

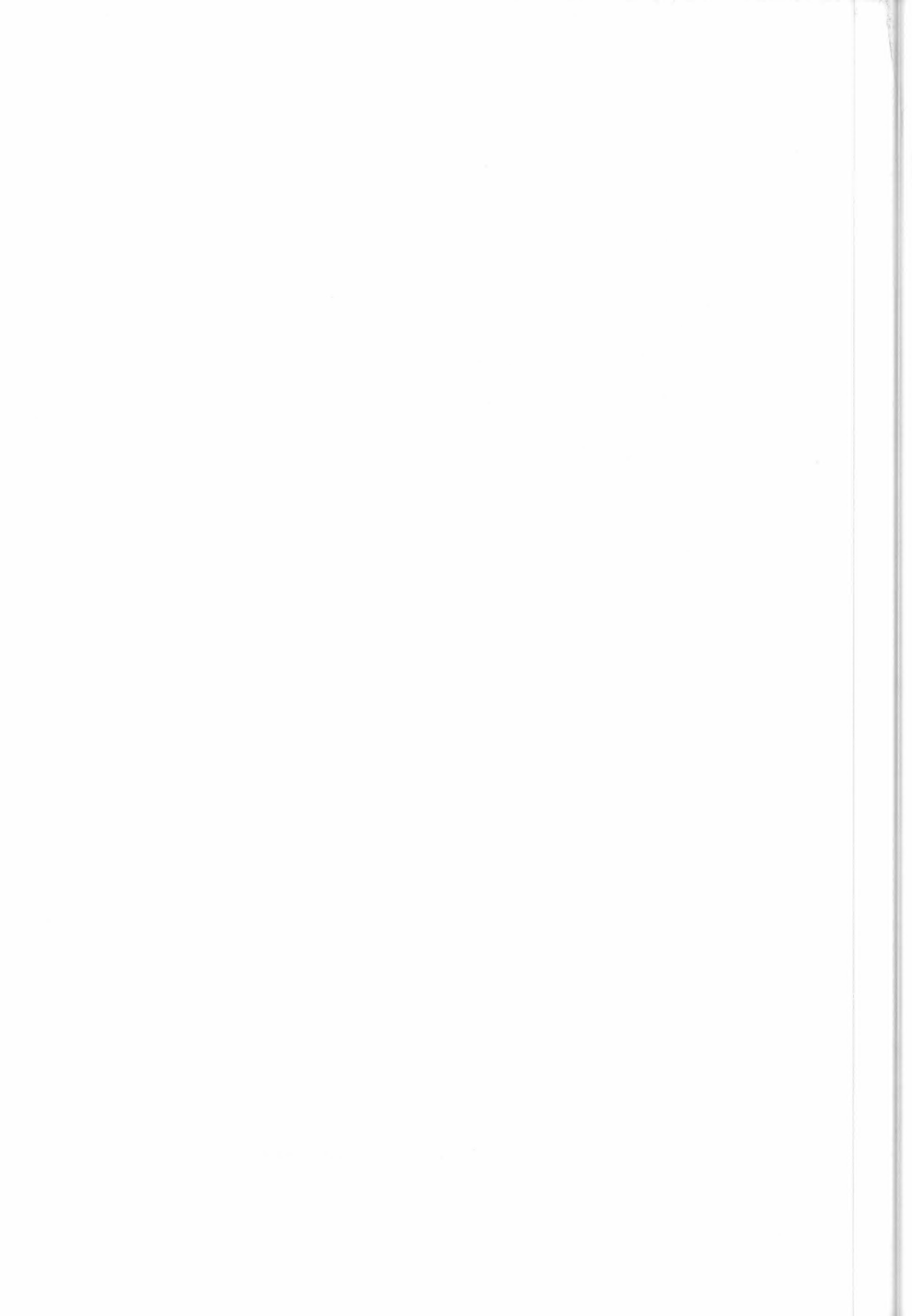
"Study of a Method to De-Alias Winds from ERS-1 Data"
Final Report of ESA Contract N°6074/87/GP-I(sc)

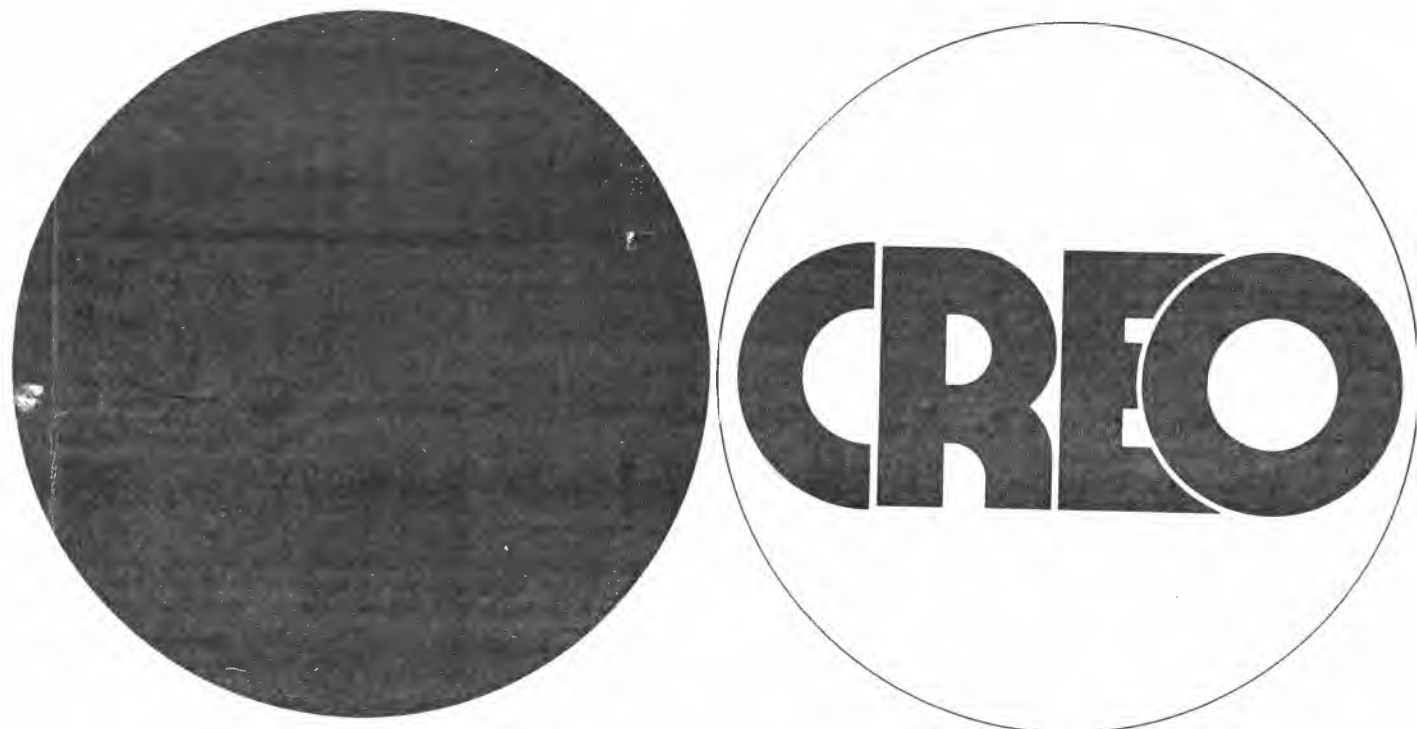
(Etude d'une Méthode pour le Lever d'Ambiguïté du Vent
Relative aux Données du Satellite ERS-1)

A. CAVANIE, P. LECONTE/CREO

AGENCE SPATIALE EUROPEENNE RAPPORT SUR L'EXECUTION D'UN CONTRAT

Les travaux décrits dans ce rapport ont été effectués au titre d'un contrat de l'ASE/ESA. Le contenu de ce rapport engage la seule responsabilité de son auteur ou de l'organisation qui l'a établi.





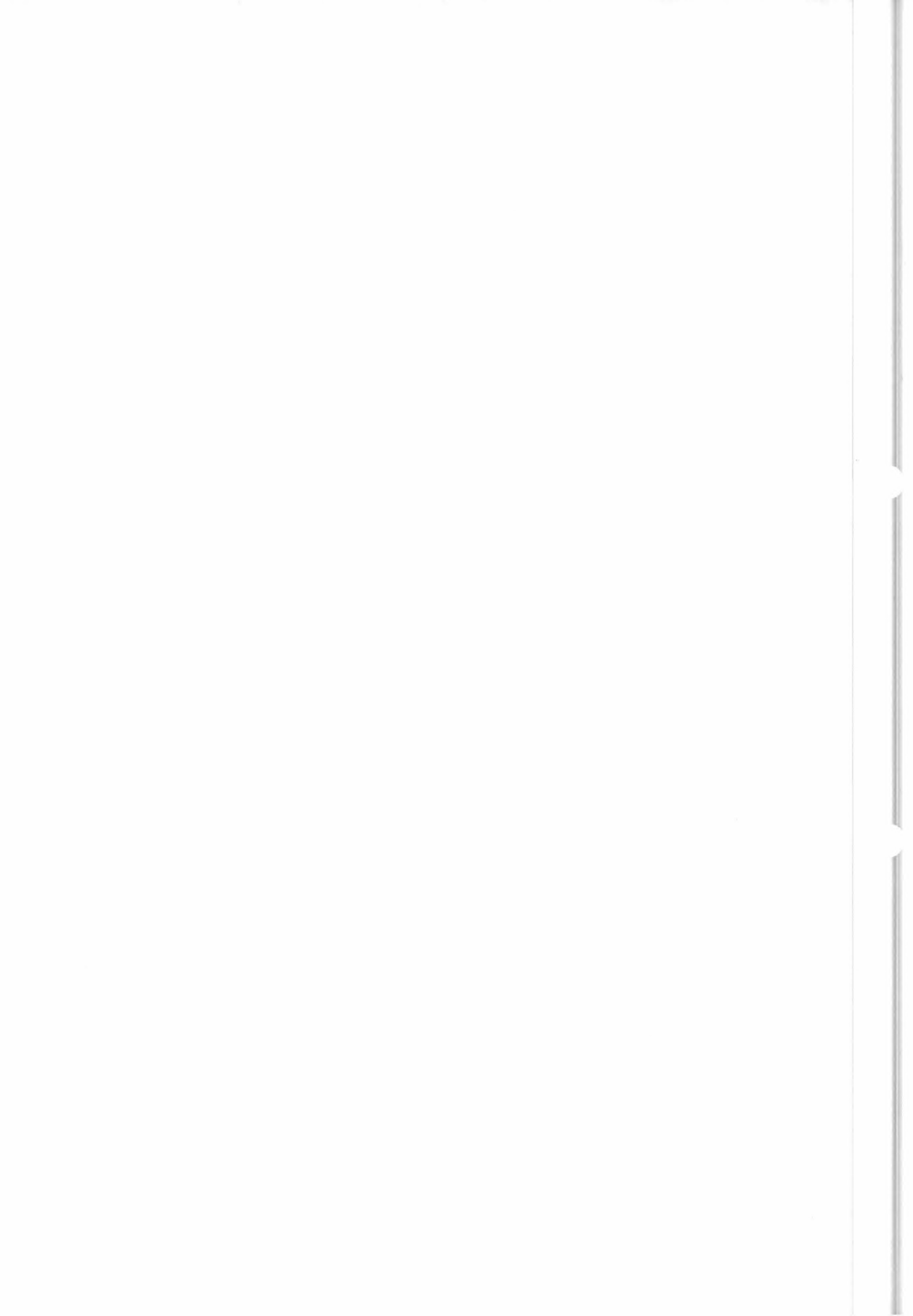
"Study of a Method to De-Alias Winds from ERS-1 Data"
Final Report of ESA Contract N°6974/87/GP-I(sc)

(Etude d'une Méthode pour le Lever d'Ambiguïté du Vent
Relative aux Données du Satellite ERS-1)

A. CAVANIE, P. LECOMTE/CREO

AGENCE SPATIALE EUROPEENNE RAPPORT SUR L'EXECUTION D'UN CONTRAT

Les travaux décrits dans ce rapport ont été effectués au titre d'un contrat de l'ASE/ESA. Le contenu de ce rapport engage la seule responsabilité de son auteur ou de l'organisation qui l'a établi.



ESA STUDY CONTRACT REPORT

No ESA Study Contract Report will be accepted unless this sheet is inserted at the beginning of each volume of the Report.

ESA CONTRACT NO: N°6874/87/GPI(sc)	SUBJECT: Study of a method to De-Alias winds from ERS-1 Data	NAME OF CONTRACTOR CREO
* ESA CR() No:	* STAR CODE	No. of Volumes 2 This is Volume No: 1
		CONTRACTOR'S REFERENCE. N°6374

ABSTRACT:

This document is the final report of ESA contract N°6874/87/GPI(sc) "Study of a Method to De-alias Winds from ERS-1 Data" (Etude d'une méthode pour le lever d'ambiguïté du vent relative aux données du satellite ERS-1).

Volume I describes primarily the principles, methods, blunder point screening, software tests carried out and their results. Possible evolutions and further work are suggested when appropriate.

A general presentation is given of the scatterometer and the problems posed in going from normalized radar cross-section (Σ_0) to unambiguous winds. Then the search for all possible solutions, which corresponds to finding local minima of a maximum likelihood function is described. De-aliasing, that is, choosing between these different solutions, is then discussed.

Influence of rapid wind changes and ice-regions are studied and general concepts of off-line manual de-aliasing presented.

The main objective is a real-time wind extraction/ambiguity removal algorithm proposal and the indication of the added value of an improved ambiguity removal algorithm to be used in the off-line mode.

Volume II is an annex containing the Detailed Program Description of WIND and WINRET and the User Manual of WIND. (WINRET and WIND are respectively the inversion and combined inversion and de-aliasing routines provided to ESA). Are also annexed test wind field figures and a description of the method used to determine maximum likelihood straight lines.

The work described in this report was done under ESA contract. Responsibility for the contents resides in the author or organisation that prepared it.

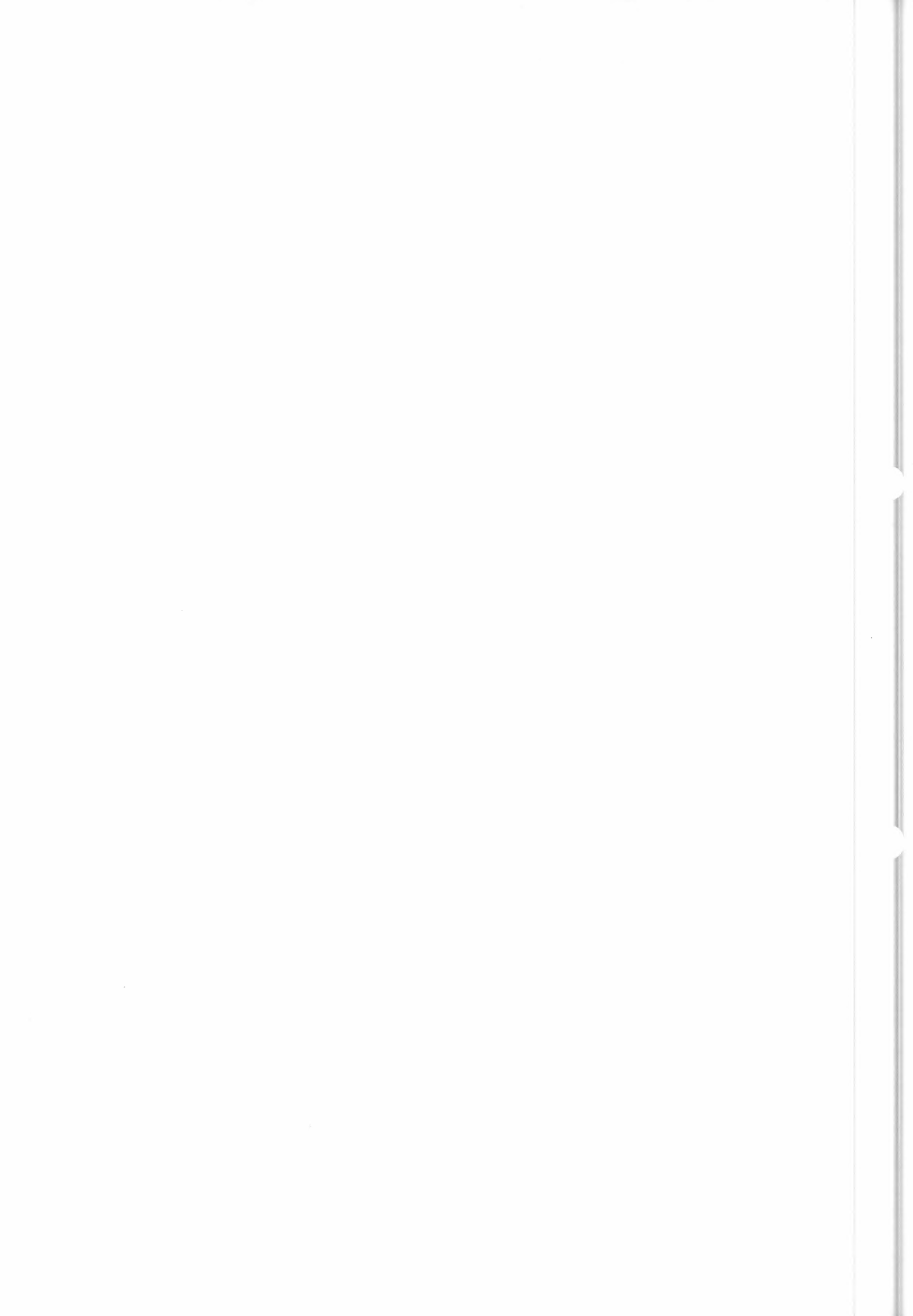
Names of authors:

Alain CAVANIE and Pascal LECOMTE

** NAME OF ESA STUDY MANAGER WILLEM WILMANS	** ESA BUDGET HEADING 65-512 / 73-512
DIV: EPO DIRECTORATE EOM	

* Sections to be completed by ESA

** Information to be provided by ESA Study Manager



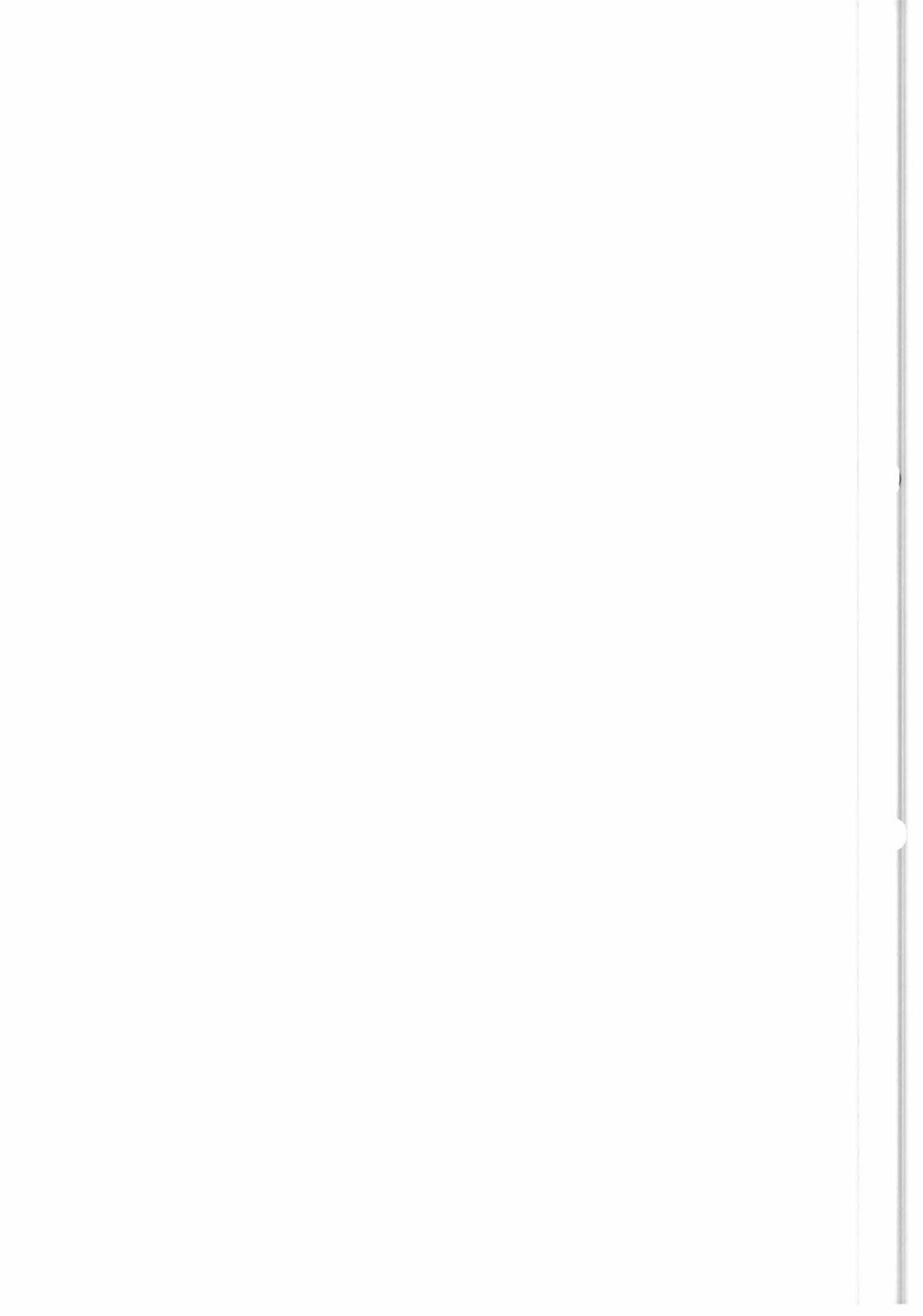
"Study of a Method to De-Alias Winds from ERS-1 Data"
Final Report of ESA Contract N°6874/87/GP-I(sc)

(Etude d'une Méthode pour le Lever d'Ambiguïté du Vent
Relative aux Données du Satellite ERS-1)

A. CAVANIE, P. LECOMTE/CREO

AGENCE SPATIALE EUROPEENNE RAPPORT SUR L'EXECUTION D'UN CONTRAT

Les travaux décrits dans ce rapport ont été effectués au titre d'un contrat de l'ASE/ESA. Le contenu de ce rapport engage la seule responsabilité de son auteur ou de l'organisation qui l'a établi.



SUMMARY

This document is the final report of ESA contract N°6874/87/GPI(sc) "Study of a Method to De-alias Winds From ERS-1 Data" (Etude d'une méthode pour le lever d'ambiguïté du vent relative aux données du satellite ERS-1).

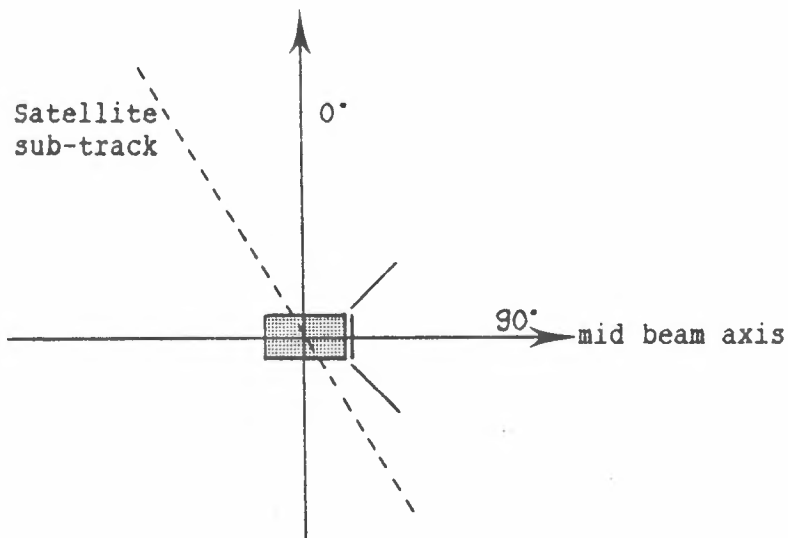
As software, user manuals and detailed program descriptions have been furnished to ESA as annexes, it describes primarily the principles, methods, blunder point screening, software tests carried out and their results. Possible evolutions and further work are suggested when appropriate.

A general presentation is given of the scatterometer and the problems posed in going from normalized radar cross-section (Σ_0) to unambiguous winds. Then the search for all possible solutions, which corresponds to finding local minima of a maximum likelihood function, is described. De-aliasing, that is, choosing between these different solutions, is then discussed.

Influence of rapid wind changes and ice-regions are studied and general concepts of off-line manual de-aliasing presented.

The main objective is a real-time wind extraction/ambiguity removal algorithm proposal and the indication of the added value of an improved ambiguity removal algorithm to be used in the off-line mode.

Throughout this report, we have chosen a system of directions (positive clockwise), the wind-beam direction being fixed arbitrarily at 90° (thus, the 0° direction is approximatively long track).



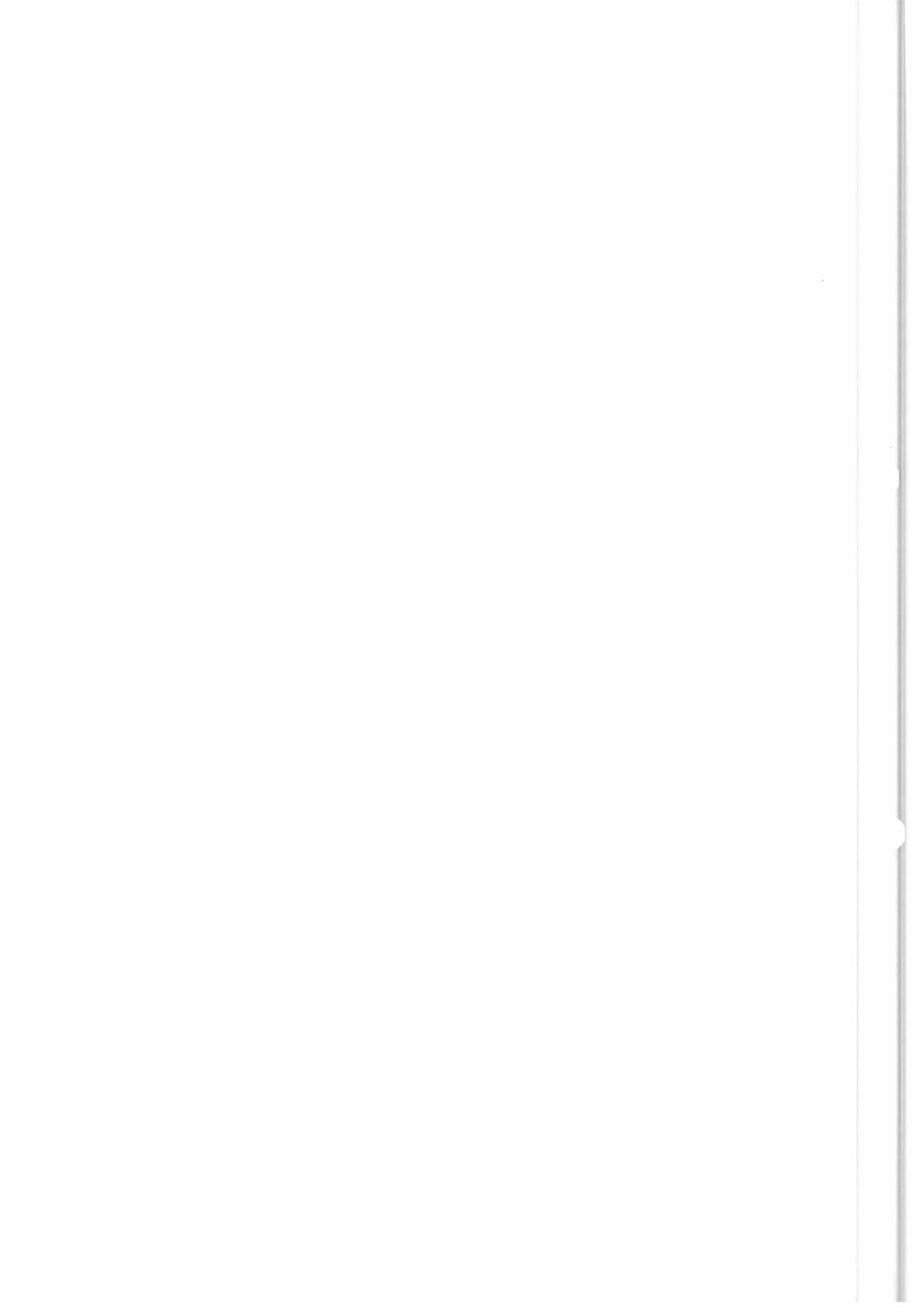


TABLE OF CONTENTS

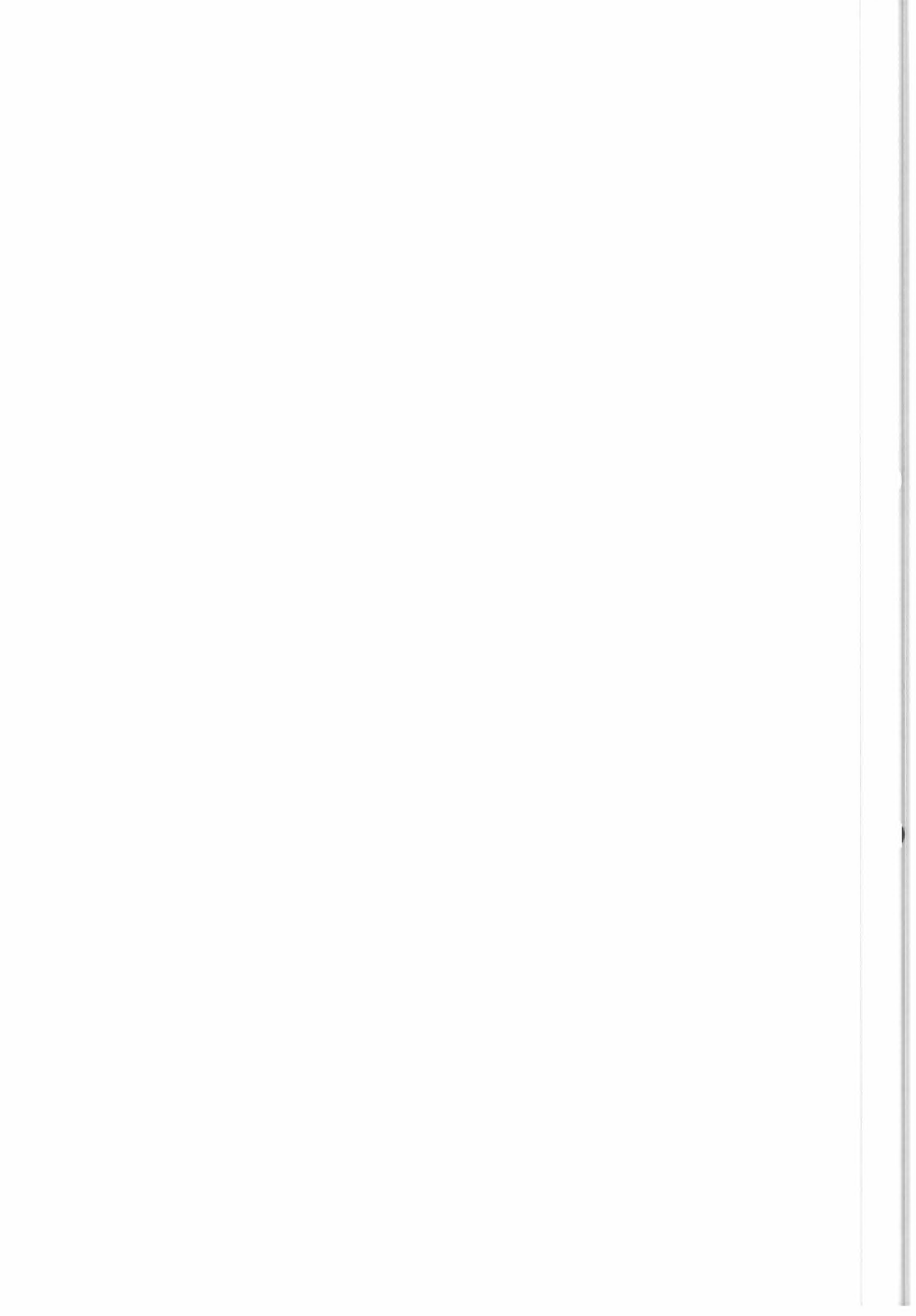
- I - BRIEF PRESENTATION OF THE ERS-1 SCATTEROMETER, THE C-BAND MODEL AND WIND EXTRACTION PROCEDURES
 - I.1 The scatterometer
 - I.2 The ESA C-band model
 - I.3 Geometrical representation of the C-band model, in three-beam data space
 - I.4 Geometrical representation of the C-band model in two-beam data planes
 - I.5 Interpretation of scatterometer data, subject to noise

- II - THE MAXIMUM LIKELIHOOD DISTANCE AND ITS USE AS A PROBABILITY LEVEL QUALITY TEST
 - II.1 Evaluation of maximum likelihood distances corresponding to given probability levels
 - II.1.A The three-beam case
 - II.1.B The two-beam case
 - II.2 Discussion concerning Ml, the limiting value of the M.L.D

- III - TESTING FOR BLUNDER-POINTS AT THE σ_0 , Kp LEVEL
 - III.1 Testing the Kp
 - III.2 Testing σ_0 values
 - III.2.A Testing σ_0 values individually
 - III.2.B Testing the sum of forward and rear beam σ_0 values
 - III.3 Possible further tests of σ_0

- IV - PASSING FROM σ_0 TO POSSIBLE WIND ESTIMATES (INVERSION)
 - IV.1 General principles of the inversion
 - IV.2 Particular features of the three-beam procedure
 - IV.3 Particular features of the two-beam procedure
 - IV.4 Testing the inversion module with simulated data
 - IV.4.A Two and three beam tests without bias
 - IV.4.B Synthesis of results including multiplicative bias
 - IV.5 Propositions for further testing

- V - INFLUENCE OF A RAPID EVOLUTION IN SPACE OF WIND SPEED OR DIRECTION ON WIND RETRIEVAL
 - V.1 A basic hypothesis in the interpretation of measured σ_0 to evaluate winds
 - V.2 Estimation of the influence of a constant wind shear
 - V.3 Estimation of the influence of a wind speed jump



V.4 Estimation of the influence of a wind direction jump

V.4.A Presentation of the problem

V.4.B Equivalent surfaces and their probability distribution for a Gaussian weighting function

V.4.B.a The Gaussian scatterometer weighting function

V.4.B.b The equivalent surface as a function of r

V.4.B.c The probability density of equivalent surfaces

V.4.C Numerical simulation of direction jumps

V.4.C.a Description of the procedure

V.4.C.b Description of results

V.4.C.c Impact on de-aliasing techniques

VI - BEHAVIOUR OF THE INVERSION MODULE IN ICE-COVERED AREAS

VI.1 Presentation of the problem

VI.2 The linear approximation of σ_0 dependence on incidence angle

VI.3 Incidence angles as a function of off-track distance

VI.4 Presentation of rank 1 and 2 "wind solutions" over ice

VI.5 Impact on wind extraction modules

VI.6 Detection of ice-covered areas

VII - DE-ALIASING PROCEDURE

VII.1 General principles of de-aliasing procedure in the 3-beam case

VII.1.A Ambiguity removal in σ -space

VII.1.B Ambiguity removal in the (V, φ) -space

VII.2 Two-beam ambiguity removal

VII.2.A Two-beam area description

VII.2.B Basis of the method

VII.3 Compatibility

VII.4 Tests

VII.4.A Tests without bias

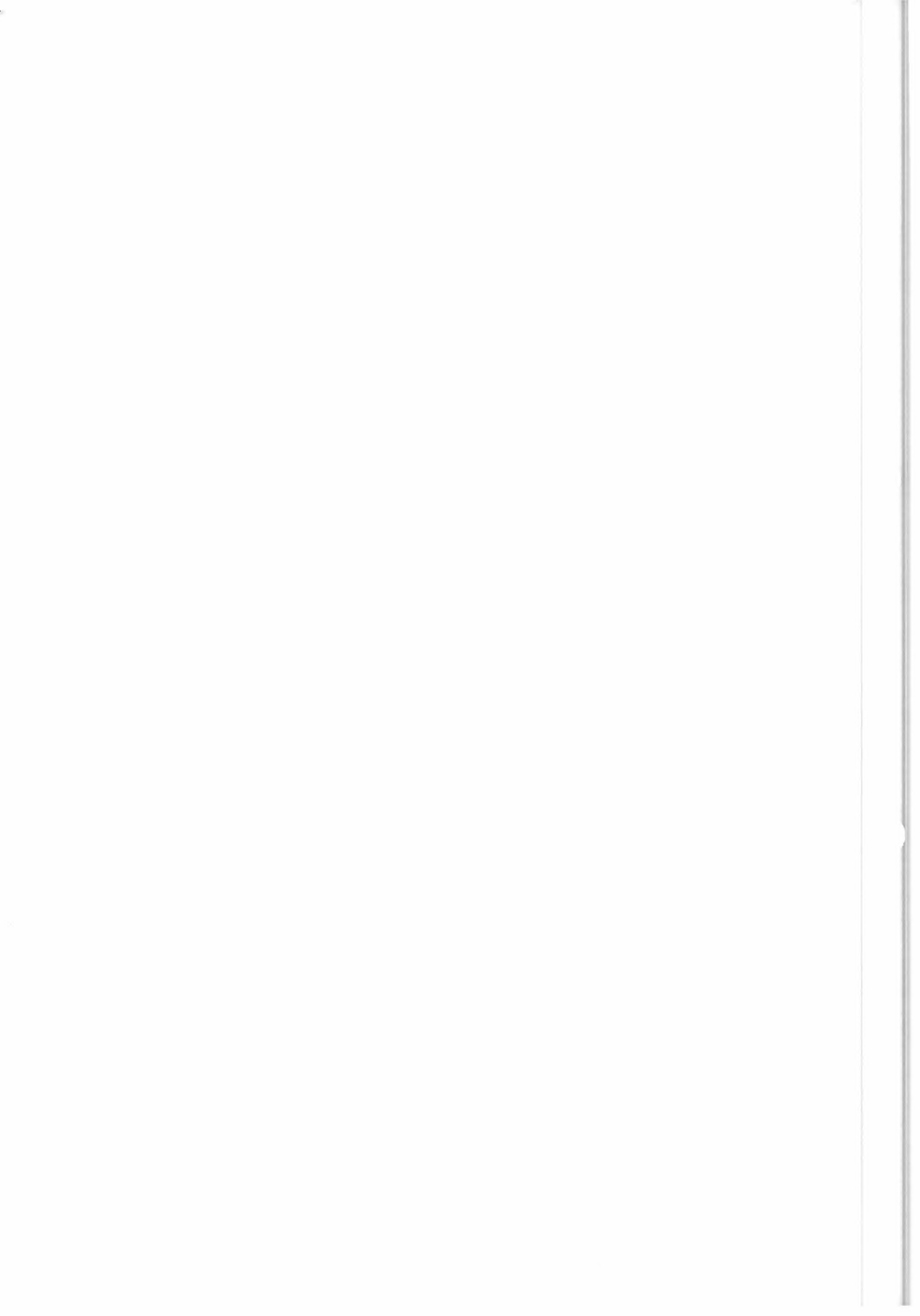
VII.4.B Tests with bias on antennas

VII.4.C Computing times

VIII - MANUAL DE-ALIASING FOR PRECISION PROCESSING

VIII.1 General presentation

VIII.2 De-aliasing three-beam zones left undetermined by automatic processing



VIII.3 De-aliasing two-beam zones

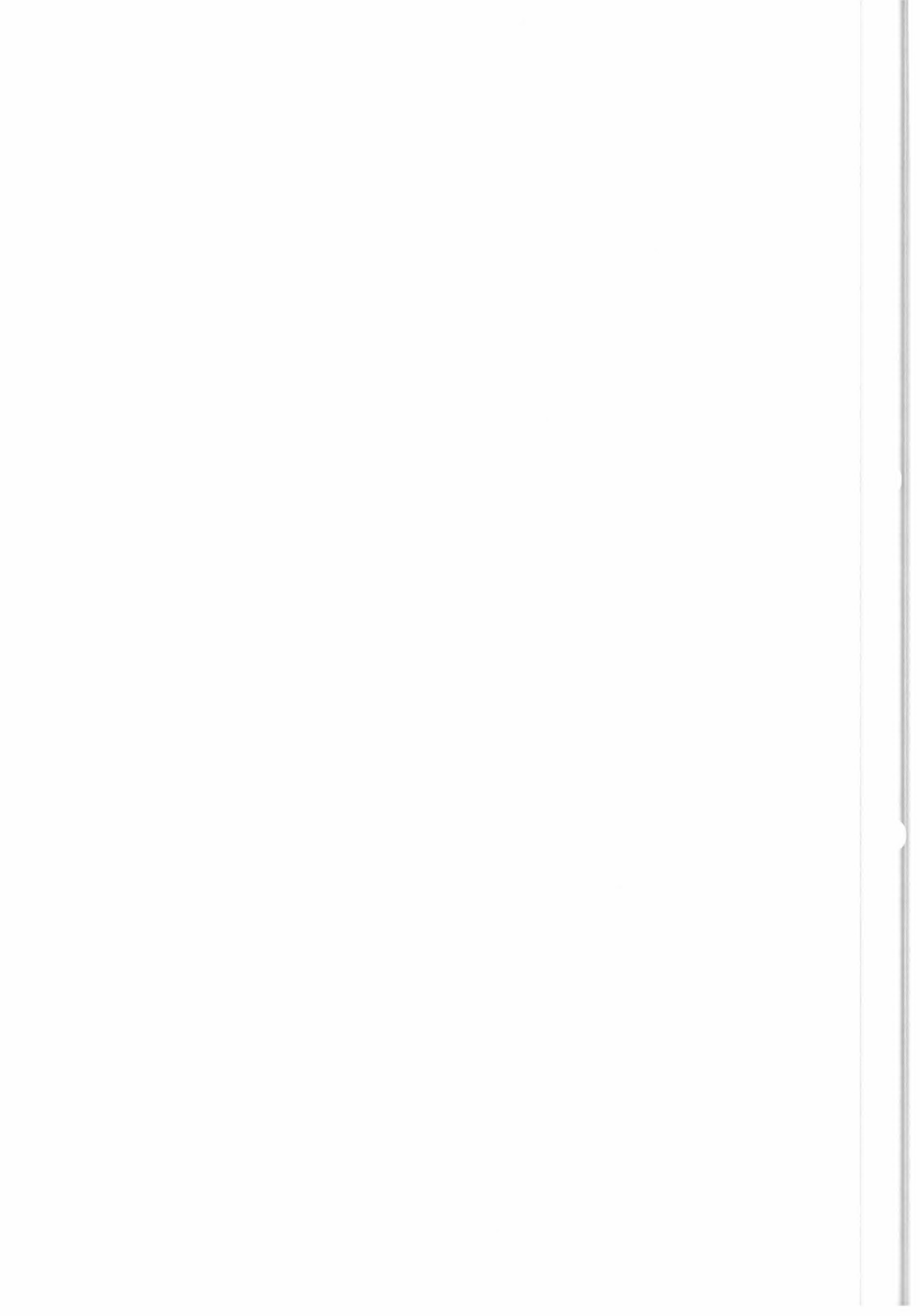
IX - SIMILARITIES AND DIFFERENCES BETWEEN FAST DELIVERY AND PRECISION PROCESSING

- IX.1 Swath preparation
- IX.2 Quality tests
- IX.3 Wind extraction
- IX.4 Manual de-aliasing

X - GENERAL CONCLUSION AND POSSIBLE FUTURE WORKS

ANNEX 1 : LAND/SEA RATIO DETERMINATION PROGRAMS

ANNEX 2 : METEOROLOGICAL SITUATIONS OF D. OFFILER'S FILES



I - BRIEF PRESENTATION OF THE ERS-1 SCATTEROMETER, THE C-BAND MODEL AND WIND EXTRACTION PROCEDURES

I.1 The scatterometer

The ERS-1 scatterometer is a three antenna instrument working in C-band (5.3 GHz), VV polarized. The beam geometry is represented in Fig. I.1, which shows the 500 km wide swath of the instrument, to the right of the satellite sub-track.

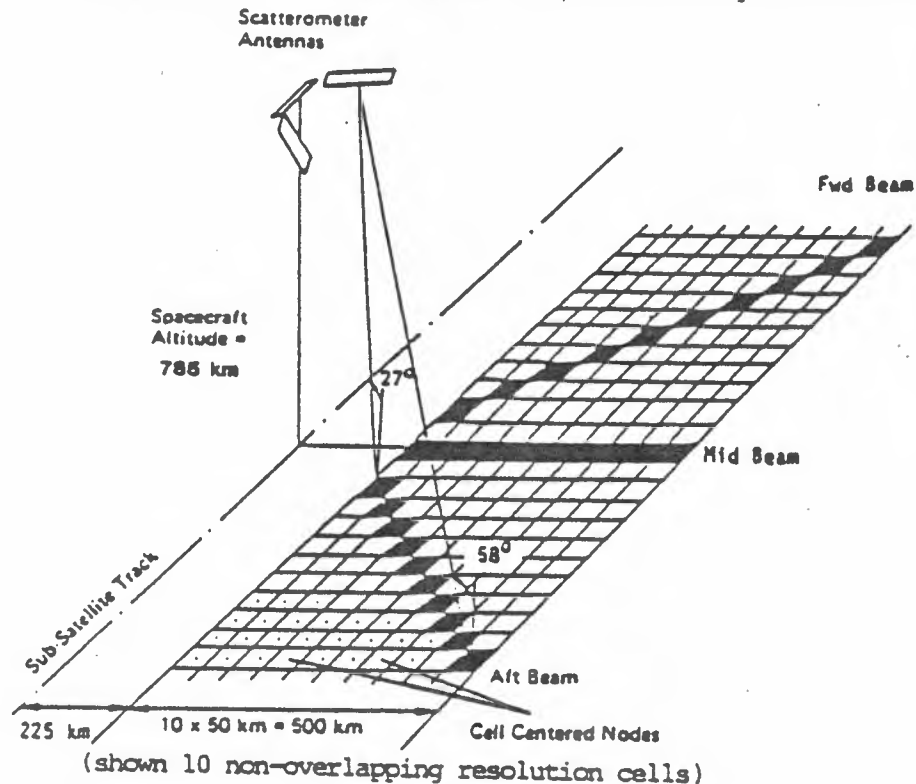


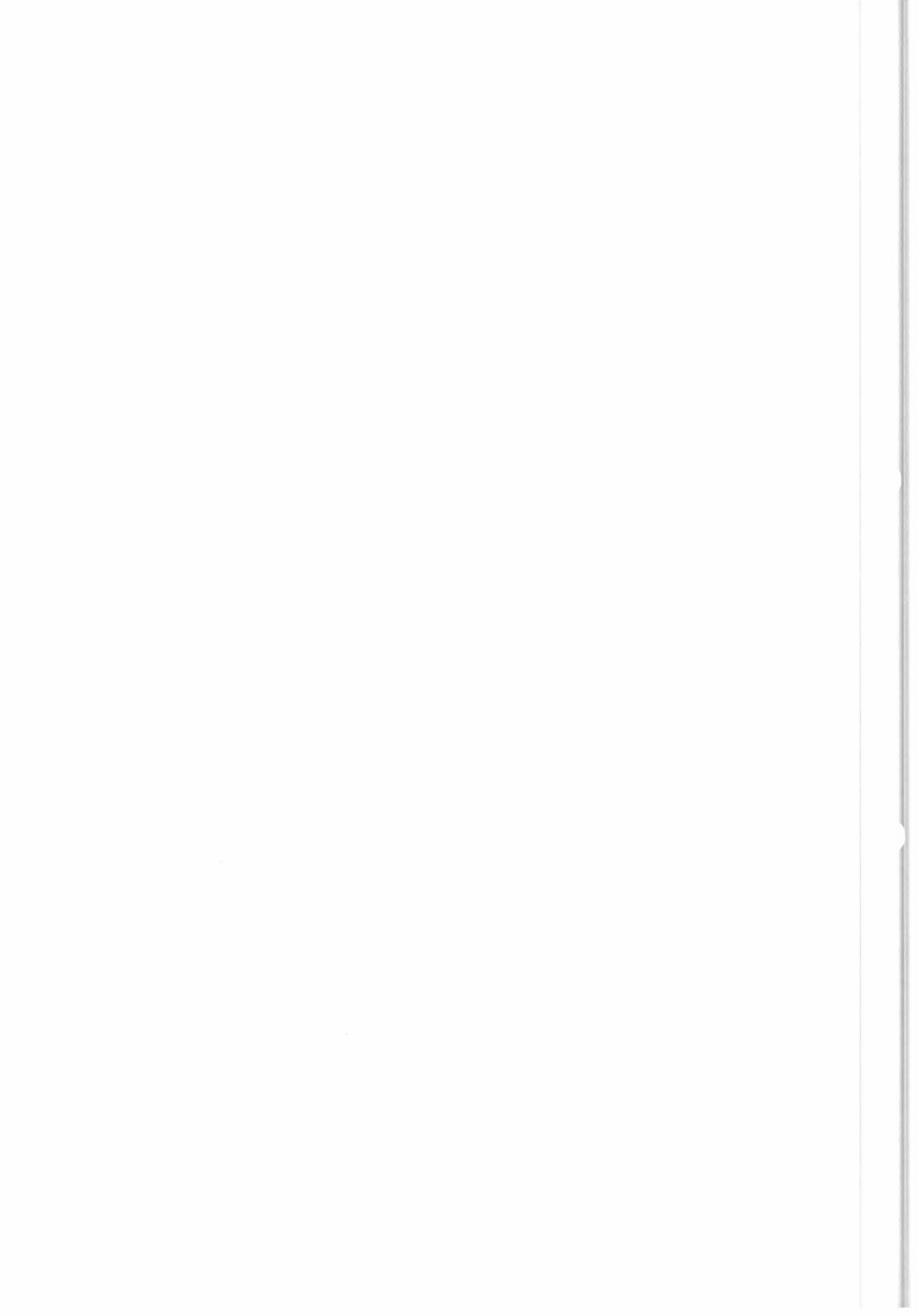
Figure I.1 ERS-1 wind scatterometer geometry

The swath is divided into 19 lines of nominally 50 km x 50 km cells. Each cell is illuminated by 128 pulses of each antenna, which through yaw-steering of ERS-1, are maintained in directions very close to 45°, 90° and 135° to the right of the sub-track direction.

The cycle of measurements (four consecutive sequences of Forward-Central-Rear beam 32 pulse bursts) takes 3.763 s and is repeated continuously during instrument operation; this fixed time interval corresponds approximately to 25 km along the satellite track, slight variations being due to satellite ground speed and altitude variations.

Although there is some instrument noise, the major part of the standard error in the measurement of σ_0 (Sigma0), the normalized radar cross-section, is caused by speckle. This noise can be approximately modelled by centered Gaussian noise, proportional to the power of the signal returned, of amplitude around 10%.

Particular aspects of the scatterometer data are the two-beam zones, formed of the central and rear beams at the beginning of the swath. If the scatterometer is lit and shut off sufficiently inland, the two-beam zones will not appear over the ocean. But mission constraints, particularly the use of the AMI imaging mode, will lead to a number of two-beam zones, whose data analysis is particular.



I.2 The ESA C-band model

ESA is pursuing work on the relationship between σ_0 and the most clearly important parameters :

θ : the incidence angle

V : the surface wind speed

ϕ : the beam direction, or azimuth, angle

Some idea of this relationship is given by the example of Figure I.2. The analysis of calibration campaigns made with air-borne scatterometers indicates that the general expression for σ_0 (in linear representation), can be correctly approached by a truncated Fourier development extending to the first harmonic :

$$\sigma_0 = U (1 + b_1 \cos \phi + b_2 \cos 2\phi) / (1 + b_1 + b_2) \quad (1)$$

where $U = Av^\gamma$

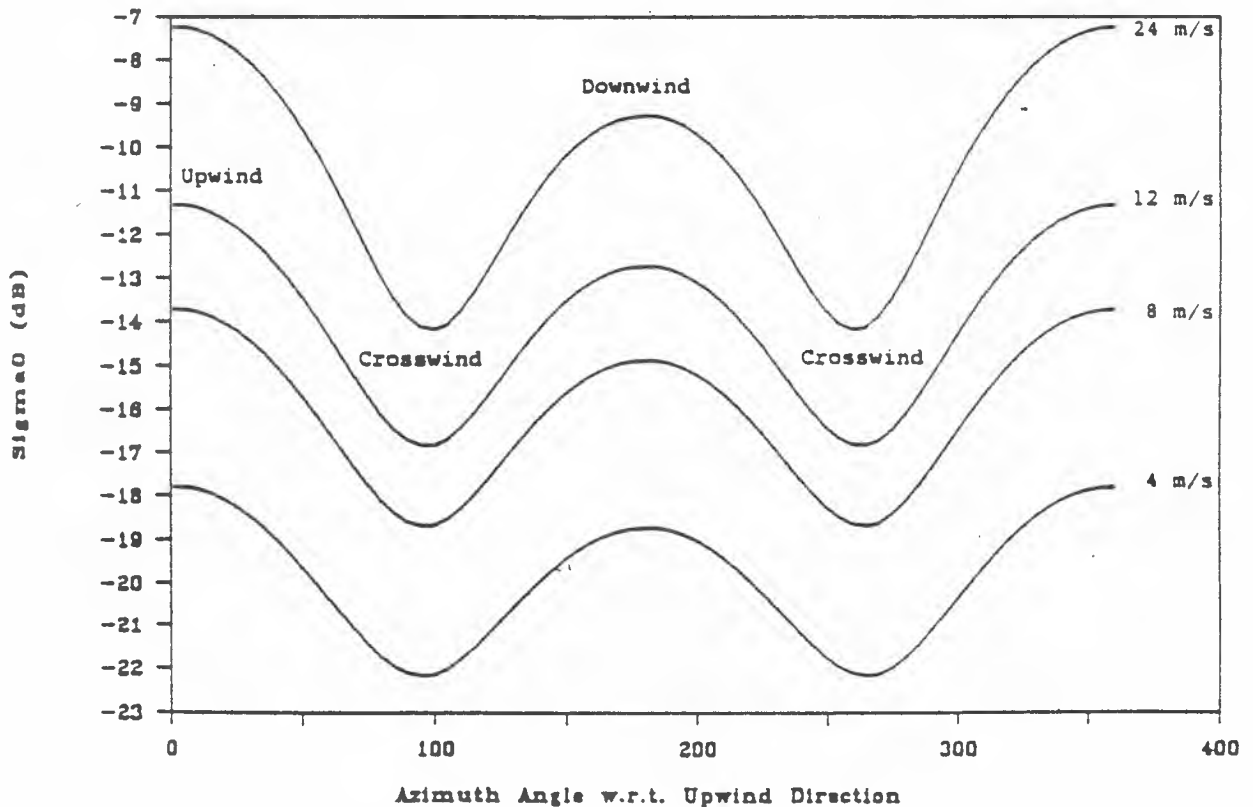


Figure I.2 Radar cross-section of the sea as a function of the wind direction and wind speed



The present ESA model, CMOD1, developed by Alfred LONG (ESTEC), specifies that A and γ depend only on incidence angle on θ , and that b_1 and b_2 are functions of both wind speed, V , and θ . Details of this model are given in the WINRET annex, and will not be here reproduced. It is probable that the model will change somewhat in the coming year (discussion with A. LONG at ESRIN in april 1987) to take into account new high wind data obtained in the Mediterranean campaign. But the basic structure with a Fourier development to the first harmonic in direction appears as appropriate, and the general observations that $0 < b_1 < 1$, and $|b_2| \ll 1$ seem will be established.

I.3 Geometrical representation of the C-band model, in three-beam data space

For a given cell, the incidence angles of the three beams are fixed parameters, and σ values for the three beams form points in the $(\sigma_F, \sigma_R, \sigma_C)$ space of forward, rear and central beam values. As the wind speed, wind direction domain is swept through, a surface is generated by the set of points created, which represents the locus of all points in σ space which could be reached if the model was perfectly exact and there was no error on the measurements. This surface is schematically represented in Figure I.3.

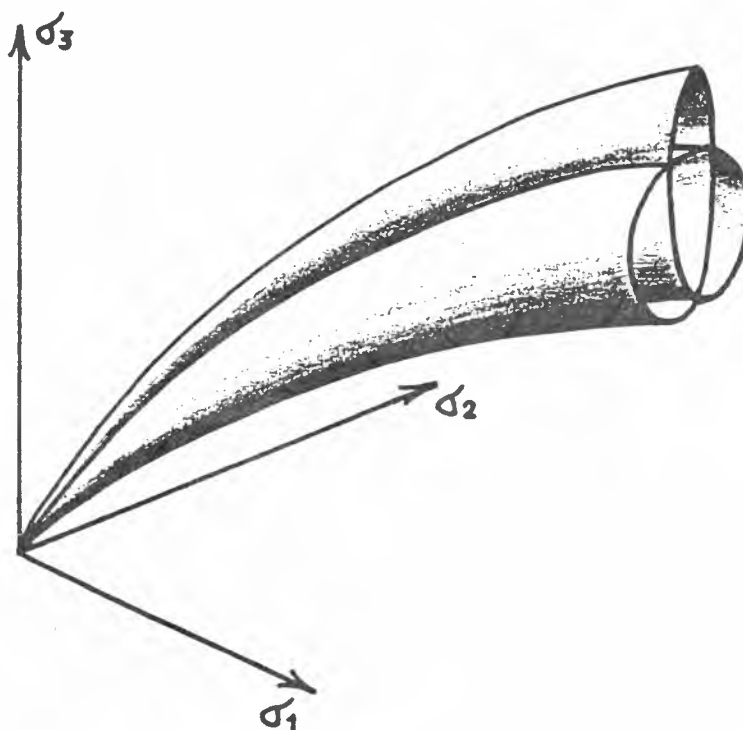
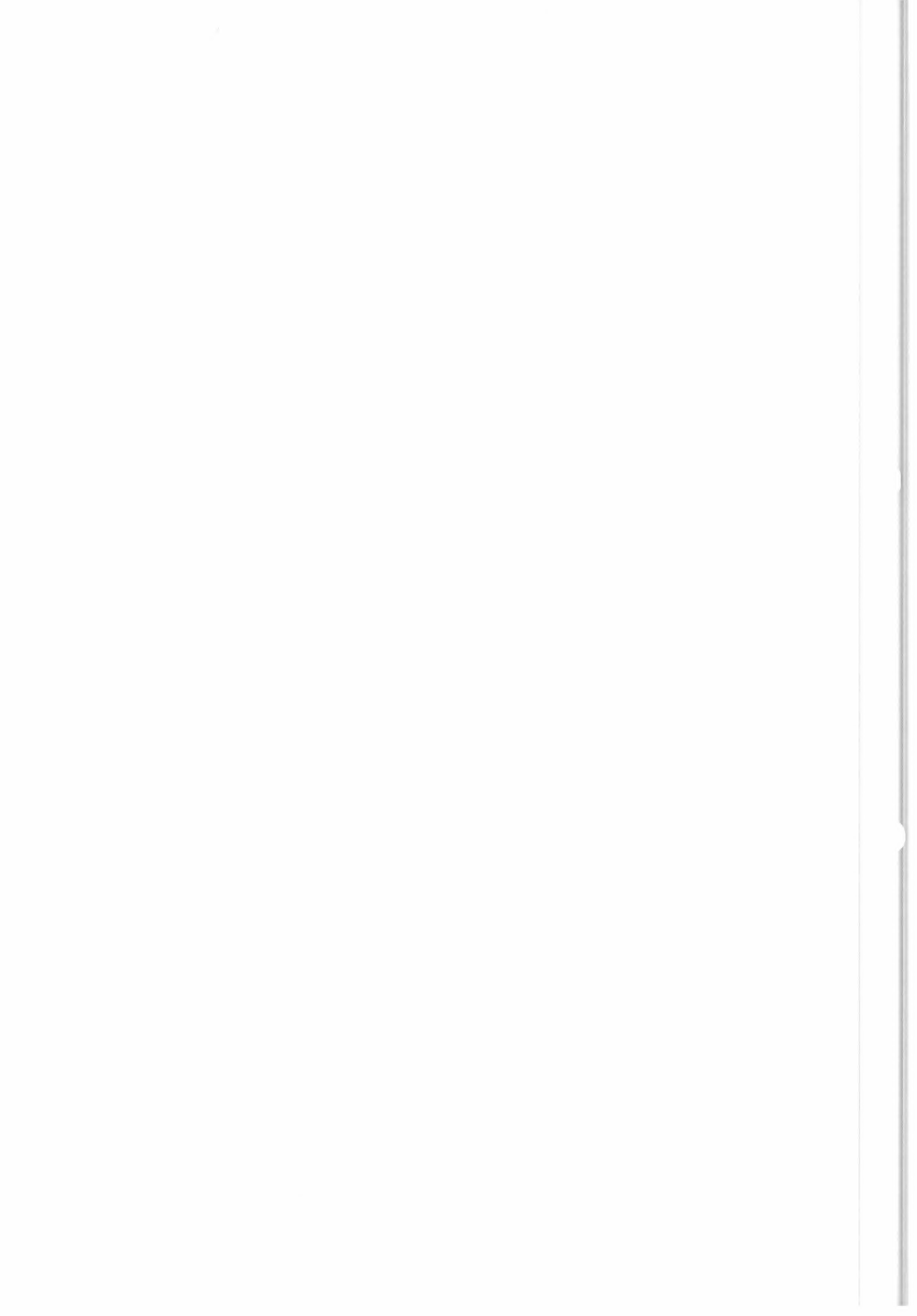


Figure I.3 Surface of the C-band model in σ space

This behaviour can perhaps be best represented after a variable transformation corresponding to a 45° rotation of the axes around the σ_C axis. Then :

$$\sigma_p = (\sigma_F + \sigma_R)/2 \quad (2a)$$

$$\sigma_m = (\sigma_F - \sigma_R)/2 \quad (2b)$$



Taking ϕ with respect to the central antenna, making the approximation that incidence angles of the forward and rear beams are exactly the same and that azimuth of the Forward, Central and Rear antennas are exactly 45° , 90° and 135° to the right of the subtrack :

$$\sigma_F = U(1 + b_{1F} \cos(\phi - 45^\circ) + b_{2F} \cos(2\phi - 90^\circ)) / (1 + b_{1F} + b_{2F}) \quad (3a)$$

$$\sigma_R = U(1 + b_{1F} \cos(\phi + 45^\circ) + b_{2F} \cos(2\phi + 90^\circ)) / (1 + b_{1F} + b_{2F}) \quad (3b)$$

(These approximations are excellent, within a few tenth of degrees in incidence angle and azimuth, because of yaw-steering). In the new coordinate system :

$$\sigma_p = U (1 + (b_{1F} / \sqrt{2}) \cos\phi) / (1 + b_{1F} + b_{2F}) \quad (4a)$$

$$\sigma_m = U ((b_{1F} / \sqrt{2}) \cos\phi + b_{2F} \sin 2\phi) / (1 + b_{1F} + b_{2F}) \quad (4b)$$

$$\sigma_c = U (1 + b_{1c} \cos\phi + b_{2c} \cos 2\phi) / (1 + b_{1c} + b_{2c}) \quad (4c)$$

For a fixed wind speed these equations describe a Lissajous figure, as ϕ goes from 0° to 360° . Because $|b_{1F}| \ll 1$ there is only a slight evolution of σ_p . The mean value of σ_m is zero, corresponding to the plane :

$$\sigma_R = \sigma_F$$

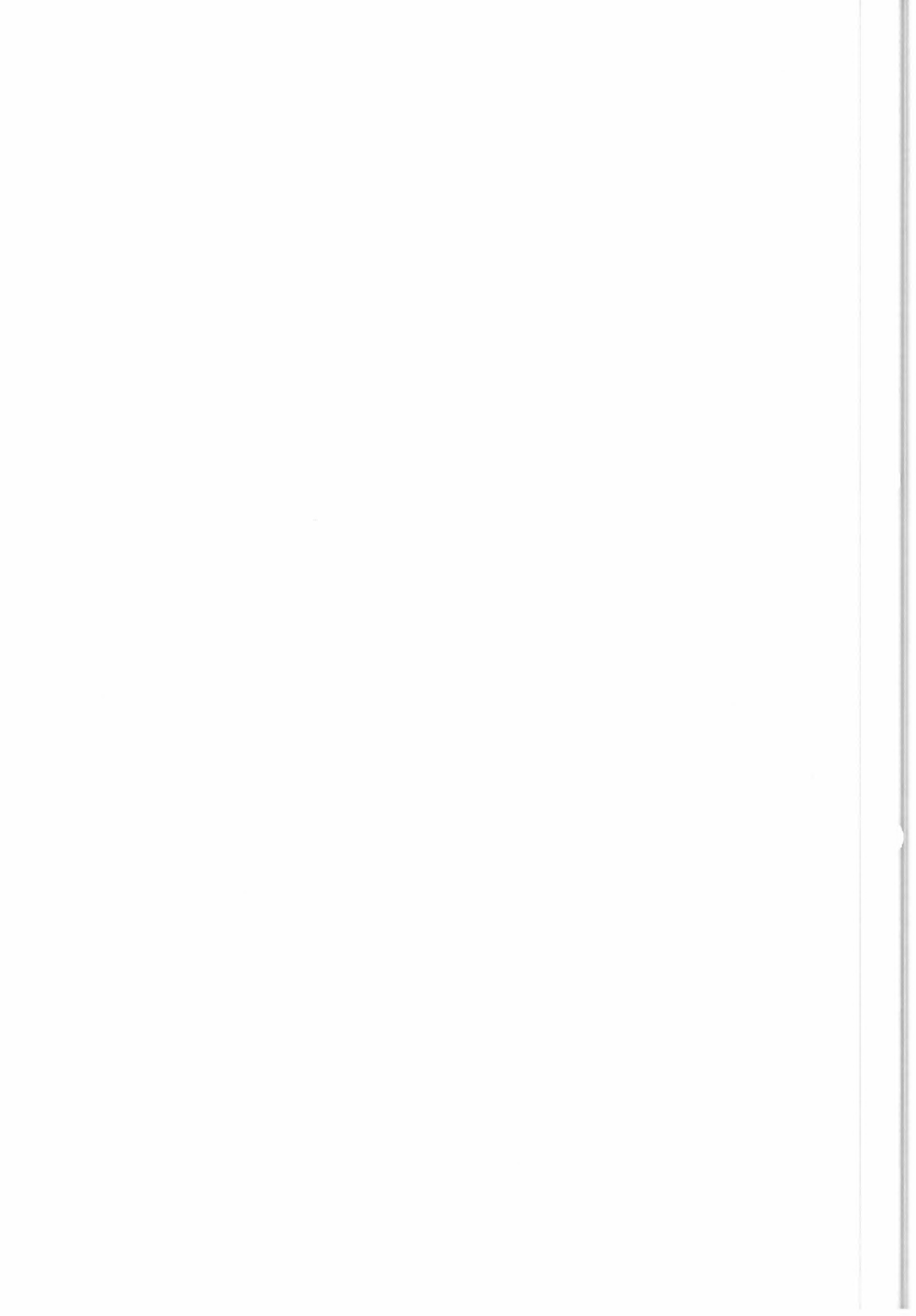
and the mean value of σ_c is $Uc / (1 + b_{1c} + b_{2c})$, which grows approximately as v , since b_1 and b_2 are always less than 1, slowly vary with wind speed.

Finally as the major variable terms in σ_m and σ_c are respectively $\sin 2\phi$ and $\cos 2\phi$, a curve at constant wind speed goes through a double loop as ϕ goes from 0° to 360° , the separation between the loops, (created by the $\cos\phi$ terms) being small because $|b_{1F} / \sqrt{2}| \ll b_{2F}$. Sweeping through all wind speeds the double-looped Lissajous figures generate the surface represented.

Whatever the evolution of the C-band model, the general nature of the surface will remain the same, as long as the Fourier development is truncated at the first harmonic. Changes in parameters would cause changes in the numerical values, such as values of ϕ where the surface intersects itself. But such variations, which are to be expected, can be understood and coped with, using this general scheme of analysis.

I.4 Geometrical representation of the C-band model in two-beam data planes

Having described the surface of points in 3D space respecting the C-band model, it is an easy task to speak of the two-beam cases, where only measurements of the central and of the forward or rear beams are made. This is because the locus of possible points is simply the orthogonal projection of the three-dimensional surface on the (F,C) or (R,C) planes. Figure I.4 shows that up to four distinct values of (V, ϕ) can correspond to one point in the plane ; beyond this central (dark) zone, there are two side regions where two distinct (V, ϕ) values correspond to a point in the plane. Beyond these areas, the



orthogonal projection shows that no point in the plane satisfies the C-band model exactly.

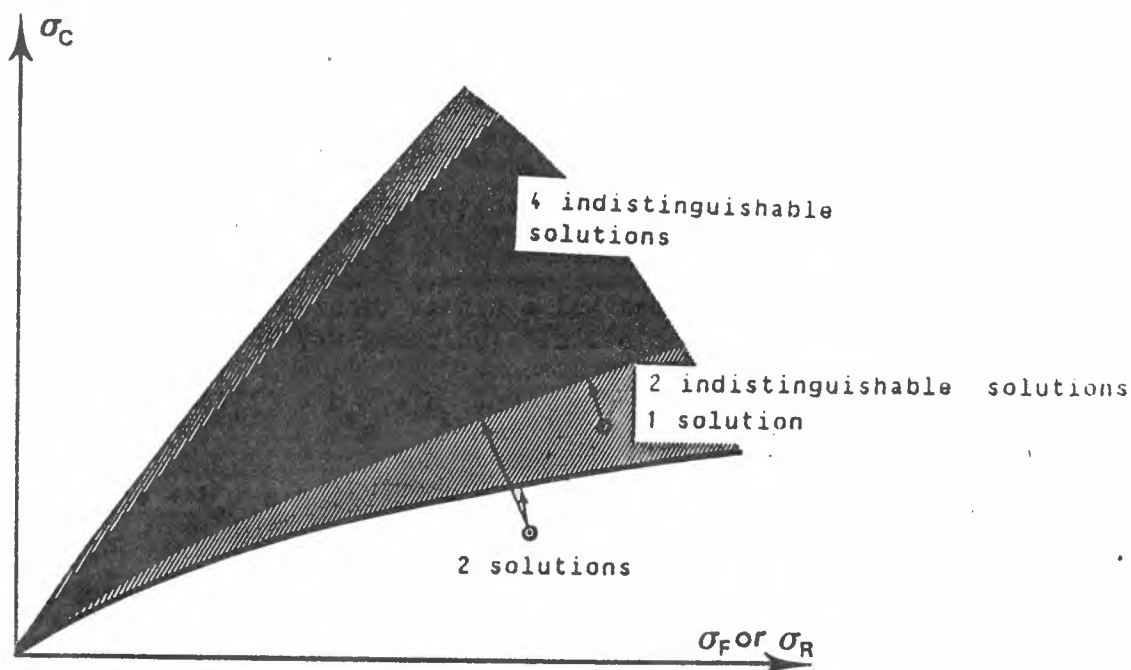


Figure I.4 Projection of the three-beam surface of the C-band model, on the (F, C) or (R, C) planes

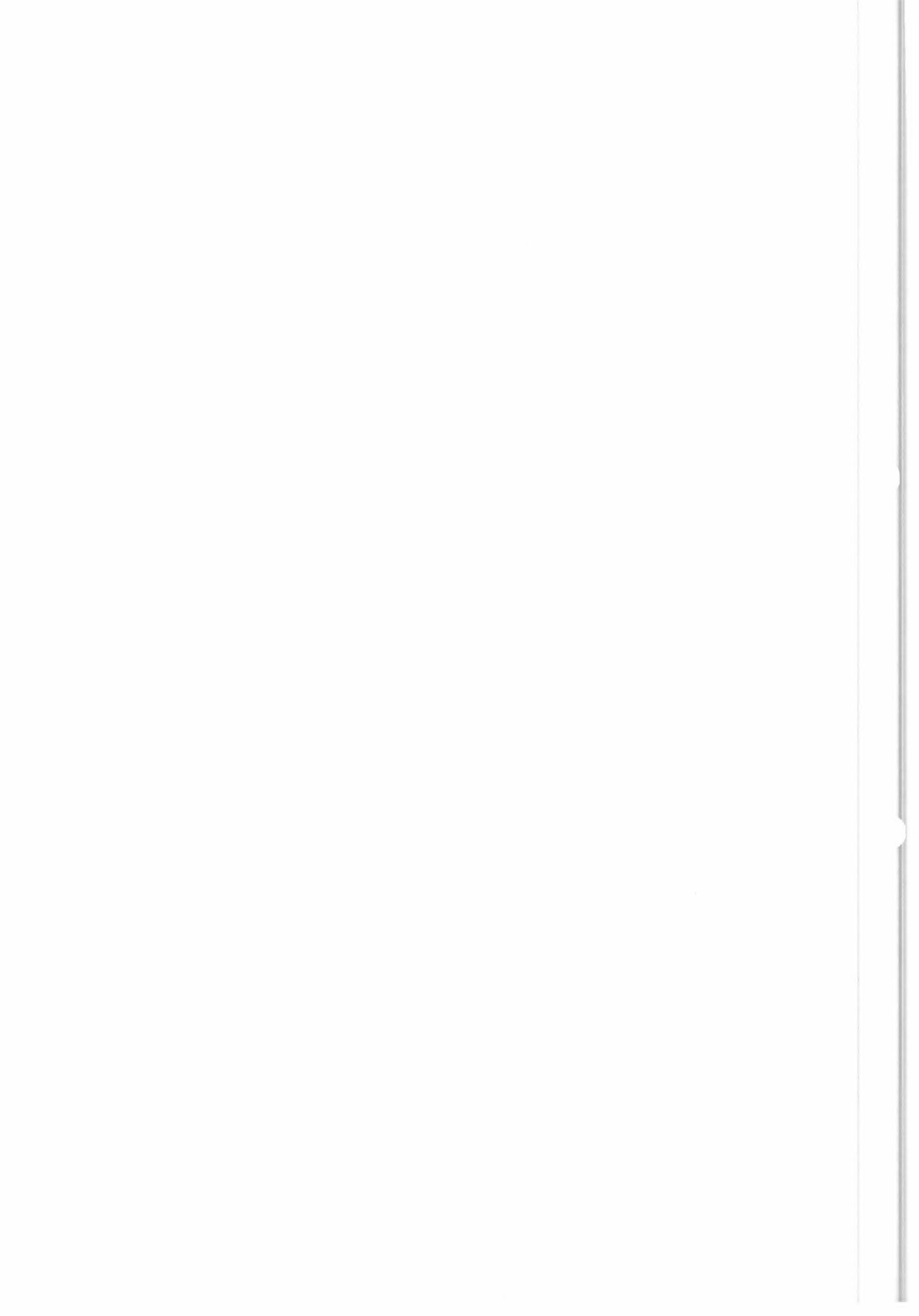
I.5 Interpretation of scatterometer data, subject to noise

So far, only the C-band model has been presented. If the model was perfect, and the measured σ_0 devoid of noise, then locating the measurement point on the C-band surface would, in the three-beam case, furnish a single value of (V, ϕ) ; the exception to this being found only for the curves where the surface intersects itself. In the two-beam case, up to four equally possible values of (V, ϕ) would be found depending on the position of the point in the (F, C) or (R, C) planes.

The presence of noise (due to speckle, electronics...) and the imperfections of the empirical C-band model will in general separate a measured triplet of σ_0 from the C-band surface. To extract wind information, the procedure must therefore be to define an appropriate distance, and find possible "solutions" defined as those (V, ϕ) pairs which correspond to local minima of the distance between the C-band surface and the measured σ_0 triplet. We have chosen, and advocate, the maximum likelihood distance because it offers a simple, probabilistic, interpretation which will be presented in detail later.

The important thing to note is that, now, because of noise, "inversion" (that is, going from σ_0 to possible wind values) offers several solutions (up to six with the present model) which have notably different directions. Selection of the "right" solution, based alone on the information furnished by the scatterometer, or using a meteorological wind field as a complementary source of information is called "de-aliasing".

The problems posed by the inversion and de-aliasing of two-beam data can be expected to be more severe than in the three-beam case. First because in the



central region (Fig. I.3) all four possible (V, ϕ) solutions are at zero distance from the point of measurement : this means that these solutions cannot be ranked according to their decreasing probability. Just as important is the fact that, unlike the three-beam case, a continuous curve in the domain of possible solutions may correspond to two different wind flow evolutions ; this is because the curves limiting the dark from the grey zones and the grey zones from the exterior zones are bifurcation lines : going through them allows the flow to pass continuously from one of the elements of the three-beam surface to another (or remain in the one previously specified), elements which are superposed on the two-beam plane by the orthogonal projection.

II - THE MAXIMUM LIKELIHOOD DISTANCE AND ITS USE AS A PROBABILITY LEVEL QUALITY TEST

II.1 Evaluation of the maximum likelihood distances corresponding to given probability levels

The choice of the maximum likelihood distance, rather than an Euclidian or least squares distance, offers the interesting possibility of obtaining rather simply the corresponding probability of occurrence.

This is really fully exploitable only in the three-beam case, a majority of points in the two-beam case being at zero distance from the theoretical surface given by the C-band model, as already said.

These two different cases must therefore be treated separately.

II.1.A The three-beam case

The maximum likelihood distance M is defined as

$$M = \sum_{i=1}^3 ((\tilde{\sigma}_i - \sigma_i)/K\pi_i\sigma_i)^2 \quad (1)$$

If measured values of Σ_0 , $\tilde{\sigma}_i$, are subject to a multiplicative Gaussian noise of standard deviation $K\pi_i\sigma_i$, (where σ_i are the noiseless C-band model Σ_0 , and the $K\pi_i$ are constants of proportionality computed previously with the $\tilde{\sigma}_i$) then the probability density of the point $(\tilde{\sigma}_1, \tilde{\sigma}_2, \tilde{\sigma}_3)$ is :

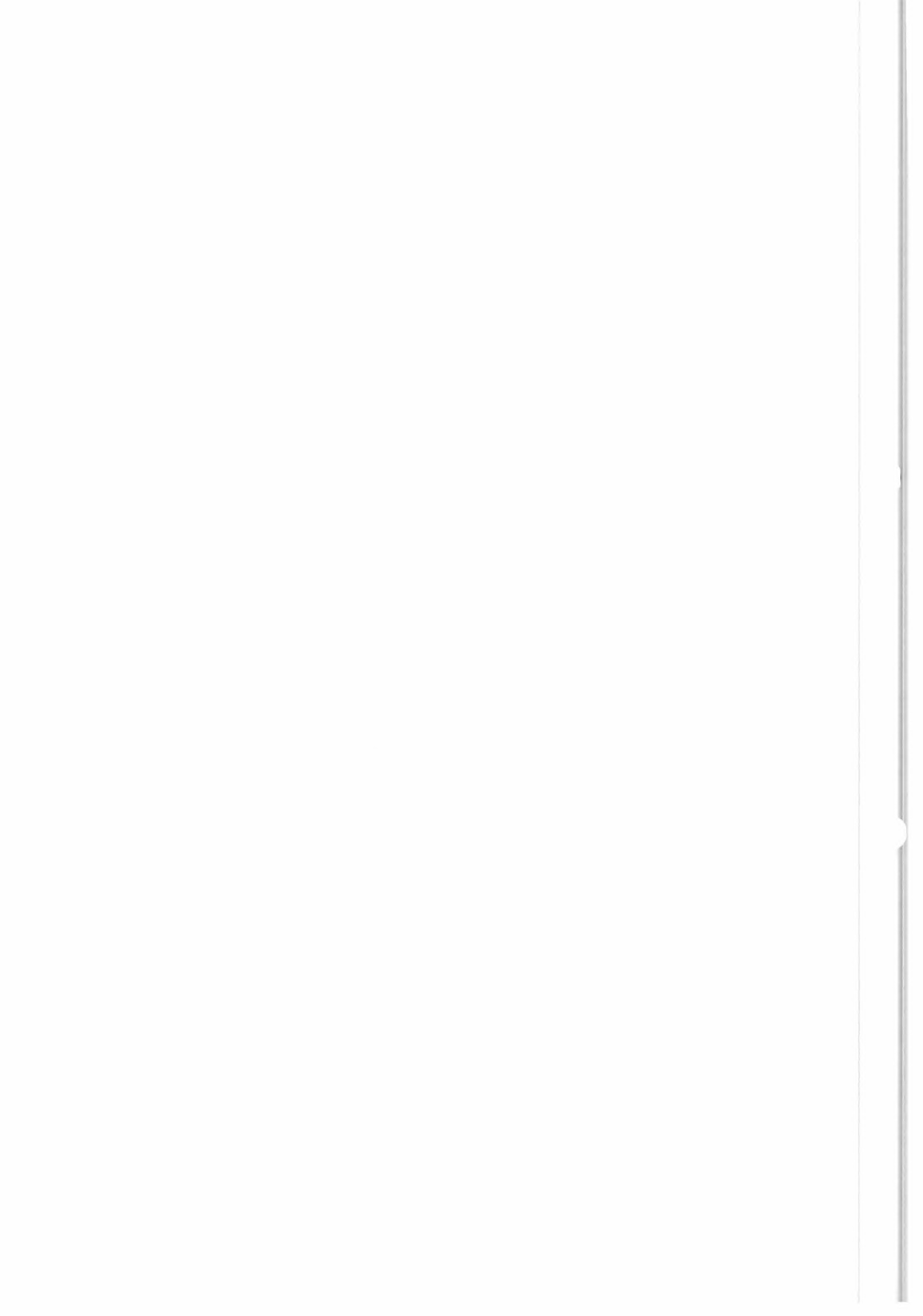
$$p(\tilde{\sigma}_1, \tilde{\sigma}_2, \tilde{\sigma}_3) = \frac{1}{\sqrt{2\pi}} \frac{\exp(-M/2)}{[(2\pi) \prod K\pi_i \sigma_i]^{3/2}} \quad (2)$$

where

$$\prod K\pi_i = K\pi_1.K\pi_2.K\pi_3$$

$$\prod \sigma_i = \sigma_1.\sigma_2.\sigma_3$$

Here it is assumed that the different noises are uncorrelated, which is quite reasonable since the three measurements are made at different instants and scatterometer noise is mainly due to speckle, whose effect, summed over 128 pulses, should be very nearly Gaussian.



The integral of p in the volume $M < M_1$ gives the cumulative probability that points $(\tilde{\sigma}_1, \tilde{\sigma}_2, \tilde{\sigma}_3)$ lie within a distance M_1 of the noiseless position $(\sigma_1, \sigma_2, \sigma_3)$. To carry out this integration, the following variable transformation is imposed to simplify notation :

$$X_i = (\tilde{\sigma}_i - \sigma_i) / K_{pi\sigma_i} \tag{3}$$

The cumulative probability $P(M_1)$ is then expressed as :

$$P(M_1) = \int_{M < M_1} \exp \left[-\sum_{i=1}^3 X_i^2 / 2 \right] dX_1 dX_2 dX_3 / (2\pi)^{1.5} \tag{4}$$

Transforming to cylindrical coordinates leads to the expression :

$$P(M_1) = \int_{-M_1^{0.5}}^{M_1^{0.5}} \int_0^{(M_1 - X_3^2)^{0.5}} \exp \left[-(R^2 + X_3^2) / 2 \right] R dR dX_3 / (2\pi)^{0.5} \tag{5}$$

which is easily integrated with respect to R, giving :

$$P(M_1) = 2 \left[\int_0^{M_1^{0.5}} \exp(-X_3^2 / 2) dX_3 / (2\pi)^{0.5} - (M_1 / 2\pi)^{0.5} \exp(-M_1 / 2) \right] \tag{6}$$

The integral is that of the normal curve of error which is tabulated in different mathematical tables ; we used the "Handbook of Mathematical Functions" (M. ABRAMOWITZ - I. STEGUN, Dover, 1970).

By successive approximations, values of M_1 for given values of P can be found. Examples are given in the following table :

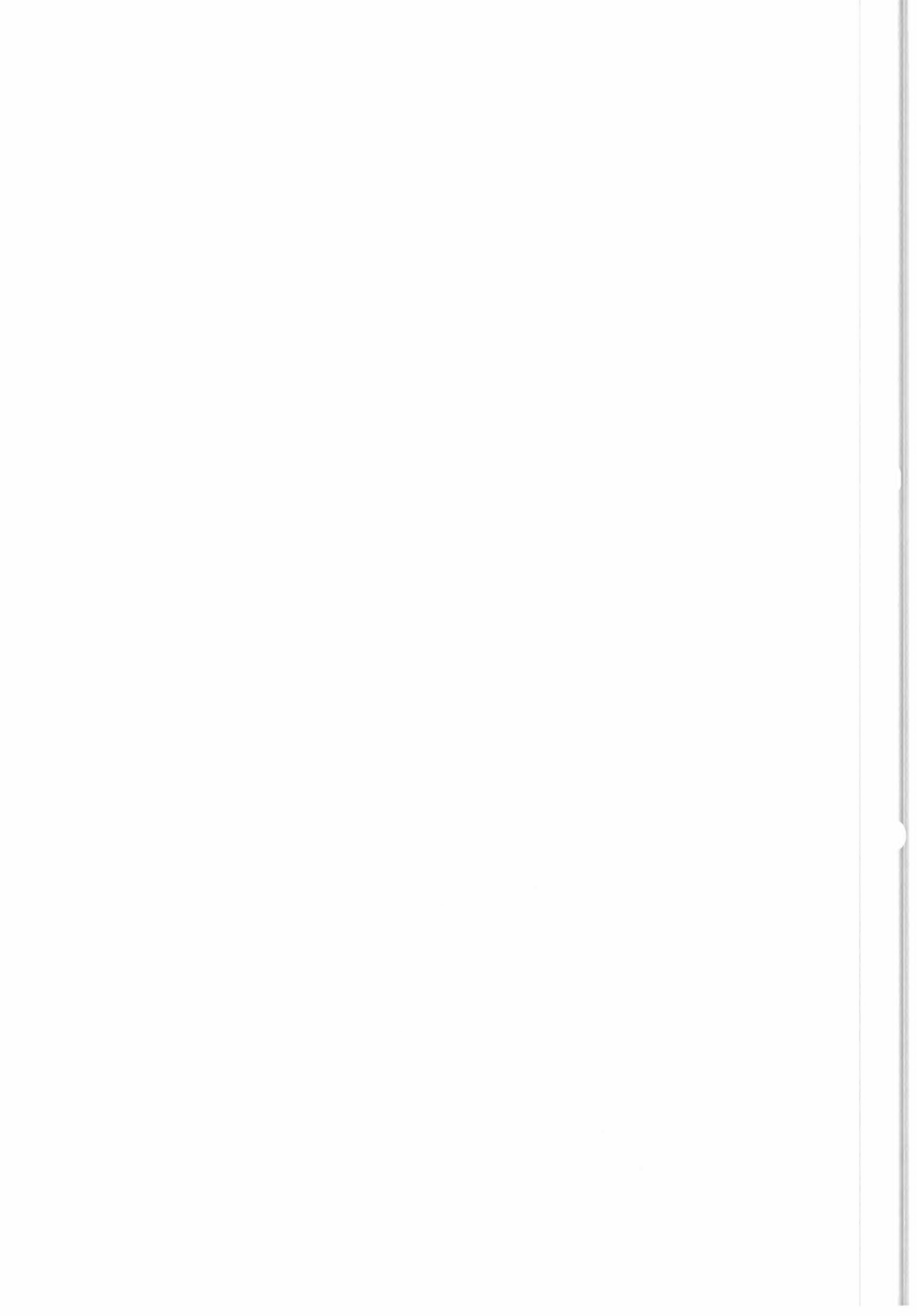
P	0.99	0.999	0.9999
M_1	11.36	16.40	21.16

In wind, we have chosen to signal three-beam measurement points having a probability of only one thousandth of being so far from the theoretical C-band surface ($M_1 = 16.40$) ; but this value, being a parameter, could of course be readily changed if desired by the user.

II.1.B The two-beam case

In the three-beam case, the set of points formed by possible wind speeds and directions forms a surface in the three-space ; therefore, noise will quite generally impose a non-zero maximum likelihood distance between the point of measurement and the model surface.

In the two-beam case, the set of points formed by possible wind speeds and directions forms a surface, continuous subset of the two-space ; therefore measurement points within this subset are at zero distance ($M = 0$) and only measurement points lying outside the subset have a non-zero value of M. Testing M is thus less efficient in the two-beam



than in the three-beam case.

The maximum likelihood distance M is now defined as :

$$M = \sum_{i=1}^2 ((\tilde{\sigma}_i - \sigma_i)/Kp_i\sigma_i)^2 \quad (1)$$

and now the probability density of the point $(\tilde{\sigma}_1, \tilde{\sigma}_2)$ is :

$$p(\tilde{\sigma}_1, \tilde{\sigma}_2) = [\exp(-M/2)] / (2\pi Kp_1 Kp_2 \sigma_1 \sigma_2) \quad (2)$$

Reasoning as in the three-beam case leads immediately to the cumulative probability P, which in the two-beam case is easily expressed in closed form :

$$P(M) = 1 - \exp(-M/2) \quad (3)$$

As in the three-beam case, to each value of P corresponds a value of M1 :

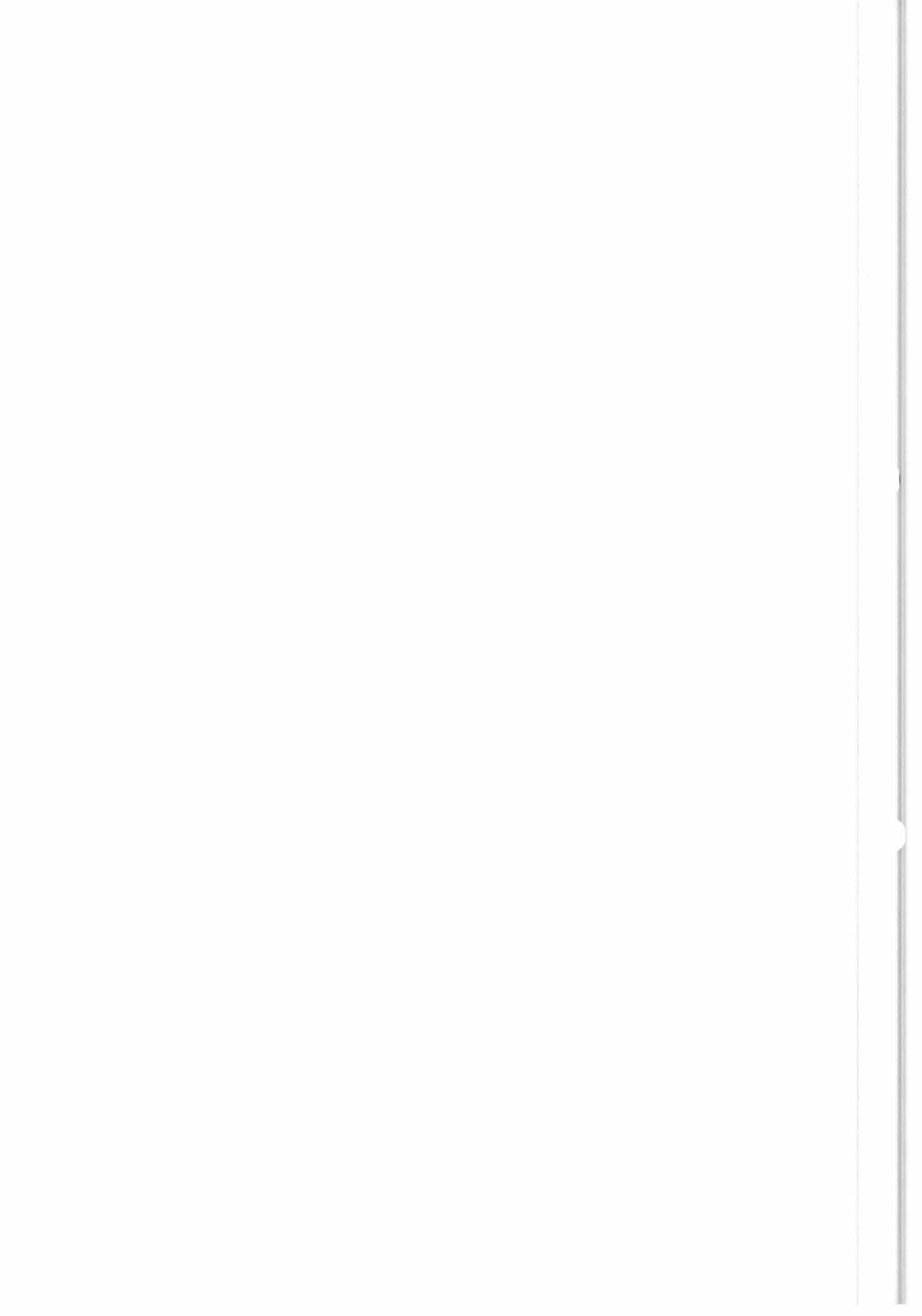
P	0.99	0.999	0.9999
M1	9.21	13.82	18.42

Choosing $P = 0.999$ in WIND has led to define M1 as 13.82. It must be re-emphasized, as previously stated, that the test of M1 is of interest only for points lying outside the subset of points generated by possible wind speeds and directions.

II.2 Discussion concerning the use of M1, upper limit of the M.L.D

The limiting value of M1, both for the two-beam and three-beam cases, has presently been set to correspond to a probability of 0.999. Any point in Sigma0 space at a distance greater than M1 is discarded by WIND for the de-aliasing phase. This should allow the elimination of some points in ice-covered regions and of points highly contaminated by noise, without discarding a significant number of points containing wind information.

It would be interesting to try another strategy : reduce M1 to values corresponding to a probability of 0.99, discard points further out ($M > M1$) temporarily in the first phase of de-aliasing (constructing and choosing between the two wind fields nominally 180° apart) and re-introduce these points in the second phase. The difference over all would of course be slight (1% of points concerned) and would require a good C-band ice model, in order to consider at the same time ice-discrimination. (see paragraph VI).



III - TESTING FOR BLUNDER-POINTS AT THE σ_0 , Kp LEVEL

III.1 Testing the Kp

To each beam measurement is associated a standard error, called Kp in the ESA notation. This value should be of the order of 10%. Much higher values would correspond to unacceptable instrument noise, or perhaps sea-land or sea-ice transitions.

We have not investigated this question in detail, but have set a maximum value of Kp (20%) beyond which the measurement point is rejected from further treatment.

With more precise knowledge of Kp across the swath, of σ_0 over land and over ice, the limits of Kp would be studied further.

III.2 Testing σ_0 values

Testing σ_0 values depends on the C-band model and the range of wind speeds to be considered. Presently, we have set the minimum wind speed, Vmin, to 2 m/s and the maximum wind speed, Vmax, to 60 m/s, in order to comply to the tables in the WIND program. These values extend beyond the 4 to 24 m/s ESA commitment for FDP winds, but we expect that this range could be increased by careful and comprehensive calibration procedures.

III.2.A Testing σ_0 values individually

Each measured σ_0 value is tested to see if it is smaller than 1.1 times the C-band model σ_0 value for that incidence angle, upwind and for a wind of value Vmax. If at least one of the σ_0 values of a cell does not meet this criterion, the point is rejected from further treatment.

III.2.B Testing the sum of forward and rear beam σ_0 values

As discussed in paragraph I.3 the sum of forward and rear beam values should be nearly independent of wind direction, since :

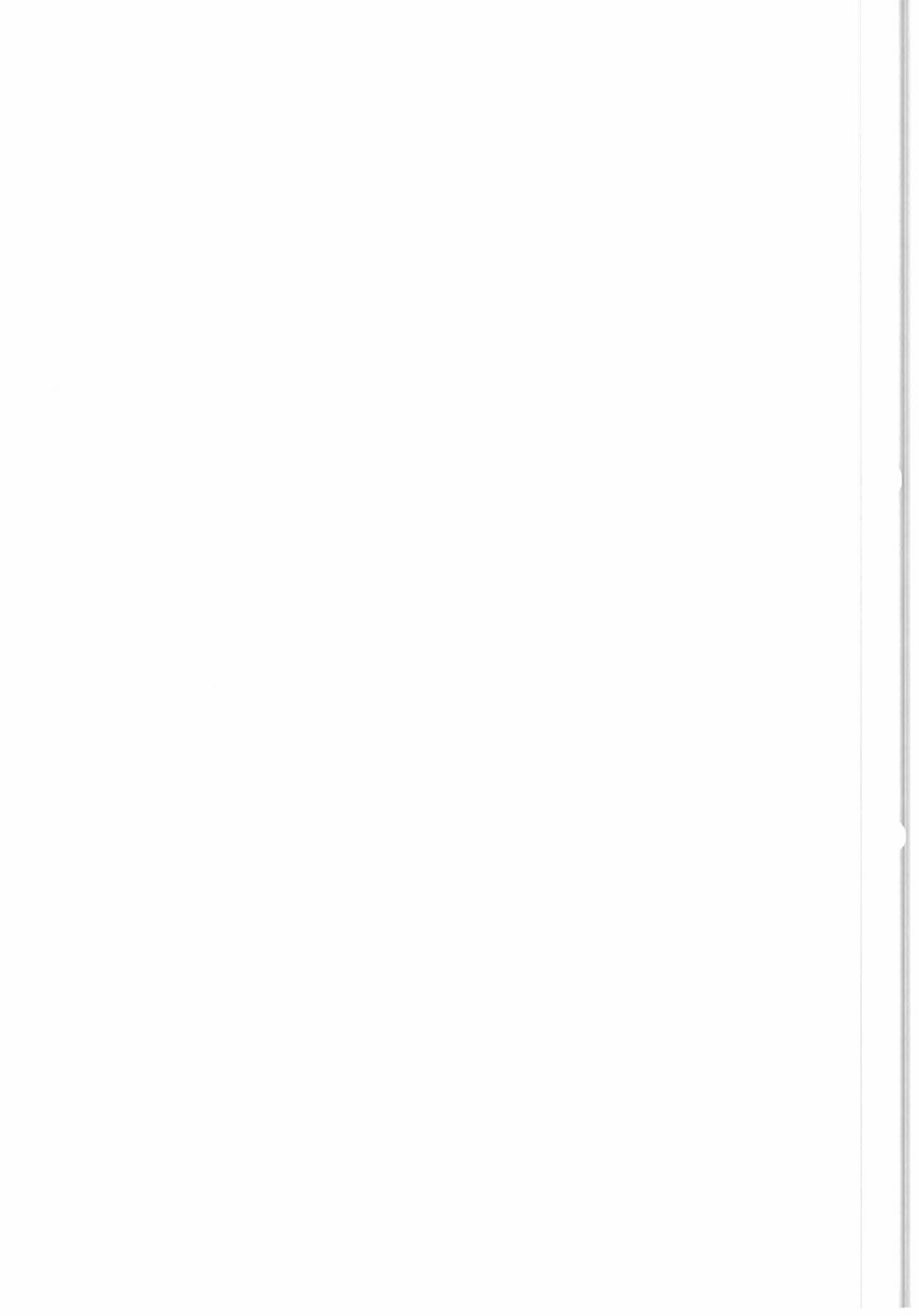
$$\sigma_0F + \sigma_0R = 2.U(1+(b_1F/\sqrt{2})\cos\phi \quad (1)$$

$$\text{and } |b_1F| \ll 1$$

This sum of measured values is tested with respect to 2U of the C-band model at Vmin ; if smaller the cell is rejected as corresponding to too-low winds. The sum is also tested with respect to 2U of the C-band model at Vmax ; if greater, the cell is rejected as corresponding to too-high winds.

III.3 Possible further tests of σ_0

There is certainly a need to further test σ_0 measurements in order to screen out ice zones, which would require considering 19 point lines as a whole. But present testing, over ocean areas, has proved sufficient. It is probable that changes in the model would not essentially modify these conclusions, as long as σ_0 remains a monotonic function of wind speed.



IV - PASSING FROM σ_0 TO POSSIBLE WIND ESTIMATES (INVERSION)

IV.1 General principles of the inversion

The detailed procedure as implemented in the WIND routine, is described in the Annexed WINRET report and will not be recopied here. Rather, the general concepts and reasons for the choices made will be insisted upon.

As already mentioned, inversion consists in finding those points in the set of C-band model compatible points which represent local minima of a "distance", M , with respect to wind speed, V , and wind direction, ϕ . All such local minima must be found which implies that the domain of V and ϕ must be thoroughly and methodically explored.

The choice has been to sweep the surfaces of Fig.2 or Fig.3 on curves of constant wind direction ϕ , and find the minima of the maximum likelihood distance, previously described, M , on each of these curves. In view of the complexity of the present C-band model, we have not been able to prove that the minimum with respect to V on each of these constant ϕ curves is unique. But the good results of many tests on simulated data indicate this to be the case. (A C-band model with much greater curvature of constant ϕ curves might not satisfy this criterion).

The minima of M are found on 72 constant ϕ curves, separated by 5° . On each constant ϕ curve, the search for minimum is abandoned when the first minimum is found. In case of multiple minima, this might mean not observing the correct minimum, but insures robustness of the algorithm. The 5° increment is well within the ESA 20° specification for FDP products wind directions, which of course is a global precision estimate taking into account all factors ; we stress here only that the numerical noise created by 5° sampling will be small with respect to this specification.

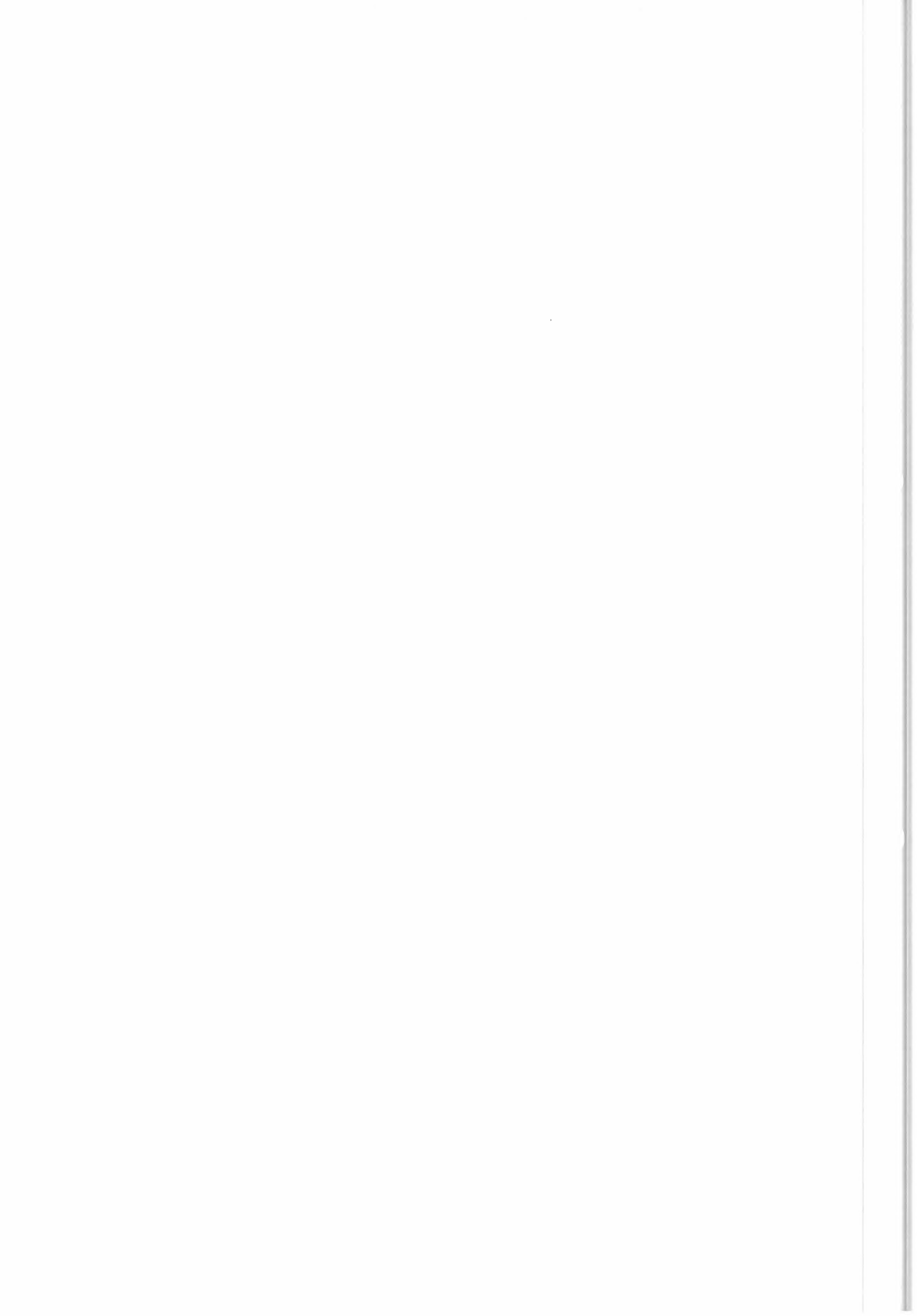
The 72 minima, in V , are now intercompared to find their minima in ϕ . This experimentally leads to up to 6 minima which are classed according to increasing distance, M ; rank 1 solutions are therefore closest to the surface.

If the value of M for the rank 1 solution is greater than that corresponding to a probability level of 0.999, the cell is discarded for further analysis. Otherwise, the set of possible solutions is retained for the de-aliasing phase. This should screen out some noisy data as well as a part of ice-covered regions as described later.

IV.2 Particular features of the three-beam procedure

Three-beam zones will form the major part of scatterometer data over the oceans. Moreover, the winds deduced should be more accurate, and exact automatic analysis will generally be achievable for these zones.

The procedure used in their inversion is a simple gradient search on each constant ϕ curve. Starting from an initial value of V , the value of M is computed for a wind speed increased by 0.5 m/s and the search continued in that direction if the new value of M is less than the previous one (otherwise the search direction is reversed). Once a minimum is found, the search is abandoned, and processing of the next constant ϕ curve is begun.



The search on each constant ϕ curve is of course accelerated by a good first estimate of the wind speed. This is obtained by evaluating the wind speed which satisfies the condition :

$$\sigma_F + \sigma_R = 2AV^Y (1 + b_1 F/\sqrt{2})$$

where $b_1 F$ is computed (rather arbitrarily) at 8 m/s. As previously discussed, the sum of forward and rear beam measured σ_0 is nearly azimuth independent, and thus a good approximation is obtained. This approach should not fail, whatever the evolution of the C-band model, as long as $|b_1/\sqrt{2}|$ remains much smaller than 1.

The simple gradient method was chosen because it allows tabulation of the C-band model σ_0 values which otherwise take very much computing time. The table of σ_0 gives values every 1° in incidence, 0.5 m/s in speed and 5° in direction. Its range is 15° to 69° in incidence, 1 to 60 m/s in wind speed and 0° to 180° only in direction, because of symmetry :

$$\sigma_0(\phi) = \sigma_0(-\phi)$$

The tabulation allows roughly a gain of ten in computing time. Should, later on, a much simplified expression for the C-band model be found, this factor would of course be reduced.

IV.3 Particular features of the two-beam procedure

Tests with the gradient method in two-beam cases rapidly indicated that the numerical precision offered was not sufficient to cope with them ; more than four minima were often observed which was not logical in view of the geometry of the problem. It was therefore decided to use a Newton-Raphson algorithm, much more precise ($+ 10$ cm/s, $+ 1^\circ$), which had been developed previously, and abandoned for FDP products, as too slow.

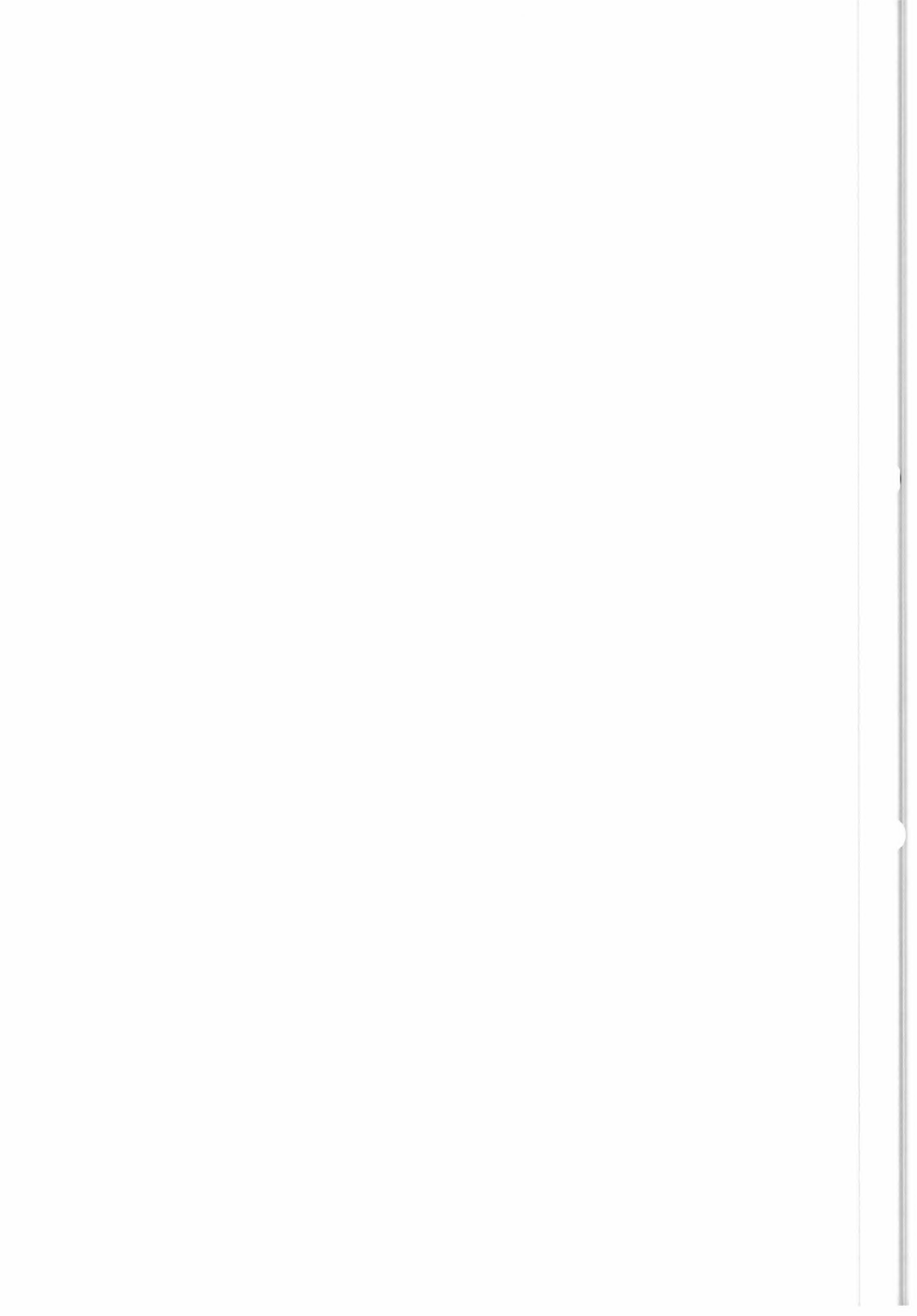
The search for the minimum on each constant ϕ curve is now done using a Newton Raphson technique, in which first and second derivatives are evaluated by finite differences. Thus the following step length V can be evaluated as :

$$-(dM/dV)/(d^2M/dV^2) \quad (1)$$

Since step size in V is no larger constant, σ_0 tables cannot be used, and only tables of cosine help to speed up the routine.

Once minima in V and ϕ with a five degree precision in ϕ are found, the search is taken up again on curves separated by 1° , around the minima ($\phi_{\min} - 4$ to $\phi_{\min} + 4$) ; this allows a precision in direction of at least 1° . Although this technique has the drawback of being about ten times slower than the gradient search with tables, it has allowed the two-beam data to be processed correctly, and has therefore been retained in the WIND procedure.

A first guess wind field is estimated, exactly as in the three-beam case, if forward and rear beams are available. But, in general, one of these beams is absent, and the first guess wind field is set to 5 m/s, which is somewhat below the SEASAT scatterometer world-ocean mean wind, approximately 7.5 m/s. This value could be optimized once ERS-1 in flight, and the final C-band model determined.



IV.4 Testing the inversion module with simulated data

Performance tests of Winret were run on five test-data files furnished by David OFFILER (U.K Met. Office), labeled WINTST01:DATA to WINTST05/DATA. These files were generated from meteorological wind fields in the North Atlantic, Sigma0 values being perturbed by Gaussian noise of zero mean and nominally 10% standard error (precisely 9.7 % on forward and rear beams, 8.5 % on the central beam data). (annexe 2).

Not only were the data files used as such, but the same tests were run again imposing the routine to run in the two antenna mode for all five files. Then a multiplicative bias (0.9 or 1.1, successively) was imposed on the central beam or on both forward and rear beams, once again for all five data sets. It is this complete set of tests which the present paragraph describes and analyses. All tests were run on a N.D. 570 (nominally 3 Mips).

IV.4.A Two and three beam tests without bias

Table IV.1 gives for each of the test data files the bias (in m/s or degrees), the standard deviation (SDD) and maximum error (Max) as well as the number of points ranked (from 0 to 6), the average computing time per point and the number of points not treated (rank 0) because of land flag, or too low wind speed.

In the same manner, table IV.2 gives the results in the case where data from the forward beam is suppressed. It is clear from these individual results that behaviour does not notably vary from one data set to another and that the two-beam algorithm is roughly five times slower (0.12s) than the three-beam algorithm (0.025s). It is also very positive to notice that the two-beam results generally fall within ESA specifications of + 2 m/s and 20° in direction.

IV.4.B Synthesis of results including multiplicative bias

Tables IV.3 and IV.4 furnish a global view of the results of tests over all five test data sets, with or without multiplicative bias ; the letters F, C, R are symbols for forward, central and rear beams respectively.

As expected, multiplicative bias creates significant bias on the wind speed and direction. If the wind speed standard deviation is not notably increased by bias in the three antenna case, it is significantly augmented in the two antenna case. All in all, the levels of bias imposed seem to remain tolerable, for the present C-band model and algorithm.

Ranking of solutions is very important in order to de-alias the scatterometer winds. Table IV.4 shows that overall ranking skill is very good, first ranked solutions being the closest to the correct wind about 70% of the time, in the three-beam case ; even 10 % bias does not affect this skill too much. It is to be noted that solutions ranked 5 or 6 are practically never correct, which implies that they could be discarded immediately.

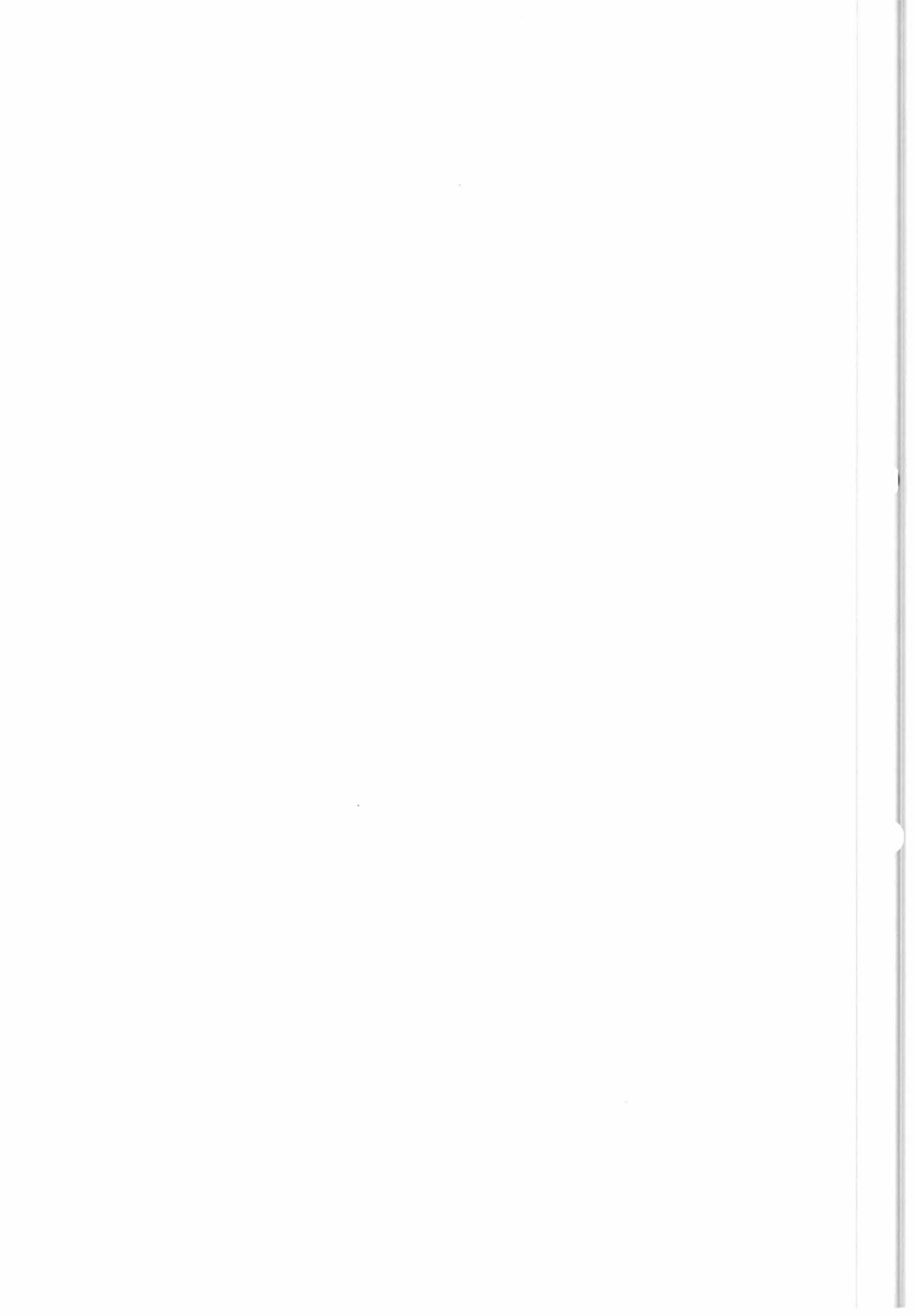


TABLE IV.1 (3 antenna, no bias)

		Bias	SDD	Max	Rank	Number
WINTST01	Speed	0.03	1.36	6.50	1	1548
	Dir	-0.1	5.7	38.3	2	408
					3	16
					4	4
	Time : 0.0268 s				5	0
					6	0
					0	24
WINTST02	Speed	.04	0.96	4.10	1	1443
	Dir	0.1	5.3	28.5	2	538
					3	16
					4	3
	Time : 0.023 s				5	0
					6	0
					0	0
WINTST03	Speed	-.01	.99	4.8	1	1421
	Dir	0.0	5.4	36.9	2	553
					3	1
					4	0
	Time : 0.025 s				5	0
					6	0
					0	10
WINTST04	Speed	.01	.45	2.3	1	1346
	Dir	.0	7.2	35.0	2	525
					3	41
					4	0
	Time : 0.0186 s				5	0
					6	0
					0	88
WINTST05	Speed	.01	.71	3.0	1	903
	Dir	-.2	6.7	26.2	2	503
					3	20
					4	1
	Time : 0.021 s				5	0
					6	0
					0	110 (108 land)

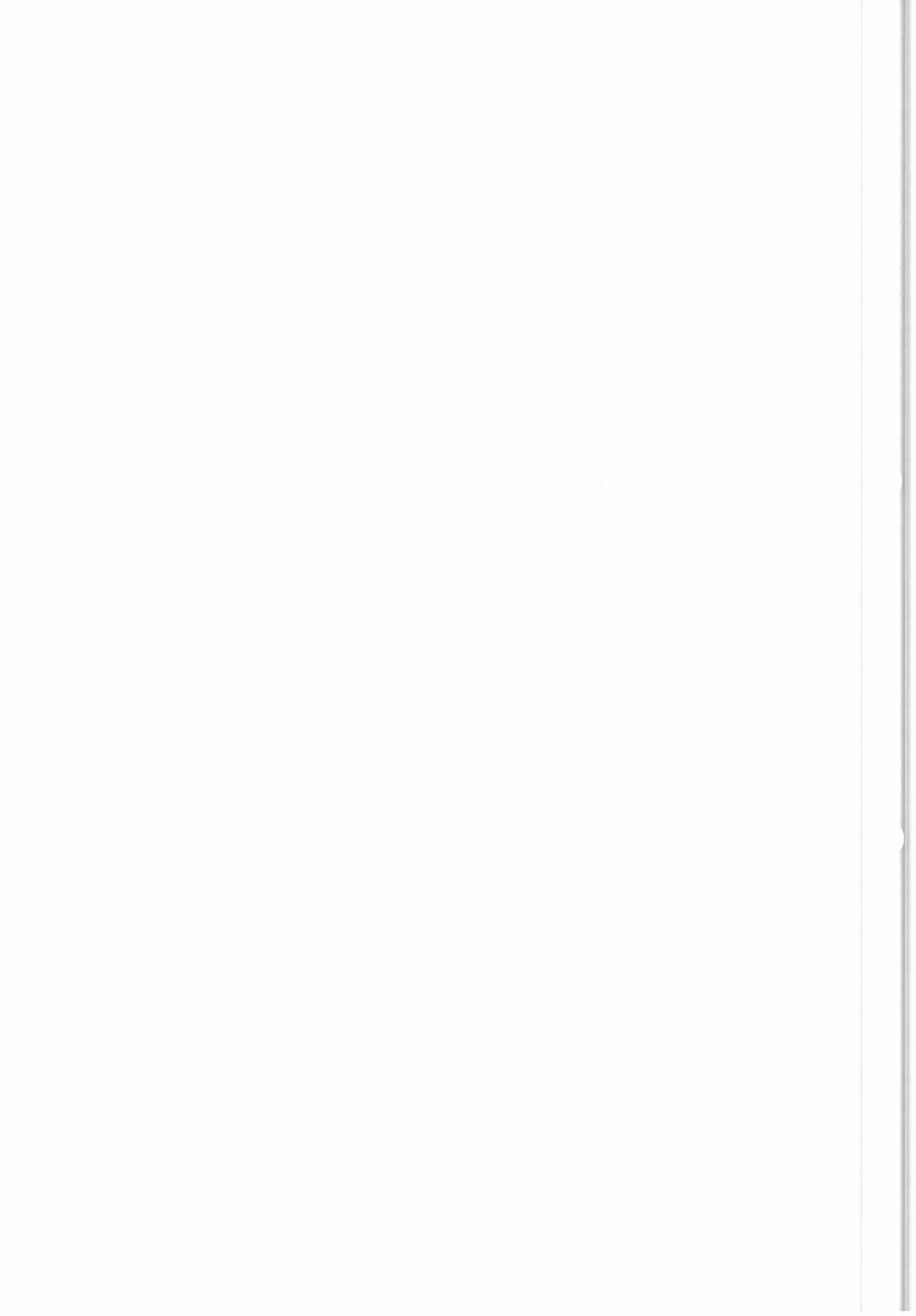


TABLE IV.2 (beams, forward suppressed, no bias)

		Bias	SDD	Max	Rank	Number
WINTST01	Speed	.03	2.2	10.64	1	586
	Dir	-.2	7.7	43.3	2	457
					3	478
					4	471
	Time : 0.122 s				0	8
WINTST02	Speed	.06	1.63	7.2	1	563
	Dir	-.1	8.2	38.3	2	630
					3	459
					4	348
	Time : 0.122 s				0	0
WINTST03	Speed	.03	1.98	13.98	1	603
	Dir	-.1	8.3	33.1	2	578
					3	491
					4	321
	Time : 0.121 s				0	7
WINTST04	Speed	-0.02	.74	5.62	1	543
	Dir	0.1	9.2	34.4	2	543
					3	388
					4	481
	Time : 0.124 s				0	45
WINTST05	Speed	0.09	1.39	7.42	1	555
	Dir	-0.3	9.6	30.5	2	478
					3	236
					4	158
	Time : 0.111 s				0	110 (108 land)

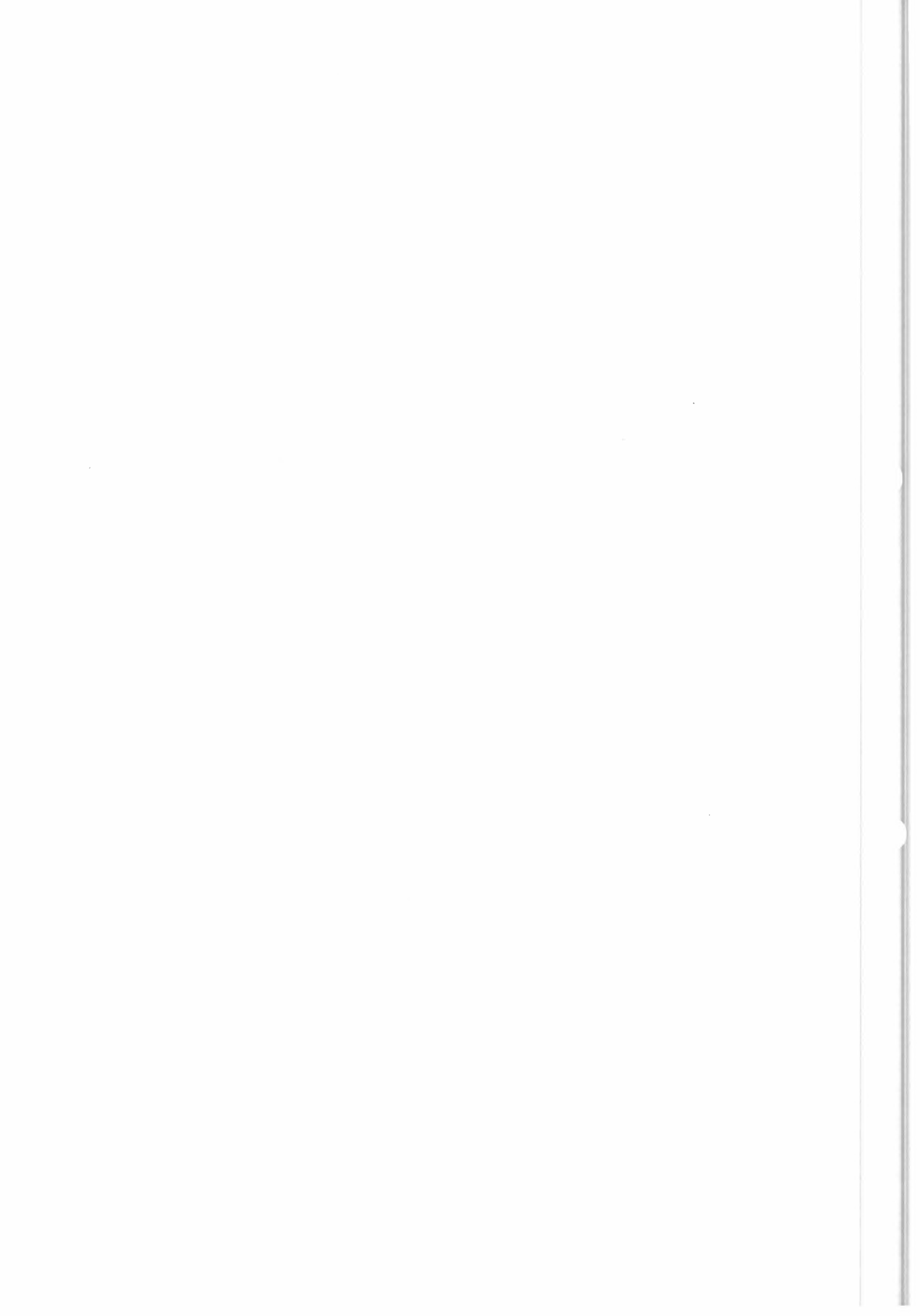


TABLE IV.3

(F.C.R) BEAMS N= 9427 VMIN = 2 M/S;

	WINDSPEED			DIRECTION		
	BIAS	SDD	MAX	BIAS	SDD	MAX
NO BIAS	.016	.959	12.3	-.03	6.1	52.2
(0.9)*C	-.28	.98	7.2	-1.9	7.1	45.6
(1.1)*C	.36	1.04	8.0	1.6	4.3	49.3
(0.9)*(F.R)	-.98	1.04	8.9	1.4	6.5	46.3
(1.1)*(F.R)	1.04	1.17	10.5	-1.4	6.7	38.9

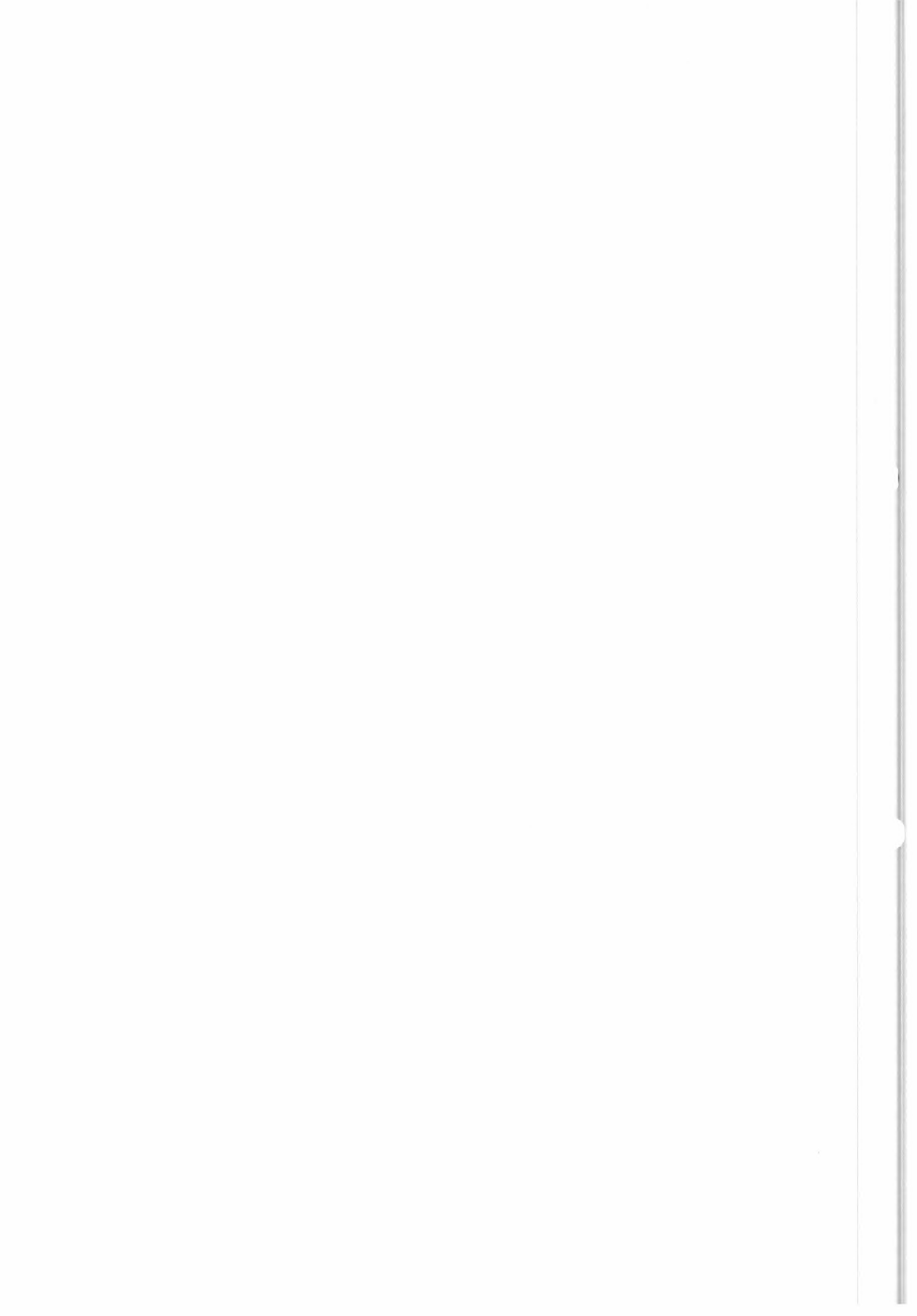
Time : 0.023 s/cell

TABLE IV.4

(-,C,R) BEAMS N= 9427 V = 2 M/S;

	WINDSPEED			DIRECTION		
	BIAS	SDD	MAX	BIAS	SDD	MAX
NO BIAS	.09	1.39	7.4	-.3	9.6	30.5
(0.9)*C	-.94	1.75	11.6	-.05	9.5	53.3
(1.1)*C	1.10	2.10	16.8	-.3	9.4	43.1
(0.9)*(F.R)	-.39	1.83	14.4	.92	9.5	43.1
(1.1)*(F.R)	.50	1.86	12.2	.04	10.2	53.3

Time : 0.12 s/cell



IV.5 Proposition for further testing

Results presented are very satisfactory but depend very much on the C-band model used. This is particularly true of the percentage of rank 1 solutions which are best fit to the underlying meteorological wind direction. It is clear that such tests must be re-run if the model is changed.

Moreover, very simplified (Gaussian noise, constant standard deviation) simulation data has been used. If, later, ESA can give a detailed behaviour of the standard deviation's evolution crosstrack, as well as realistic beam bias evolutions (aging, temperature effects, ...) these problems should be taken up a new. But we suggest that this be done after a new version of the C-band model is written, taking into account high wind speed data of the Mediterranean campaign, and perhaps data from further campaigns.

V - INFLUENCE OF A RAPID EVOLUTION IN SPACE OF WIND SPEED OR WIND DIRECTION ON WIND RETRIEVAL

V.1 A basic hypothesis in the interpretation of measured σ to evaluate winds

A fundamental hypothesis made in going from σ to possible winds is that the wind field is sufficiently regular (slowly varying in speed and direction) that the mean of σ over the area covered, $\bar{\sigma}(v)$, is close to the value of σ which would be obtained for the mean wind ; $\sigma(\bar{v})$.

If our present knowledge concerning extreme wind variations in space is sufficient, and, in fact, this is one of the research tasks assigned to the scatterometer, at least we can make preliminary investigations of the behaviour of the scatterometer using simplified models of wind speed or wind direction evolution in space.

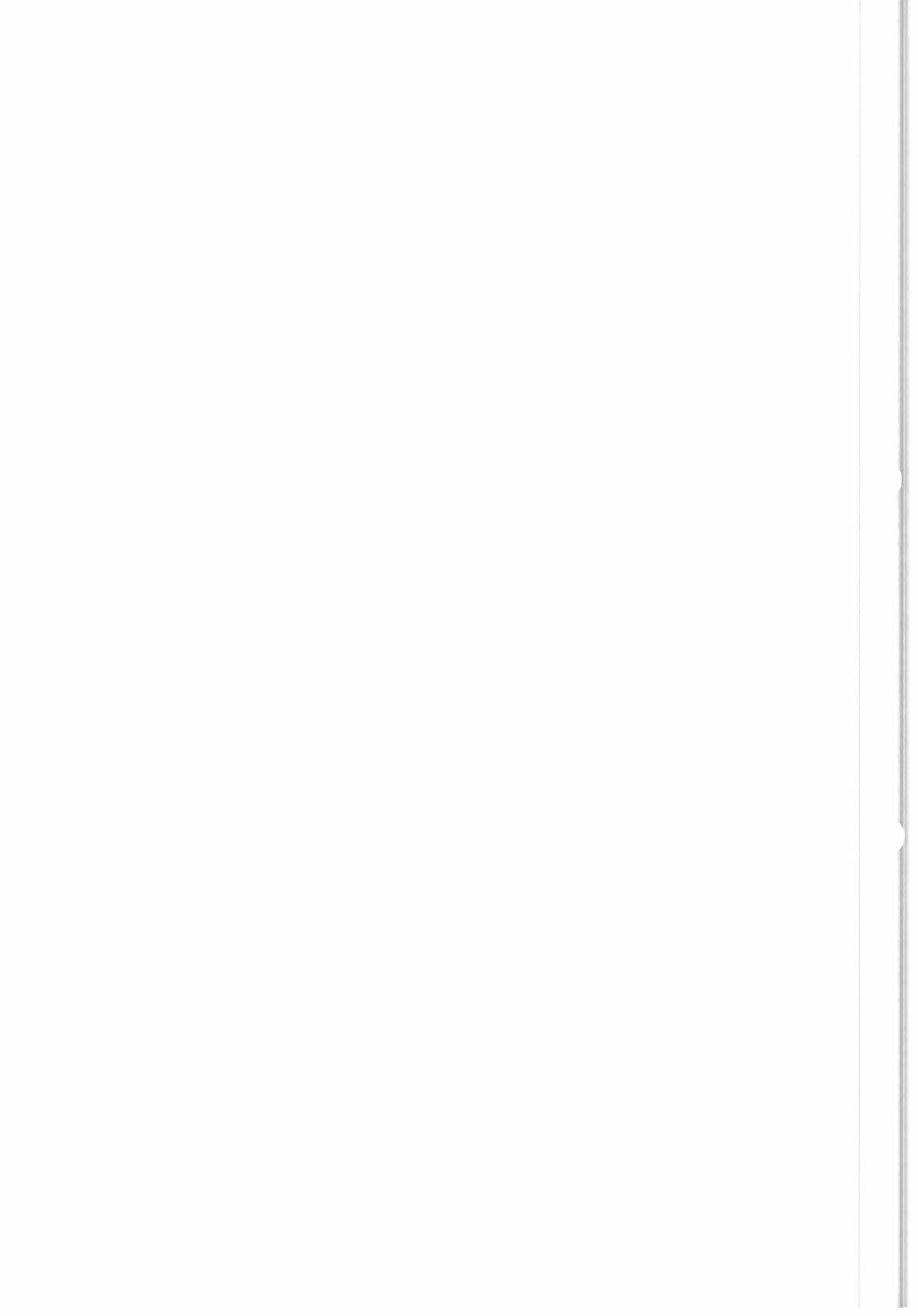
The tentative conclusion to be drawn from the simplified approach presented in detail in the following paragraphs, is that wind speed variations in space should not lead to important differences between $\bar{\sigma}(v)$ and $\sigma(\bar{v})$. However, jumps in wind direction, if they occur over a narrow transition zone, and are 60° or more, may cause the different wind directions of the possible solutions after inversion, to be quite far from the mean direction of the actual wind field. This is a potential source of error, whose importance will have to be evaluated in more detail.

V.2 Estimation of the influence of a constant wind shear

Let us assume that the wind direction remains constant and that a linear wind speed variation occurs in the scatterometer footprint ; to simplify matters, the footprint is supposed rectangular, one side parallel to the wind. Further, we neglect the variations in the Fourier coefficients in the truncated Fourier series with respect to wind direction ; this appears reasonable as their evolution with wind speed is slow.

Then, over the normalized distance, x :

$$v = \bar{v} (1 + ax) \text{ for } -0.5 \leq X \leq 0.5 \quad (1)$$



The parameter "a", of course, describes the wind rate of change with distance. The mean value of σ over the footprint is :

$$\begin{aligned}\bar{\sigma}(v) &= \bar{v}^{\gamma} * \int (1 + a * X)^{\gamma} * dX \\ &= [\bar{v} / (a * (\gamma + 1))] [1 + 0.5 * a]^{\gamma + 1} - (1 - 0.5 * a)^{\gamma + 1} \quad (2)\end{aligned}$$

$$= \sigma(\bar{v}) * R \quad (3)$$

Here, the function R expresses the ratio of $\bar{\sigma}(v)$ to $\sigma(\bar{v})$, the value of σ for the mean wind over the footprint.

The value of R for the extreme values of γ expected are given in the following :

	a →	0.1	0.6	1.0	2.
For $\gamma = 0.8$,	R →	.9999	.9976	.9931	.9673
For $\gamma = 1.4$,	R →	1.002	1.008	1.024	1.0996

Thus it appears that a wind shear that triples the wind speed from one side to the other of the scatterometer footprint creates only a 2.4 % difference between $\bar{\sigma}(v)$ and $\sigma(\bar{v})$. This is tolerable in view of the noise level which is of the order of 10%. It is only when the ratio of the minimum wind to the maximum wind in the footprint tends toward zero ($a = 2$) that the difference between $\bar{\sigma}(v)$ and $\sigma(\bar{v})$ approaches 10%, and that, only for the highest value of γ . Figure V.1 once again represents R, but as a function of "r", the ratio of the minimum wind to the maximum wind in the footprint. It appears there, perhaps more evidently that R is within a few percent of 1, except for very small values of the V_{min}/V_{max} ratio.

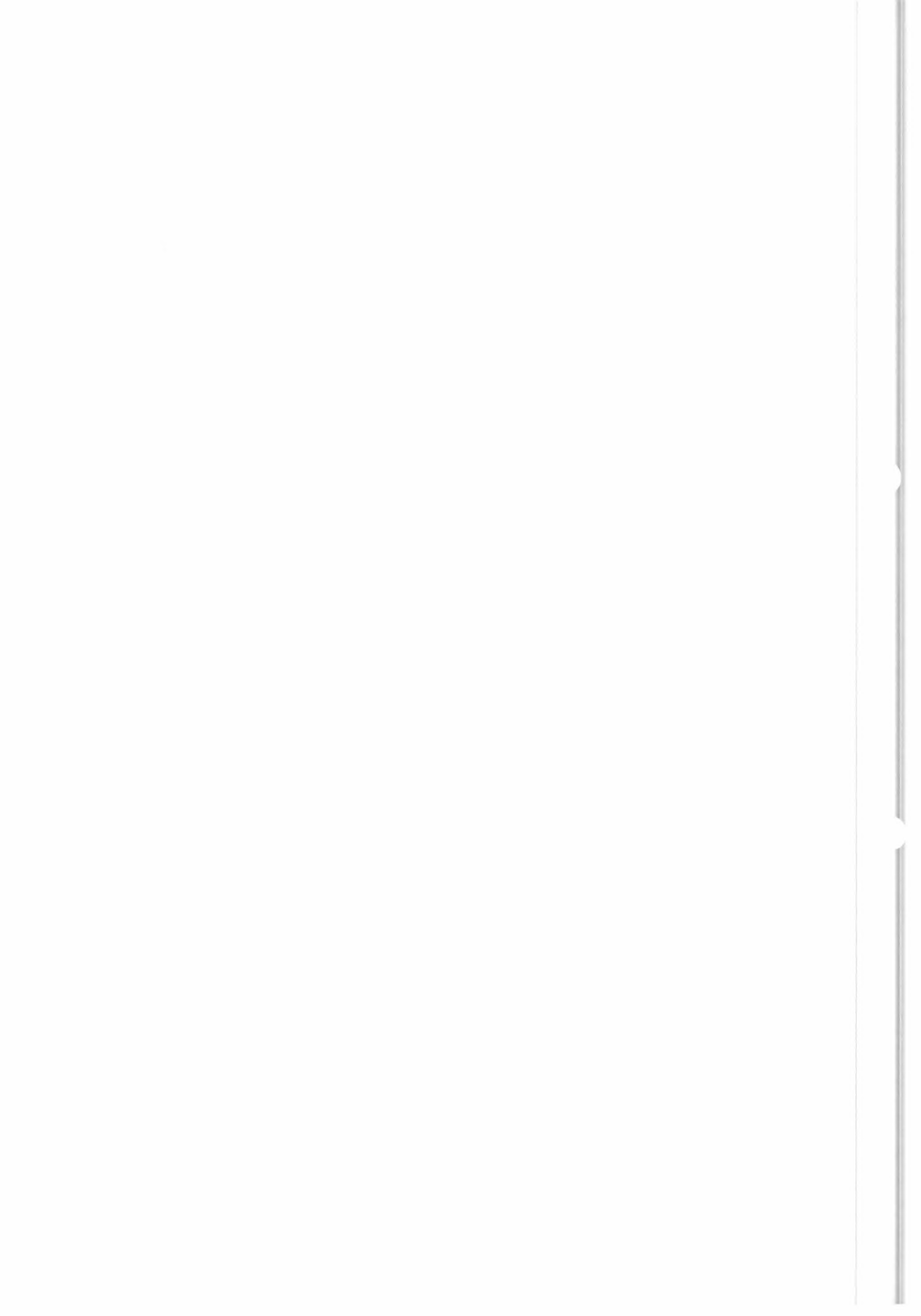
V.3 Estimation of the influence of a wind speed jump

The previous paragraph showed that a linear wind speed gradient would create a significant difference between the measured σ , $\bar{\sigma}(v)$, and that of the mean wind $\sigma(\bar{v})$ only in the case of small V_{min}/V_{max} ratio. Here will be considered a wind speed jump across a straight-line boundary, wind directions being conserved across the boundary, winds being constant in speed and direction on each side of the boundary.

The mean wind over the scatterometer footprint is thus :

$$\bar{v} = s(v_1) + (1 - s) v_2 \quad (1)$$

where v_1 and v_2 are the wind speeds on each side of the jump s and $(1 - s)$ the normalized equivalent surfaces attributed to side 1 and side 2 respectively ($0 \leq s \leq 1$).



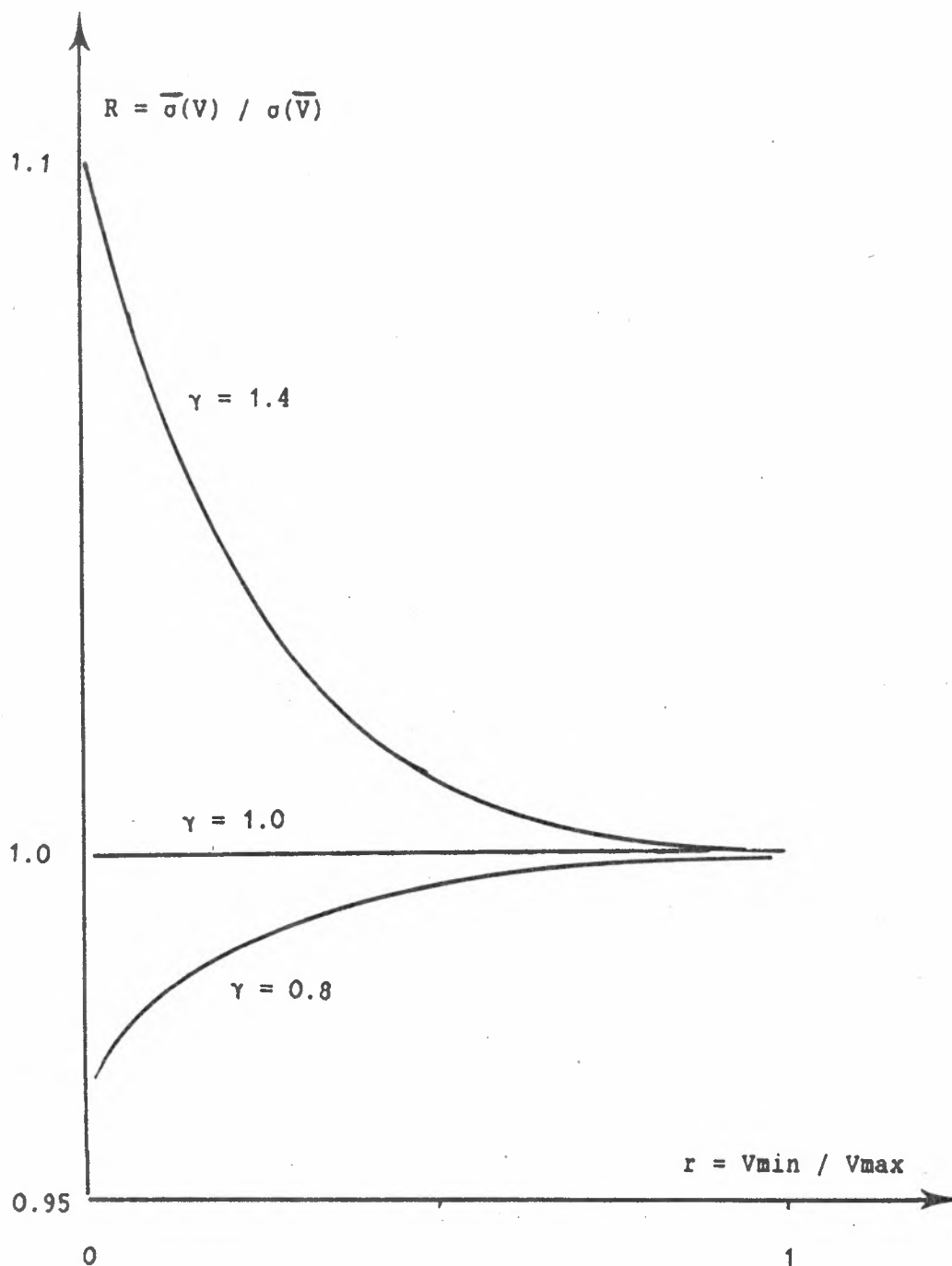
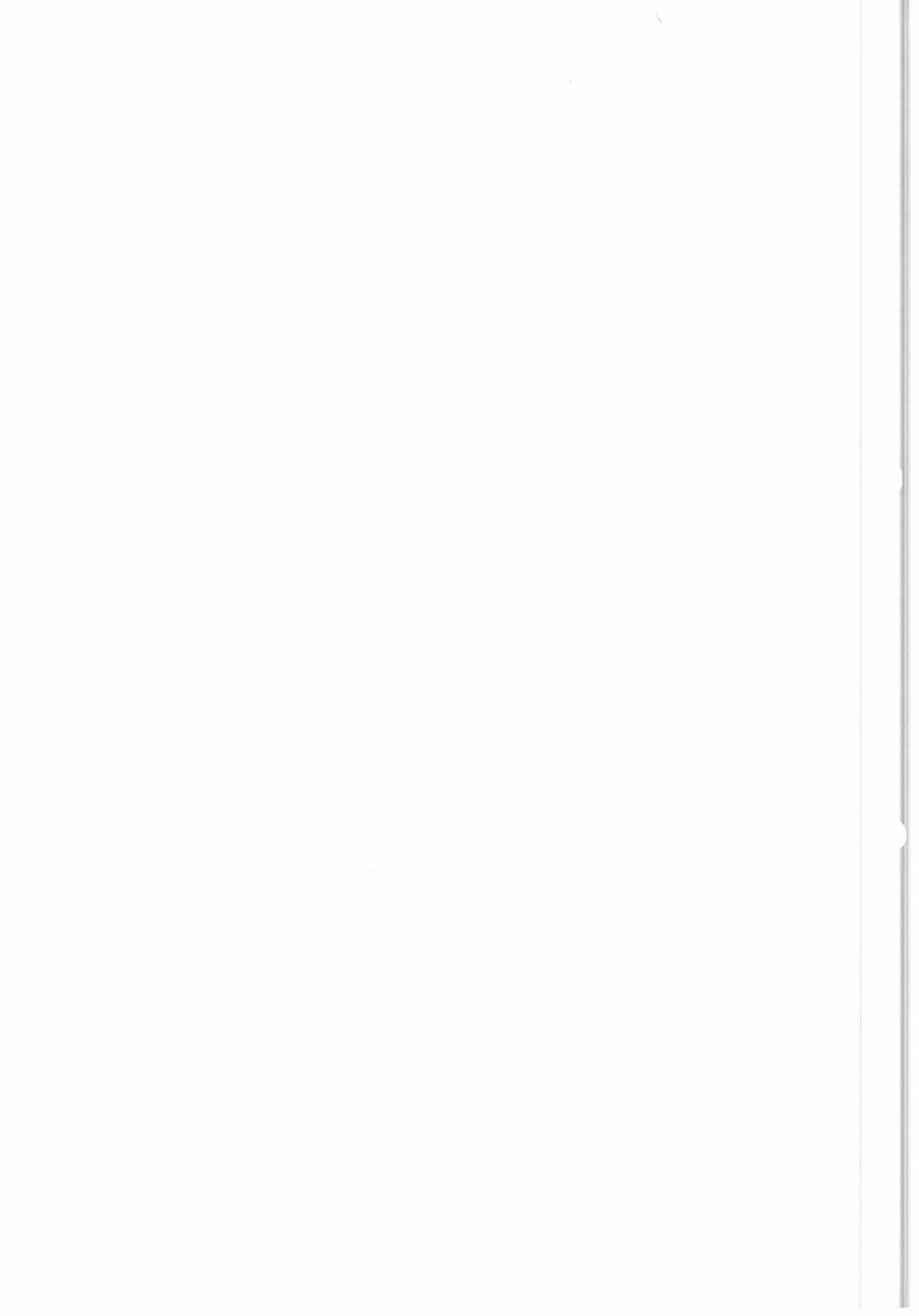


Fig. V.1 $R(r)$ for a linear wind speed gradient



Then making the same simplifications as in the previous paragraph :

$$\bar{\sigma}(v) = s v_1^\gamma + (1 - s) v_2^\gamma = v_1^\gamma (s + r(1 - s)) \quad (2)$$

$$\sigma(\bar{v}) = \bar{v}^\gamma = v_1^\gamma (s + r(1 - s)) \quad (3)$$

where $r = v_2/v_1$

The parameter r may be constrained to lie in the domain :

$$0 < r < 1$$

by simply imposing that side 1 have the greater wind speed. Figure V.2 gives R , ratio of $\bar{\sigma}(v)$ to $\sigma(\bar{v})$, as a function of r , the ratio of lesser to greater wind speed. As in the case of a linear wind speed gradient, R deviates most from a desired value of 1, for small values of r . Curves above $R = 1$ correspond to $\gamma = 1.4$, curves below, to $\gamma = 0.8$. Note that variations in R are one order of magnitude greater than for the constant shear case.

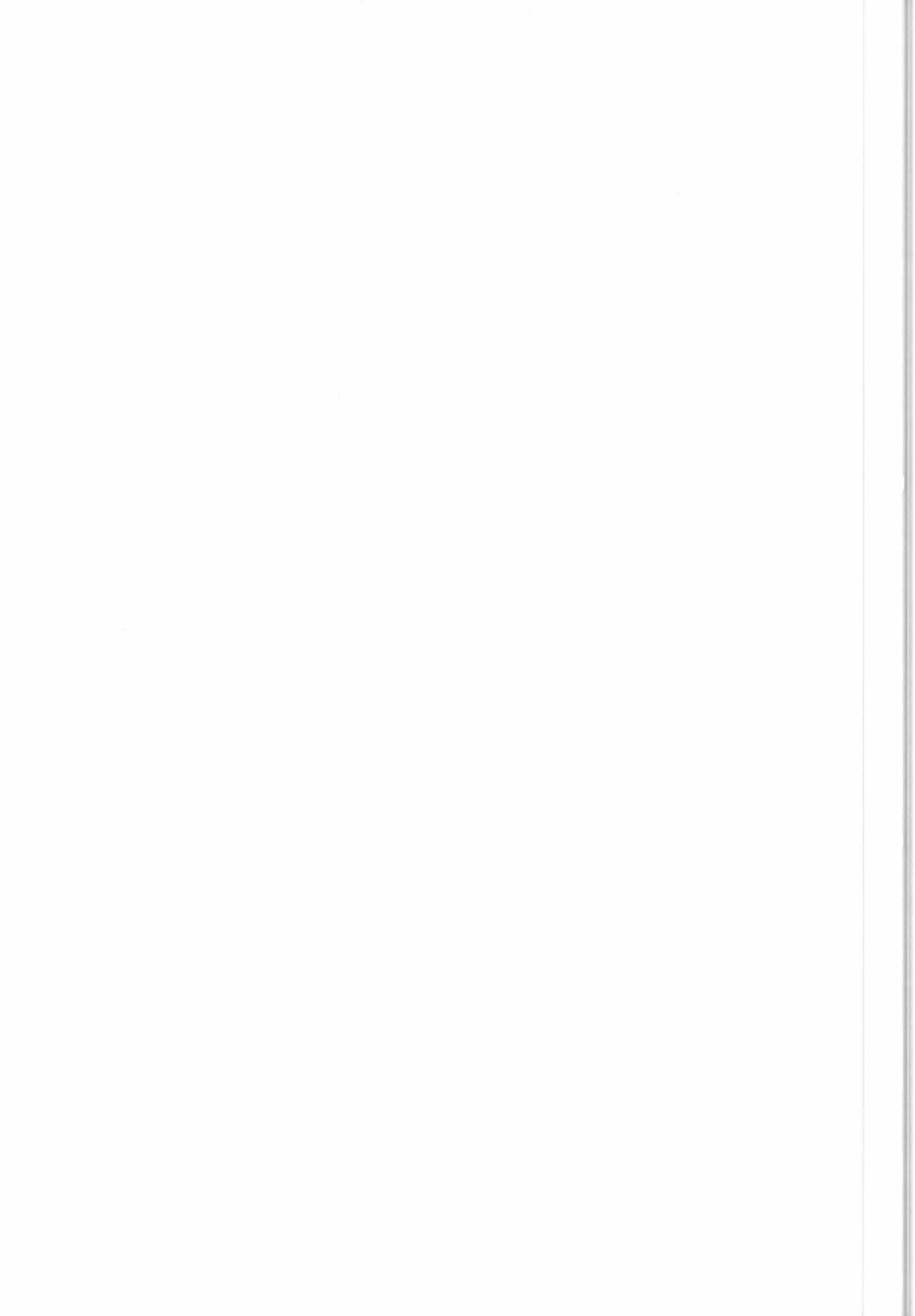
V.4 Estimation of the influence of a wind direction jump

V.4.A Presentation of the problem

Through a front and more typically through a cold front, important variations in wind direction are often observed. As an example, Figure V.3 (furnished by P. QUEFFEULOU, TOSCANE Group, IFREMER) shows continuous recordings of wind speed and direction during the Promess campaign, taken at 10 m height on the west coast of Brittany. Here a direction jump of 70° occurs in about ten minutes ; the width of the front will of course depend on the instantaneous value of its propagation speed. Taking the value given by the weather chart (55 km/h) gives a width of roughly 9 kms. This value is small with respect to the footprint characteristic length (~ 50 kms), and leads to think that modeling a front as a direction-jump across a straight-line segment is a reasonable first approximation.

Because the curvature of the surface of solutions in the $(\sigma_1, \sigma_2, \sigma_3)$ three-space is important on constant wind speed curves, which form characteristic "double loop" figures (see paragraph I.3) an approximate analytic approach as in the previous paragraphs is not possible. It must be remembered that points nominally 90° apart in direction lie roughly on opposite sides of the double loop, while points 180° apart lie rather close together on two different loop segments. Thus taking the weighted mean of positions of points lying close to 90° apart, and using such a mean position in the inversion algorithms, can appear a priori dangerous on the basis of geometrical intuition ; depending on the importance of the direction jump, and the percentage of the surface on each side of the front, quite different results of the inversion are to be expected.

To simplify notations, units of length will be 25 km, the distance between two points on the scatterometer grid. The front, represented as a straight-line direction jump, is assumed at a distance "ro" from the point of the grid studied ; in fact, depending on the weighting function all points on the grid may be more or less affected by the front, so it is really the normalized equivalent surfaces (function of the weighting function) which are important. Their values are G_1 and, of course,



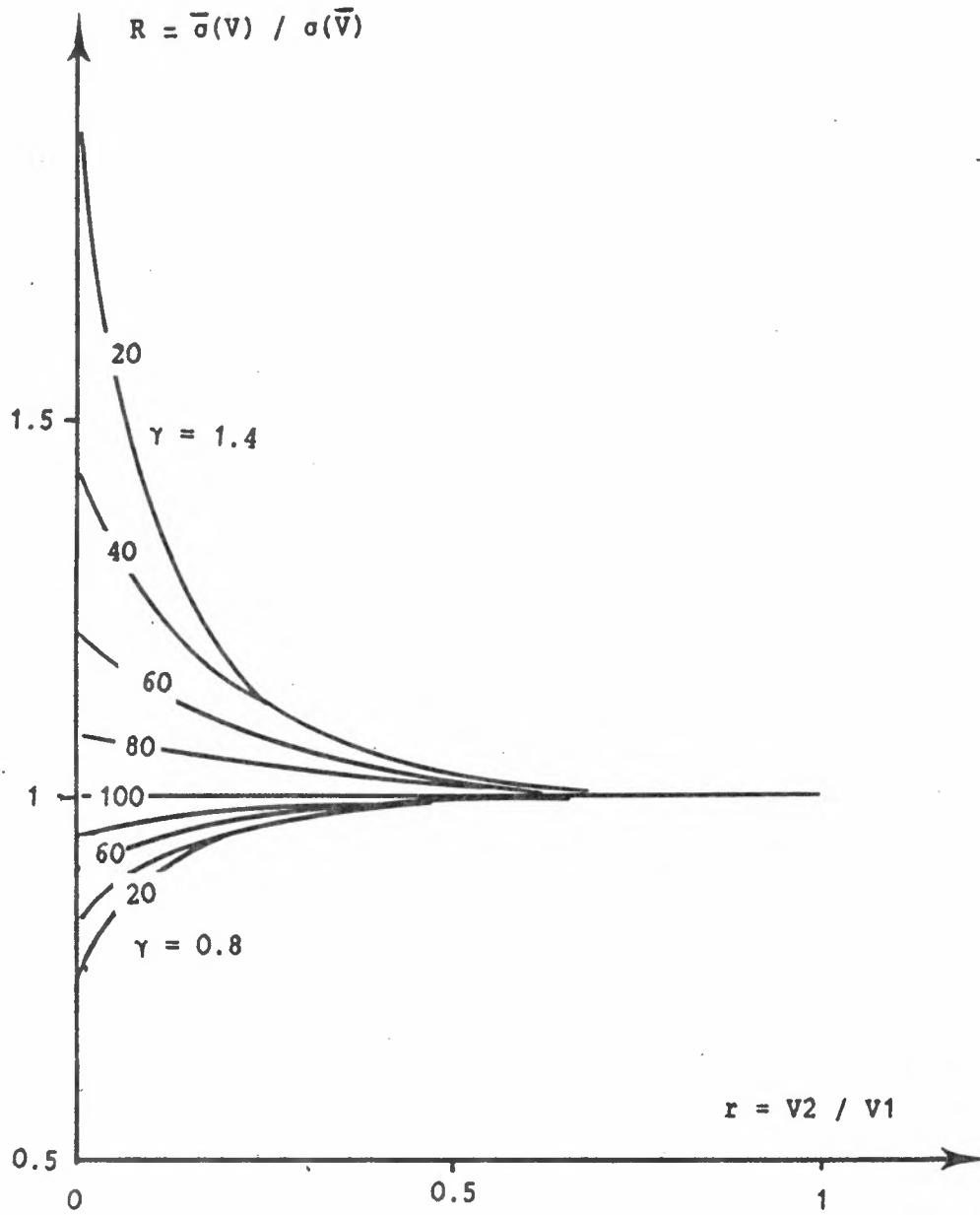
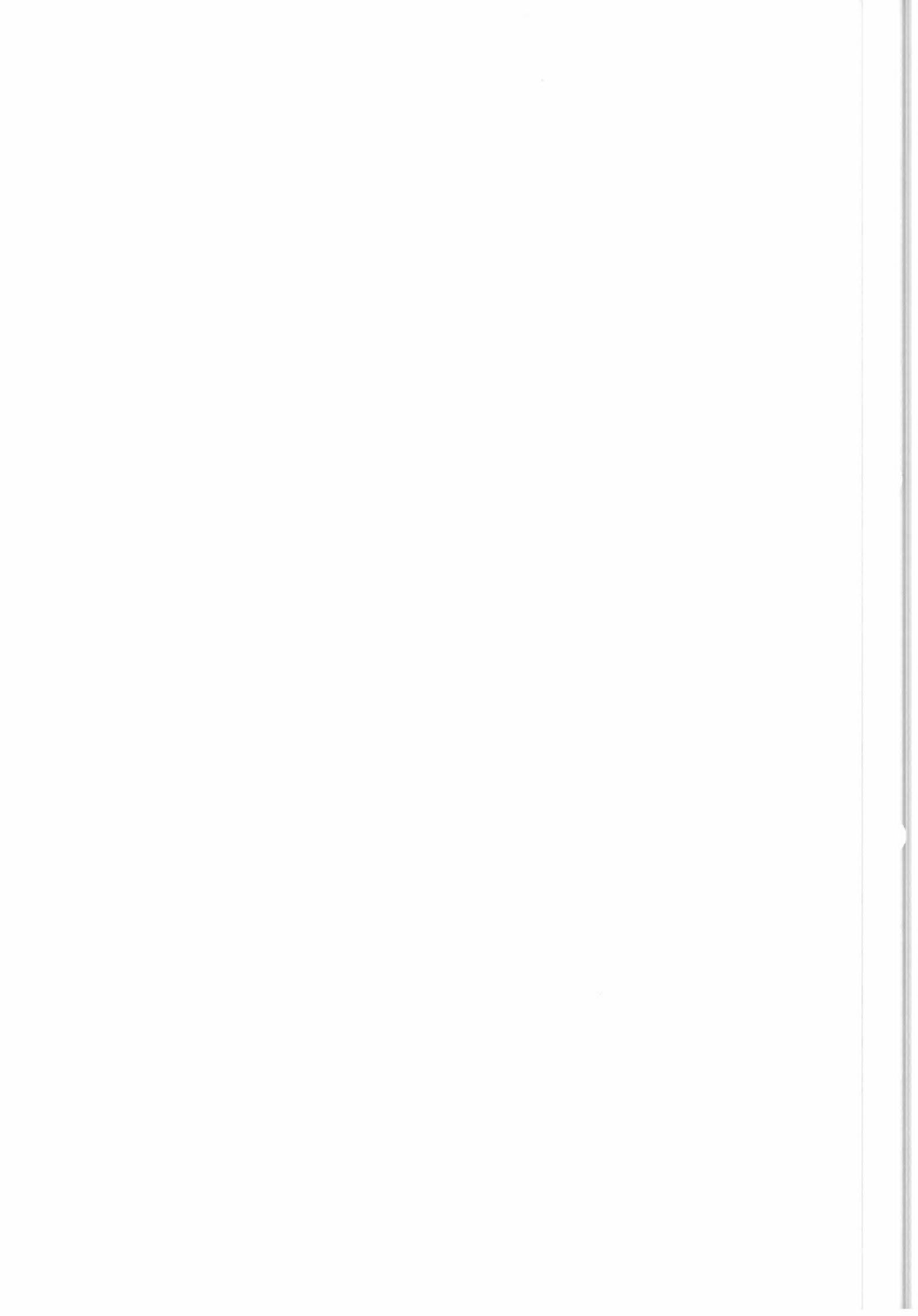


Fig. V.2 $R(r)$ for windspeed jumps
(S_1 in %, indicated for each curve)



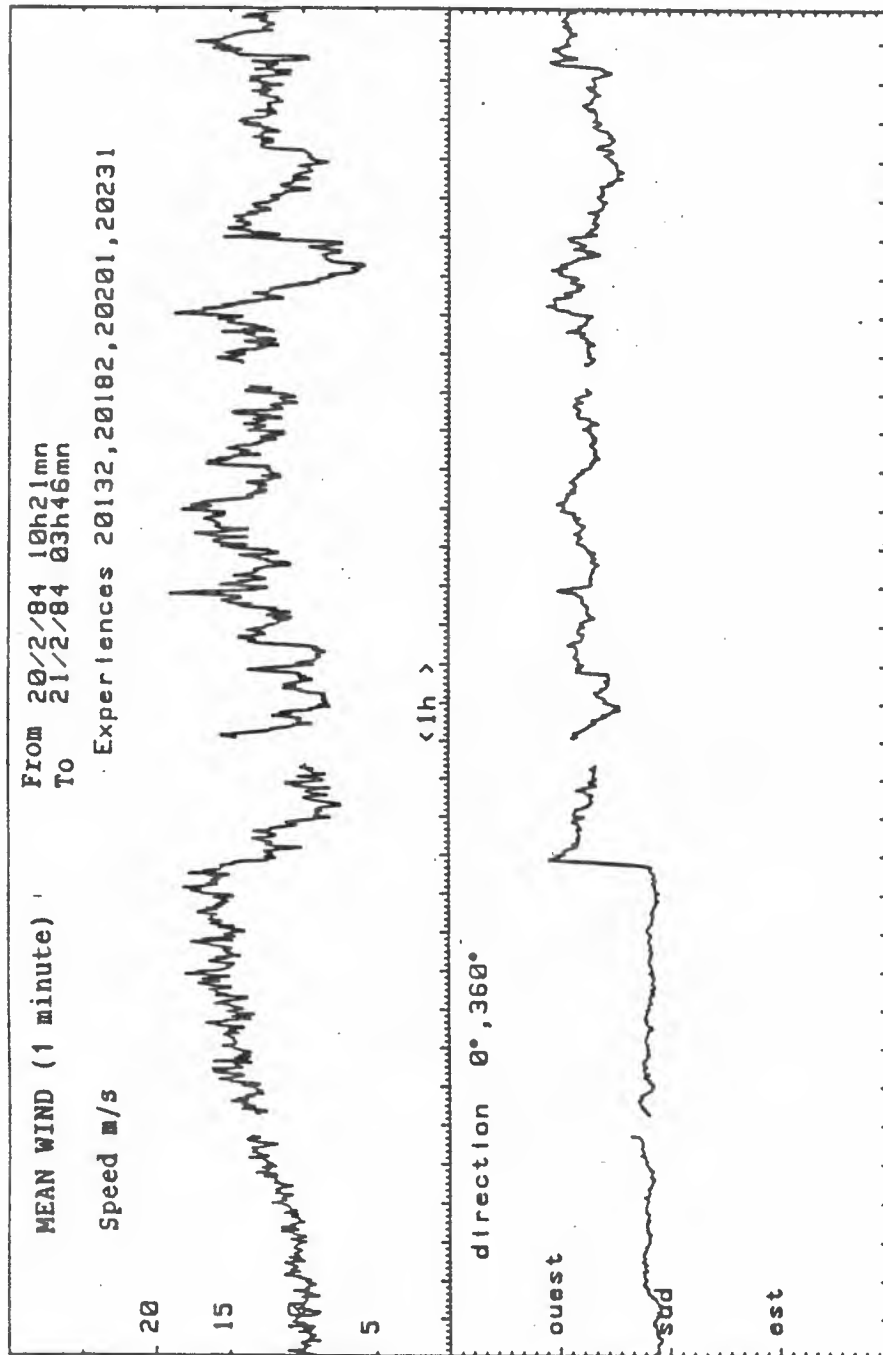
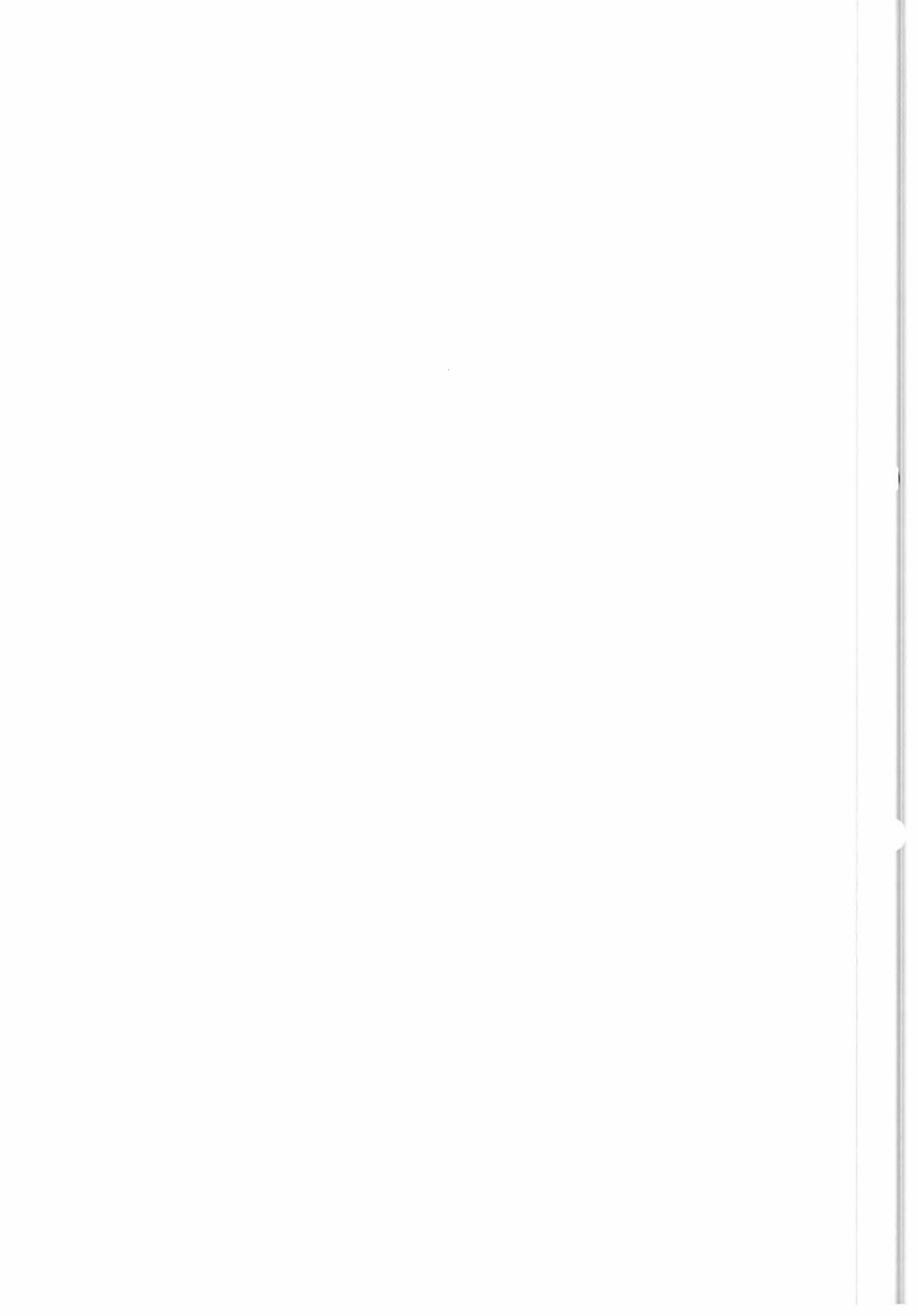


Fig.V.3 Wind structure on passing a cold front
 (TOSCANE1/PROMESS campaign)



$S_2 = 1 - S_1$; S_1 will be expressed in per cent (%). It will be assumed that the weighting function has a cylindrical symmetry so that S_1 depends only on the radial distance "r". The jump in direction from side 1 to side 2 is noted by Δ , measured in degrees. Finally, we must expect that the results will depend both on the wind speed value and the distance cross-track. This has been considered as indicated in the following paragraphs.

V.4.B Equivalent surfaces and their probability distribution for a Gaussian weighting function

In order to be more specific, it is interesting to fix tentatively the scatterometer footprint weighting function " $g(r)$ " which should fall to half its maximum value at $r = 1$; that is :

$$g(0) = 2 * g(1)$$

A reasonable candidate, which has here been chosen, is a Gaussian function, which choice will allow us to represent $S_1(r)$ and also the probability density of S_1 fairly simply.

V.4.B.a The Gaussian scatterometer weighting function

The conditions that the Gaussian weighting function for $r = 1$ be one half its value at $r = 0$, determines its parameters such that :

$$g(r) = (k^2/2\pi) \exp - [(kr)^2/2] \quad (1)$$

$$\text{where } k^2 = 2 \ln 2$$

Fig. V.4 shows that $g(r)$ is a smoothly decreasing function, as might be expected.

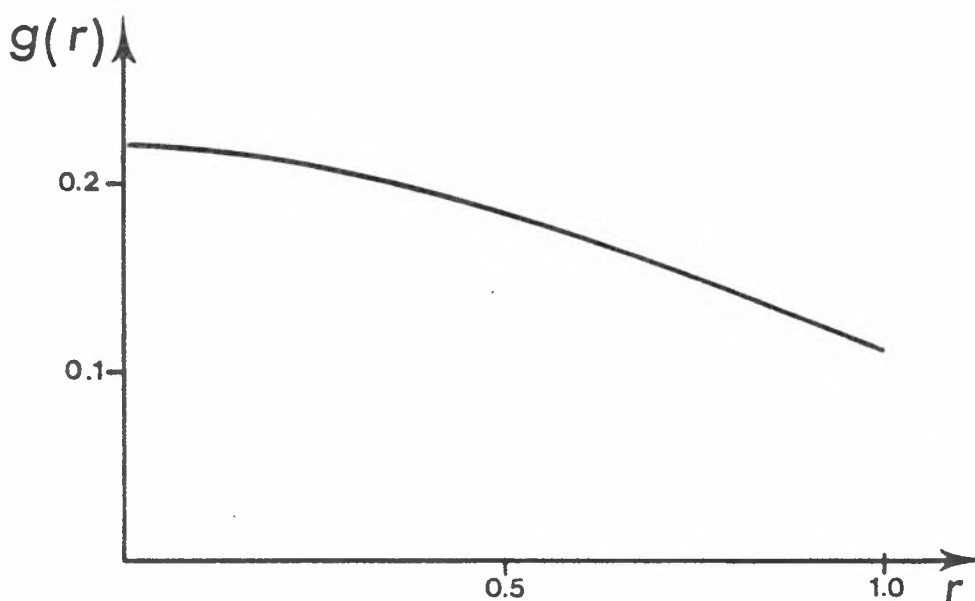
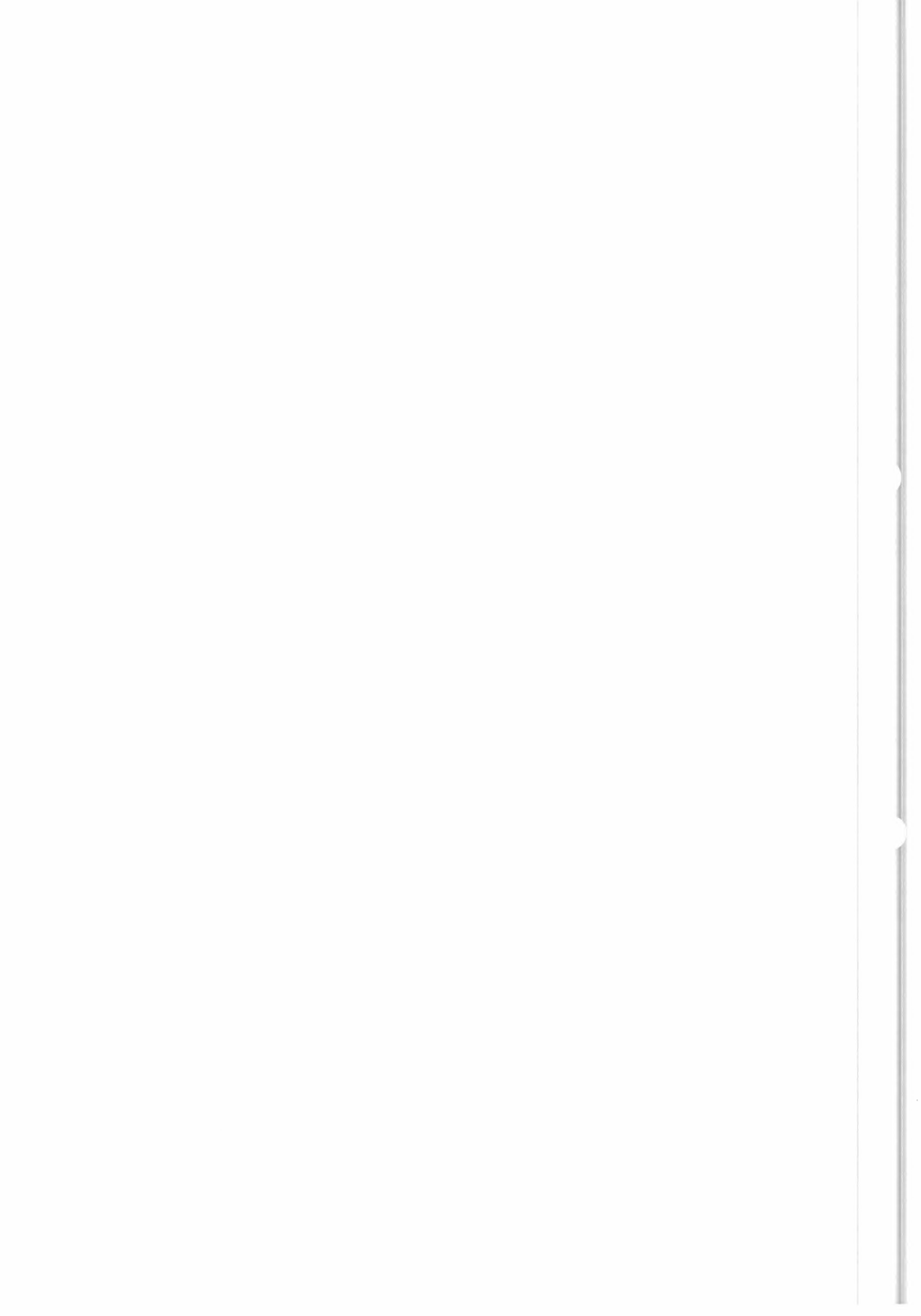


Figure V.4 Gaussian weighting function, $g(r)$



V.4.B.b The equivalent surface as a function of r

Because the weighting function is specified, the value of S_1 , the equivalent surface of the side which does not contain the central point, can be determined as the integral :

$$S_1 = \int_{-\infty}^{\infty} \int_{r_0}^{\infty} g(r) \, dx dy \quad (1)$$

where $r^2 = x^2 + y^2$

Integrating over y (Gaussian definite integral) leaves :

$$S_1 = (k/(2\pi)^{0.5}) \int_{r_0}^{\infty} \exp - [(kx)^2/2] \, dx \quad (2)$$

which integral is readily found tabulated (Math. Tables, Chem. Rubber Pub. Co., 1984). Figure V.5 shows S_1 as a function of r_0 .

As to be expected, S_1 , falls off first rapidly for small values of r_0 , decreasing from 0.5 to 0.1 as r_0 goes from 0 to 1.

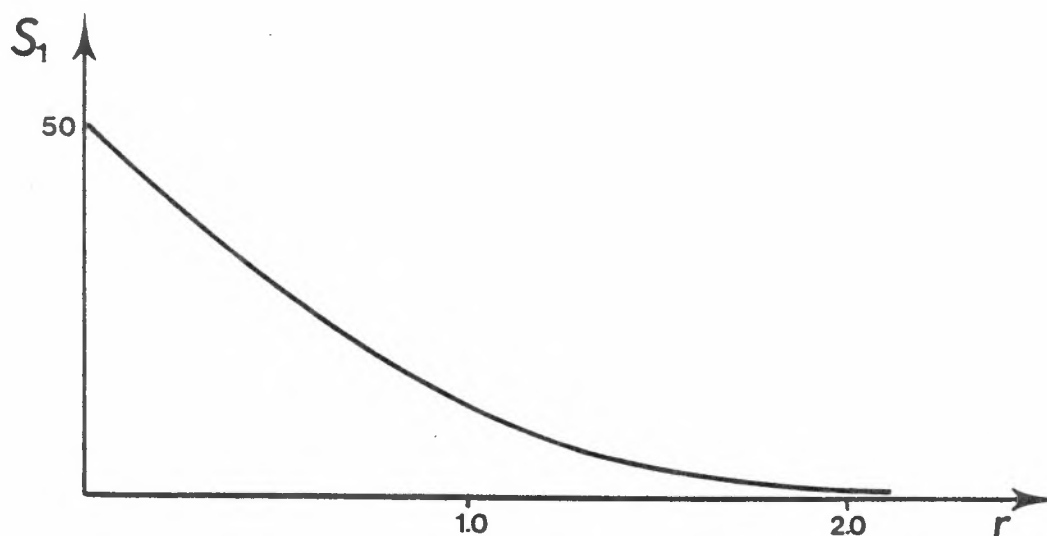
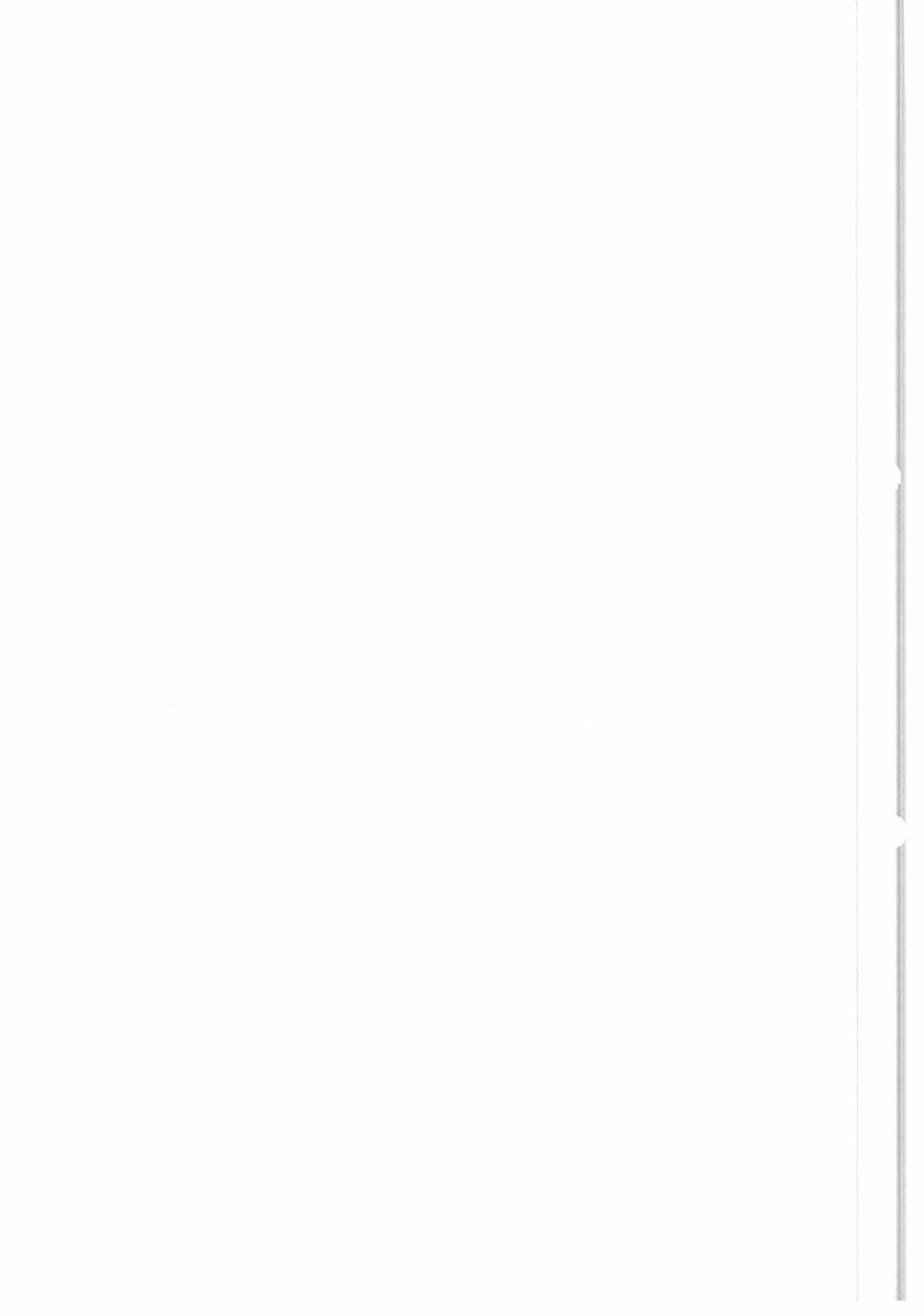


Figure V.5 The equivalent surface, function of r (in %)



V.4.B.c The probability density of equivalent surfaces

It is of some interest to determine the probability density $p(S_1)$ for fronts lying within a normalized distance of 1 from the footprint center. This is because points which are closest to the front will be most affected by it, and any front crossing the swath will come closer than 1 (the normalized distance between points on the scatterometer grid) to certain points.

Because fronts will be randomly distributed with respect to the scatterometer grid, the probability distribution of r_0 must be uniform ($p(r_0) = 1$). Since, by definition :

$$p(S_1) |dS_1| = p(r_0) |dr_0| \quad (1)$$

the probability density of S_1 takes the simple form :

$$p(S_1) = -1/(dS_1/dr_0) = [k/(2\pi)^{0.5}] \exp [-(k r_0)^2 / 2] \quad (2)$$

Knowing both S_1 and $p(S_1)$ as a function of r_0 , the curve $p(S_1)$ as a function of S_1 can be drawn (Fig. V.6). This curve indicates clearly that small values of S_1 will be somewhat more frequent than values of S_1 close to 50%, but that all values of S_1 have reasonable probabilities of occurrence.

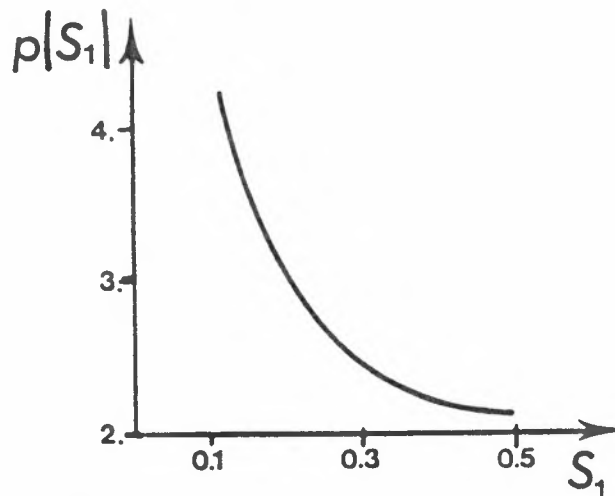


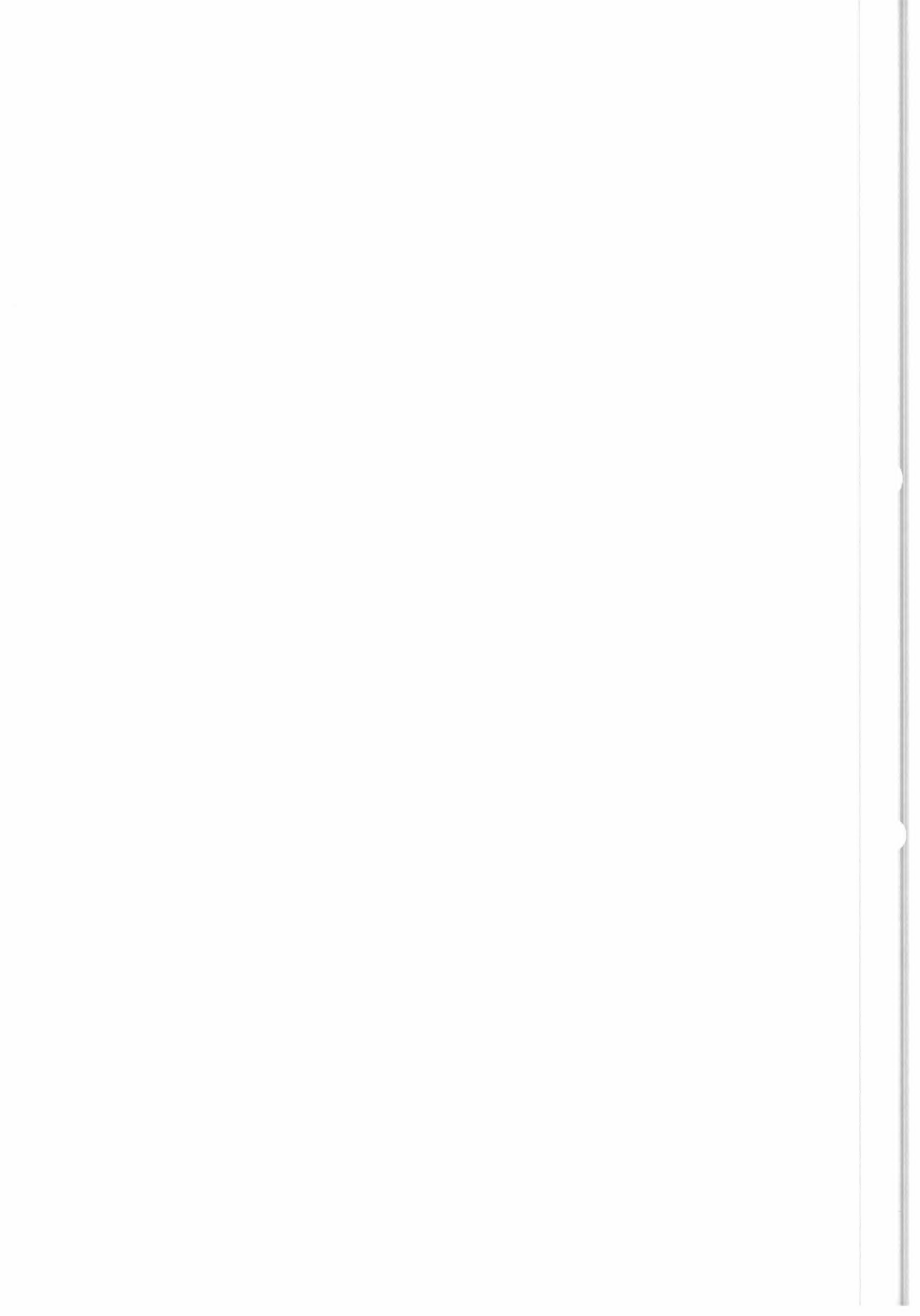
Figure V.6 Probability density of S_1

V.4.C Numerical simulations of direction jumps

V.4.C.a A description of the procedure

The procedure is the following ; for a given speed v , and direction D_1 on the side of the front having equivalent area S_1 , and a wind speed and direction v and $D_1 + \Delta$ on the other side :

- 1) Generate $(\sigma_1, \sigma_2, \sigma_3)$ on each side of the front



2) Take the weighted mean $(\overline{\sigma_1, \sigma_2, \sigma_3})$:

$$(\overline{\sigma_1, \sigma_2, \sigma_3}) = S1 (\sigma_1, \sigma_2, \sigma_3)_1 + (1 - S1)(\sigma_1, \sigma_2, \sigma_3)_2$$

3) Invert, using WINRET the point $(\overline{\sigma_1, \sigma_2, \sigma_3})$ to obtain the different possible winds to be de-aliased

4) Present results in synthetic form in an appropriate format so as to simplify interpretation

The wind directions are given in satellite track oriented system such that upwind for the central antenna is 90° , wind directions increasing in the geographical sense (upwind for the forward beam corresponding to 45°). Parameters explored are :

- Distance from track : 250, 500, 729 kms
- Wind speeds : 5, 10, 15 m/s
- Wind directions, D1 : -90° to 90° in 15° steps
- Wind direction jump, Δ : D1 - D2 : $60^\circ, 90^\circ$
- Equivalent surface S1 : 10, 30, 50 %

(In view of yaw-steering it is not necessary to explore D1 beyond the range chosen, because of the symmetry in antenna orientation).

V.4.C.b Description of results

As might be expected, as S1 and Δ increase, the direction of rank 1 or rank 2 solutions closest to the mean direction :

$$\overline{D} = S1D1 + (1 - S1)(D1 + \Delta)$$

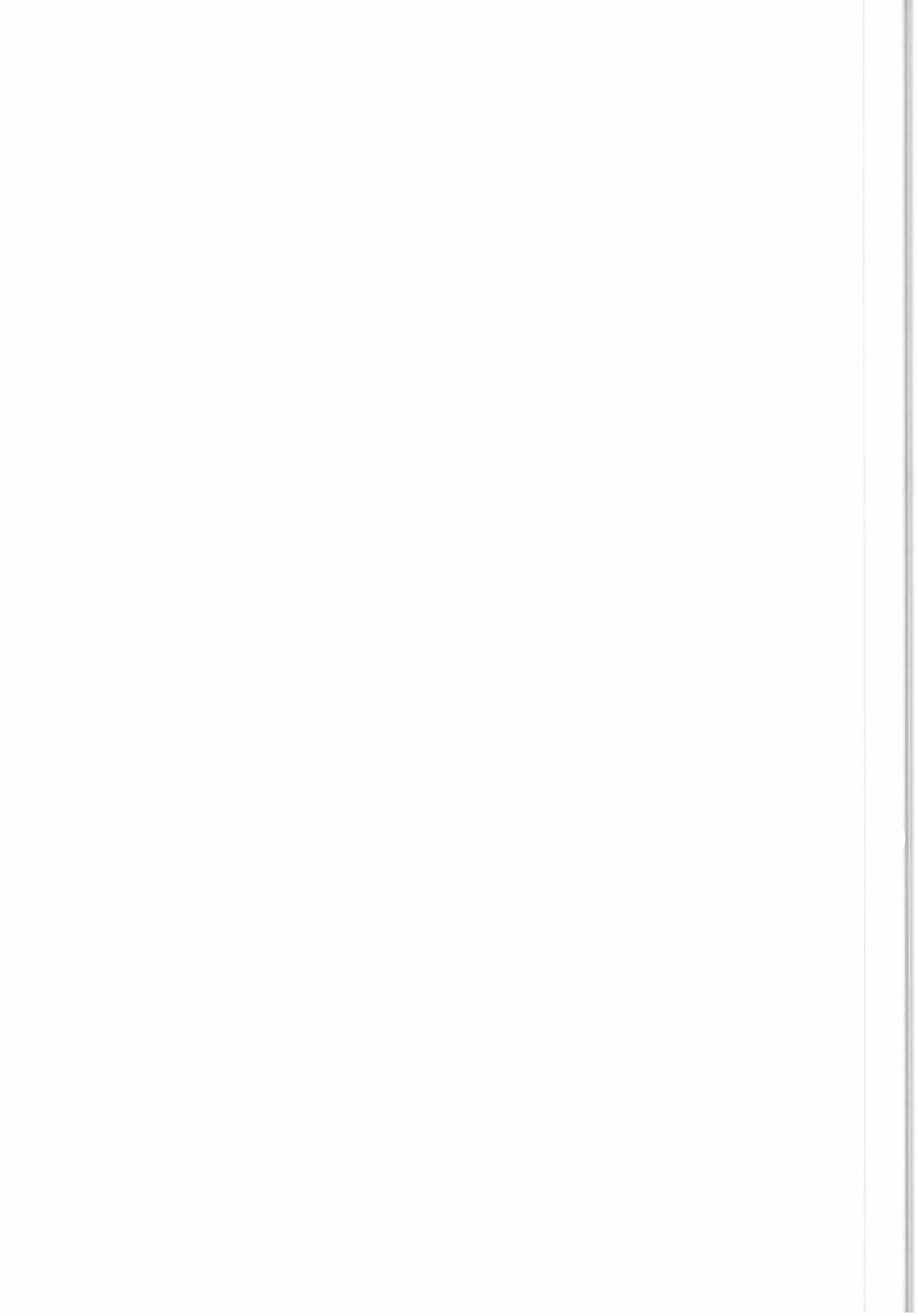
departs more and more from it. Although all three distances (250, 494, 729 km) have been computed and drawn, only cases at 494 km will be shown, as being typical.

On figures V.7a to V.7c are plotted, every 15° , the directions of rank 1 and rank 2 solutions for $\Delta = 60^\circ$ and $S1 = 10\%$.

The two continuous straight-line segments represent D1 and \overline{D} , the upper being D1, the lower \overline{D} . Notice simply that there is always one solution within 20° of \overline{D} .

As S1 increases ($S1 = 30\% \rightarrow$ Fig. V.7b ; $S1 = 50\% \rightarrow$ Fig. V.7c) discontinuities appear in the curves representing solutions closest and farthest from the \overline{D} line.

This behaviour is enhanced if $\Delta = 90^\circ$ (Fig. V.8a to V.8c). For the most severe case ($\Delta = 90^\circ, S1 = 50\%$; Fig. V.8c) rank 1 and rank 2 directions are attracted into four directions, nominally $-150^\circ, -90^\circ, -30^\circ$ and 90° . In such extreme cases, which should occur only very rarely because they imply a very improbable wind jump associated to a 50/50 cut through the scatterometer footprint, there is practically no correlation between \overline{D} and the directions proposed by the inversion of the mean σ values.



DELTA = 60 DEG. X = 10. DISTANCE = 494 KM

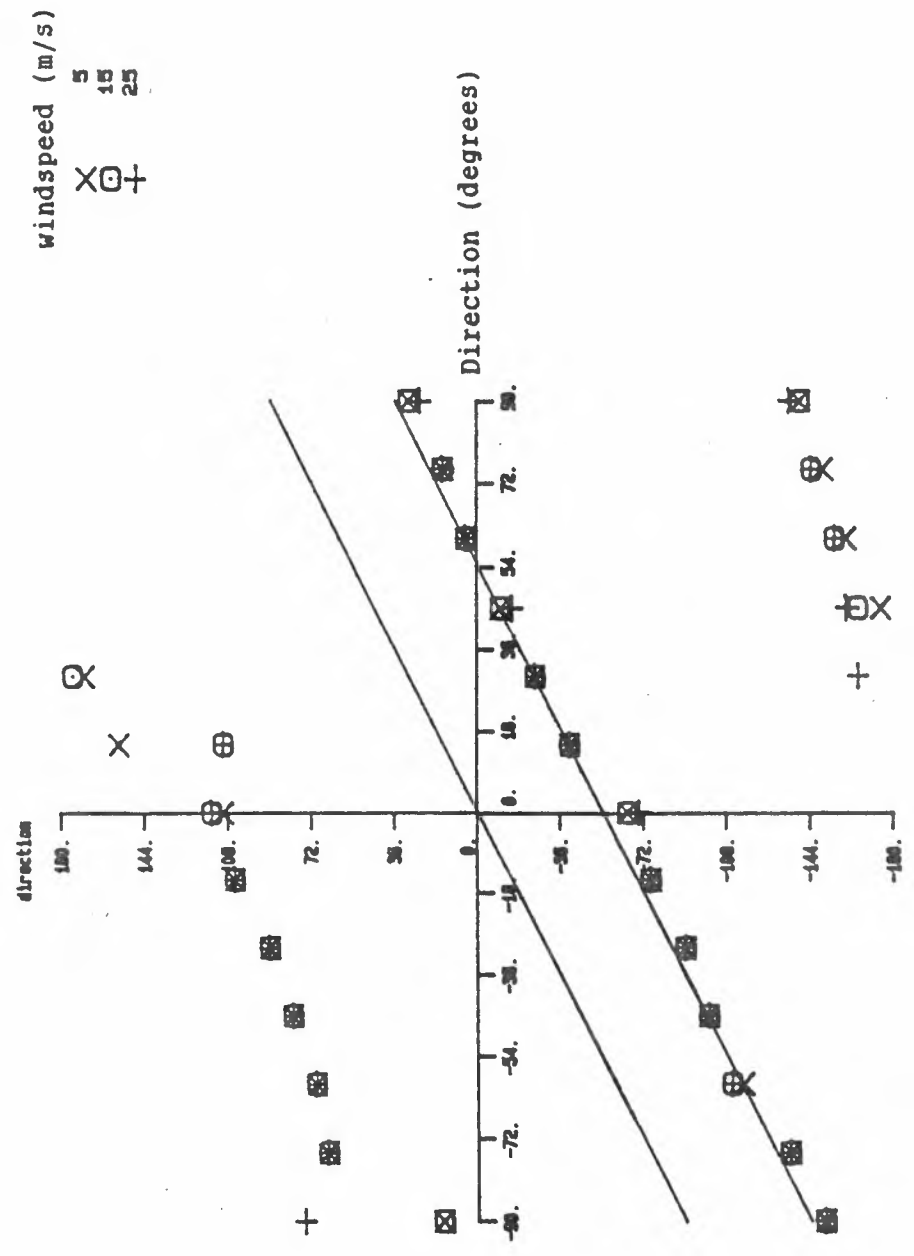
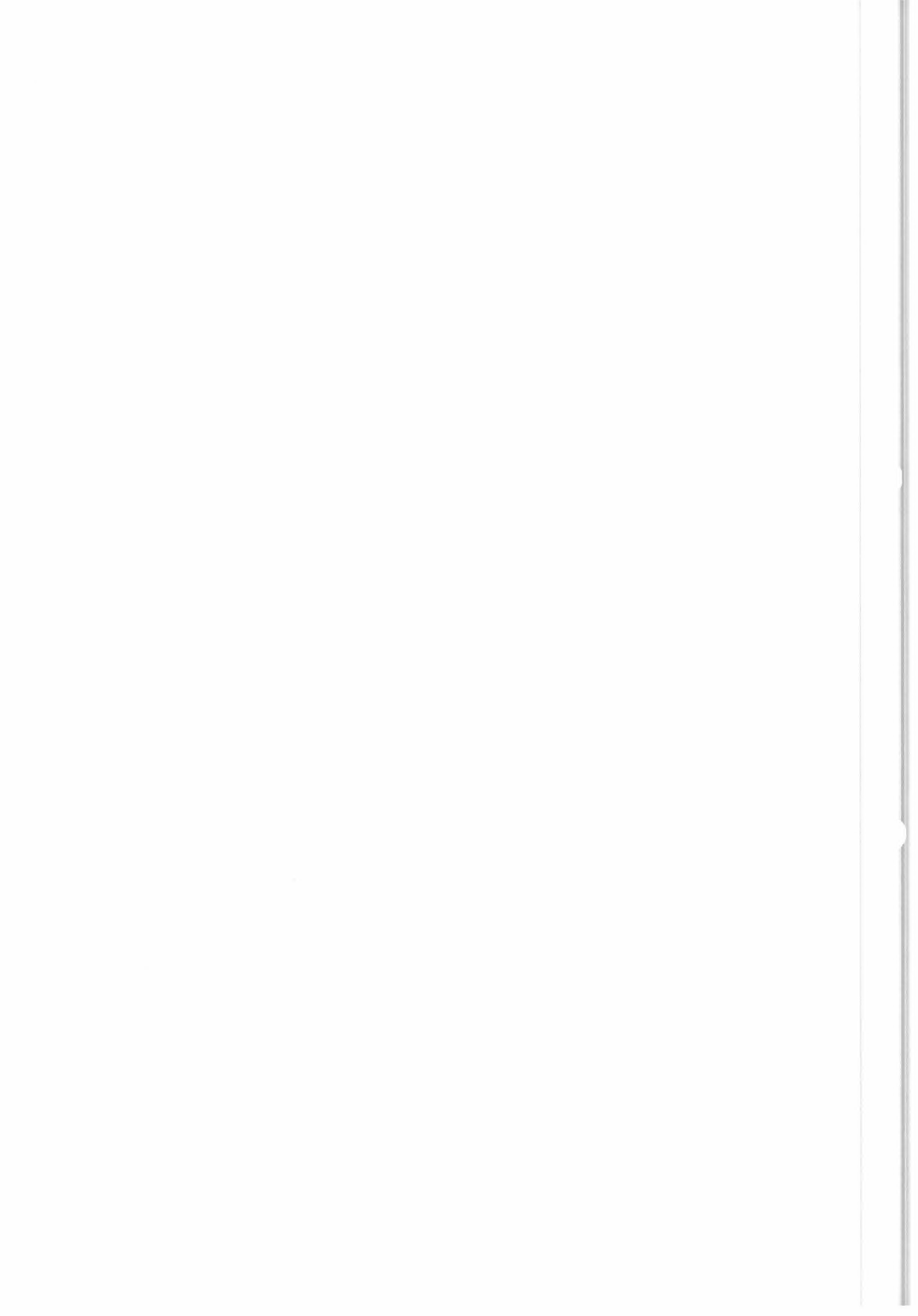


Fig. V.7.a Rank 1 and rank 2 directions



DELTA = 60 DEG, X = 30, DISTANCE = 494 KM

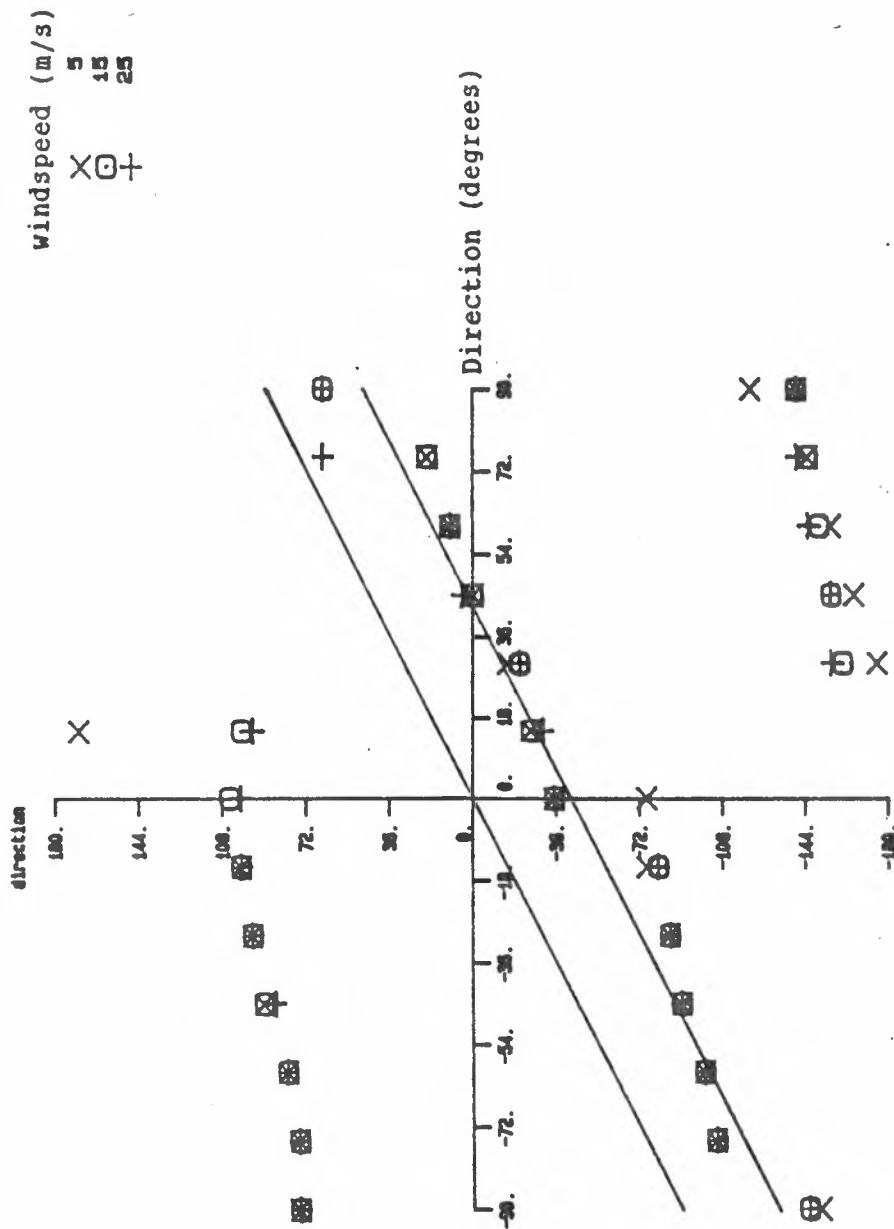
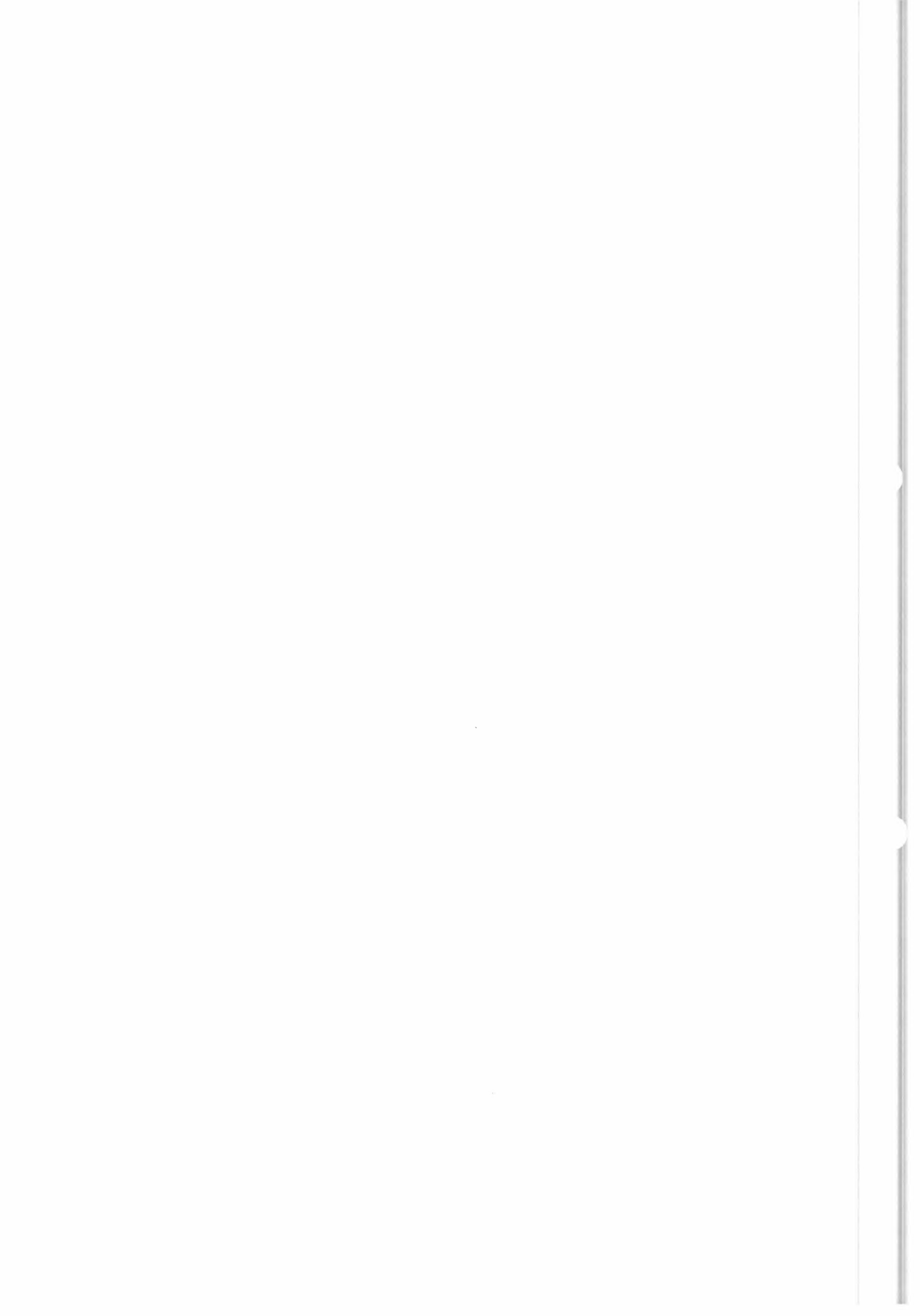


Fig. V.7.b Rank 1 and rank 2 directions



DELTA - 60 DEG, X - 50, DISTANCE -494 KM

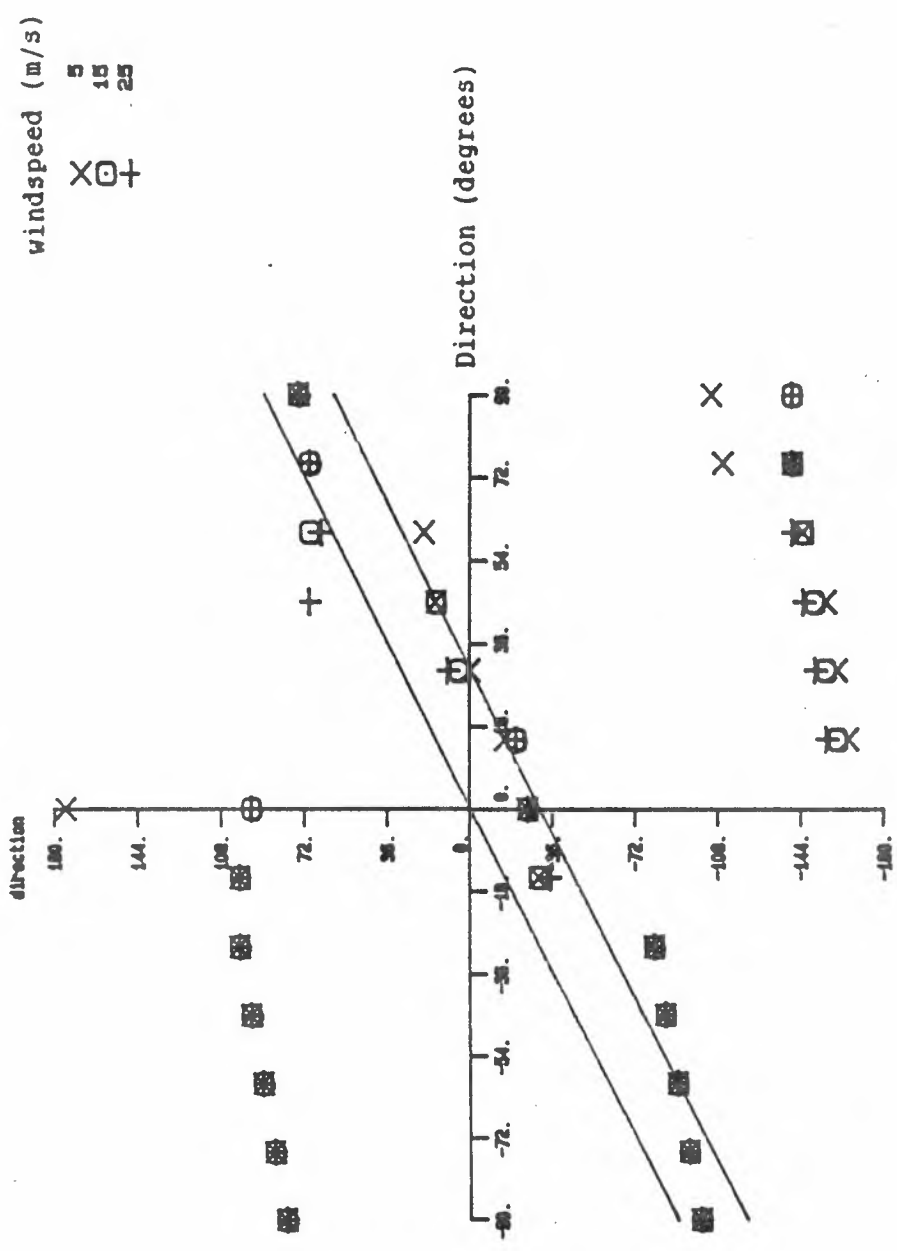
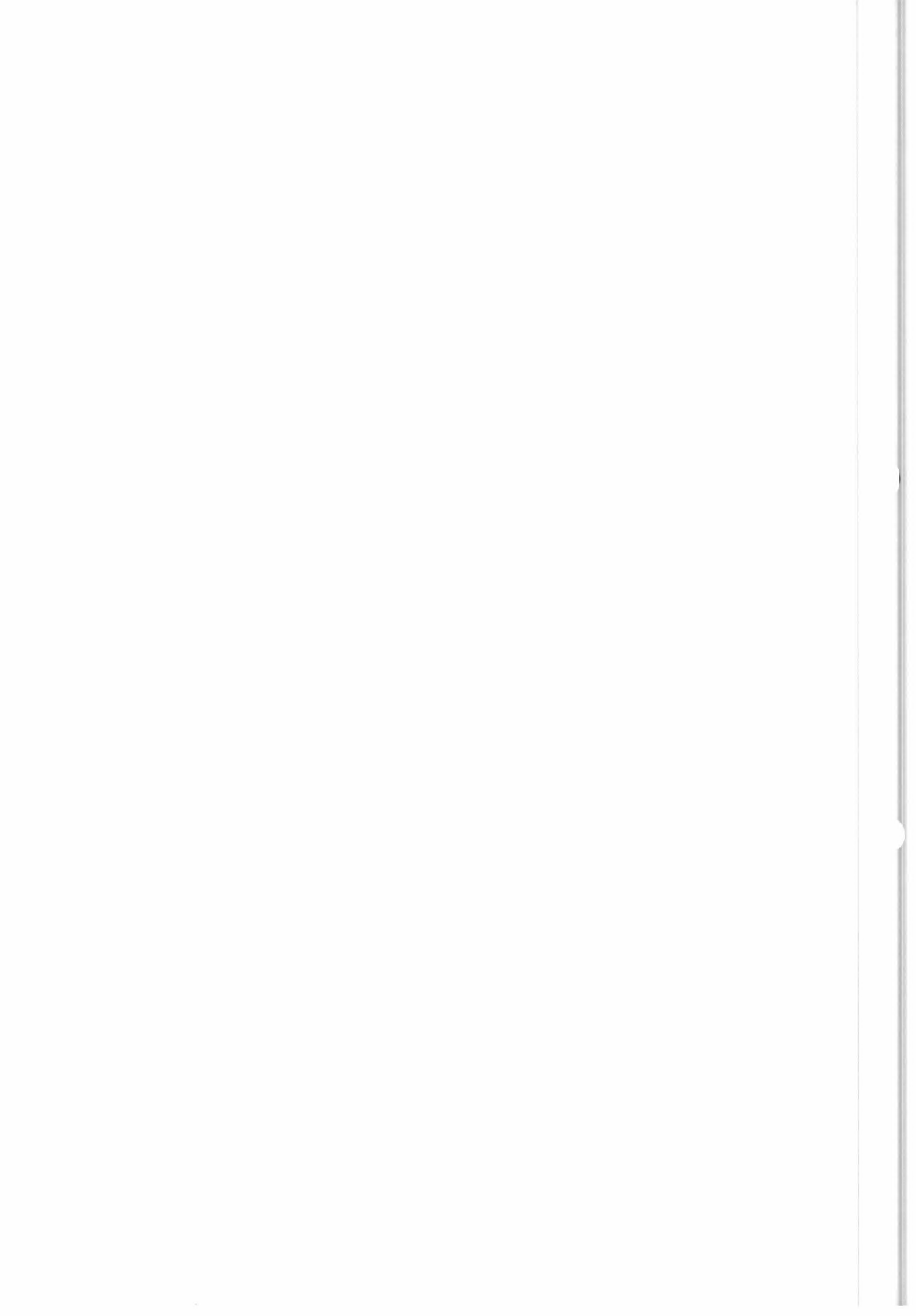


Fig. V.7.c Rank 1 and rank 2 directions



DELTA = 90 DEG. X = 10. DISTANCE = 494 KM

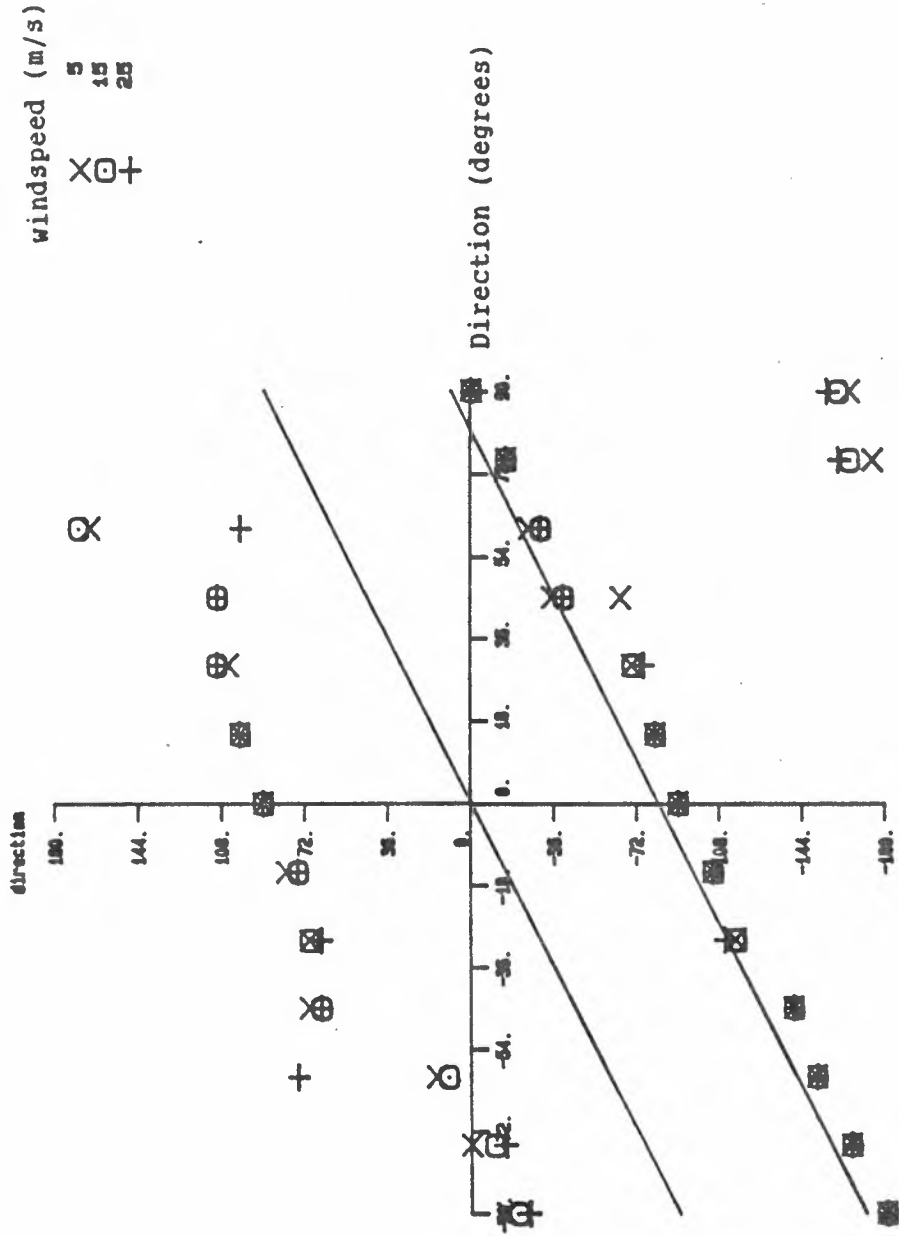
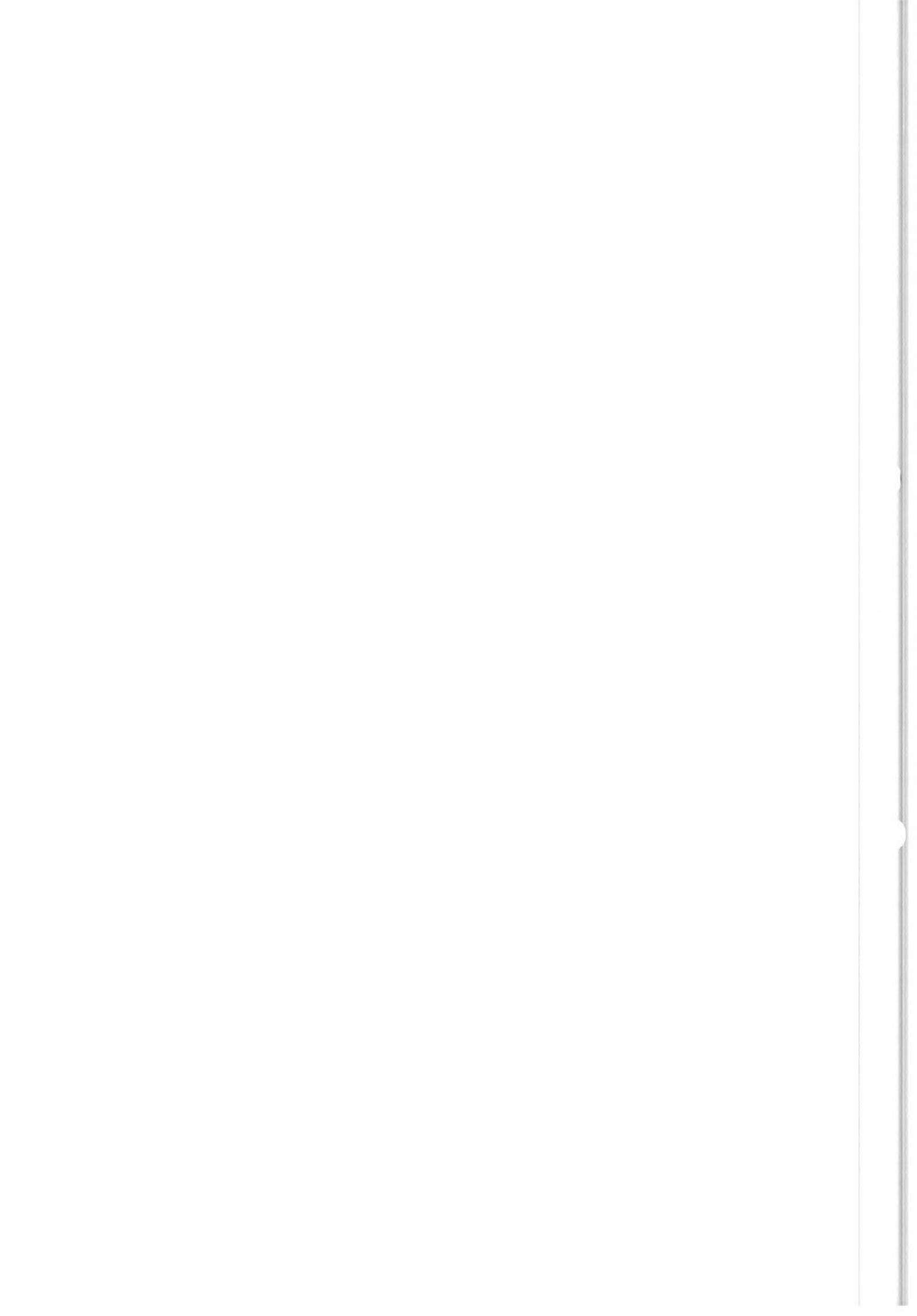
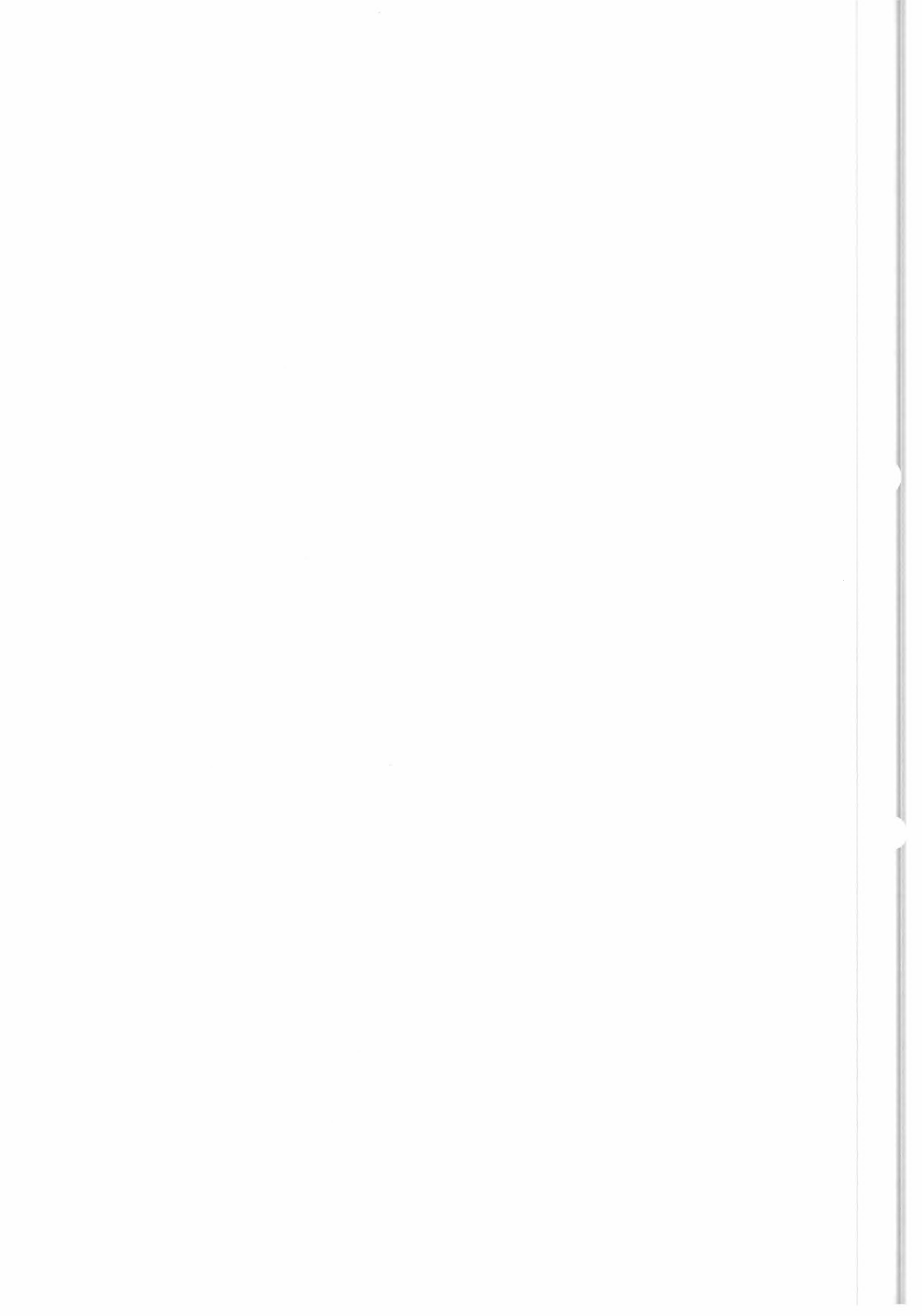


Fig. V.8.a Rank 1 and rank 2 directions





DELTA = 90 DEG. X = 50. DISTANCE = 494 KM

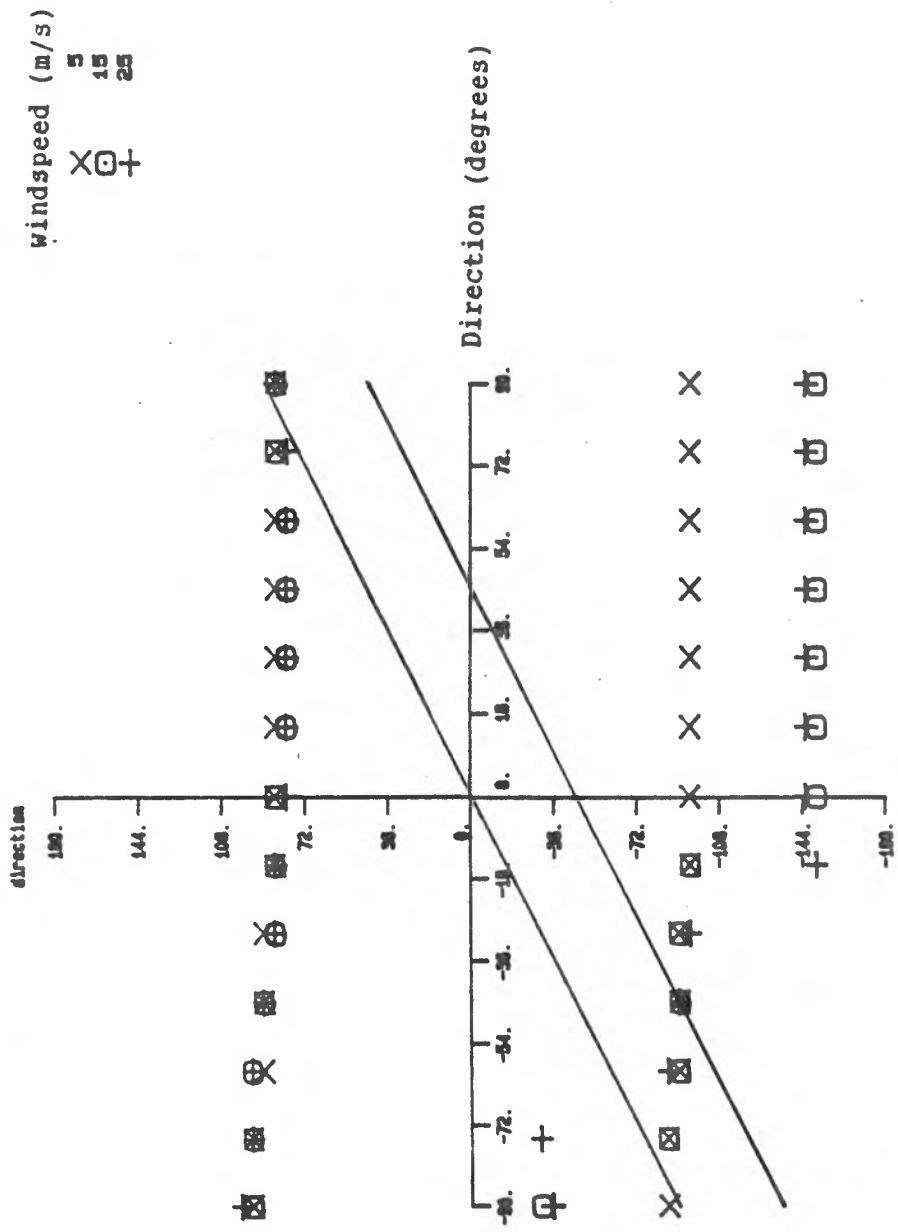
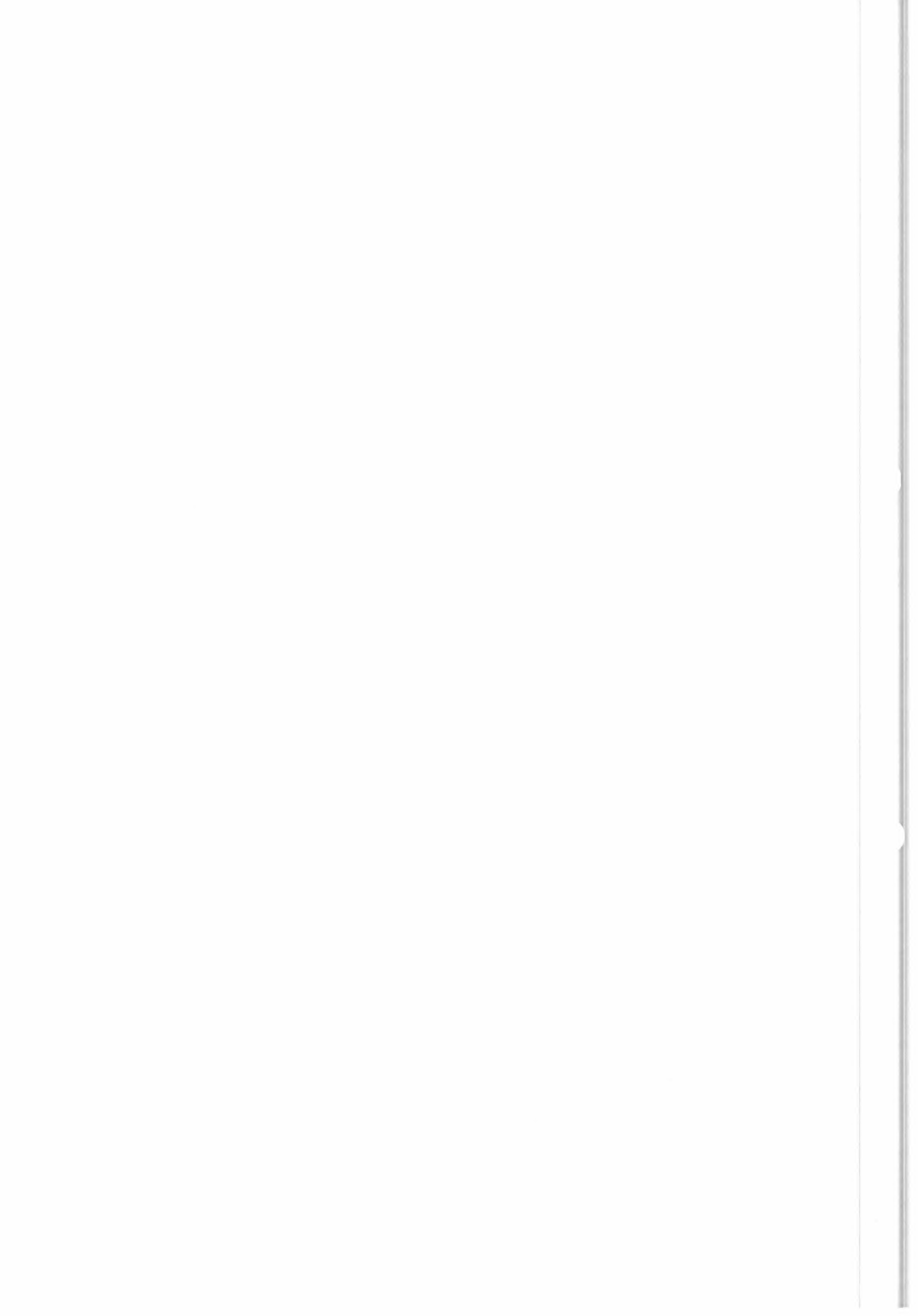


Fig. V.8.C Rank 1 and rank 2 directions



Notice that curves for cases $\Delta = 60^\circ$, $S1 = 30\%$ or $S1 = 50\%$, as well as $\Delta = 90^\circ$, $S1 = 30\%$, are also deviated to the four "attracting" directions. The geometrical interpretation of this is the fact that -150° , -90° , -30° , 90° (nominally) are closest to the center line of the surface of solutions.

V.4.C.c Impact on de-aliasing techniques

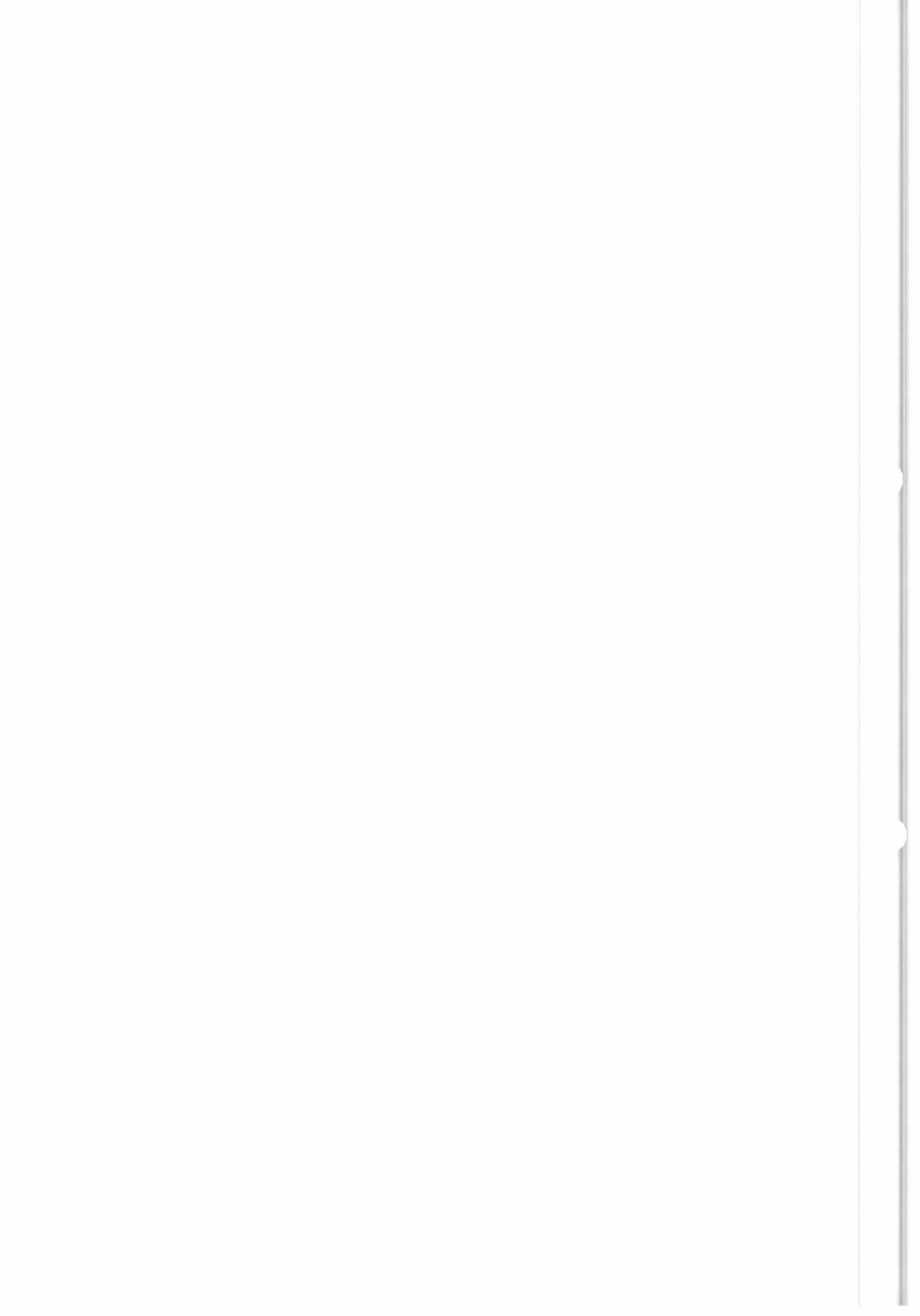
De-aliasing techniques (described in section VII) such as the routine CHOIX in the FDP production chain for the ERS-1 scatterometer are based on choosing the direction of the "next" point as being that which is closest to that of the previous points (the number of previous points used to get a previous mean direction, we have chosen this number to be two as in CHOIX).

The presence of "attracting" directions would cause wrong choices to be made in the following way. As an example take Fig. V.8b ($\Delta = 90^\circ$, $S1 = 30\%$) ; for all wind speeds considered, when $D1 = 15^\circ$, the possible wind directions to choose from are 90° and -90° . If 90° is chosen as is reasonable because closest to 15° , then in the next step, nominal directions of -75° and 115° will have to be chosen from, and of course 115° will be chosen (closest to the mean previous direction $(15 + 90)/2$), the bad choice.

Scrutiny of the different figures corresponding to $\Delta = 90^\circ$ shows that this same behaviour occurs for all wind speeds, distances off-track and values of $S1$. However, this is never observed for $\Delta = 60^\circ$, whatever the values of the other parameters chosen.

It is an open question whether nature creates direction jumps so important, over a short enough distance, to cause the difficulties in de-aliasing (due to poor inversion) which have just been described. But having posed this question may lead to refine the de-aliasing routines before launch date sufficiently to avoid the problem altogether. This may mean creating a "forbidden zone" around the center-line of the surface of solutions, or discovering the positions of fronts automatically and treating zones to the left and right independently, or checking to see if a point is surrounded by two neighbours whose direction lines are close to 90° apart.

A useful side study would be to better our model of front simulation, the transition zone between the two constant direction zones being given a finite width which would draw points out of the center zone of the Σ_0 three-space. The transition zone would be of order 10 kms in width, and the hypothesis would be made that gravity waves of a few centimeter wavelengths remain roughly in equilibrium with the local wind under such conditions. Then mean values of σ_0 in σ_0 -space would be constructed not only from two points on the surface of solutions corresponding to the outer zones, but also from elements on a curve on the surface of solutions joining these two points.



VI - BEHAVIOUR OF THE INVERSION MODULE IN ICE COVERED AREAS

VI.1 Presentation of the problem

Figure VI.1 shows the behaviour of σ_0 over ice-covered areas as a function of incidence angle, for VV polarization, at a frequency of 5.2 GHz. These values are close enough to those observed over the open ocean in the region 18° to 60° to warrant further investigation. The purpose of the following paragraphs is to investigate the order of wind speeds, directions and maximum likelihood distances which would be determined by the σ_0 to wind (F.D.P) inversion module, assuming that the data of Fig. VI.1 is correct.

The procedure used is the following :

- 1) Approximate the ice σ_0 (in dB) relationship to incidence angle by a linear one
- 2) Approximate the incidence angle relationship to off-track distance for the forward, rear and central antennas by a second order relationship
- 3) Determine the σ_0 of the three antennas over ice at different distances off-track, introduce these values in the inversion routine, and present wind speed, wind direction and maximum likelihood distances of the rank 1 and 2 solutions found.

Only rank 1 and rank 2 solutions are presented since they play a major role in the de-aliasing routine. Moreover solutions of rank 3 and higher generally have high values of the maximum likelihood distance which would cause them to be discarded in any case.

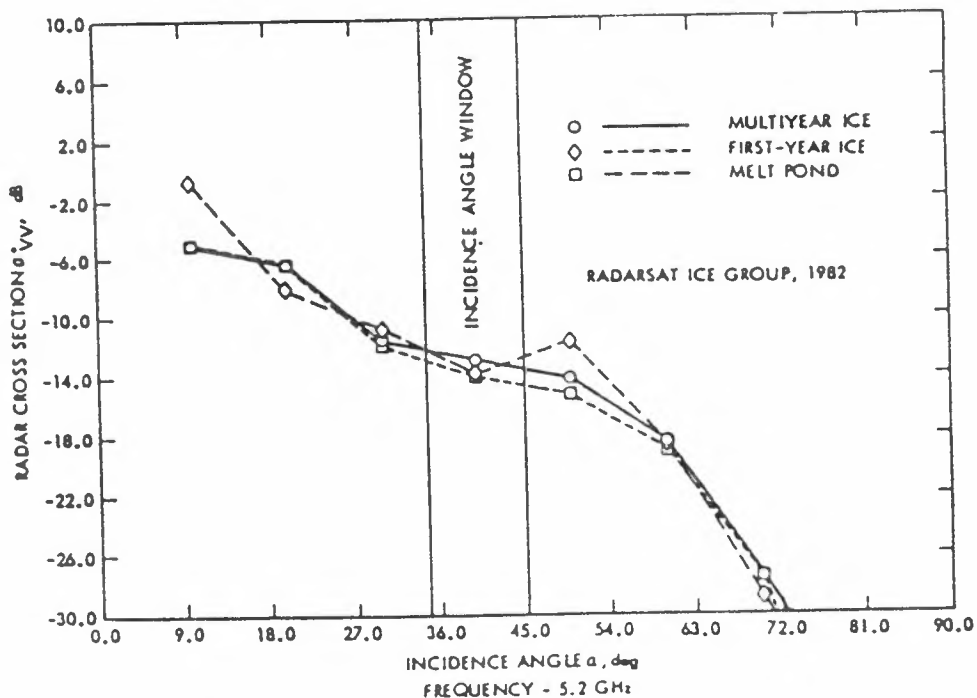
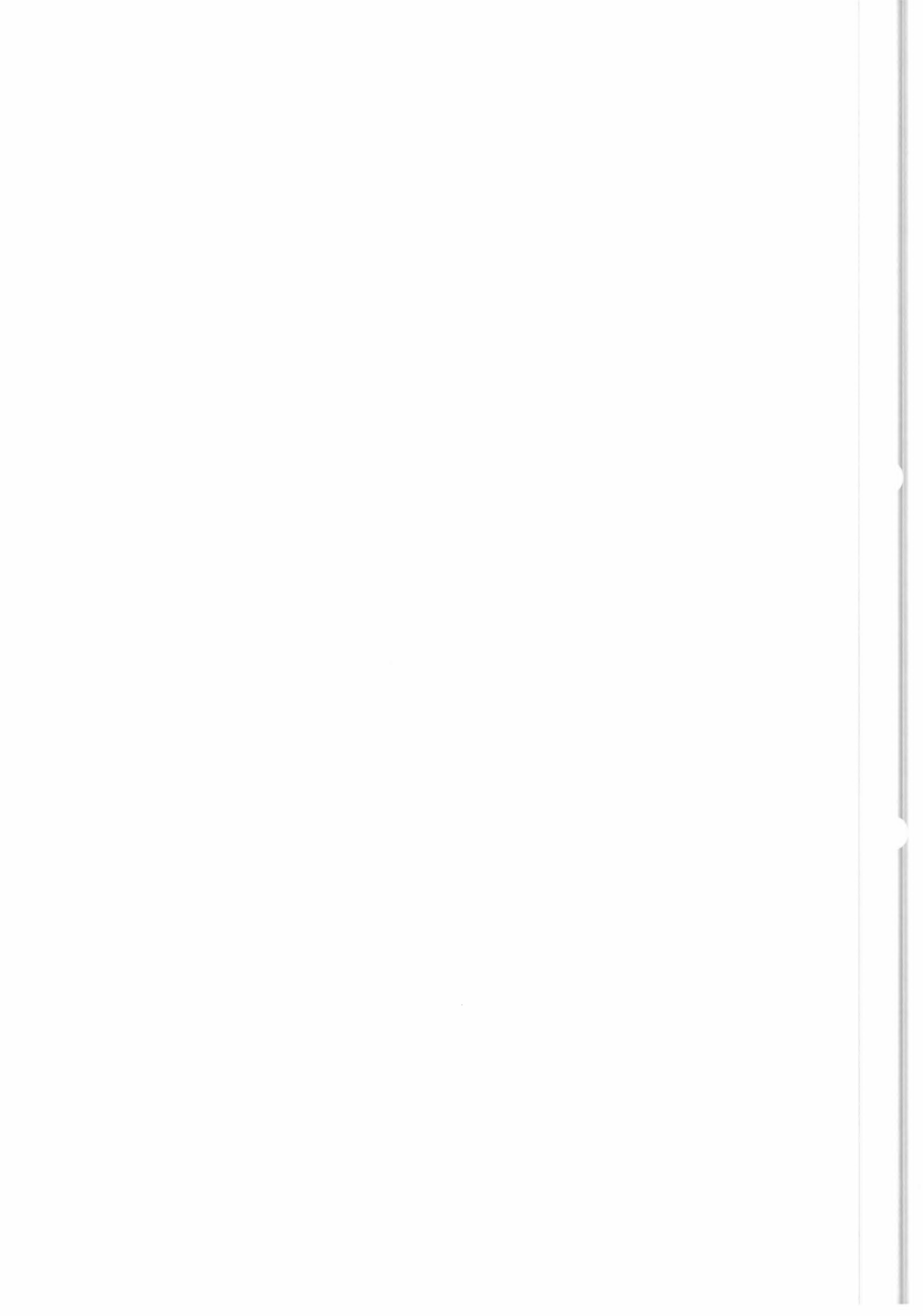


Figure VI.1 C-band ice back-scattering as a function of angle of incidence



VI.2 The linear approximation of Sigma0 dependence on incidence angle

In dB, the Sigma0 to incidence angle relationship appears to be approximately linear from 18° to 60°. The straight-line passing through the points :

$$\begin{aligned} \theta = 18^\circ & \quad \text{Sigma0} = -8.0 \text{ dB} \\ \theta = 60^\circ & \quad \text{Sigma0} = -19.0 \text{ dB} \end{aligned}$$

satisfies the equation :

$$\text{Sigma0 (dB)} = -0.2169 \theta - 3.2857 \quad (1)$$

This may appear as too crude an approximation later, but at the present time, C-band data at the precise ERS-1 frequency is not available to our knowledge.

VI.3 Incidence angles as a function of off-track distance

Here nominal values have been taken, since the relationship will vary slightly with altitude of the satellite ; values taken correspond to previously computed incidence angles at 52.75°N. A parabolic curve is passed through the incidence angle values at 250, 494 and 729 km. This gives for the central beam :

$$\theta(2) = -.7361142 + .0904297 L - .000031701 L^2 \quad (2)$$

and for the forward or rear beams :

$$\theta(1) = \theta(3) = .498356 + .1208467 L - .00005424 L^2 \quad (3)$$

Here differences in incidence angles between forward and rear beams (of the order of 0.05°) have been neglected.

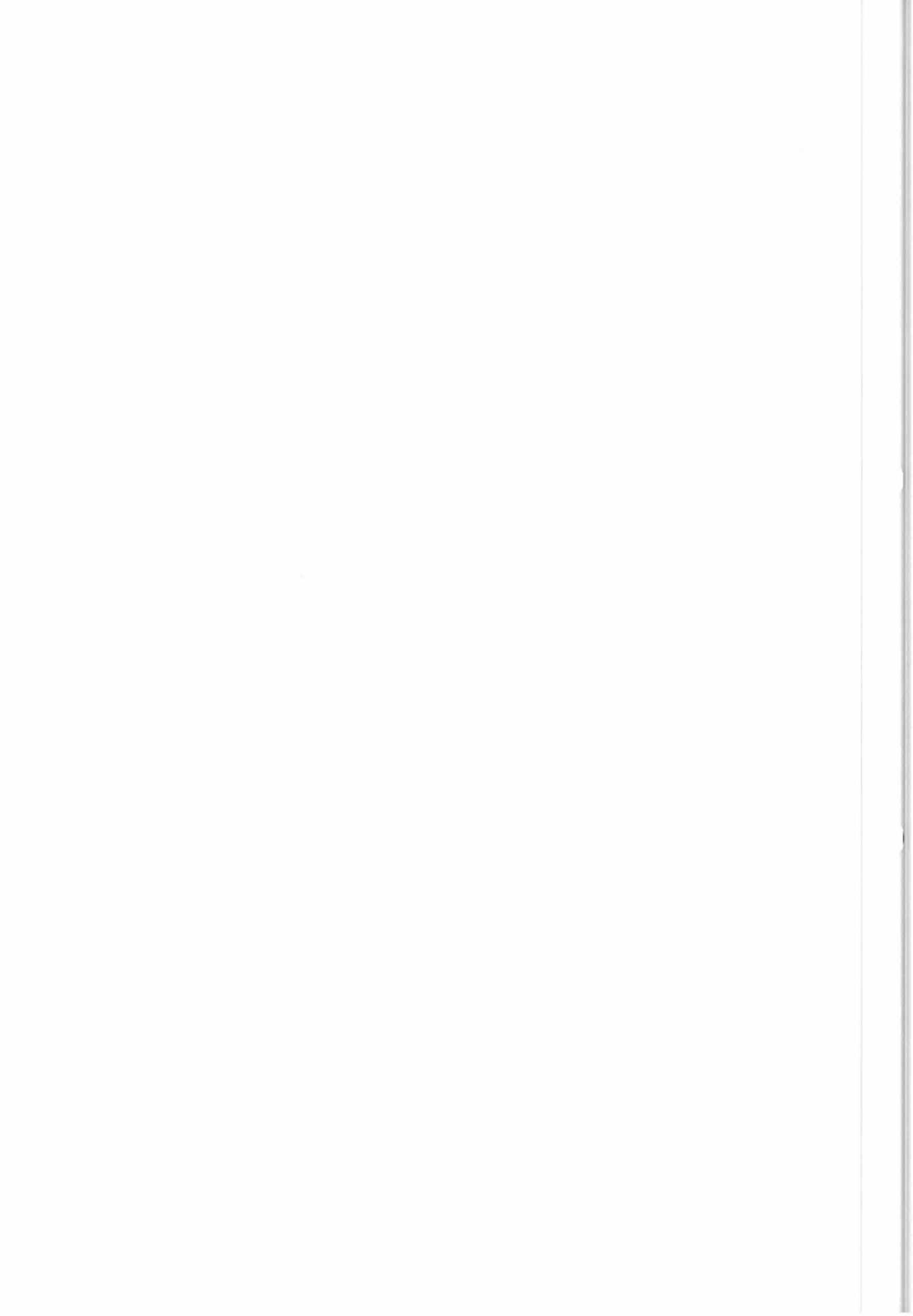
VI.4 Presentation of rank 1 and rank 2 "wind solutions" over ice

Sigma0 triplets over ice at distances from 250 to 750 km off-track were introduced in the Sigma0 to wind inversion module (WINRET), assuming isotropy of ice back-scattering in azimuth. Resulting rank 1 and rank 2 maximum likelihood distance M, wind speeds V and directions ϕ for rank 1 and rank 2 solutions are presented in figures VI.2 to VI.4.

M, as shown in Fig. VI.2, has values greater than M1 (limiting value of M, corresponding to a probability of 0.999) only for the first three points (250, 275, 300 kms) and falls to small values, between 350 and 600 kms, rendering this parameter useless for a point by point screening of ice points in this region.

Wind speed, V, (Fig. VI.3) increases regularly over most of the swath with distance off-track, taking on values which are quite reasonable in amplitude (2.5 to 14 m/s). Only to be noted is the fact that exactly the same wind speeds are obtained for rank 1 and rank 2 solutions over the swath except for the region 700 to 750 kms off-track.

Most interesting is the behaviour of the rank 1 and 2 wind directions (Fig. VI.4). These lie, at first, nearly parallel to the satellite track (180° and 360°) evolve slowly from L = 250 to 700 kms then jump to the pair of solutions corresponding to upwind/downwind for the central beam (90° and 270°).



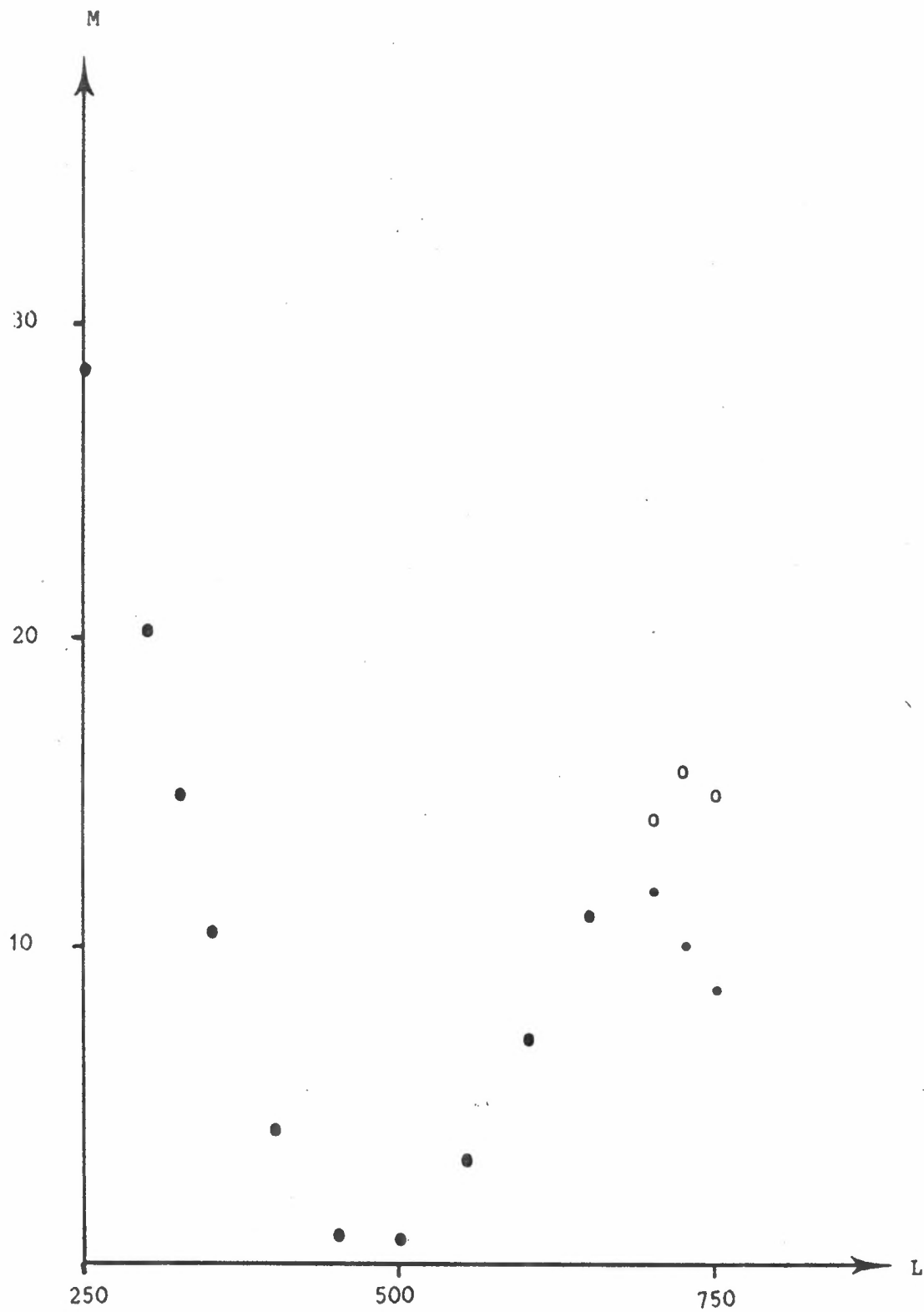
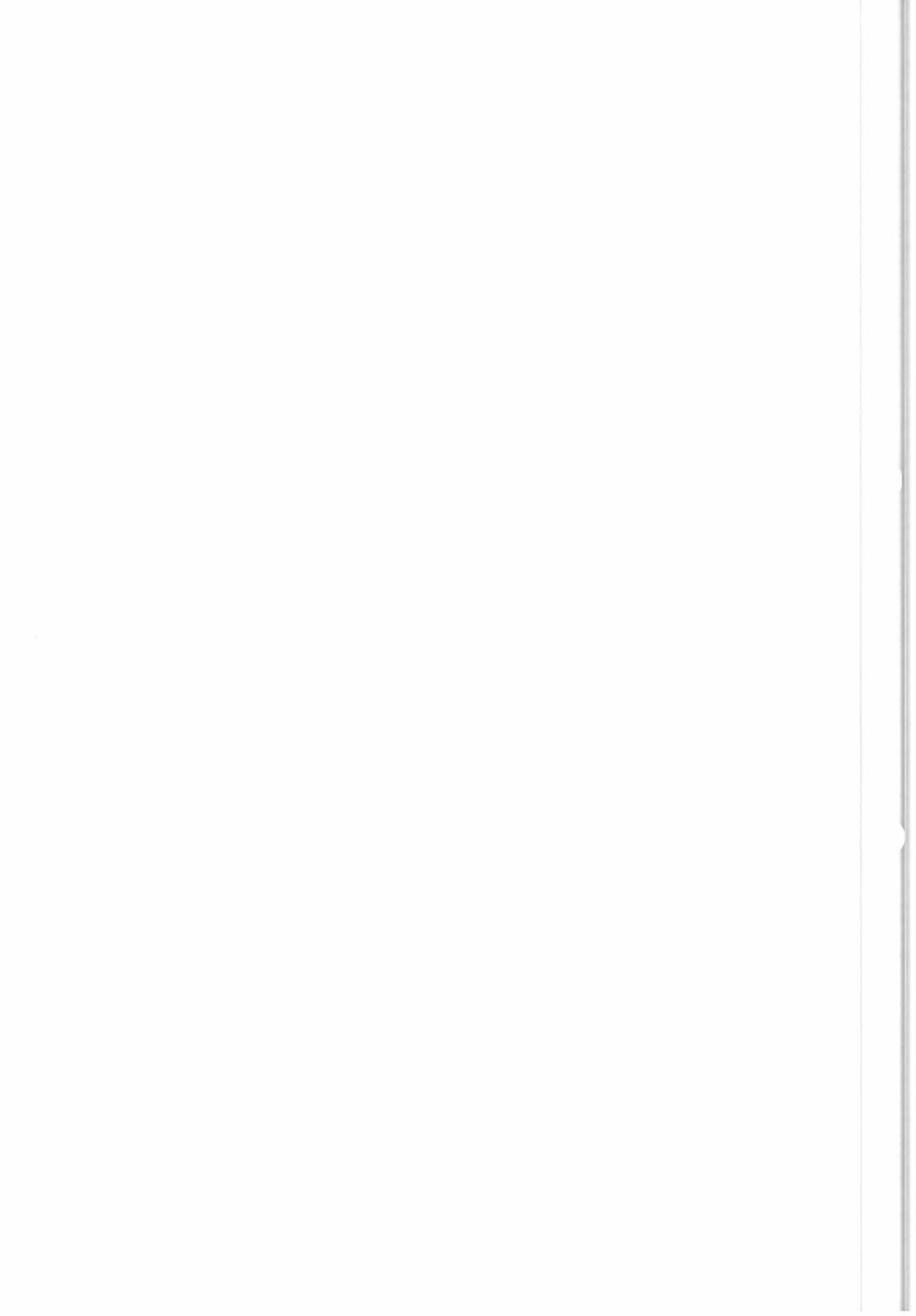


Fig. VI.2 Max. likelihood distance over ice as a function of distance off-track, L(km)
rank 1 (●), rank 2 (○), together (●)



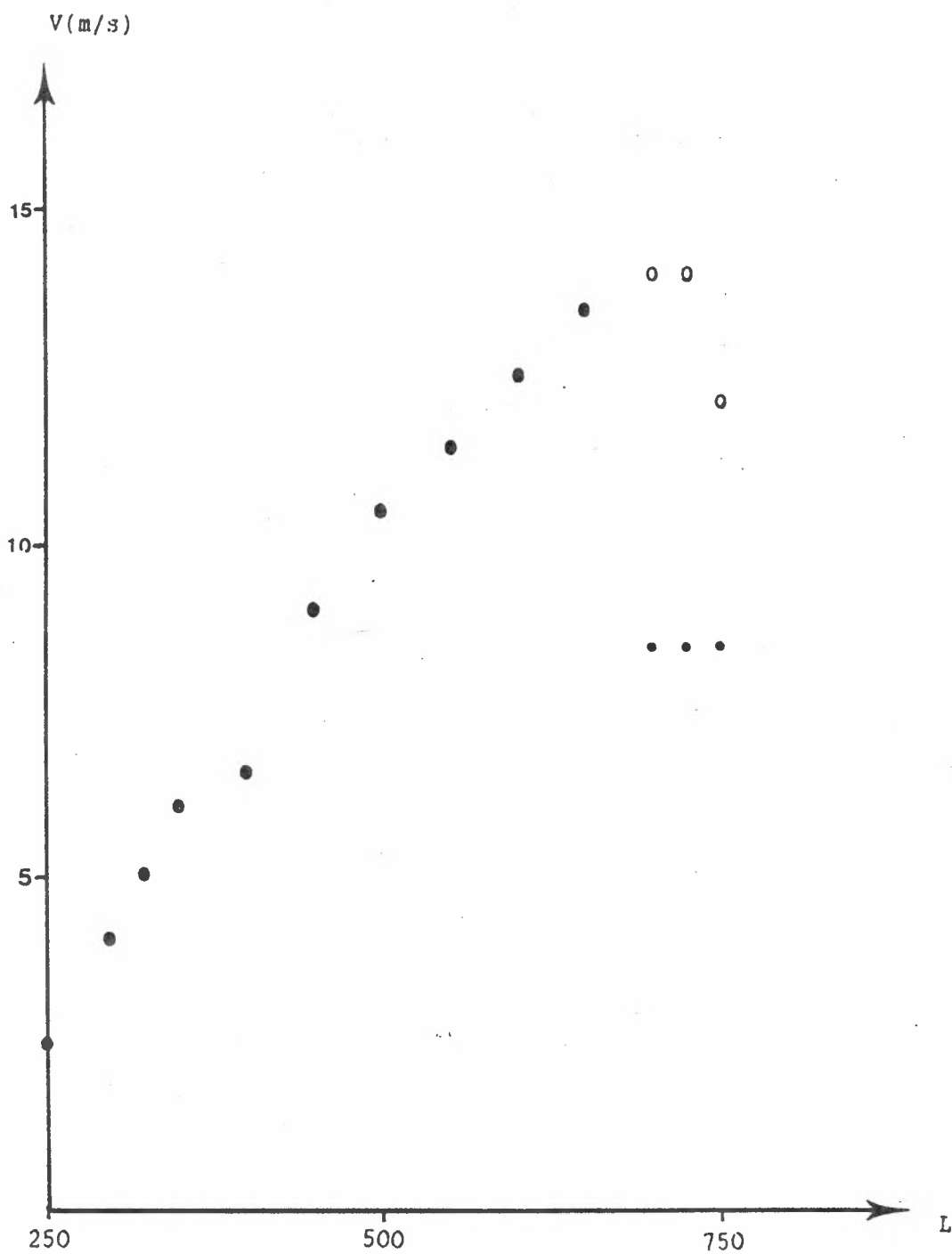
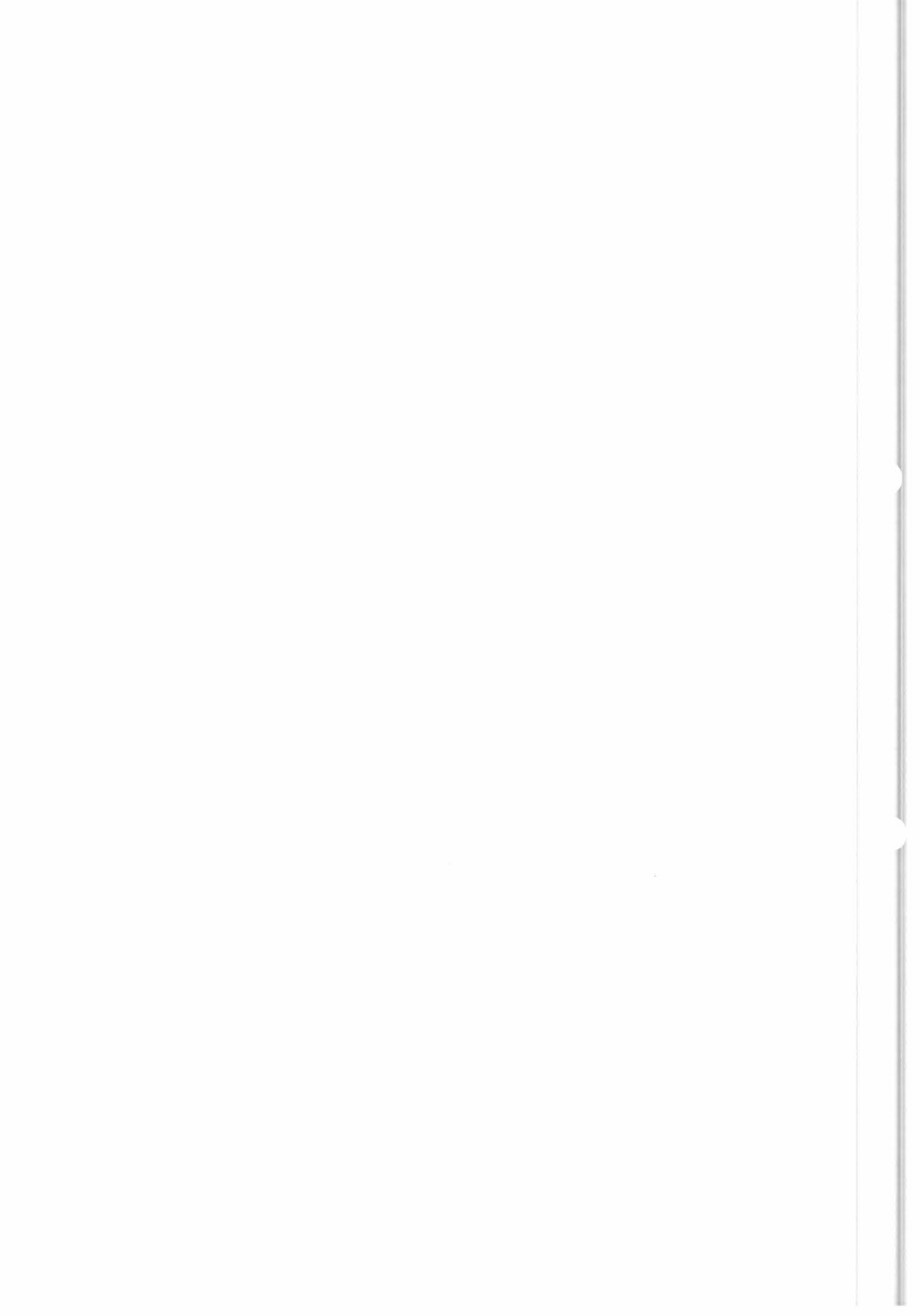


Fig. VI.3 Windspeed solutions over ice as a function of distance off-track, L (km)
rank 1 (\bullet), rank 2 (\circ), together (\bullet)



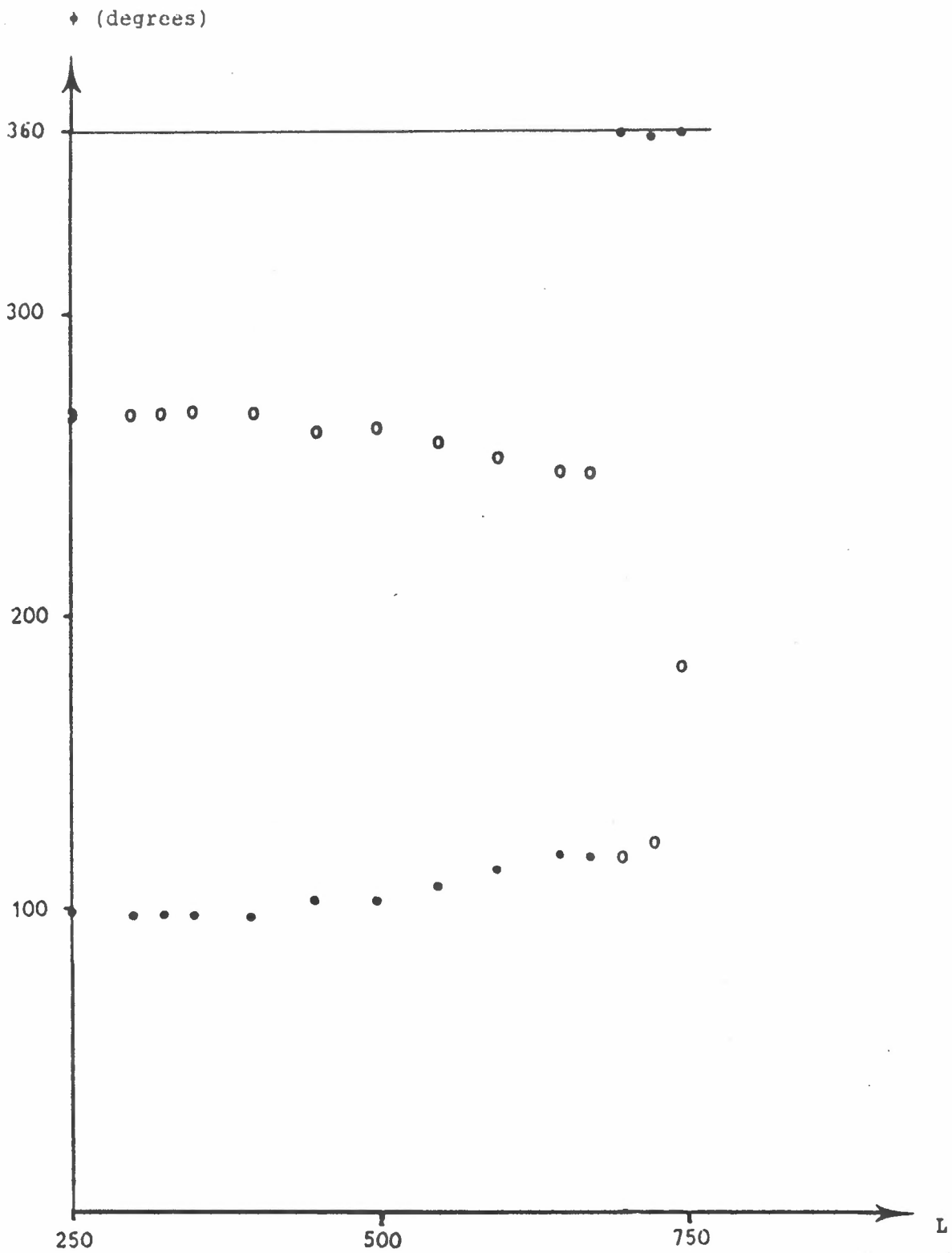
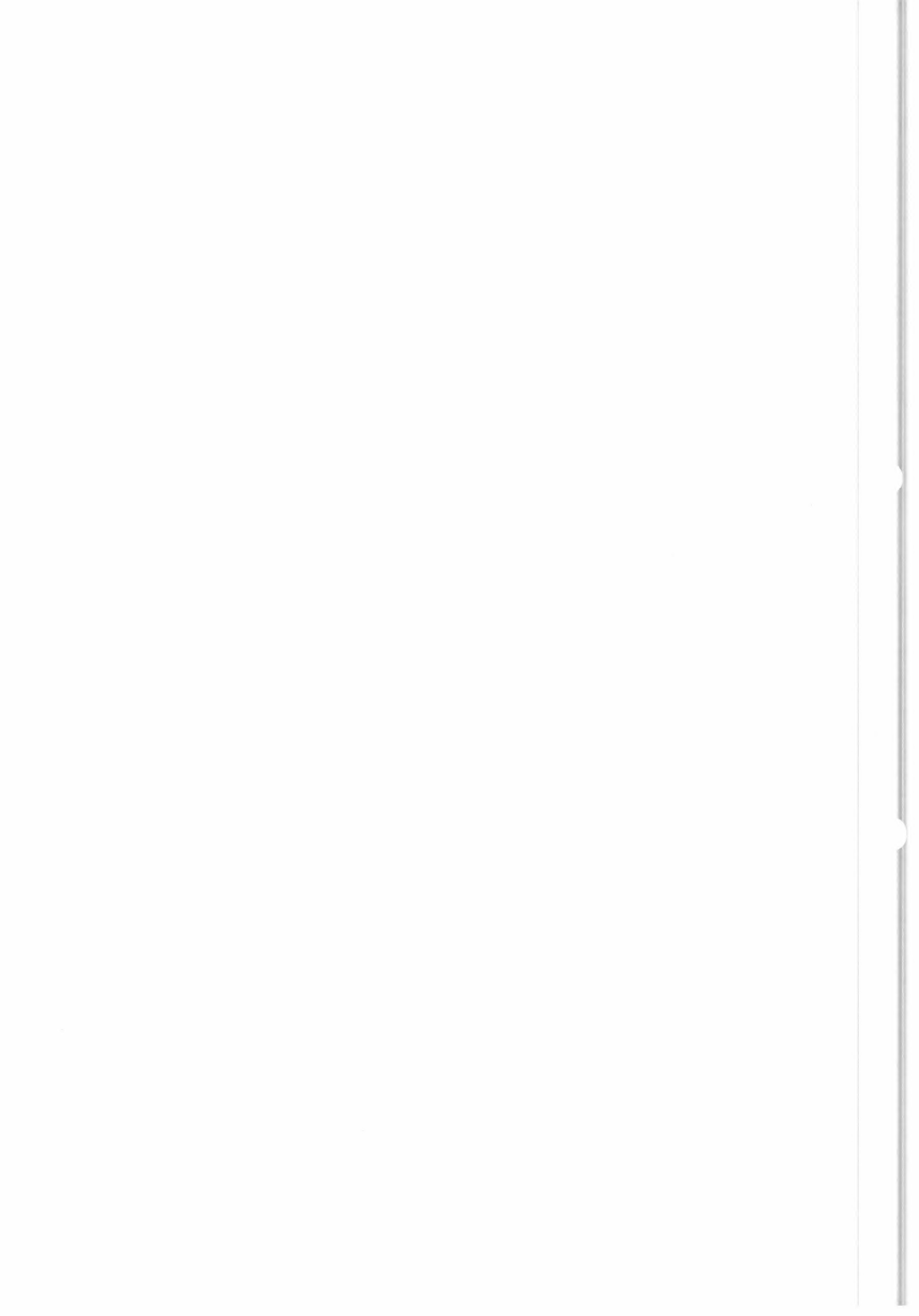


Fig. VI.4 Wind direction

Solutions over ice as a function of off-track distance, L (km).
rank 1 (•), rank 2 (○), together (●).



VI.5 Impact on wind extraction modules

It is to be expected that continuous ice-sheets will have little influence on the WIND module as it stands because the "wind" directions over ice are outside the bounds of the privileged direction sectors used in the autonomous wind de-aliasing. This fact is intrinsic to the azimuth isotropy of back-scattering from ice and will therefore remain true whatever the evolution of C-band wind back-scattering model over water. However, because ice has a "wind over water" signature, apparent winds will be computed over undetected ice areas.

VI.6 Detection of ice-covered areas

The present WIND module takes no account of possible presence of ice, counting on previous processing to discard such points, as with land. The three-day repeat period and the fairly constant nature of ice back-scattering might allow ice-detection by an appropriate correlation technique, either of the σ values of the three antennas, or using wind speed, direction and maximum likelihood distances separately.

This, done off-line, would allow an efficient and autonomous discrimination of points over the ice, considered otherwise as reasonable winds.

VII - DE-ALIASING PROCEDURE

The detailed procedure as implemented in the WIND routine, is described in the Annexed WIND report and will not be recopied here. Rather, general concepts, different methods tested and reasons for the choices made will be insisted upon.

Two automatic methods were developed, corresponding to two-beam and three-beam cases.

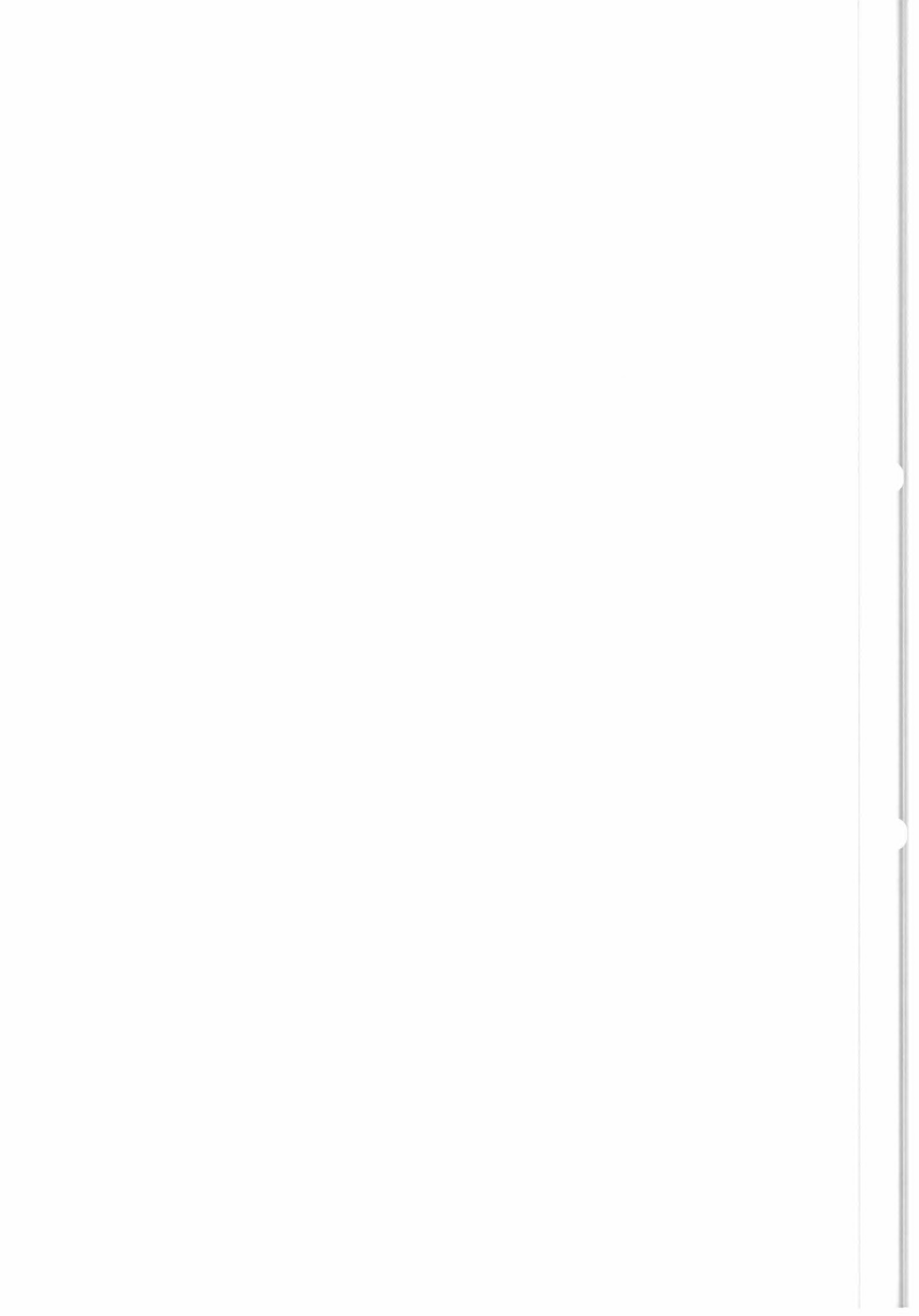
* Going from three-beam σ values to unique winds implies two successive steps : inversion and de-aliasing. We tested the two possible ways of linking these modules :

- De-aliasing before inversion
- De-aliasing after inversion

* In the two-beam cases it was evident that inversion must go before de-aliasing. In this case, as described in Par. I.4, it would be necessary to define the limits between different zones corresponding to two, three or four possible solutions. This problem is not tractable in σ -space because of the complexity of the equations, and the simplest way to treat this question is to carry out the inversion directly. Seasat experiments furnished some informations on this treatment.

An isolated two-beam zone cannot be automatically treated without human intervention because different solutions are equally probable and internal informations are insufficient.

However, two-beam zones in contact with an adjacent three-beam zone, can be partially treated, using three-beam zone information.



VII.1 General principles of de-aliasing procedure in the 3-beam case

The first idea is to determine the geographical regions of the swath where data (or possible de-aliased winds) indicates that wind directions belong to certain privileged directional windows. If direction can be determined for these data sets, direction in neighbouring zones can be determined by continuity. An area characterization module was created to connect in the same "islet" all neighbouring points having similar characteristics (in this case, belonging to one directional window).

An "islet" is formed of the subsets of points which are neighbours and share common characteristics.

For our applications, neighbourhood between two points is defined in three different ways ; two points of positions indexes (i,j) and (k,l) are :

- horizontal neighbours if $i = k$ and $j = l \pm 1$
- vertical neighbours if $j = l$ and $i = k \pm 1$
- diagonal neighbours if $i = k \pm 1$ and $j = l \pm 1$ or
 $i = k \pm 1$ and $j = l \mp 1$

After this area characterization, the swath separated into three types of islets corresponding to two mean-directions pairs : 30° or 220° and 150° or 320° ; the third type includes all others points.

In each islet, an evaluation of the data distribution is made to choose the correct direction using a statistical model.

These directional windows correspond to regions where sheets of the surface of solution are most separated (Figure VII.1).

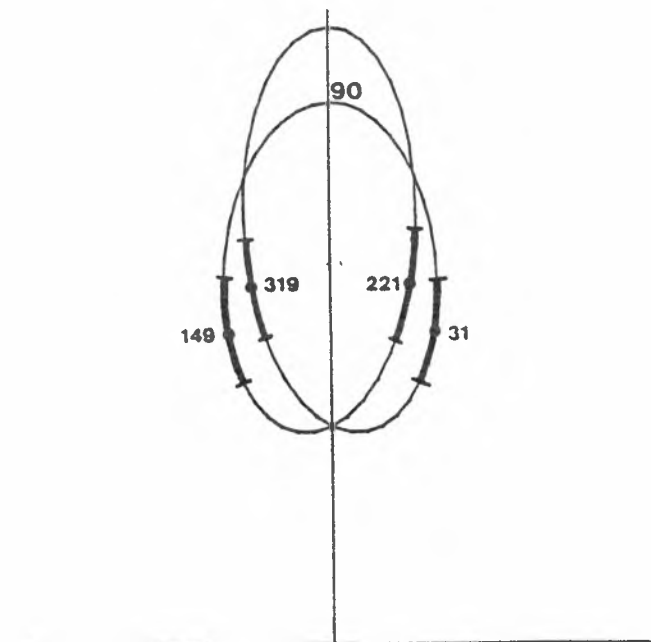
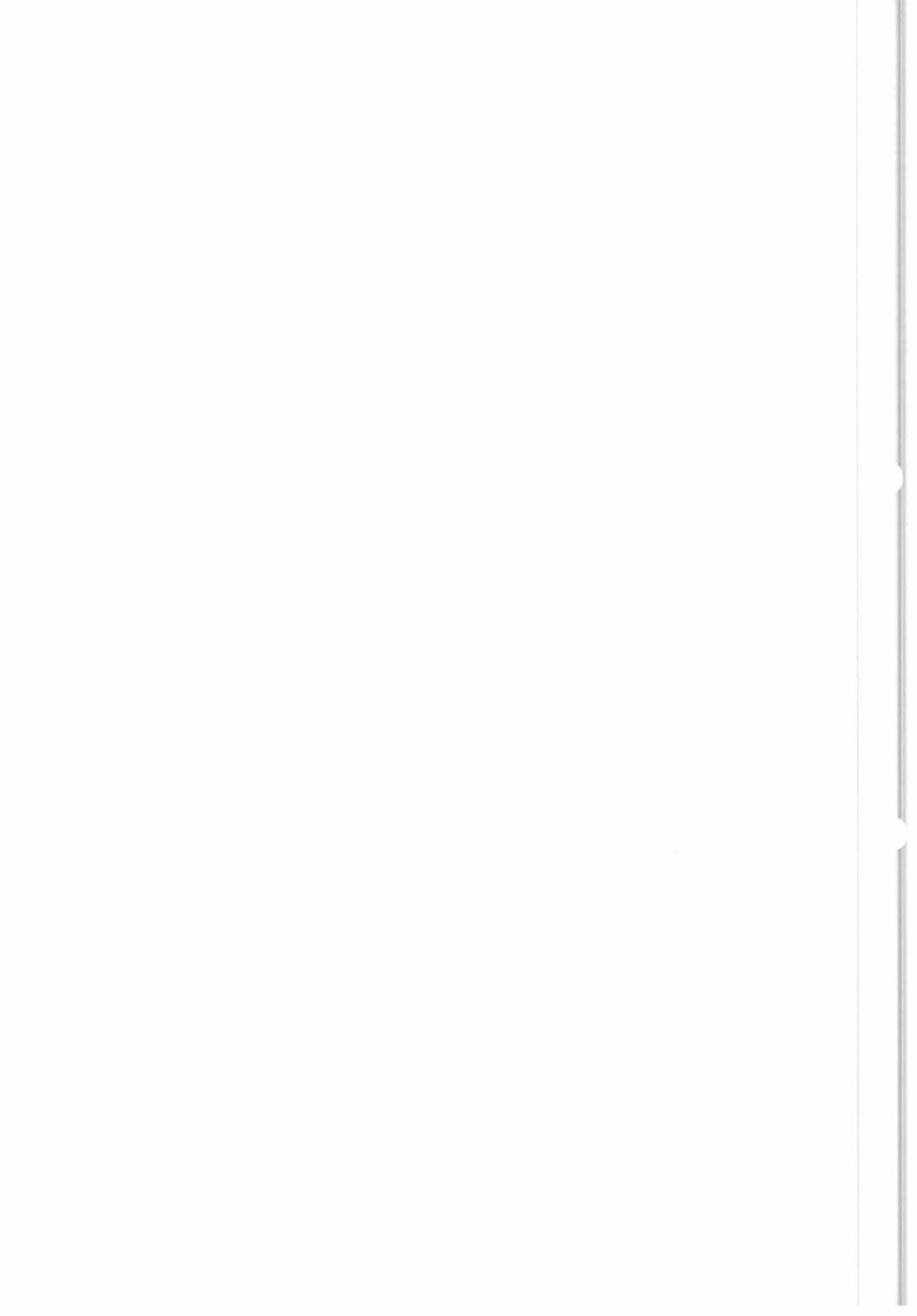


Figure VII.1 : Directional windows and corresponding mean-directions in the (V, ϕ) space



VII.1.A Ambiguity removal in σ -space

The Sigma0 model relates σ -space to (V, φ) -space. Therefore, inversion is not necessary to determine if a point belongs or not to a directional window, which can be directly defined as subsets of σ -space.

These subsets are defined as the set of points which fall within a maximum likelihood distance limit to curves on the surface of solutions whose points are at a maximum distance from the opposite sheet of solutions.

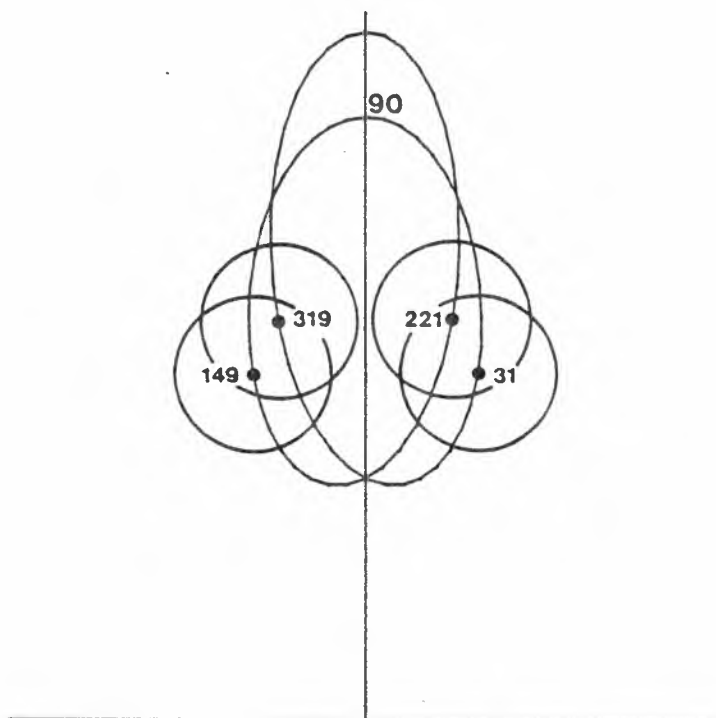
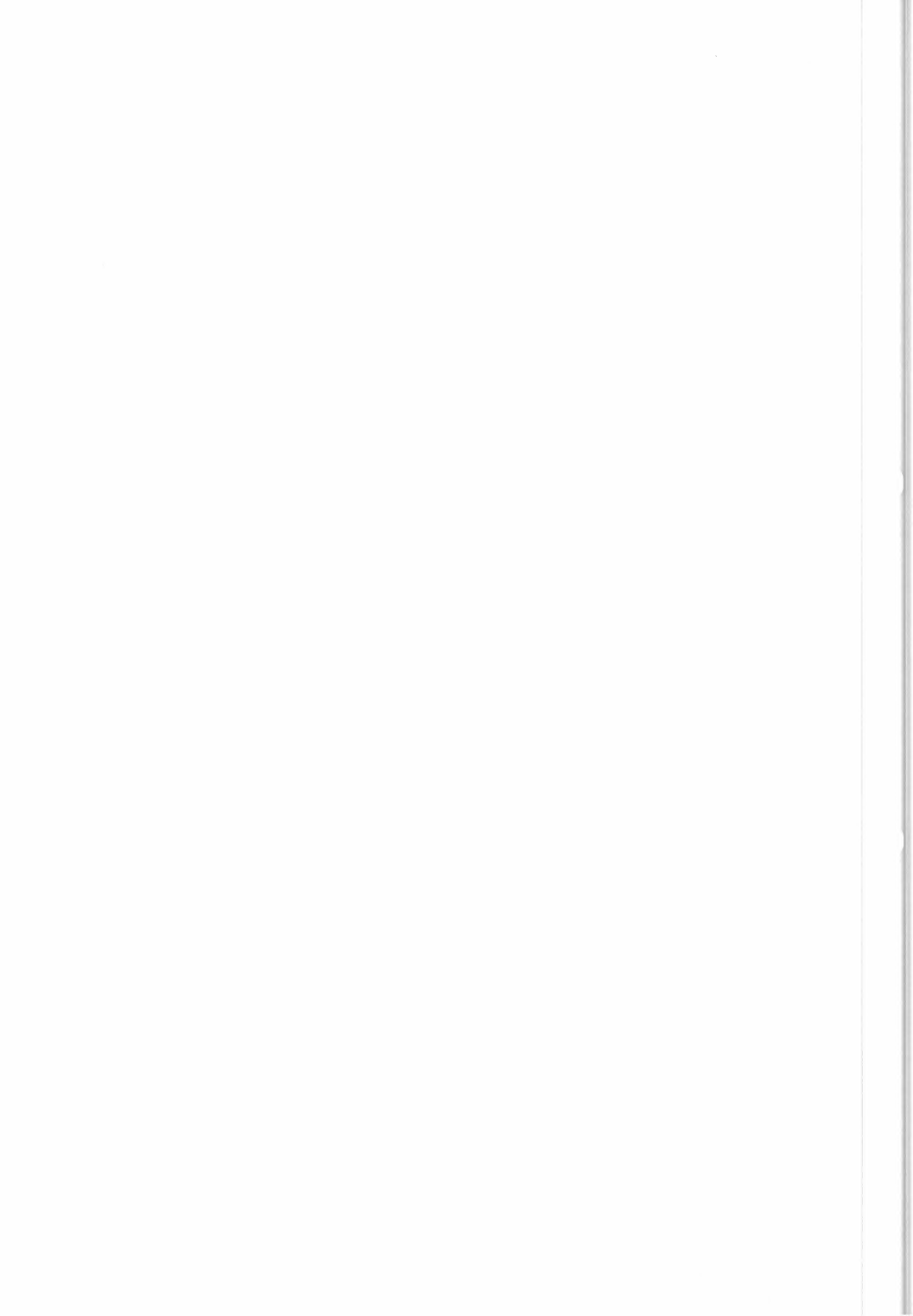


Figure VII.2 Directional windows in the σ -space

This idea is interesting because it could divide computing time by four (search of solutions could be made over 90° instead of 360°) ; but it presents three important drawbacks :

- Because of the complicated geometry of the model in σ -space, there is no rigorous test associated to a level of probability which can be found. The method arrived at was to count the number of points in subsets of σ -space corresponding to each directional window and to choose the direction of the subset having the largest number of points.
- Noise on Sigma0 triplets creates many small islets which are not

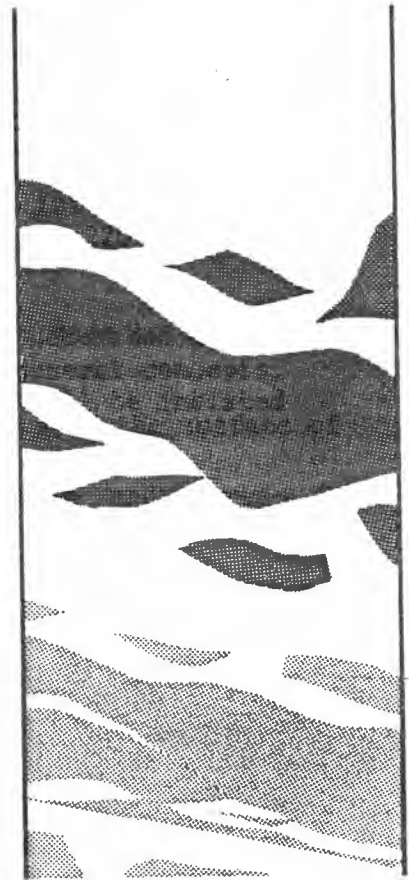


significant in size. It is possible to fix a minimum number of points in an islet to discard those that are too small, but this limit is difficult to determine. In fact, if wind direction variations are important, islets will be narrow (geographically) and may even be fragmented into small segments.

On the other hand, a slow variation of the wind direction will provoke a large islet accompanied by a lot of little islets (Figure VII.3).

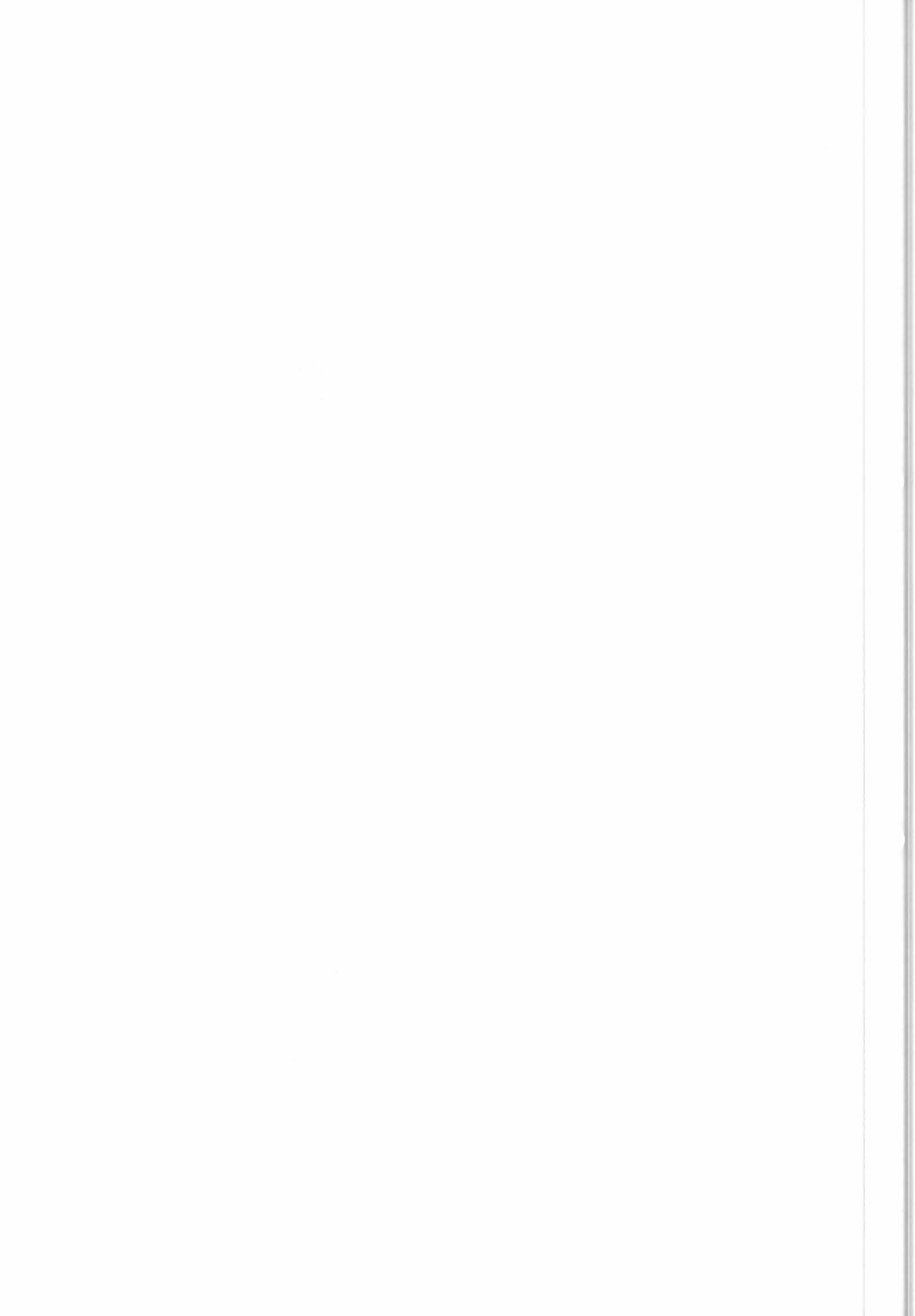


a : narrow islet



b : large islet

Figure VII.3 : Examples of islet



- The last problem is the geographical non-homogeneity of an islet following the wind variation. The Figure VII.4 shows that σ -space subsets used to construct islets are not superposed

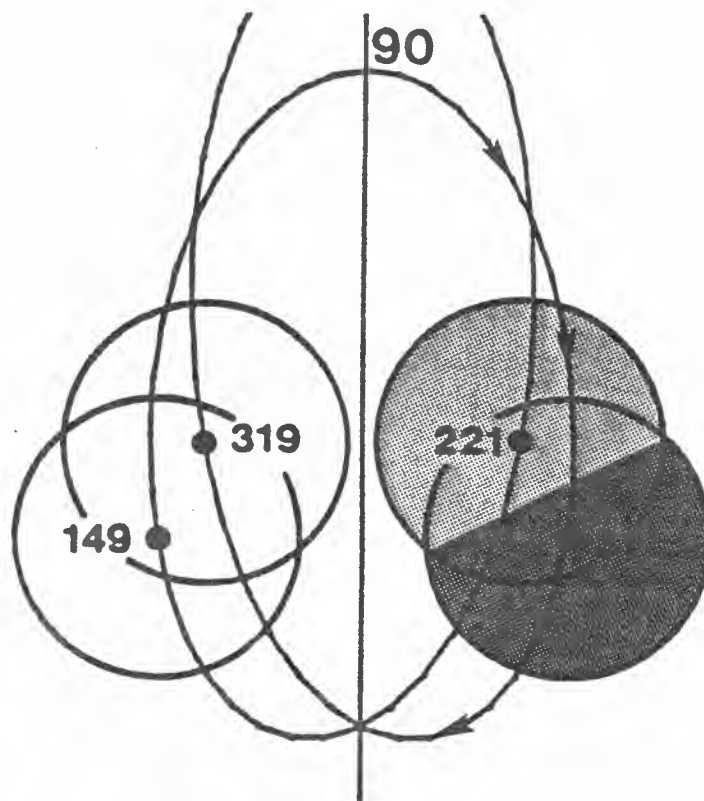


Figure VII.4 : Detail of the Figure VII.2

If the wind direction variation follows the arrows along the continuous line, σ -triplets fall first in the pale grey region and only afterwards in the dark grey region (which corresponds to the good solution).

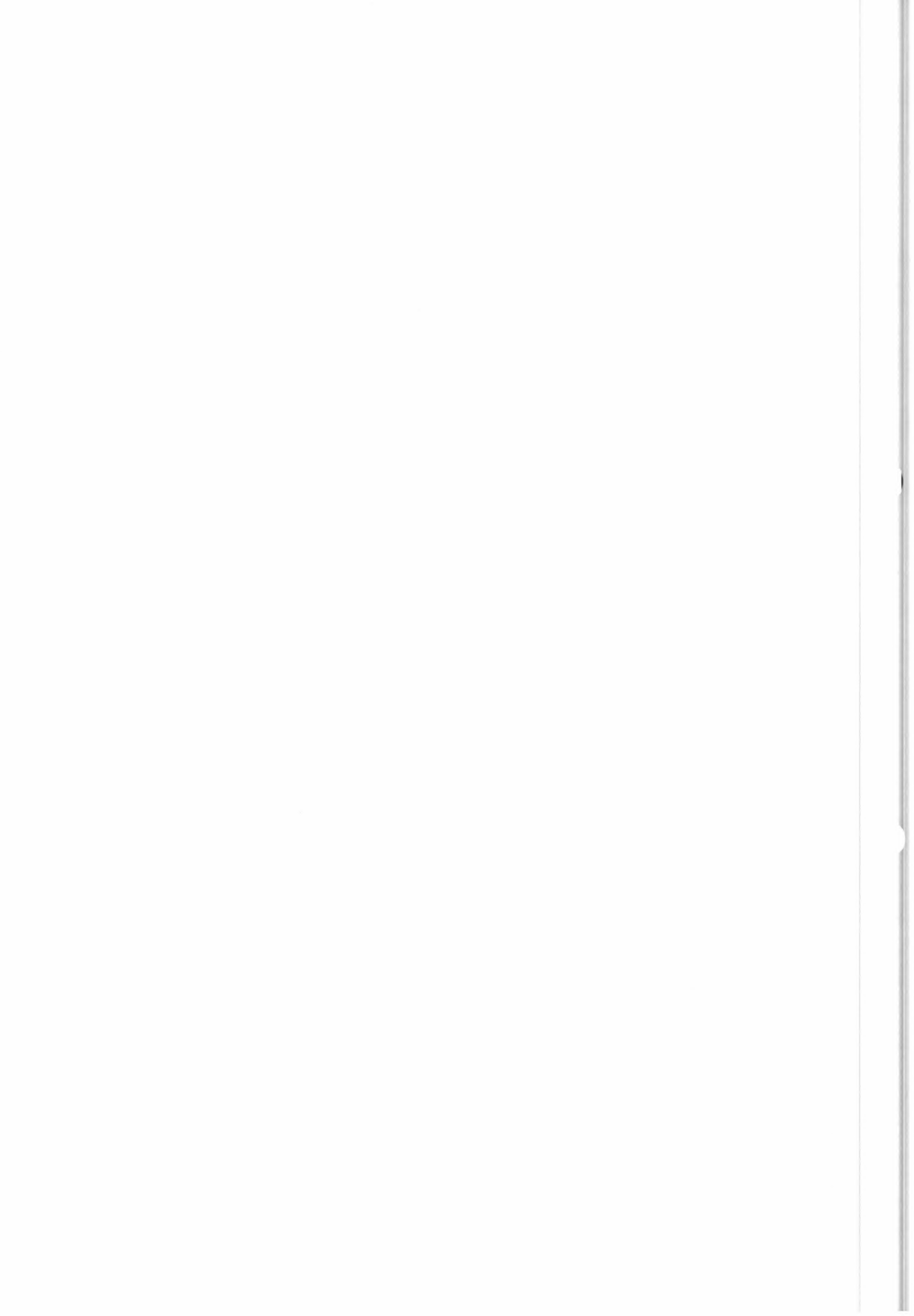
For a given geographical islet, the quality of de-aliasing will depend on the direction distribution of points in it. If too many points fall in the pale grey zone, the wrong direction will be chosen.

The problem of finding optimal subsets in σ -space proved too difficult because it depends on incidence angle (or cross-track distance). This difficulty made it impossible to resolve the two problems previously mentioned.

This method was finally abandoned on account of these problems.

VII.1.B Ambiguity removal in the (V, φ) space

The procedure was, initially, exactly the same with the four regions of the σ -space replaced by four regions on the (V, φ) space (surface of solutions, see Figure VII.1), because inversion is simply a projection of the σ -space on the V, φ space. This method avoids the first two problems of de-aliasing in σ -space :



- It is possible to estimate the distribution of good solutions (table VII.1).

Rank	1	2	3	4	5	6
Number	6588	2532	122	12	1	0
%	71.2	27.4	1.3	0.1	0.0	0.0

Table VII.1 Distribution of good solutions by rank (calculated over 9255 points)

- Noise on (V, φ) is less than an σ -triplets (1 dimension less)

The geographic non-homogeneity remains ; to suppress it, continuity of the wind field is invoked. Starting from the first point in the swath, either with the rank 1 or 2 direction, two wind fields are constructed, nominally 180° apart. (this is done line by line, from the outside to the inside of the swath). The direction of a point in the line is determined as being the closest to the mean of the (previously determined) directions of the two preceding points. In the same way the direction of the first point in the line is determined from the first point in the two preceding lines. A detailed description of procedures used in case points are missing or doubtful is given in the Detailed Program Description.

The good field has the greater number of rank 1 solutions. Moreover, because the field is continuous, points in islets belong to the same sheet of solutions. The bad one has a small number of rank 1 solutions.

At this point of our study, we come to the conclusion that using islets was really useless and unnecessarily complicated. It is much simpler to choose between the two wind fields directly using a global count of rank 1 (N_1) and rank 2 (N_2) solutions in the swath.

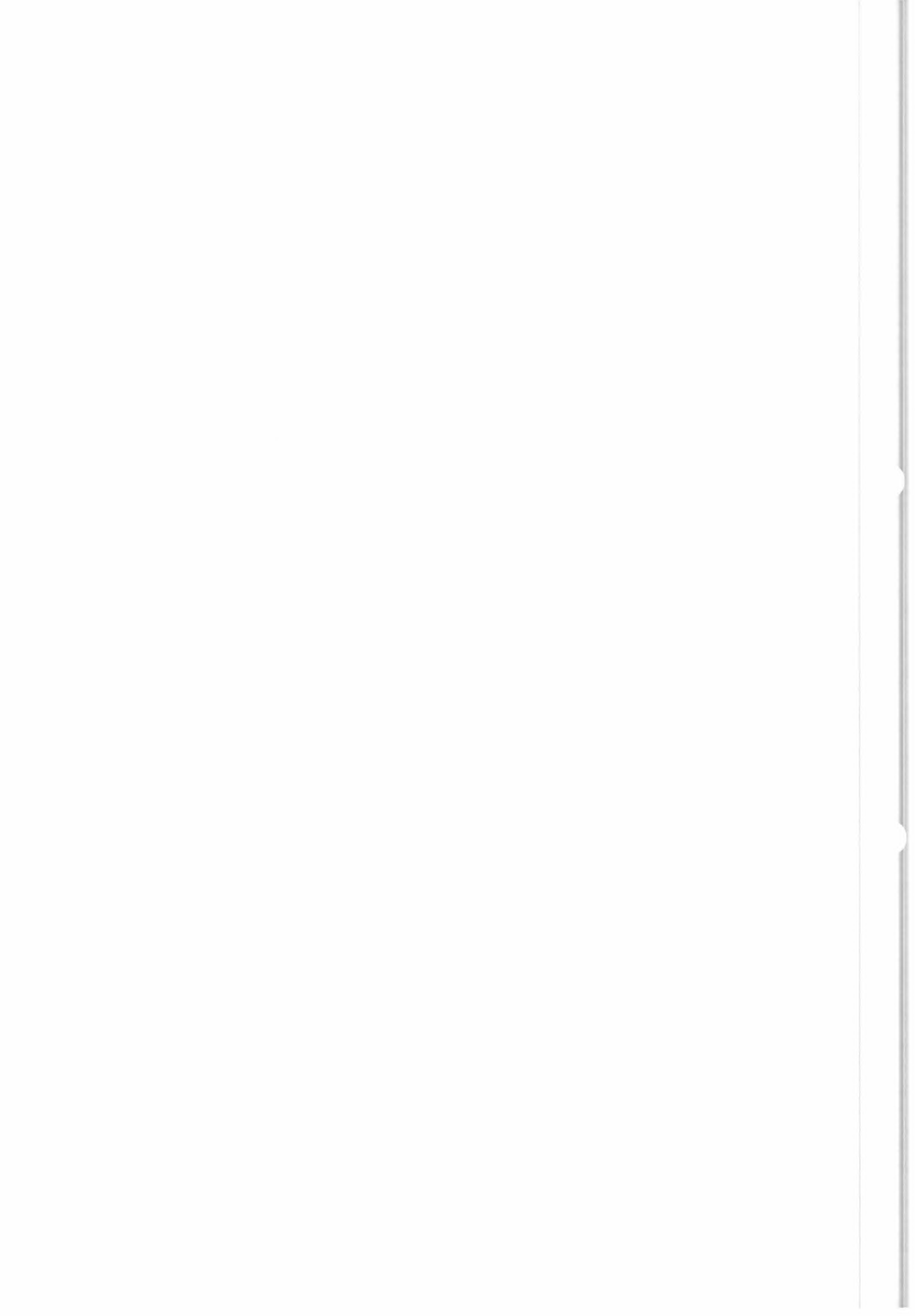
The ratio $N_1 / (N_1 + N_2)$ is the criterion chosen to test these two possible wind fields. Normally, it takes a value close to 0.7 for the good wind field and close to 0.3 for the other.

To increase this ratio, the N_1 and N_2 calculation is limited to the directional windows already described. Then, for the good wind field $N_1 / (N_1 + N_2)$ can increase to 0.9.

The confidence in this ratio decreases as the number of points in directional windows ($N_1 + N_2$). If this value is too small, (actually fixed at 100, to be confirmed by experience) this autonomous criterion is replaced by comparison with a meteorological wind field.

The meteorological test is simply a comparison of the two wind fields with a meteorological wind field using a Normalized Scalar Product (NSP) defined below.

For each point of the scatterometer grid, the North-South and East-West components of the distance to the nearest point of the meteorological grid are computed. If these distances are less than



12.5 km, informations (wind speed and direction) of this meteorological point are taken to calculate the normalized scalar product with the formula :

$$NSP = \frac{\sum V_m * V * \cos (D_m - D)}{\sum V_m * V} \quad (1)$$

where V_m and D_m are the meteorological wind speed and direction, and V and D are the scatterometer wind speed and direction.

The NSP can take any values between -1 and +1, depending on whether fields are badly or well correlated.

If in real-time processing the meteorological wind field is not available, the NSP is set to -1. In this case meteorological de-aliasing is not carried out ; a flag indicates that it was not successful.

Up to now, we have only considered rank 1 and rank 2 solutions, and some errors can remain. A test on $N_1 / N_1 + N_2$ or on the normalized scalar product, ensures that globally the field chosen is good.

To find errors, each point will be compared to its eight neighbouring points. Three methods were tested and give similar results.

$$1) S = \min_j \sum_{i=1}^8 (\varphi_j - \varphi_i) \quad (2)$$

$$2) \bar{\varphi} : \text{direction of } \vec{V} = \frac{1}{8} \sum_{i=1}^8 \vec{V}_i \quad (3)$$

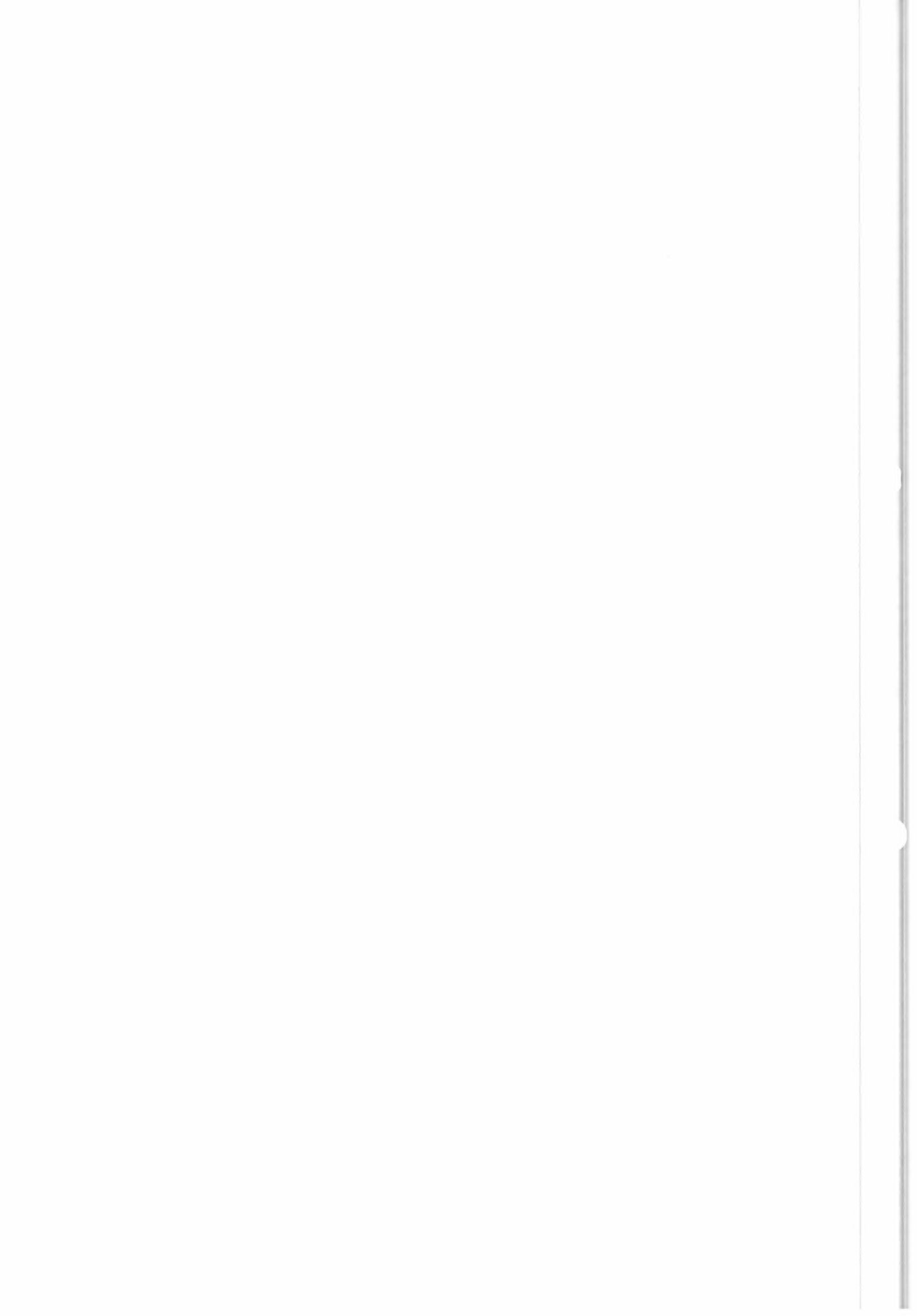
$$S = \min_j |\bar{\varphi} - \varphi_j|$$

$$3) S = \min_j \frac{1}{n} \sum_{i=1}^8 ||\vec{V}_j - \vec{V}_i|| \quad (4)$$

i is the neighbouring points index and j the rank of the central point.

The solution of the central point is replaced by that found, if one difference $|\varphi_j - \varphi_i|$ is greater than a threshold (ecmini). This algorithm is used twice with different values of threshold :

- To correct possible errors (ecmini = 60°). This pass is only applied on rank 1 and 2 solutions, the test on ecmini speeding up the operation
- To consider the four solutions (ecmini = 0°). This allows the insertion of good rank 3 or 4 solutions



VII.2 Two-beam ambiguity removal

This method deals only with the beginning and end of swaths, which correspond to scatterometer switchings on and off.

All neighbouring three-beam areas must be previously treated. In fact, the method consist in extending three-beam information into two-beam areas.

VII.2.A Two-beam area description

When the scatterometer is switched on, fore beam will not illuminate a trapezoid including 361 pixels (Figure VII.5). Consequently, this surface will have only informations coming from central and aft-beam.

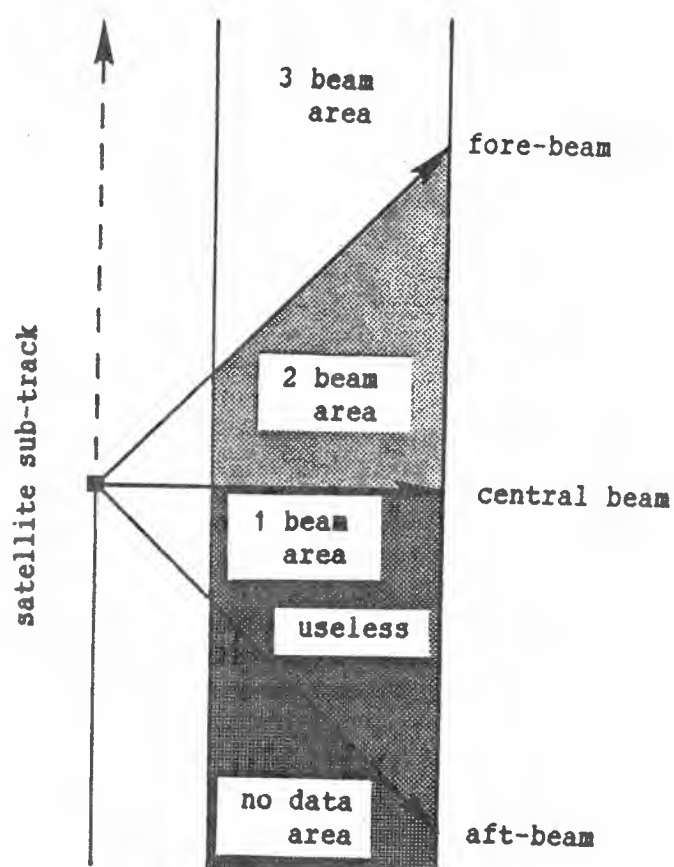
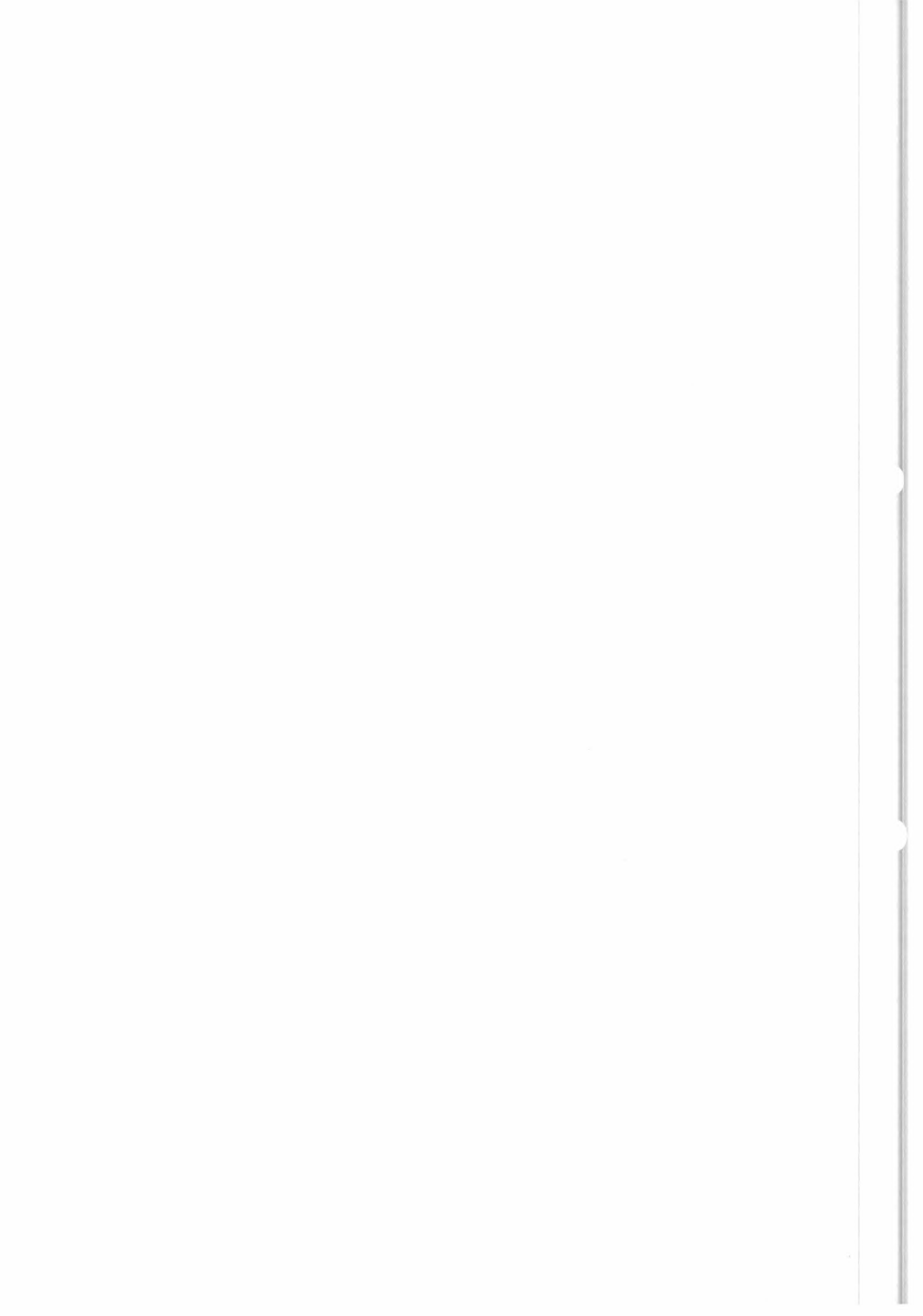


Figure VII.5 Scatterometer switching on



VII.2.B Basis of the method

Projection of the surface of solution (presented on Figure I.3), on $\sigma_F - \sigma_C$ or $\sigma_R - \sigma_C$ planes presents three types of points (indices F, C and R correspond respectively to fore, central and rear beam) (Figure VII.6).

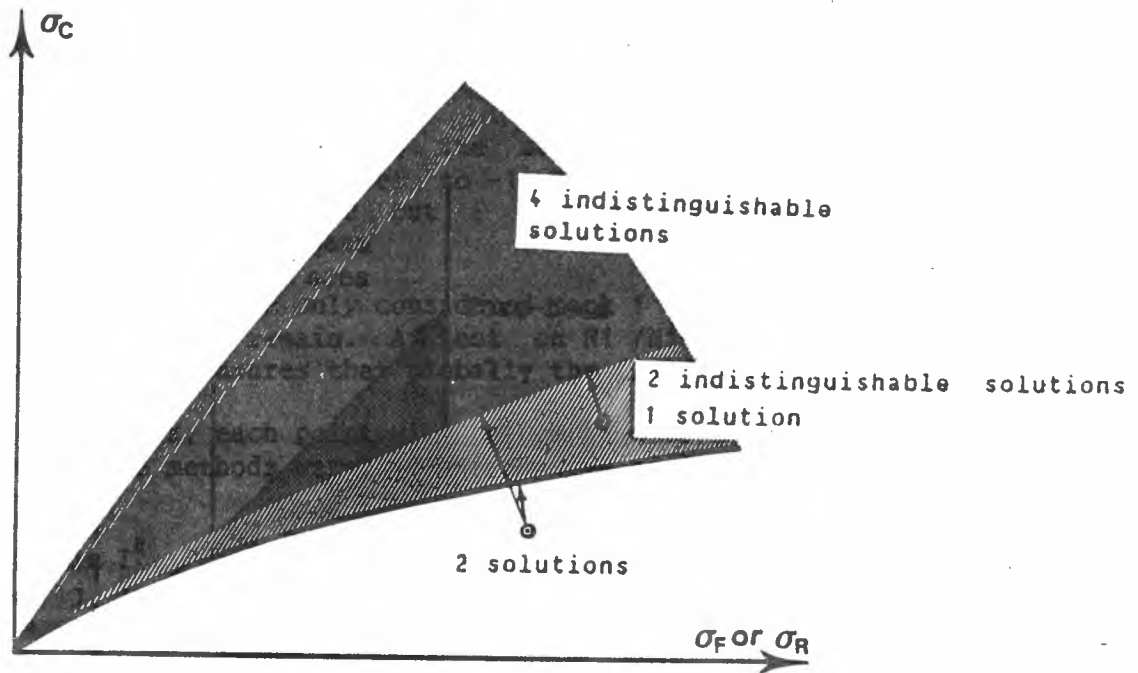
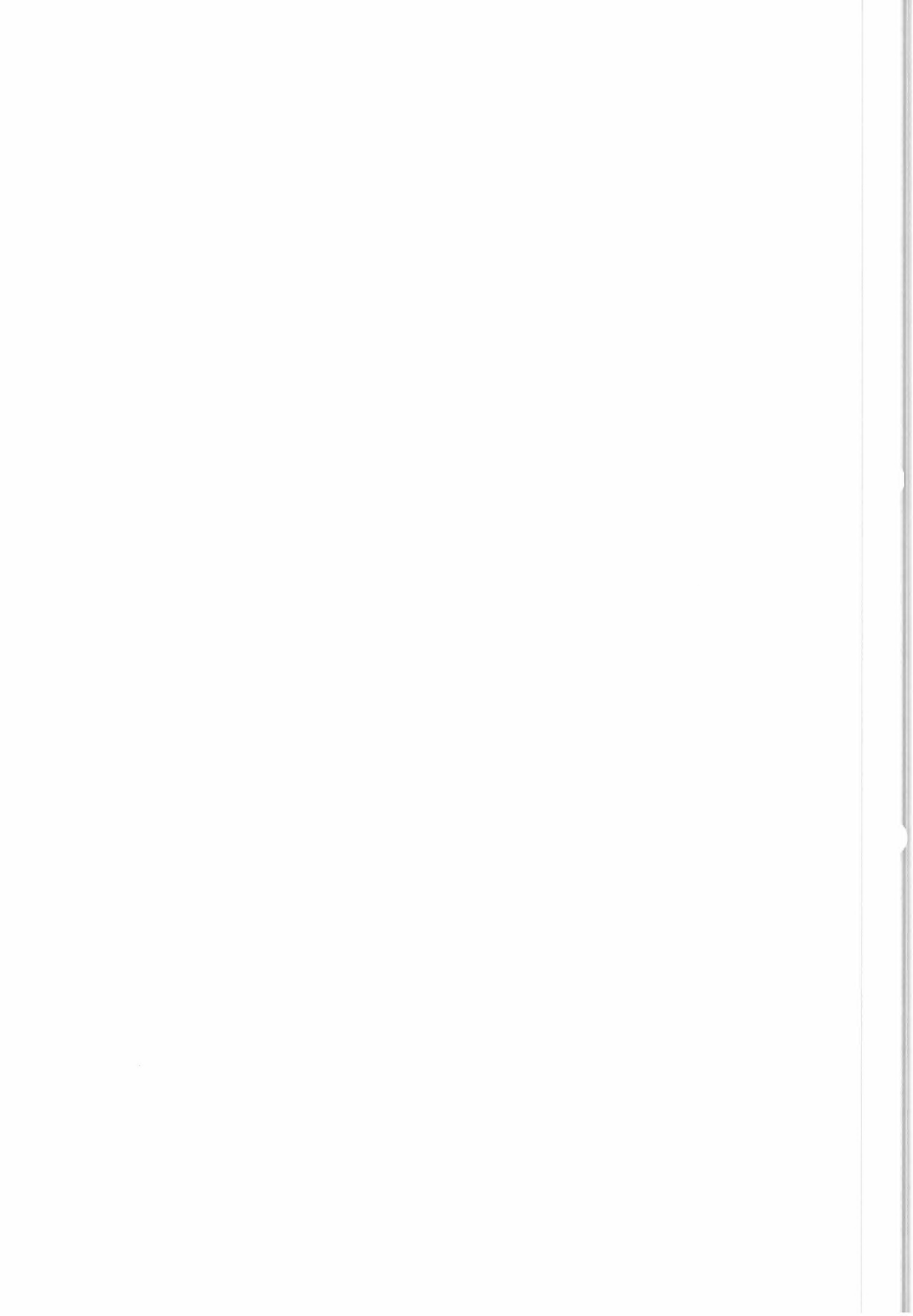


Figure VII.6 Projection of the surface of solution of the $\sigma_F - \sigma_C$ or $\sigma_R - \sigma_C$ planes

The central area corresponds to four indistinguishable solutions. Intermediate areas correspond to two indistinguishable solutions, plus one solution on the curve limiting this area to the central one. Outer areas have two solutions on the two curves limiting different areas.

Directions corresponding to each limit depend only of the model used and can be a priori calculated.

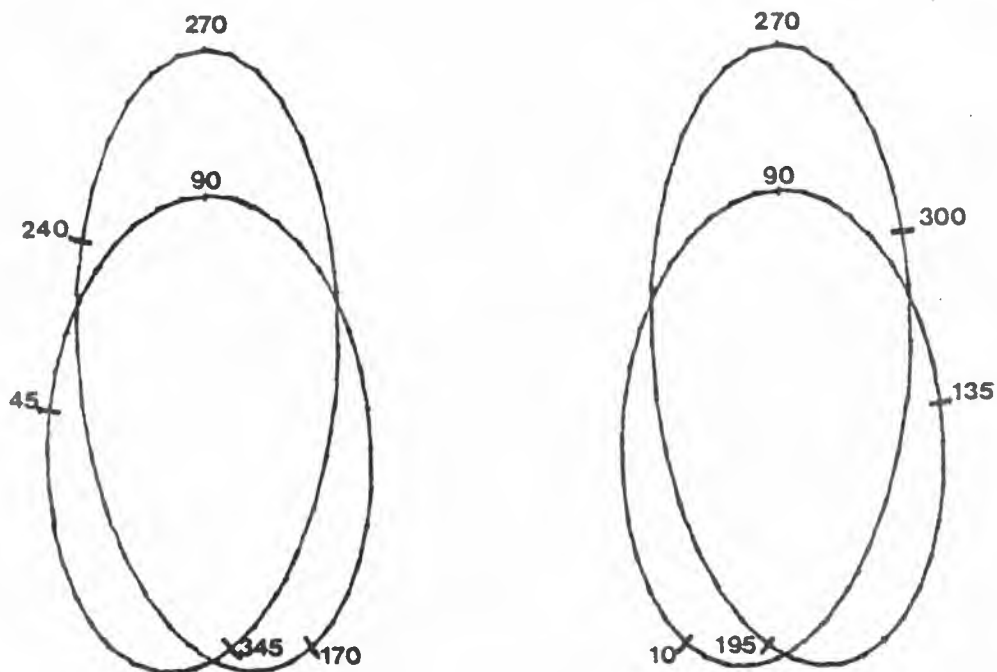
After wind retrieval, a point outside the surface will always give two solutions corresponding to one of the two possible direction pairs presented in table VII.2.



Swath	Couple 1	Couple 2
beginning	240°/45°	170°/345°
end	300°/135°	10°/195°

Table VII.2 Possible pairs of solutions for an outer point
(rank1/rank2)

Those directions can be found on the surface of solutions (cut by a vertical plane perpendicular to its plane of symmetry) (Figure VII.7).



a : Beginning of the swath

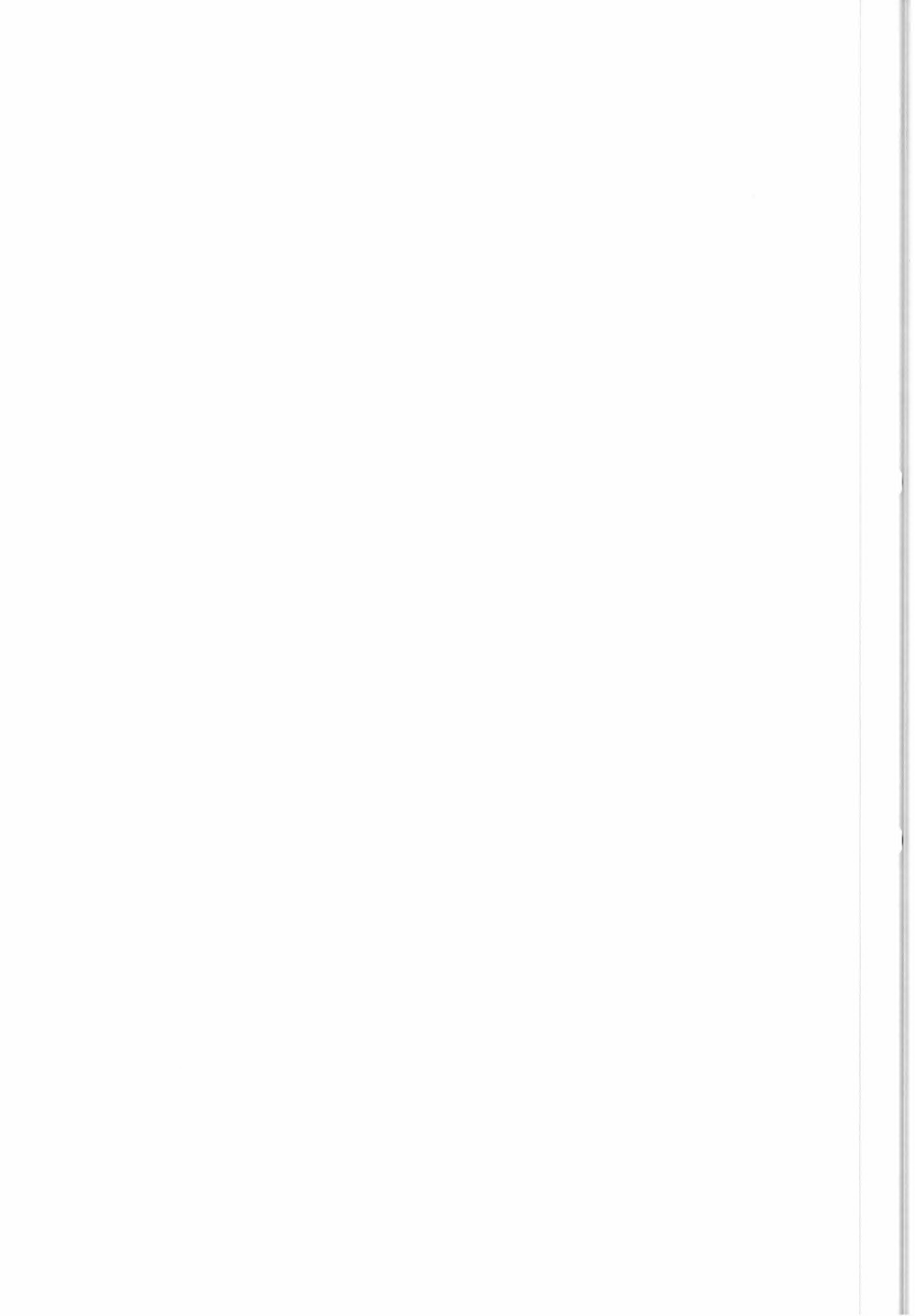
b : End of the swath

Figure VII.7 Direction of limiting curves (degrees)

They are also presented on a compass-card for a switching-on situation (Figure VII.8).

This compass-card is divided in four sectors with mean directions : 15°, 107.5°, 250°, 292.5°. A point in the central area will have four solutions in each of these four sectors.

In each two-beam area, it is possible to draw a fitting curve through points of each two-solution type.



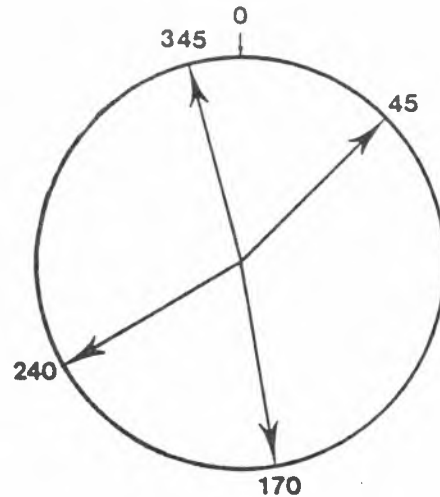


Figure VII.8 Direction of limiting curves at a beginning of the swath

These curves limit intermediate zones. Each zone in contact with three-beam points previously de-aliased can be treated using directions of those three-beam points.

All curves running along those intermediate zones can also be de-aliased.

Remaining zones can be treated if boundary curves give at least two different compatible directions.

In this algorithm, we substitute curves by maximum likelihood straight-lines. The small extent of two-beam areas makes this approximation reasonable in general.

VII.3 Compatibility

De-aliasing procedures are made on segments of 114 lines (6 products of 19 lines) to respect memory space constraints.

Overlapping of consecutive segments allows verification of compatibility. This overlap is of two-products length, in order to completely cover two-beam areas when necessary.

In this procedure, de-aliased directions and wind-speeds of the two segments are compared ; they are declared compatible if less than 5 points (out of 2×361) are different ; this is because a few points may be different because of end effects. If compatibility is not verified, the segment considered is re-treated a second time, imposing a meteorological wind field comparison.

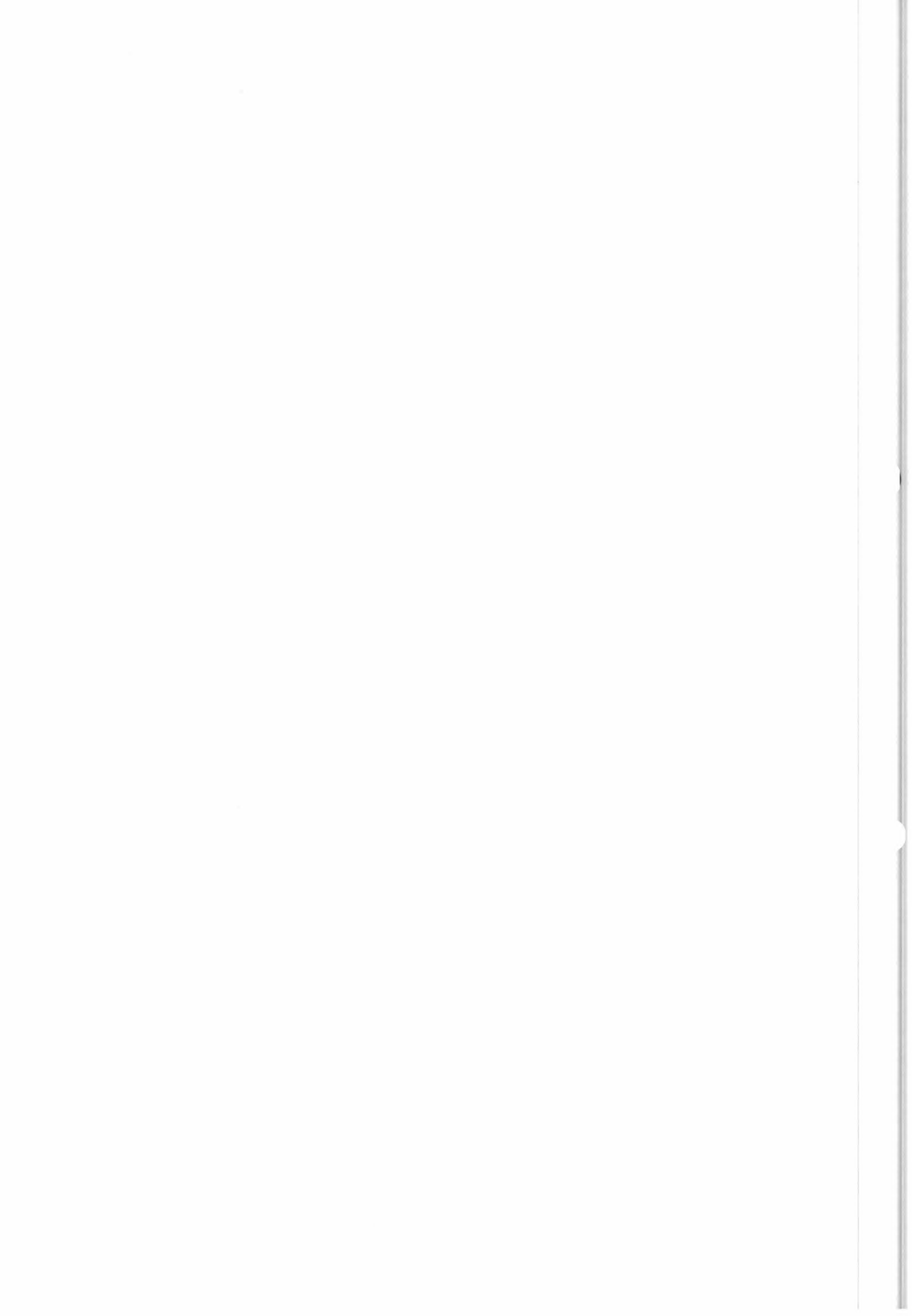
VII.4 Tests

Tests are made on two groups of five files, furnished by David OFFILER.

Informations are not identical in these two groups, and the WIND calling program is different.

WINTO tests files WINTST01 to WINTST05, and WINT1, files WINTST11 to WINTST15.

No file has more than 114 lines. To test segmentation of the swath in segments of 114 lines, the files of the first group were completed by their mirror image (line 107 is identical to line 106, 108 to 105, ..., line 212 to line 1).



This method gives 212 lines for files 01 to 04 and 162 line for files 05. This last file contains two 2-beam areas at each extremity of the swath.

VII.4.A Tests without bias

Adjustment of wind was made with the first group of files. The second group of files was used to verify behaviour of the algorithm without modification in WIND.

Tables 7, 8 and 9 present these results and give respectively :

- Distribution of each type of points (land, low winds, not calculated by WINRET, 3-beam cases, 2-beam cases)
- Results of three beam cases
- Results of two beam cases

WIND tests results

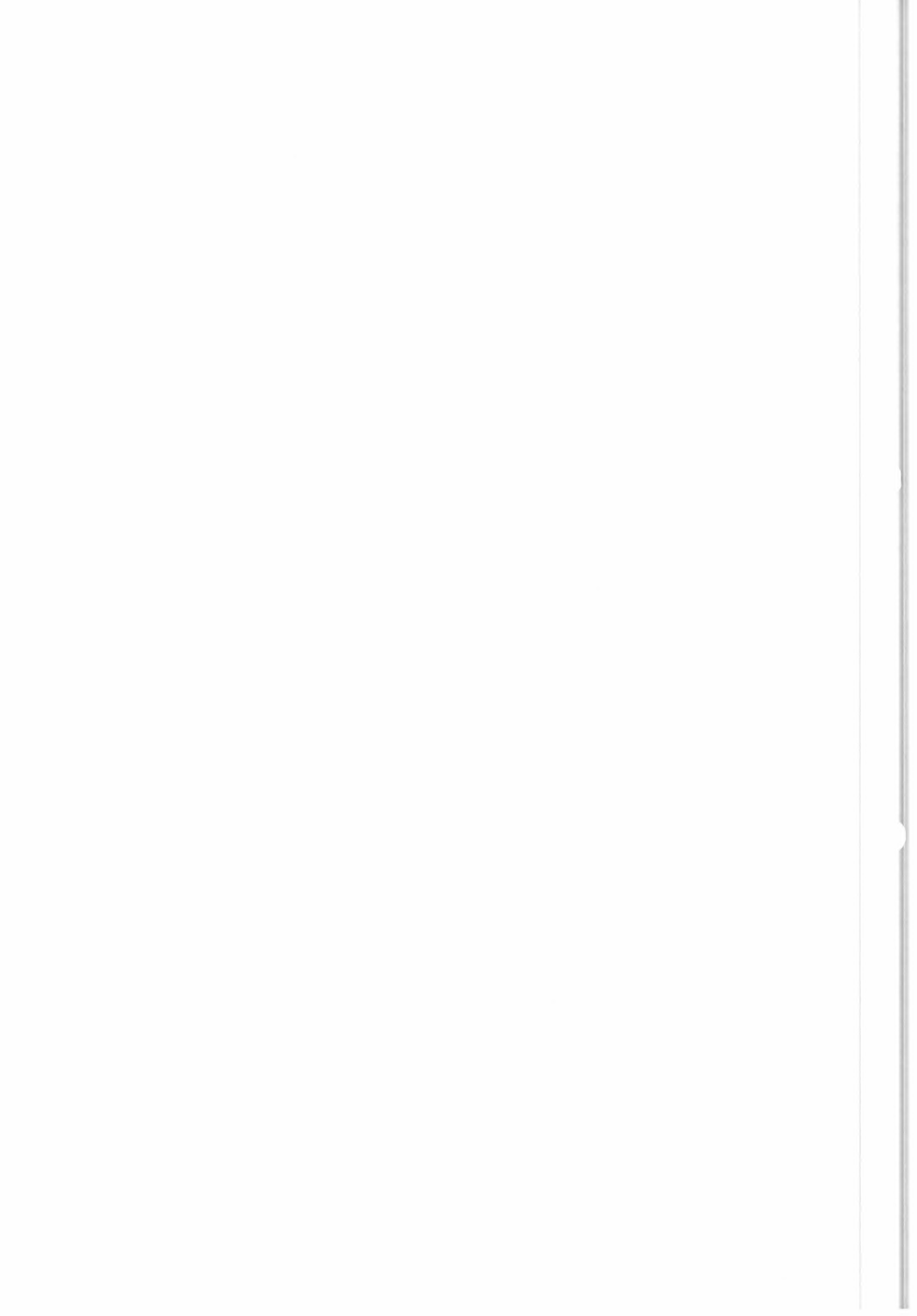
File	01	02	03	04	05	11	12	13	14	15	Total	%
Land	30	28	30	30	220	32	97	4	1	50	406	1.45
Low wind	48	0	18	174	4	75	13	5	28	241	582	2.07
No wind retrieval	0	0	0	0	0	0	1	0	0	0	1	0.00
3 beam	3950	4000	3980	3824	2618	1067	1090	1136	1140	883	23688	84.41
2 beam	0	0	0	0	236	631	594	660	636	628	3385	12.06

Table 7 : Points distribution

WIND tests results

File	01	02	03	04	05	11	12	13	14	15	Total	%
3 beam	3950	4000	3980	3824	2618	1067	1090	1136	1140	883	23688	100.00
No amb. removal	0	0	0	0	0	0	0	0	0	3	3	0.01
$ei < 30^\circ$	3948	3999	3978	3816	2618	1067	1089	1131	1139	879	23661	99.89
$30^\circ < ei < 60^\circ$	2	1	2	8	0	0	1	5	1	4	24	0.10
$60^\circ < ei$	0	0	0	0	0	0	0	0	0	0	0	0.00

Table 8 : 3 beam cases



WIND tests results

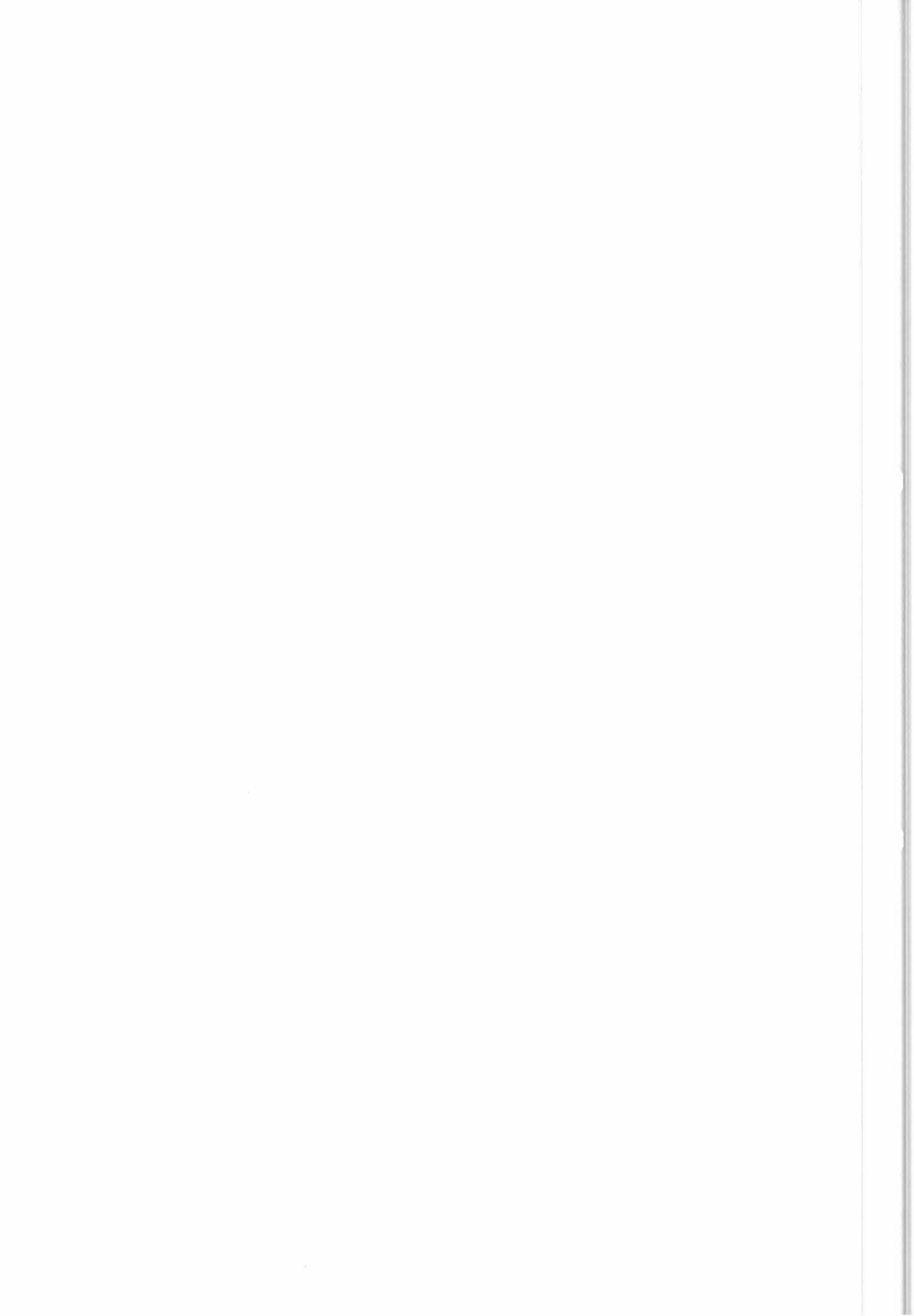
File	01	02	03	04	05	11	12	13	14	15	Total	%
2 beam	0	0	0	0	236	631	594	660	636	628	3385	100.00
No amb. removal					9	43	121	337	552	0	1062	31.37
$ei < 30^\circ$					227	575	450	322	84	625	2283	67.44
$30^\circ < ei < 60^\circ$					0	0	9	1	0	3	13	0.38
$60^\circ < ei$					0	13	14	0	0	0	27	0.20

Table 9 : 2 beam cases

Table 10 gives bias and standard deviation on wind speed and wind direction for the ten test-files.

WINTST	Bias		Standard deviation	
	V	φ	V	φ
01	0.001	-0.143	0.062	5.687
02	0.002	0.080	0.058	5.394
03	0.000	-0.064	0.060	5.456
04	0.001	-0.002	0.062	7.250
05	0.002	-0.271	0.065	6.903
11	0.027	1.478	0.084	15.687
12	0.032	-1.187	0.095	12.039
13	0.025	-0.057	0.072	6.103
14	0.015	0.298	0.063	5.509
15	0.020	-0.260	0.078	7.450

Table 10 : Bias and standard deviation on V and φ for the ten files ; these results include 3-beam and 2-beam cases and all bad choices



VII.4.B Tests with bias on antennas

Different multiplicative bias were tested on the first group of files for three-beam cases.

Table 11 presents these tests :

A1 : autonomous ambiguity removal : first pass

A2 : autonomous ambiguity removal : second pass

Md : meteorological ambiguity removal directly (N1+n2 too small)

Ma : meteorological after autonomous ambiguity removal

* : CHOIX found the good field bus was hindered by anormal points

— : LVDOUT3 could not make a choice

† : incompatibility between two segments

169 : number of bad ambiguity removals

Table 12 summarizes these informations :

	no bias (x2)	5%	0%	5%	10%	0%	10%	0%	10%	0%
A1	24		15		11				19	
A2	2		2		1				1	
Ma	0		10		15				5	
Md	2		1		1				3	
†/18	0		0		1				0	
Error Nb	0		0		169*				0	

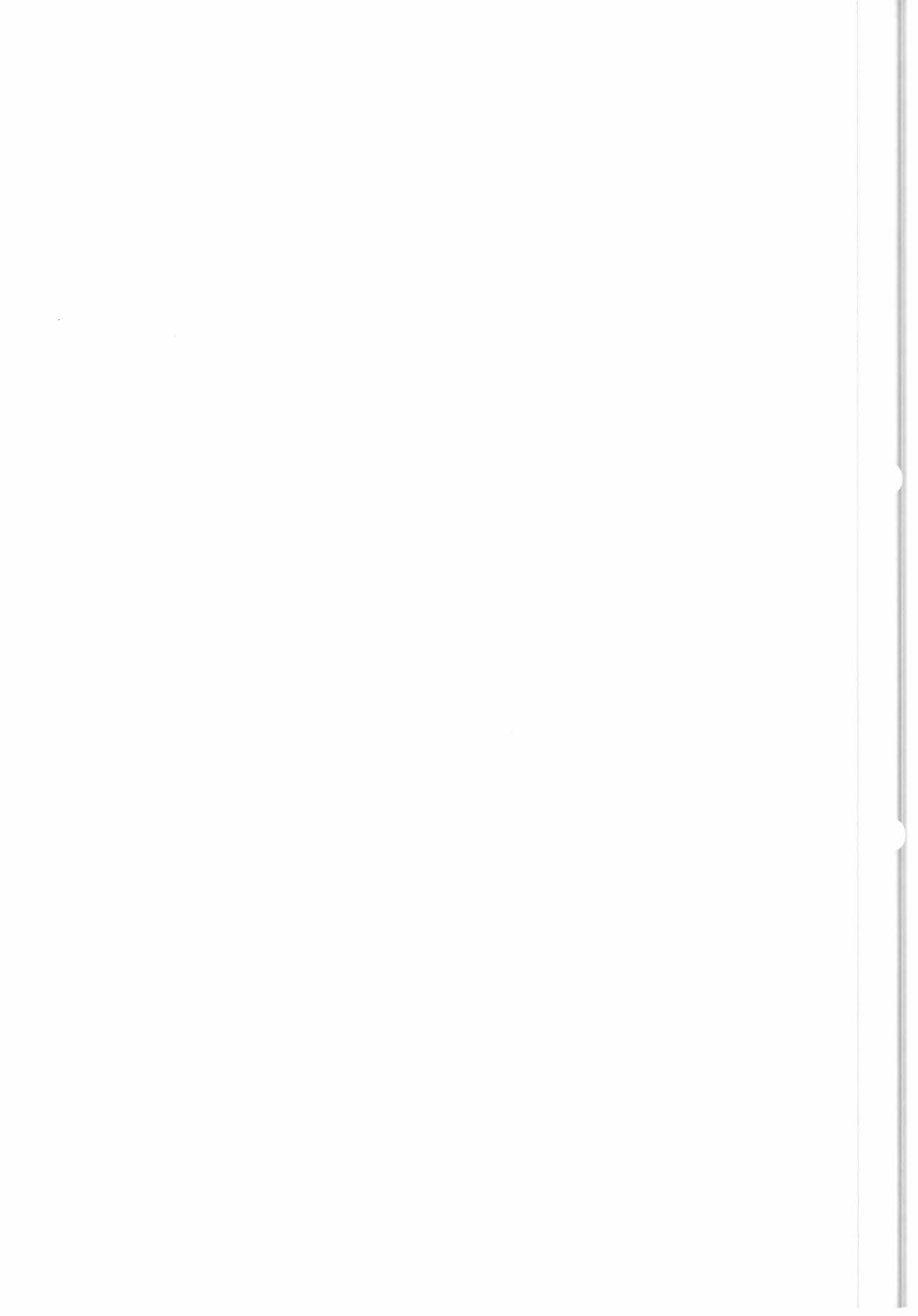
* All errors come from the case of incompatibility

Table 12 : Summary of table 11

Notice that a bias between antennas limited to 0.4 dB (~10%) can be accepted by WIND. WINRET always finds solutions, but a lot of these solutions are abnormal. This fact hinders CHOIX and provokes a few malfunctions. These malfunctions become more numerous if bias increases.

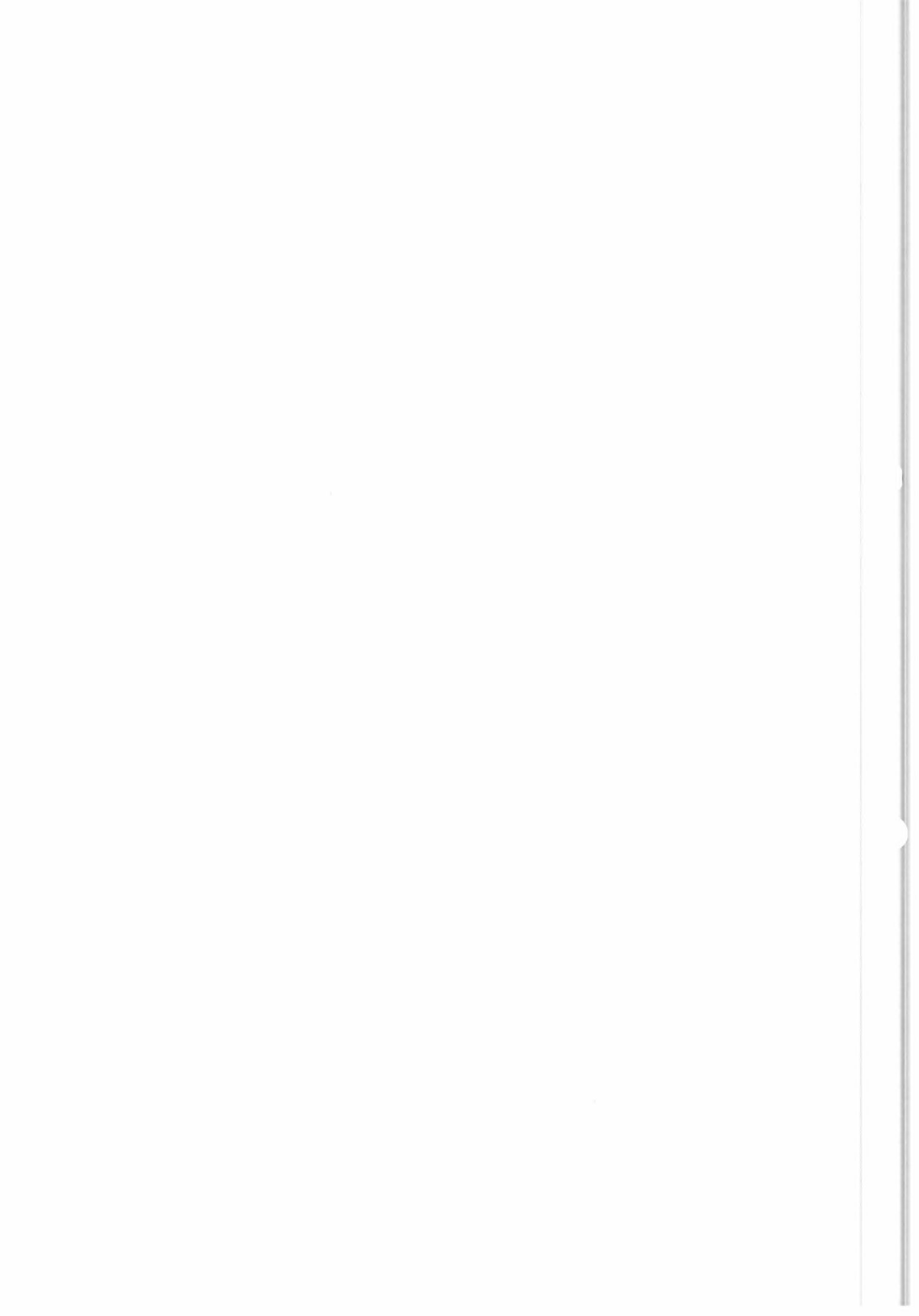
Another effect of bias is to change the signification of N1 /N1+N2 test. In fact, bias changes position of measured surface of solution, and this surface no longer coincides with the surface model.

This difference changes the rank distribution of good solutions. With an important bias, distribution of rank 1 and 2 can be inverted ; the algorithm cannot work in this situation.



file	no bias	+10%	0%	-10%	+5%	0%	-5%	+10%	0%	-5%	+5%	0%	-10%	0%
1	A1.A1.A1 0	A1.A1.Ma 0	A1.A1.Ma [*] 0	A1.A1.A1 0	A1.A1.A1 0	A1.A2.A1 0	A1.A1.A1 0	A1.A1.A1 0	A1.A1.A1 0	A1.A2.A1 0	A1.A1.A1 0	A1.A1.A1 0	A1.A1.A1 0	A1.A1.A1 0
2	A2.A1.Ma 0	Ma.Ma.Ma 0	Ma.Ma.Ma [*] 0	Ma.Ma.Ma 0	Ma.Ma.Ma 0	Ma.Ma.Md 0	Ma.Ma.Ma 0	Ma.Ma.Ma 0	Ma.Ma.Ma 0	Ma.Ma.Md 0	Ma.Ma.Ma 0	Ma.Ma.Ma 0	Ma.Ma.Ma 0	Ma.Ma.Ma 0
3	A1.A1.A1 0	A1.A1.A1 0	Ma.Ma.A2 [*] 0	A1.A1.A1 0	A1.A1.A2 0	A1.A1.A2 0	A1.A1.A1 0	A1.A1.A2 0	A1.A1.A2 0	A1.A1.A2 0	A1.A1.A2 0	A1.A1.A2 0	A1.A1.A1 0	A1.A1.A1 0
4	A1.A1.A1 0	A1.Ma.A1 169	Ma.Ma.Ma [*] 0	A1.Ma.A1 0	A1.Ma.A1 0	Ma.Ma.A1 [*] 0	Ma.Ma.A1 0	Ma.Ma.A1 0	Ma.Ma.A1 0	Ma.Ma.A1 0	Ma.Ma.A1 0	Ma.Ma.A1 0	Ma.Ma.A1 0	A1.A1.A1 0
5	A1.A1 0	A1.A1 0	Ma.Ma [*] 0	A1.A1 0	A1.A1 0	Ma.Ma 0	Ma.Ma [*] 0	A1.A1 0	A1.A1 0	Ma.Ma 0	Md.Md [*] 0	Md.Md [*] 0	A1.A1 0	A1.A1 0

Table 11 : Test results of biased files



We can summarize tests in three sentences :

- The algorithm chosen works correctly with no bias.
- A little bias, up to 0.4 dB, does not provoke a brutal failure but malfunctions appear. These correspond to having rank 1 and 2 solutions close in direction, which may provoke errors in de-aliasing.
- An important bias, more than 0.4 dB, is an upper limit above which this method must not be expected to give satisfactory results.

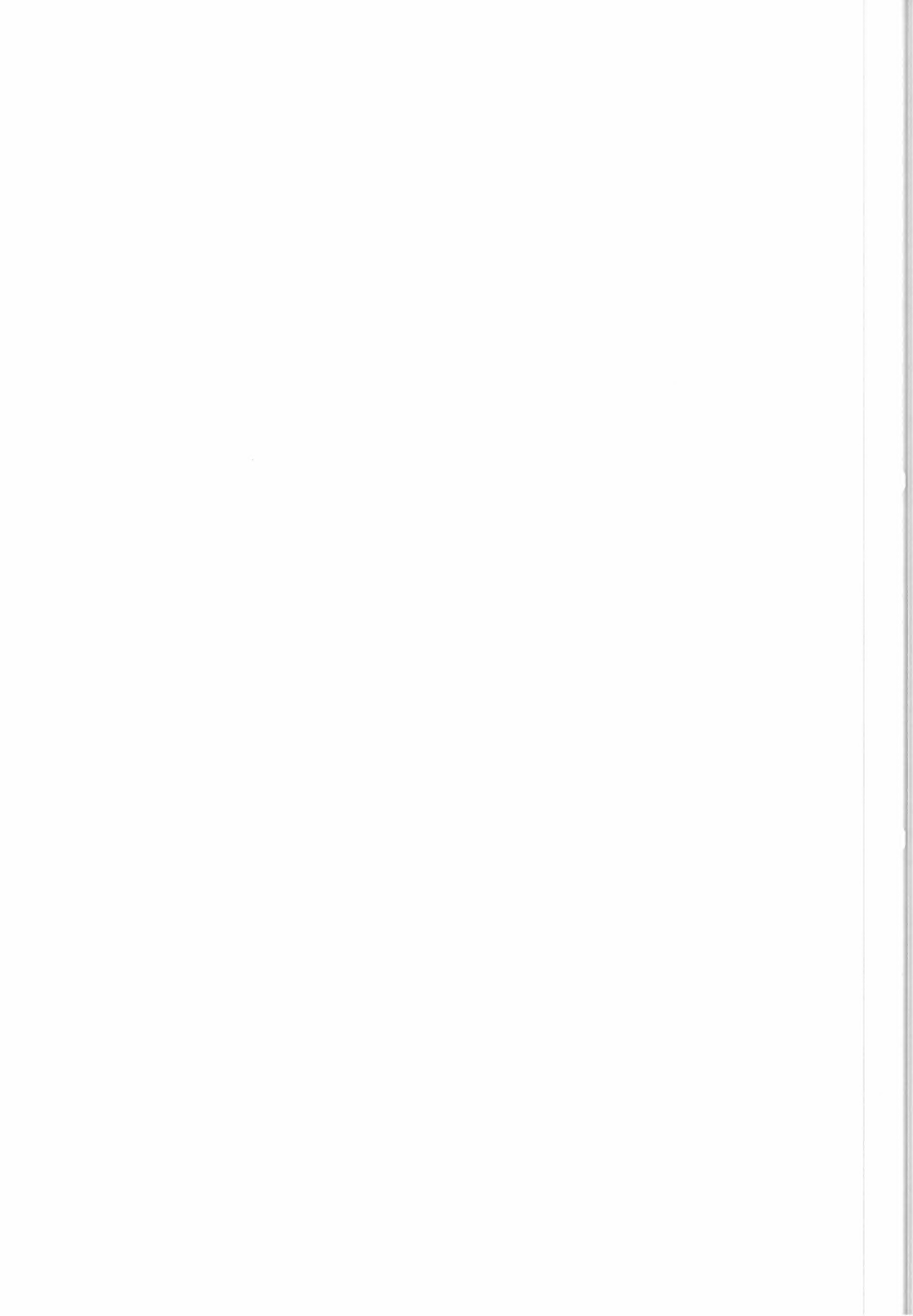
Only a precise evaluation of the inflight calibration results will allow a fine investigation of bias effects.

VII.4.C Computing times

We tested WIND on all ten of David Offiler's test files. Tables 13 and 14 summarize respectively CPU times and elapsed times measured.

File N°	01	02	03	04	05	11	12	13	14	15
Table reading	2.18	2.18	2.32	2.16	2.10	2.32	2.40	2.38	2.30	2.22
Products writing (products number)	5.74 (12)	5.02 (12)	5.60 (12)	4.72 (12)	3.98 (9)	2.60 (5)	2.50 (5)	2.24 (5)	2.32 (5)	2.24 (5)
Computations	127.78	111.68	117.98	84.36	100.02	113.96	105.80	109.90	113.26	100.58
TOTAL (s)	135.70	118.80	125.90	91.24	106.10	118.88	110.70	114.52	117.88	105.04
Node number										
3 beam	3950	4000	3980	3824	2618	1067	1090	1136	1140	883
2 beam	-	-	-	-	236	631	594	660	636	628
Time per node (ms)										
3 beam	32.3	27.9	29.6	22.0	25.8	28.2	23.8	23.2	23.2	23.3
2 beam	-	-	-	-	136.2	132.7	134.1	126.1	136.4	126.7

Table 13 : CPU times.



File N°	11	12	13	14	15
Table reading	126.40	171.98	190.28	188.46	131.60
Products writing	97.54	88.56	132.08	86.12	121.74
Computations	839.00	809.26	890.80	809.10	792.40
TOTAL (s)	1062.94	1069.80	1213.16	1083.68	1045.74

Table 14 : Elapsed time. These estimations had to be used carefully. They depend very much on the computer configuration.

For a nominal orbit of 25000 points, all of which are three-beams, the CPU time would be approximatively 650 seconds and the elapsed time eight or nine times more.

If now, the nominal orbit contains 10% of two-beam points, the CPU time would be about 915 seconds.

VIII - MANUAL DE-ALIASING FOR PRECISION PROCESSING

VIII.1 General presentation

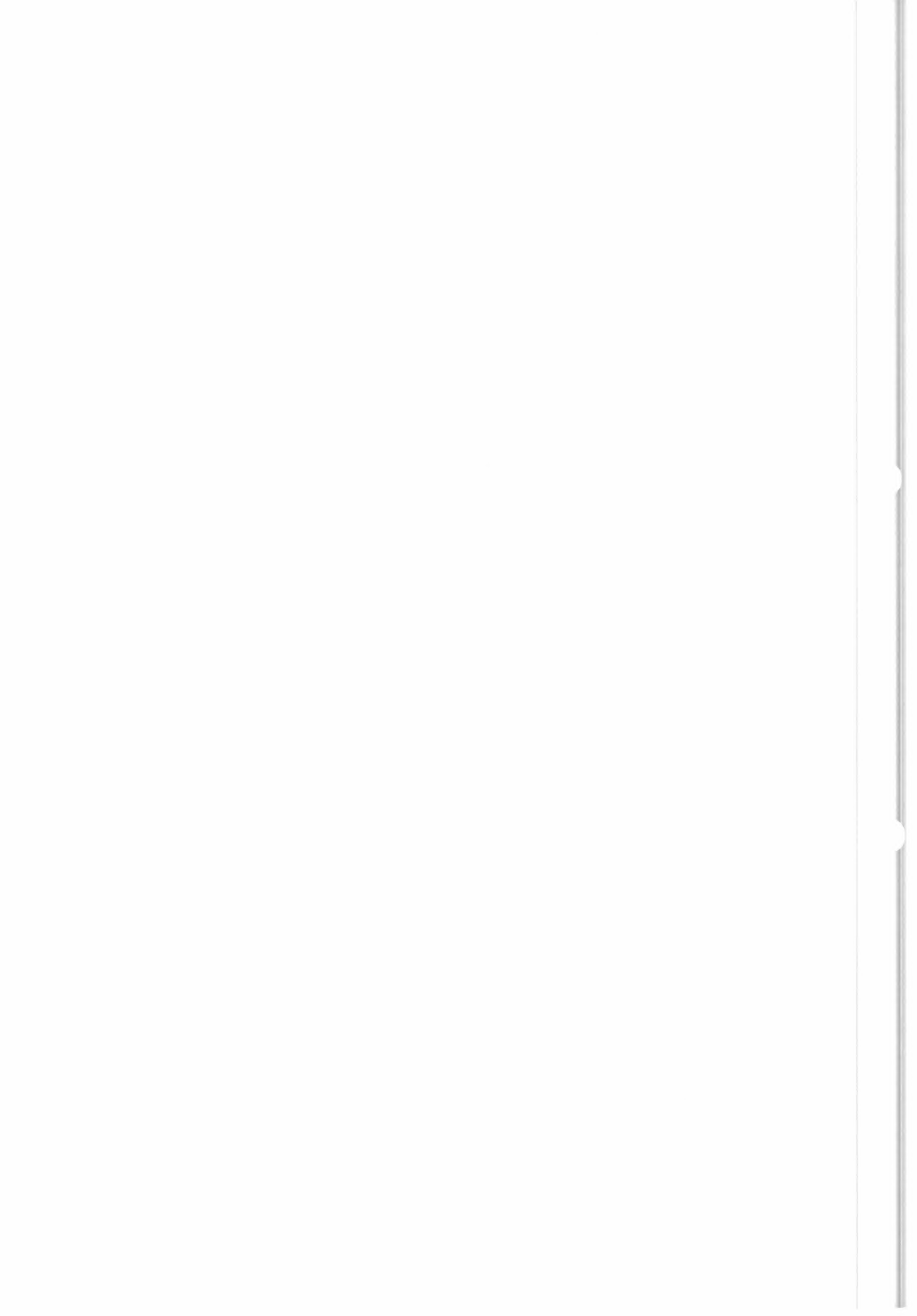
Manual de-aliasing will be required to extract all of the wind information contained in the wind data. In view of the time required, this is not feasible for Fast Delivery Products, but must be developed for off-line, Precision Products (P.P). Manual de-aliasing will require externally supplied meteorological surface wind fields.

Two distinct types of data sets will be declared "Undetermined" after passing through the automatic analysis P.P chain :

- Three-beam segments, incoherent with the previous or succeeding segment, or for which the quality tests for automatic de-aliasing have not been met
- Two-beam segments in general, the drawbacks of the automatic procedure used in F.D.P. processing (straight-line approximation for limiting curves, no de-aliasing of regions completely separated from three-beam regions by a limiting curve), appearing impossible to resolve without manual intervention

Conclusions concerning this manual treatment presented in this paragraph are only preliminary, as tests have only begun using a Tektronix graphics terminal connected to a N.D 570. If the graphic language used, GKS, has proved sufficient as a tool, the data exchange rate between computer and terminal is much too slow ; the answer to this technical problem which has delayed progress is a dedicated work-station.

The operator's choices are, of course, made as a function of the meteorological wind field which he can represent on the screen either at the exact scale of the scatterometer data, or over a much larger region, to gain information concerning the general situation. We propose that the two wind fields, before and after the scatterometer measurement time, be available to the operator.



VIII.2 De-aliasing three-beam zones left undetermined by automatic processing

Here, as in the automatic treatment, a choice must first be made between rank 1 and rank 2 solutions. To make this choice efficiently, sparing the operator's time, the double vector field is first drawn on the work-station screen as in the example chosen (Fig. VIII.1, data taken from David OFFILER's WINTSTO1 file). The meteorological wind field (not shown in the figure), when superposed on the screen, indicates a saddle-point flow, which could be guessed from the scatterometer field, a priori.

Curves, formed of straight-line segments whose end points are charted on the screen by the operator, are drawn through regions where wind directions are nominally parallel or perpendicular to the swath direction. The operator's task is simplified by an automatic color coding (red) of these privileged directions. Figure VIII.2 shows the straight-line segments, and the points on the scatterometer grid closest to the segments, which are chosen automatically. The operator is given the choice between the two (opposite) directions possible, choice which determines the directions of points on the curves. Choice between the two directions is made by comparison with the superposed meteorological wind vectors. We expect that extensive meteorological knowledge will not be required of the operator, but this is certainly to be verified by extensive testing.

Once all such curves have been drawn, the segment is separated into the different zones separated by these boundaries as well as land, low-wind zones and, perhaps later, ice-zones. (Area characterization) Fig (VIII.3). Wind directions of points in zones having boundary curves of two different directions are compared to the mean direction of the boundaries (45° , 135° , ... relative to swath direction) and the closest of the two directions at each point chosen, automatically. If a zone has only one boundary direction, (zone 4 of Figure VIII.3, limited on one side by a boundary curve, on the others by the edge of the swath and low-wind zone, is an example) the program asks the operator for the second direction, necessary to fix the mean direction for that zone.

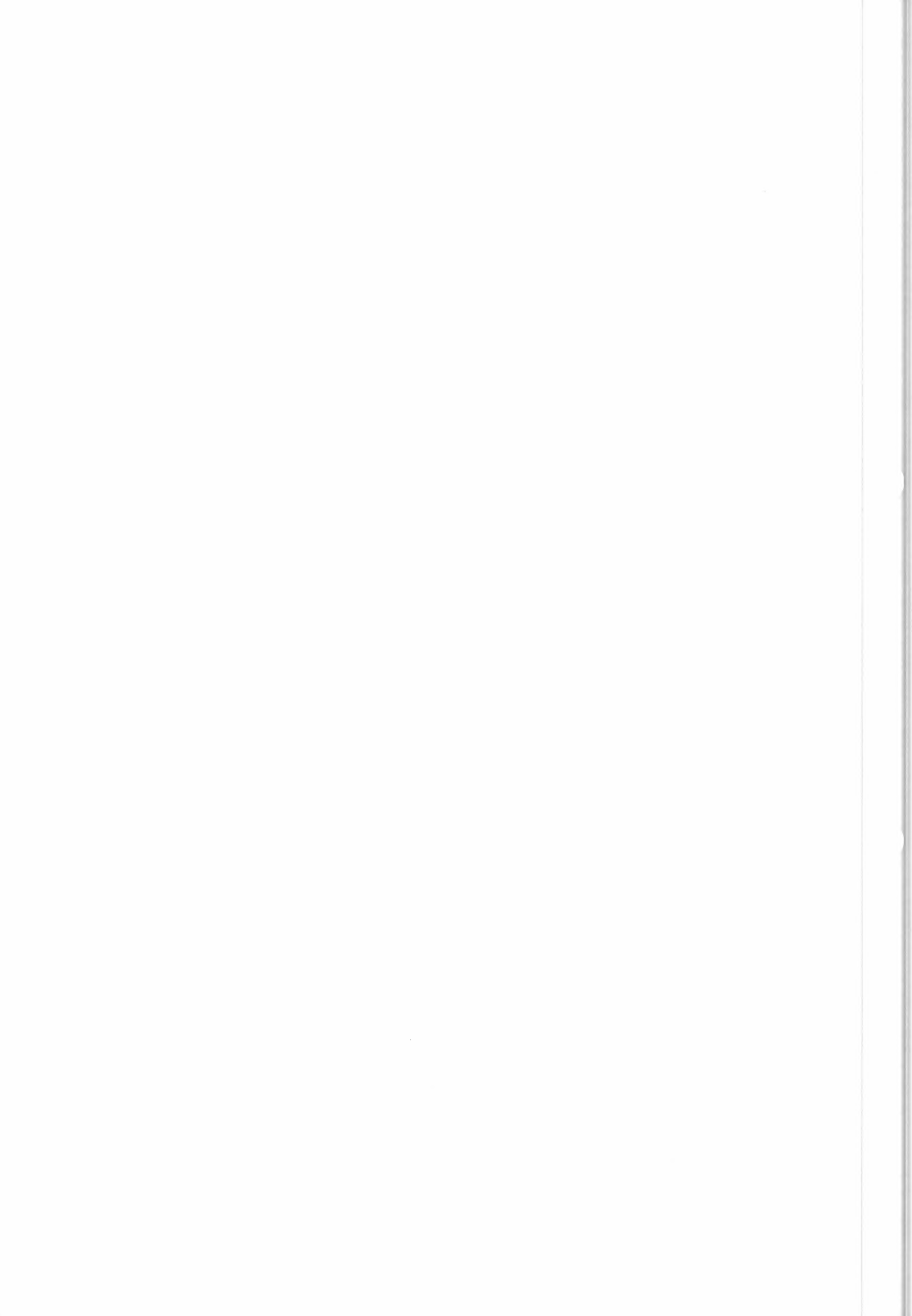
Notice that since the test is made relative to the mean direction, and not by imposing that the direction be in a given quadrant, slight errors in the operator's tracing of boundary curves are not important.

The end result is given in Figure VIII.4, which shows the de-aliasing wind vectors presented for the operator's scrutiny. The segment is then submitted to further treatment (coherence, compatibility) as previously described for the automatic analysis.

VIII.3 De-aliasing two-beam zones

This will be the major part of the manual de-aliasing effort, if the scatterometer is only turned on or off on crossing the coast-lines. We suspect, from very limited experience, that normal de-aliasing of a two-beam sector will take between a quarter and a half-hour, on the average. Thus only privileged regions will be covered by a single operator.

The two-beam manual de-aliasing will proceed quite similarly to that of the three-beam zones, except that the limiting curves drawn will pass through regions where these are only two, or three, wind-vectors to choose from. These cases correspond to the outer border of the surface of noise-free solutions indicated in Figure I.3.



These pairs of solutions are different at the beginning and end of the swath (rear and central beam, or forward and central beam data available, respectively). Figure VIII.5 indicates these directions as they now appear using the present C-band model. It is to be expected, if the model changes, that these directions be modified somewhat, but the general principle will remain the same.

In practice, the curves will be drawn by the operator through points which have two or three solutions. Then the two possible directions will be evaluated by the computer using two-solution points near the curve (thus these direction require no a priori estimation).

The operator having chosen the correct direction on each limiting curve, based on the meteorological wind field comparison, the work-station will choose correct wind vector solutions in the same manner as for the three-beam cases, the vast majority of points in a zone having only one solution satisfying the direction limits set by the boundary curves.

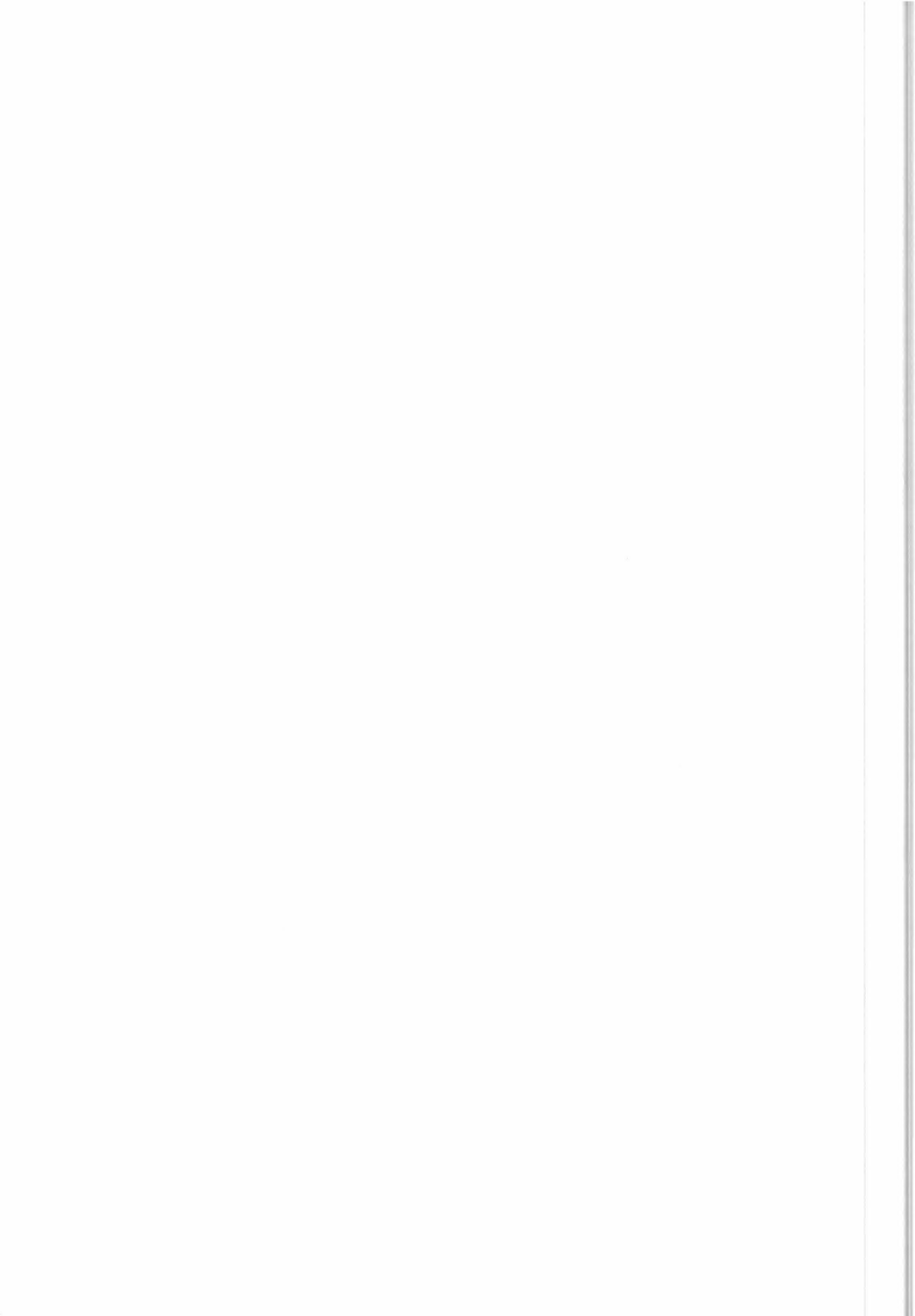
The following four colour plates are in that order :

Fig. VIII.1 Vector field of rank 1 and 2 solutions

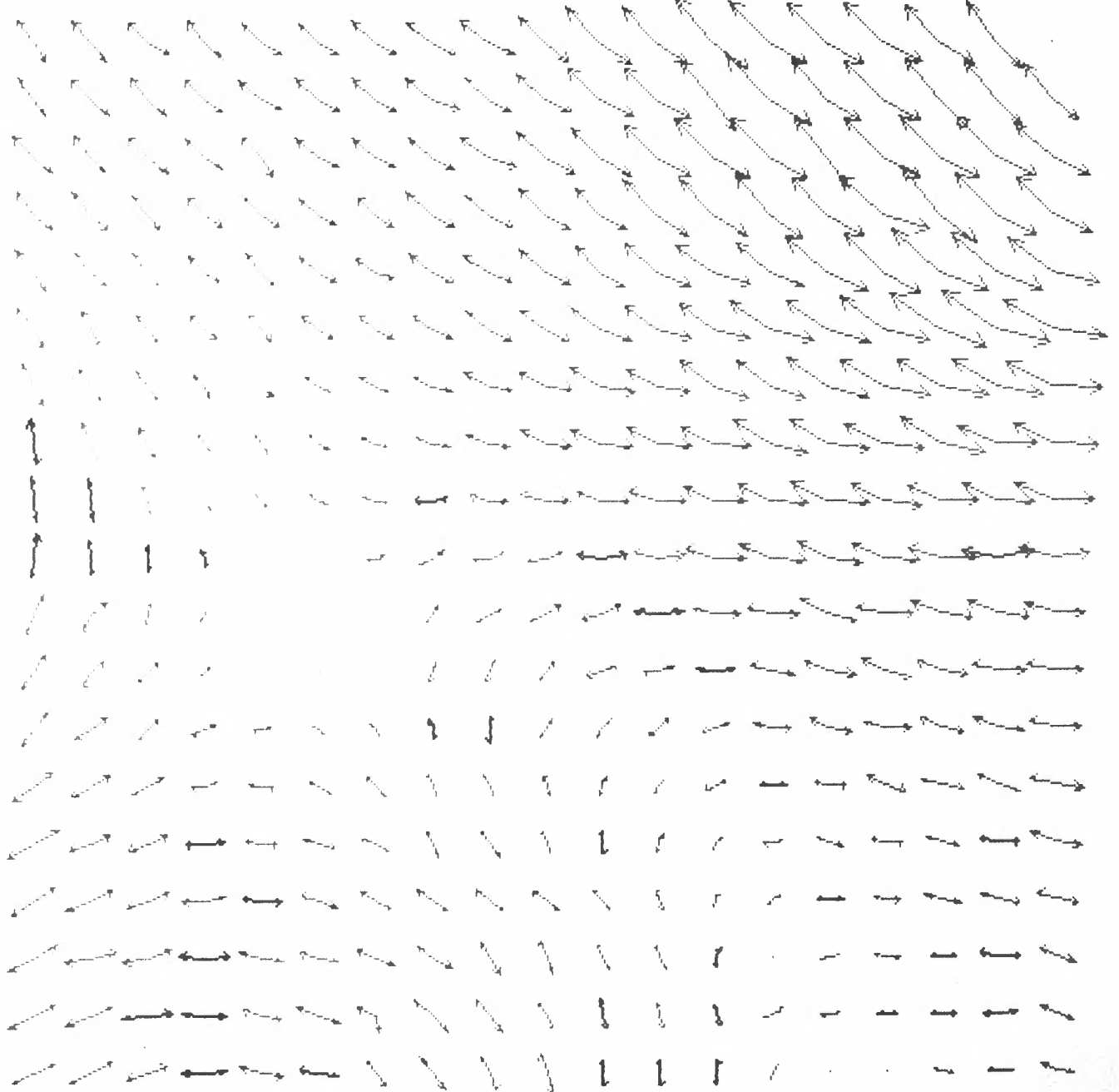
Fig. VIII.2 Operator-drawn boundary curves

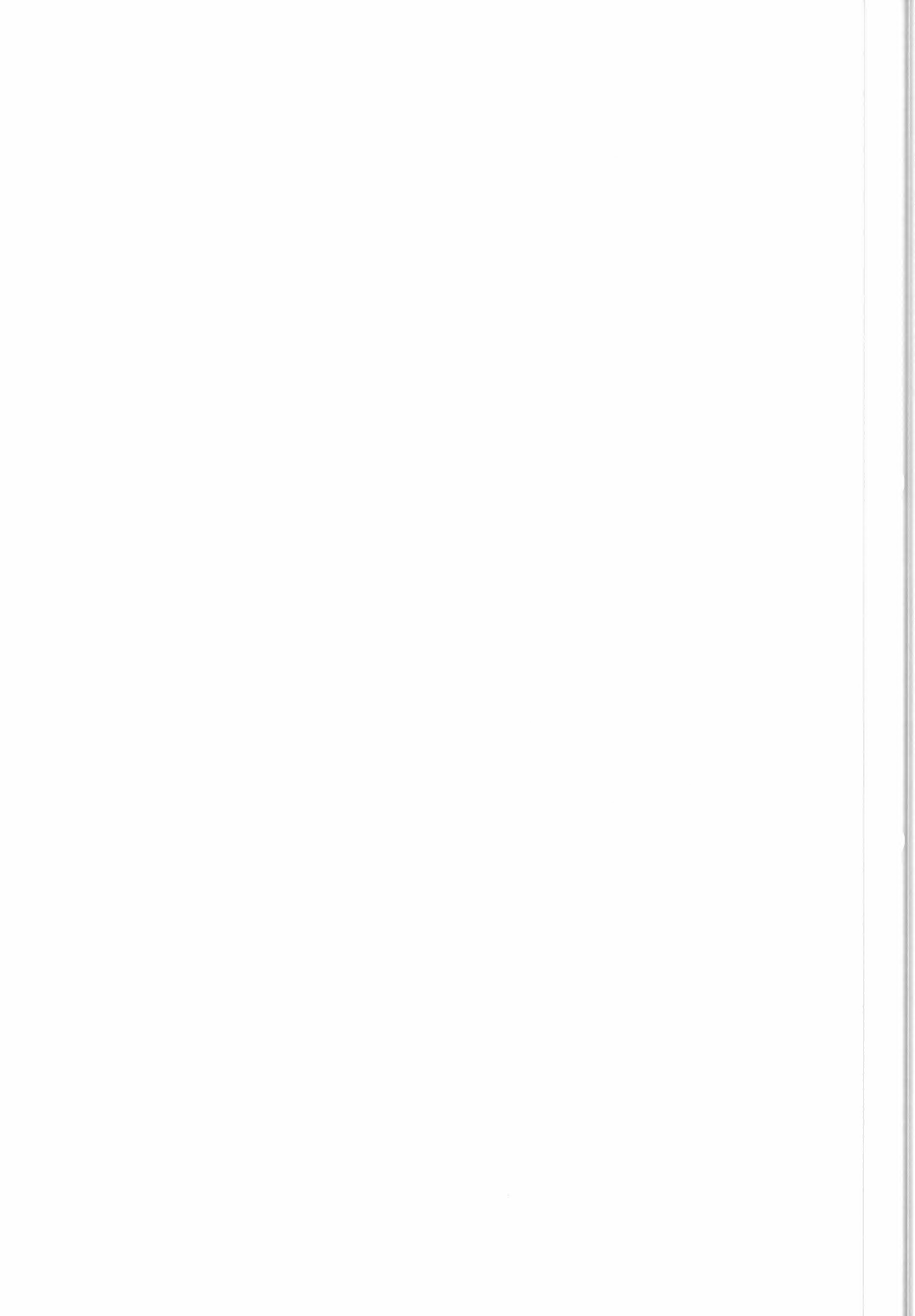
Fig. VIII.3 Area characterization

Fig. VIII.4 De-aliased wind field

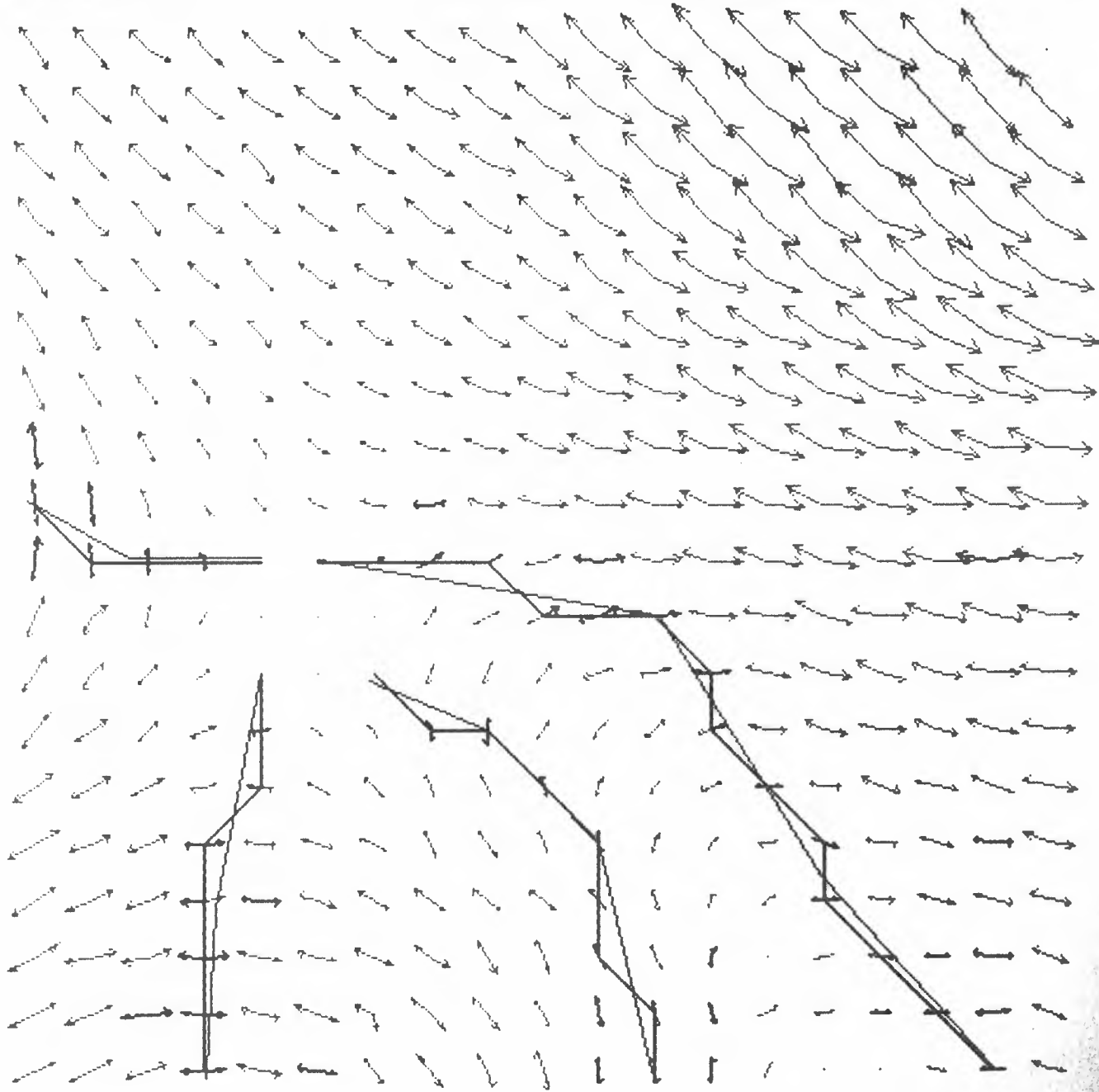


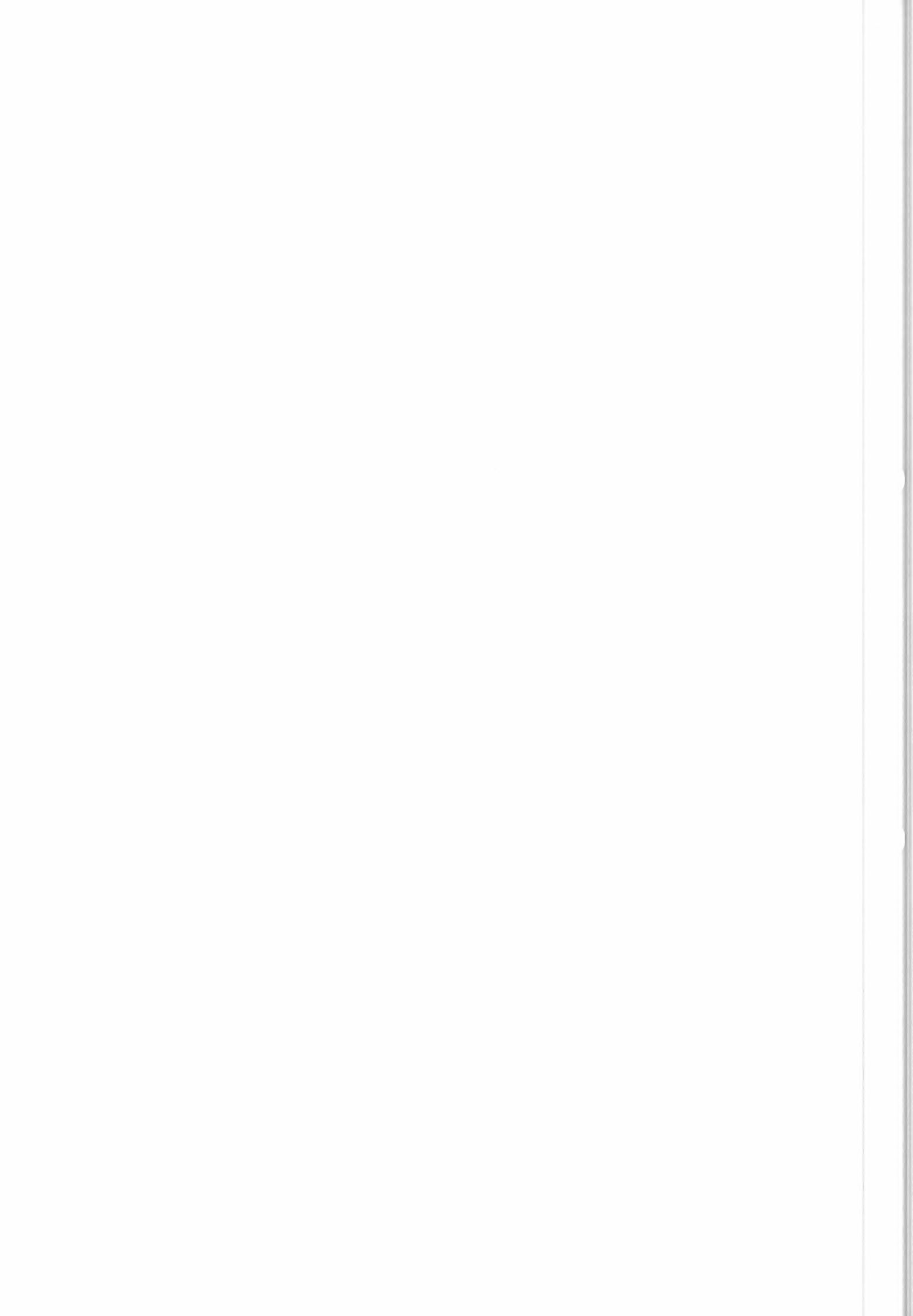
MENU
AFFICHAGE CHAMP METEOR
CHAMP METEOR INVISIBLE
ZOOM AVANT
ZOOM ARRIERE
TRACER DE LIMITES
LEVER DE DOLITE
FIN

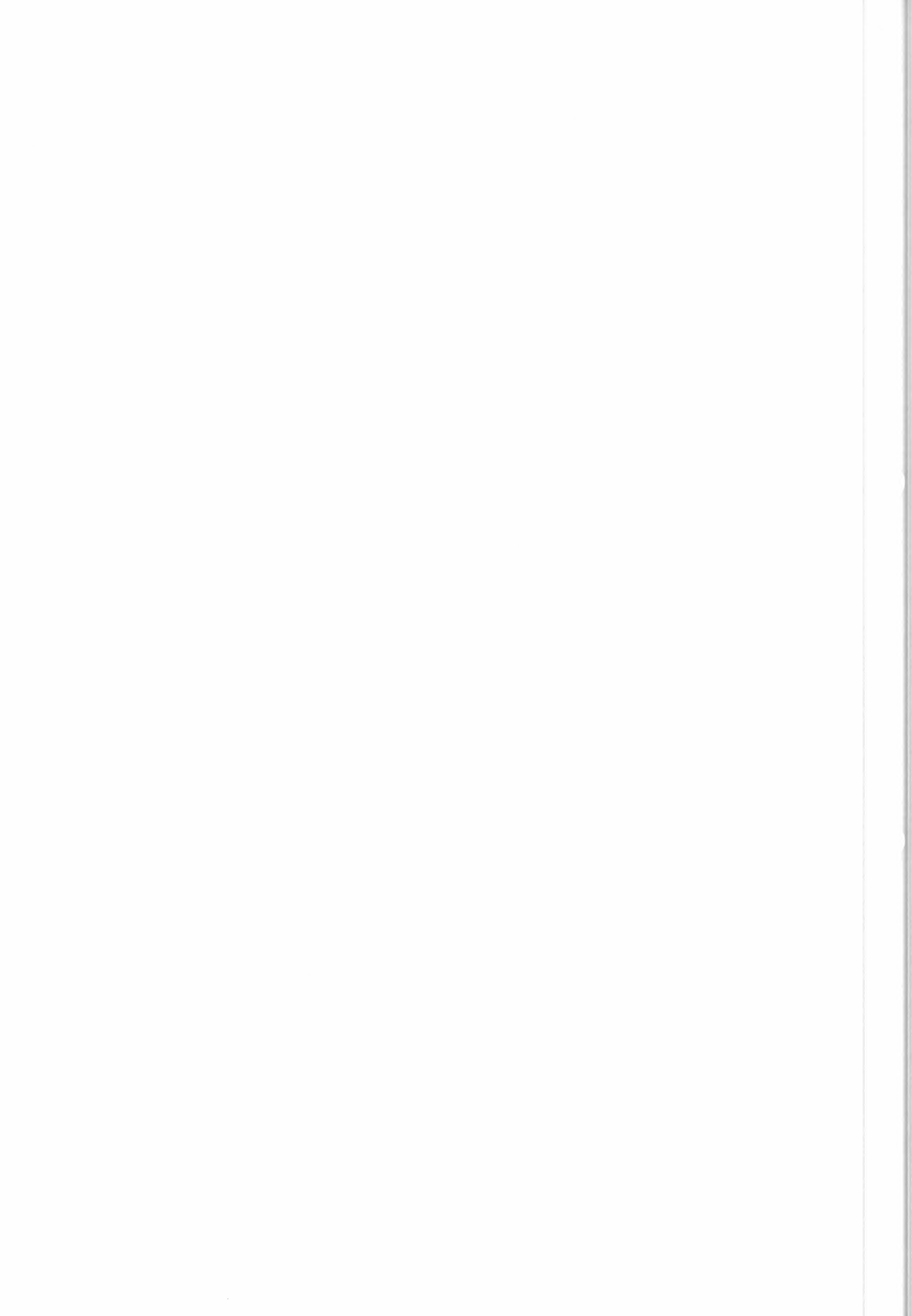




MENU
AFFICHAGE CHAMP METED
CHAMP METED INVISIBLE
ZOOM ALANT
ZOOM ARRIERE
TRACER DE LIMITES
LEVER DE DOLITE
FIN







MENU

AFFICHAGE CHAMP METED

CHAMP METED INVISIBLE

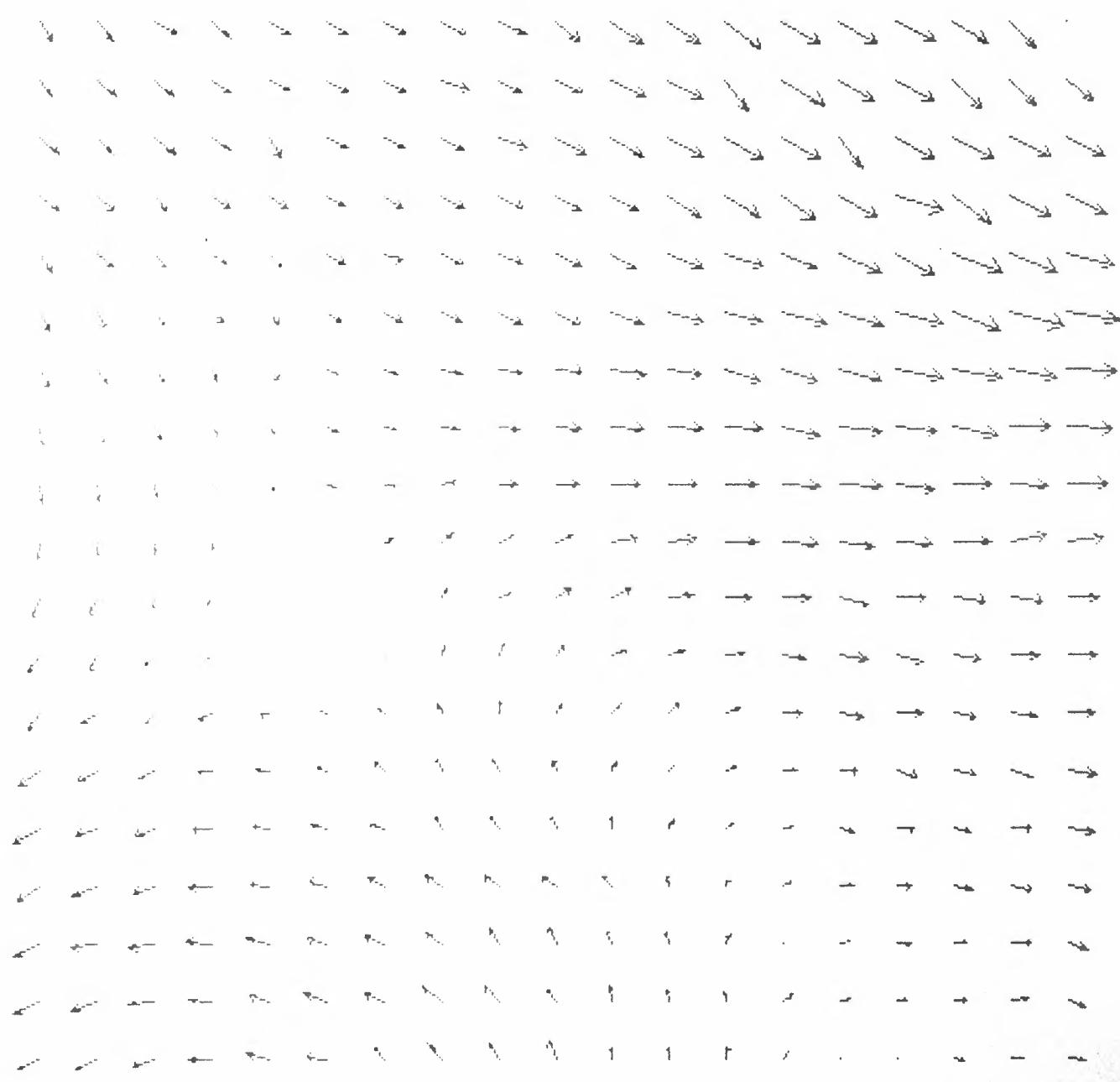
ZOOM AVANT

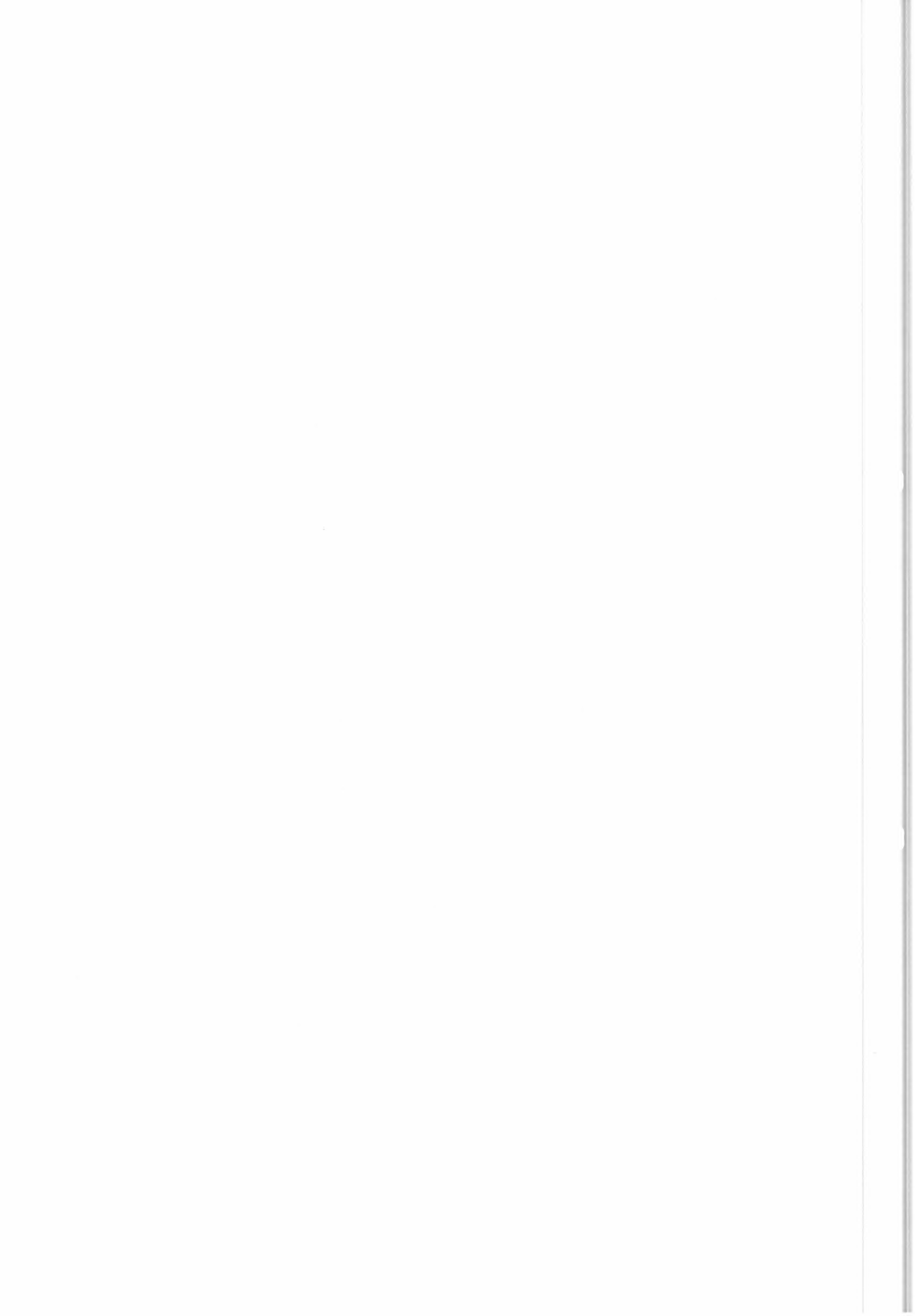
ZOOM ARRIERE

TRACER DE LIMITES

LEVER DE DOUTE

FIN





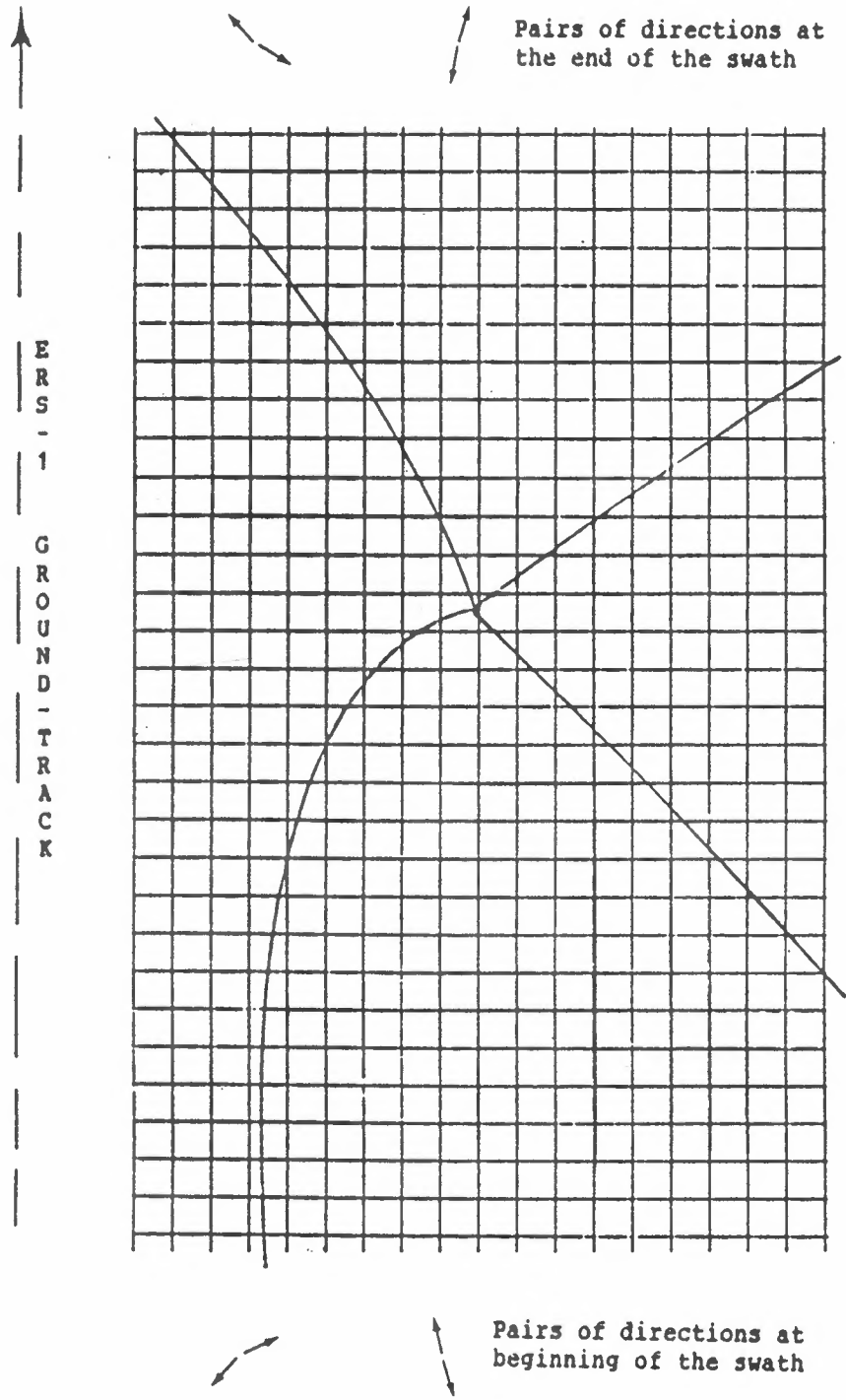


Fig. VIII.5 Manual de-aliasing : two-beam zones



IX - SIMILARITIES AND DIFFERENCES BETWEEN FAST DELIVERY AND PRECISION PROCESSING

Fast delivery (F.D) processing must meet time and personnel constraints which impose that it be a fully automatic process. Moreover, because a slow computer is used (1 Mips), tables of Σ_0 as a function of wind speed, azimuth angle and incidence angles have had to be used in the inversion algorithm we have developed for the 3-beam cases ; to maintain the size of these tables within reasonable limits, precision in computation must be kept to 50 cm/s and 5° in wind speed and direction respectively. This precision is sufficient for F.D product users, but may be inadequate to study fine points of the calibration or of the time evolution of the overall instrument chain. Moreover, two-beam inversion proved unsuccessful with tables and we had to use the previously developed Newton-Raphson scheme in this case, with a precision of 1° and 10 cm/s.

Precision processing (P.P), carried out off-line with larger computers and work-stations, can benefit from loosening of technical constraints. For the PAF segment in France, we have advocated :

- Inversion to find possible wind vectors to a precision of 10 cm/s and 1° (Newton-Raphson scheme)
- Automatic de-aliasing of three-beam regions
- Interactive de-aliasing of two-beam regions on a graphic work-station

Figure IX.1 presents the major elements of the off-line precision processing chain. They will now be considered in sequence in order to present in a systematic way differences and similarities with the F.D processing as we understand it today.

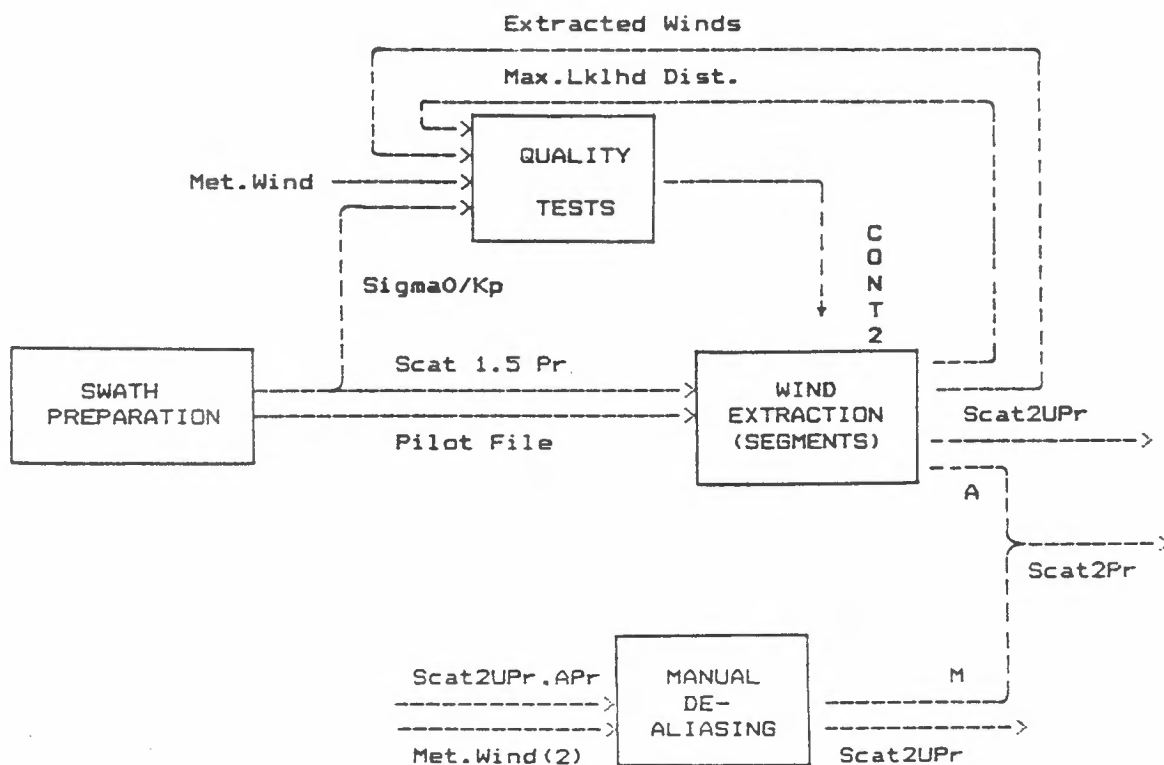


Figure IX.1 General presentation of the Precision Processing (off-line)



IX.1 Swath preparation

We must first define terms : a precision product is 500 km long (20 x 19 points), a segment is formed of six (or less) consecutive products, and a swath is the consecutive set of products to be passed through the precision processing. (Generally the swath will correspond to the region covered between turning on and off the scatterometer, but if regional treatment is carried out, the swath could be much shorter).

To prepare data for automatic precision processing from level 1.5 (oo) to level 2 (de-aliased wind vectors), consecutive products at level 1.5 will be put on temporary files with their accompanying meteorological model winds, forming the swath data. The pilot file will give parameters of the processing as well as the name of the level 1.5 data files to the Wind Extraction processing.

This module has necessarily an equivalent in the F.D processing, but the module we have written for ESA works by a line by line (19 points) input, so that it does not have any information about the length of the swath until data input is terminated by a "last line" signal.

IX.2 Quality tests

These must be separated into three classes :

- 1) Tests on data at the 1.5 level (oo, Kp)
- 2) Tests of the maximum likelihood distance after inversion
- 3) Tests of the de-aliasing quality

The first two classes of tests will be those described in paragraphs II and III. Whether automatic screening out of ice regions will be carried out or not depends on further information concerning C-band ice cross-sections which may be available only after ERS-1 launch.

Tests of automatic de-aliasing quality in three-beam regions will be different for the precision processing because both autonomous and meteorological wind field parameters ($N1 / N1+N2$, NSP) will be systematically computed. Thus the field chosen will be that for which either :

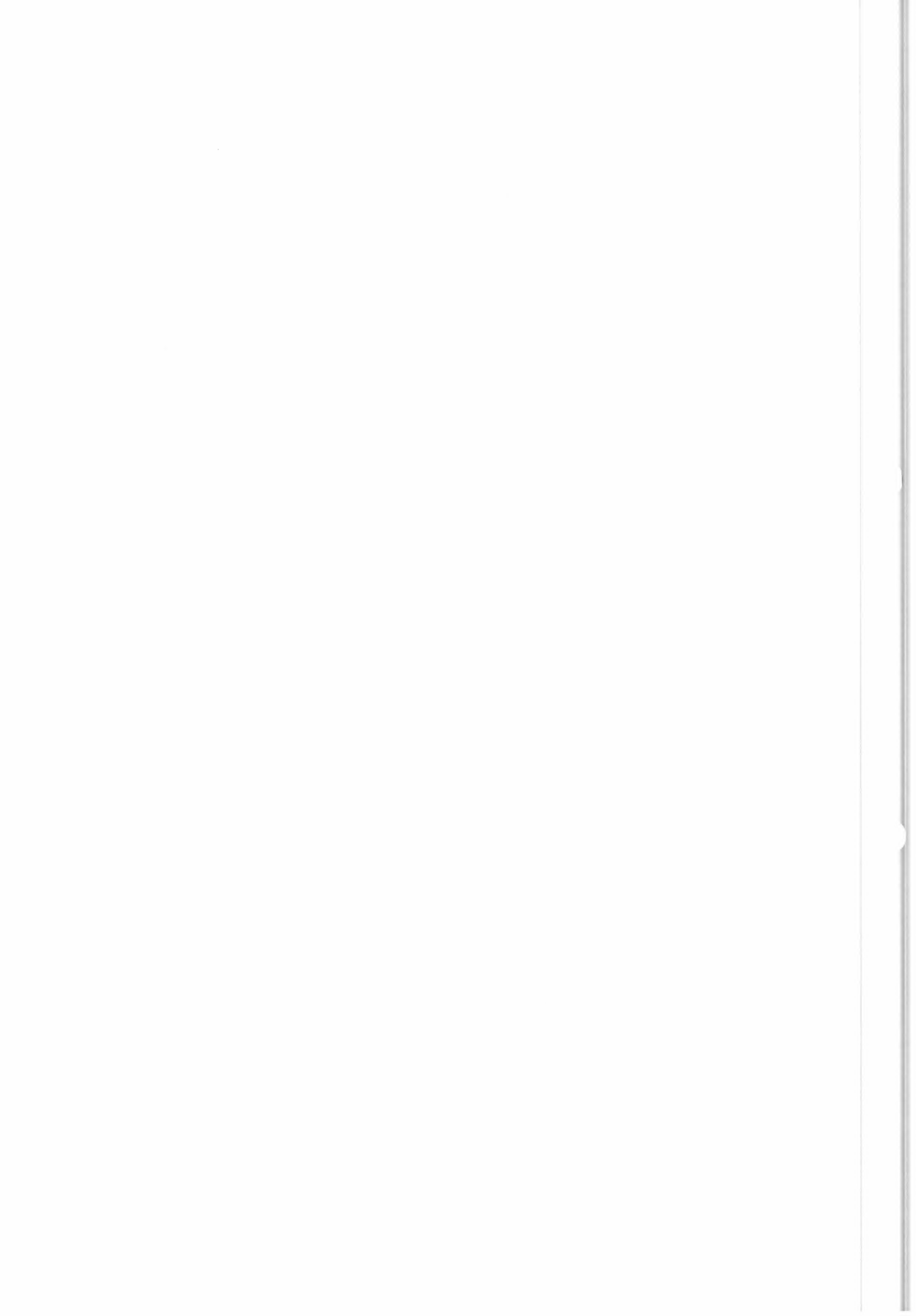
$$N1 / N1+N2 > Rmin \text{ for } N1+N2 > 100$$

or $NSP > NSPmin$

(Present values of Rmin and NSPmin have been set to 0.7 ; should the calibration of the C-band model leave substantial bias, values of Rmin would be increased. We expect some tuning of Rmin and NSPmin to optimize de-aliasing, but would be very surprised to see their present values considerably modified).

If neither of the two fields meet at least one of these criteria, the level 2 products of the segment will be declared undefined, and stored so as to be ready for interactive de-aliasing on a work-station.

If de-aliasing of the segment has been successful, compatibility of the wind field with those of the previous and following segments, when they exist, will be tested as described in paragraph VII.3. The products corresponding to two necessarily consecutive segments with incompatible wind fields will be marked



as such. Thus investigation of incompatible fields as well as undetermined fields will be later possible on the work-station.

Here the advantage of off-line precision processing with respect to F.D processing is clear. Incompatibility can be signaled for products of both segments while for F.D processing only the "products" of the second segment can be declared incompatible, because WIND has no access to the previously processed data. Moreover, systematic calculation of $N1 / N1+N2$ and NSP will furnish insight concerning the respective merits of the autonomous and meteorological field de-aliasing procedures, which will vary regionally. (Antartic ocean wind fields cannot be as good as those of the North Atlantic, for example). This should lead to more sophisticated criteria on Rmin and PSNmin than those we are presently advocating.

IX.3 Wind extraction

The series of steps of the wind extraction module for precision processing will be similar to that for F.D processing. A notable difference will be that inversion will be carried out to a numerical precision of 10 cm/s and 1' using the Newton-Raphson scheme described in paragraph IV.3 both for three and two-beam cases. This will lead to inversion times of the order of 0.15 s/cell, roughly six times greater than for the three-beam F.D inversion using tables (ND 570).

We shall continue work on the de-aliasing algorithm (construction of the two wind fields), but expect that any improvement here could be immediately carried over to the F.D processing.

The increase in computing time to obtain greater precision is certainly not justified for general application. But we expect it to prove useful in long term controls, such as the time evolution of the mean maximum likelihood distance which would indicate sensor drift or regional variations of the model.

IX.4 Manual de-aliasing

As already described, manual de-aliasing of undetermined or incompatible 3-beam zones as well as of all two-beam zones will be possible in precision processing. This is important not only to increase the amount of data de-aliased and its quality, but also to understand why and where automatic de-aliasing has failed. This will serve to produce more robust and efficient automatic de-aliasing techniques as time goes on. But it must be recognized that manual de-aliasing will be slow, perhaps 5 minutes per product and only the most important data will be treated this way.

X - GENERAL CONCLUSIONS AND POSSIBLE FUTURE WORK

It is clear that the quality of wind extraction (inversion and de-aliasing) depends very much on that of the empirical C-band model as well as the precision of this calibration. Within the limits of the present model, the procedure we have developed for three-beam zones is very successful as long as bias and noise remain within the limits specified by ESA. Should the model change these conclusions could be severely modified, and tests concerning these factors would have to be run again.

In case of a C-band model change, directions corresponding to a maximum distance between the two sheets of the surface of solutions would have to be recomputed as well as the limiting curves separating zones of two, three and four solutions



in the two-beam cases. Numerical values would vary but the principles involved would be the same.

The approach to automatic treatment of two-beam zones leaves roughly 30% of points unresolved, this being due to the nature of the information. Only manual de-aliasing, as described, can possibly fully resolve two-beam zones, but this will take too much effort to be done systematically if two-beam zones are frequent (switching on and off the scatterometer on crossing coast lines).

The procedure developed in order to construct the two wind fields nominally 180° apart, starting from rank 1 and 2 solutions, is very much ad hoc, and although surprisingly successful, should be looked into further to study it against effects of noise, frontal situations, mixed sea/ice regions. This will be done for the precision processing and can be introduced in F.D processing, later on.

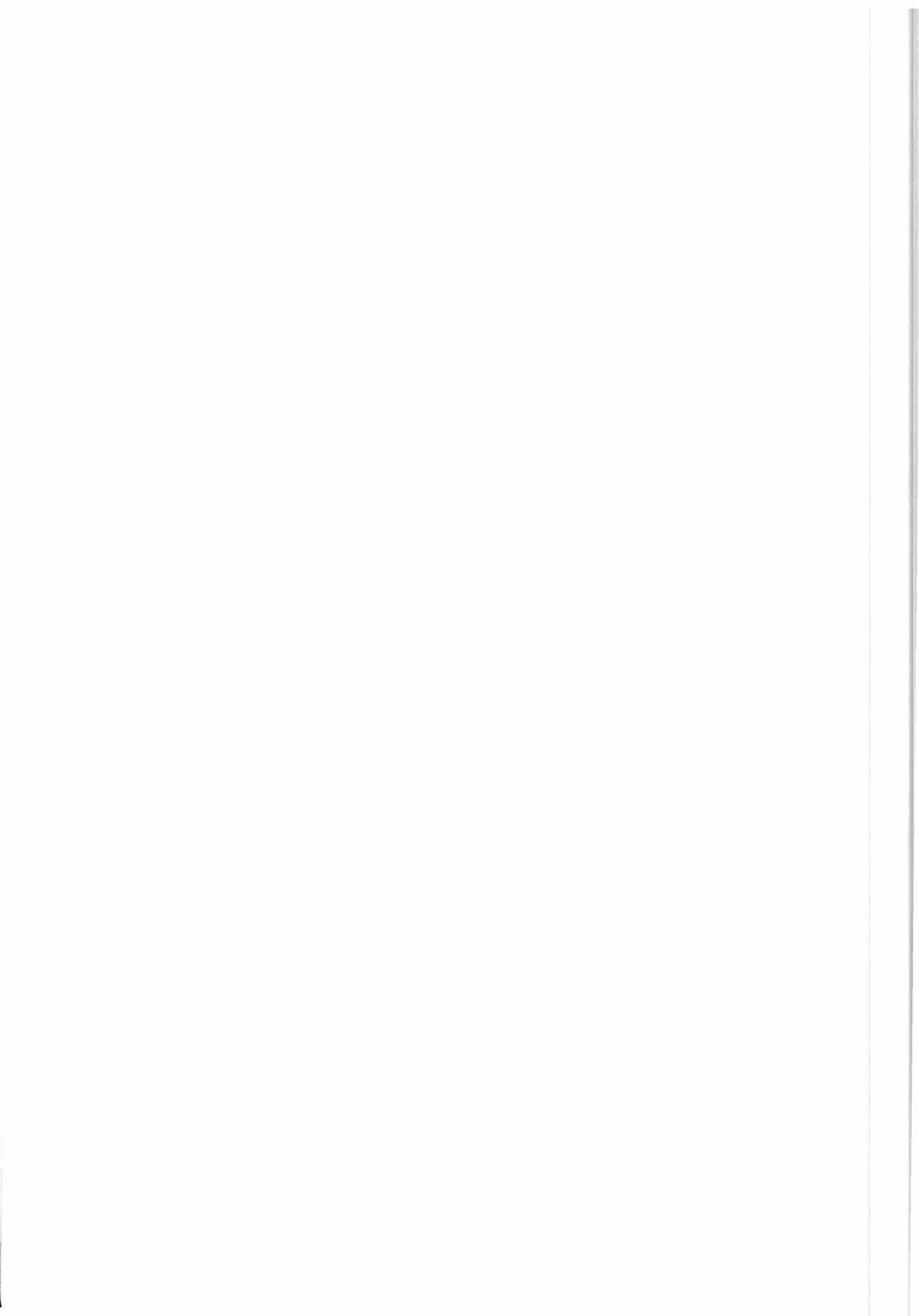
Screening of ice-covered regions could be possible by study of correlation coefficients of $\sigma\sigma$ triplets across the swath, line by line, if C-band VV $\sigma\sigma$ -behaviour over ice was well known. This could then be done in real time if the F.D computer was rapid enough. This could also be considered for off-line processing, no longer correlating measured $\sigma\sigma$ triplets with values of an ice-return model, but with $\sigma\sigma$ triplets of a previous pass over the same area, measured one or several satellite periods before.

An important field of work must now be to determine parameters best suited to monitor the scatterometer's behaviour in time or regionally (Temperature variations, drift of the electronics,...). For example, one might investigate and monitor :

- Mean, over the satellite's period, of M (maximum likelihood distance)
- Mean, over the satellite's period, of $(\sigma_e - \sigma)/\sigma$ where σ_e are, for each antenna, the measured values of $\sigma\sigma$ and σ the corresponding value deduced from the extracted wind

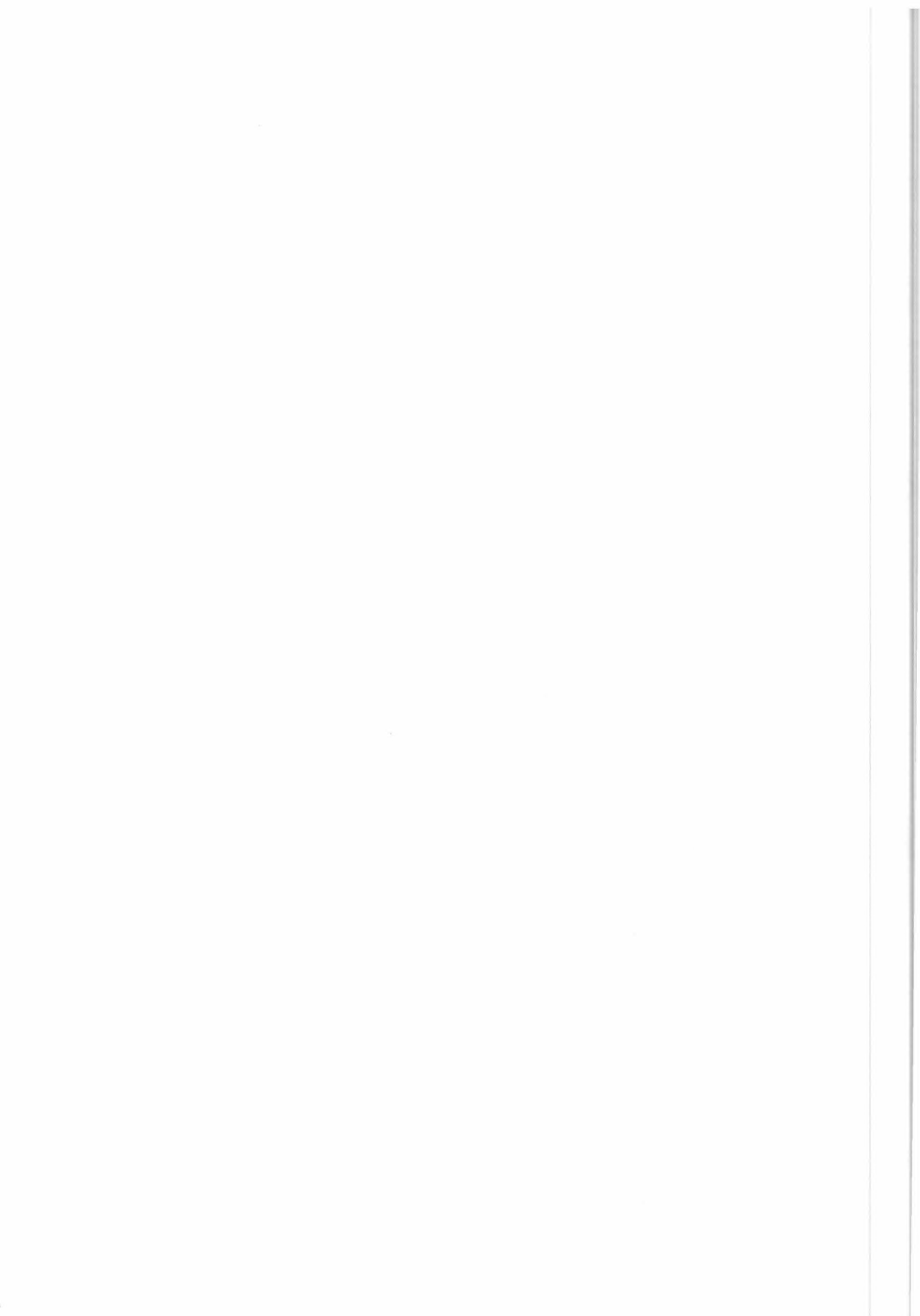
Of course, these two types of parameters could be restricted to given positions of the ERS-1 track, which would allow regional studies or investigations of transitions between night and day. Further, these parameters might be studied in off-track distance or speed, or antenna-relative direction bins, to see where problems may arise.

This being said, we are confident the procedure proposed to ESA for processing of 3-beam regions will be robust to an evolution of the C-band model function. If calibration coefficients vary so much, regionally, or are so poorly determined that autonomous de-aliasing is not feasible, then meteorological de-aliasing will have to be used alone ; this may prove to be a great disadvantage in regions such as the Antarctic ocean where meteorological models give poor results because of an insufficient number of observations.



ANNEX 1

LAND/SEA RATIO DETERMINATION PROGRAMS
V. HARSCOAT / CREO



I - INTRODUCTION

To determine if wind extraction for a given scatterometer point in the swath should be carried out, a test must be applied to see how much land might be present in the area corresponding to the Sigma0 estimates.

This requires as a starting point a land/sea table as fine as possible. The one furnished by E.S.A. to prepare the scatterometer-specific table has a resolution of 5' x 5' in latitude and longitude, from 87° S to 87° N, Antarctica and the Arctic Ocean filling the uncovered areas.

In order to accelerate the determination of percentage of land in a 50km x 50km scatterometer cell, we have generated a new table, still at a resolution of 5' x 5', indicating whether land areas represent less or more than a certain number of 5' x 5' cells in a larger zone including in its center the 5' x 5' area. The larger zone extends (beyond the 5' x 5' area) outwards at least 25 kms, and no more than is necessary to meet this requirement as well as the constraint imposed by the 5' x 5' resolution of the initial land/sea table. For the fast delivering products a scatterometer point falling within a given 5' x 5' area will be processed only if no surrounding cell is indicated as land in the larger zone. But the programs have been written so that this criterium might be made less severe.

Once the scatterometer-specific 5' x 5' table is created it must be compacted ; otherwise the number N of elements in it, would be too large :

$$N = 180^\circ \times 360^\circ \times (60/5)^3 = 9.33 \times 10^6$$

II - CONSTRUCTION OF A SCATTEROMETER SPECIFIC, SMALL SCALE TABLE

Figure 1 shows one of the 5' x 5' rectangles, the outer zone extending 15 nautical miles in latitude above and below the central rectangle, and to the left and right a sufficient number (varying with latitude) of 5' longitude segments to extend at least 25 kms beyond the central rectangle. This number of 5' x 5' elements extending to the East or West is given by the formula :

$$25 / (5 * 1.852 * \text{COS} (\text{Lat}))$$

rounded off to the next integer value. Fifteen n. miles corresponding to 27.78 kms, the northward and southward extensions of the outer zone respect rather well the 25 kms nominal value.

The scatterometer-specific, small scale table has been developed by carrying out the following steps :

- 1) Decompacting the 5' x 5' table furnished by ESA/ESTEC, and placing the decompacted table on a direct access file. This first phase is carried out by the program VH-LECT:DATA.
- 2) Creating a sequential access file containing the scatterometer - specific land/sea table in its compacted form. This second phase is done by the program LAND-5:SYMB.



III - USING THE COMPACTED TABLE TABLES:DATA

To obtain information contained in TABLE5:DATA, a logical function LAND (XLAT,XLON) is used. LAND returns a TRUE value if land is present, otherwise a FALSE value. The first call to LAND loads the file in rapid access memory (tables IND and XLONG). XLAT and XLON are the latitude and longitude of the scatterometer point ; XLAT has a range of -90.0 to 90.0 (going from 90°S to 90°N) and XLON a range of 0. to 360. (going eastward from the Greenwich meridian).

This function is used in the program VH-LAND:SYMB.

IV - VH-LECT : DATA program description

The program VH-LECT:SYMB, reads the file SEALAND:DATA furnished by E.S.A. and creates the direct access file VH-LECT:DATA. (9979200 bytes, composed of 64800 records of 154 characters (1 byte) each). It is organized in 12° longitude records (12° x (60/5)=144 + 10) from 90° South to 90° North (180(60/5)). This format is repeated 30 times to cover the longitudes from 0° to 360°.

1) Tables used in the program

- To read the file SEALAND:DATA

KOAST (6227) integer*2 : contains for each 12 degrees wide longitude band, all informations on transitions sea-land or land-sea in latitude.

INDEX (14) integer*4 : index numbers necessary to use the array KOAST

If LON is the longitude index varying from 1 to 144, then we have :

IND = INDEX(LON) and KOAST(IND) = LON

where NUM = KOAST(IND+1) is the number of transitions in latitude for the longitude LON

and from KOAST(IND+2) to KOAST(IND+1 + NUM) we have the latitude index values for all transitions land-sea or sea-land.

- To create the file VH-LECT:DATA

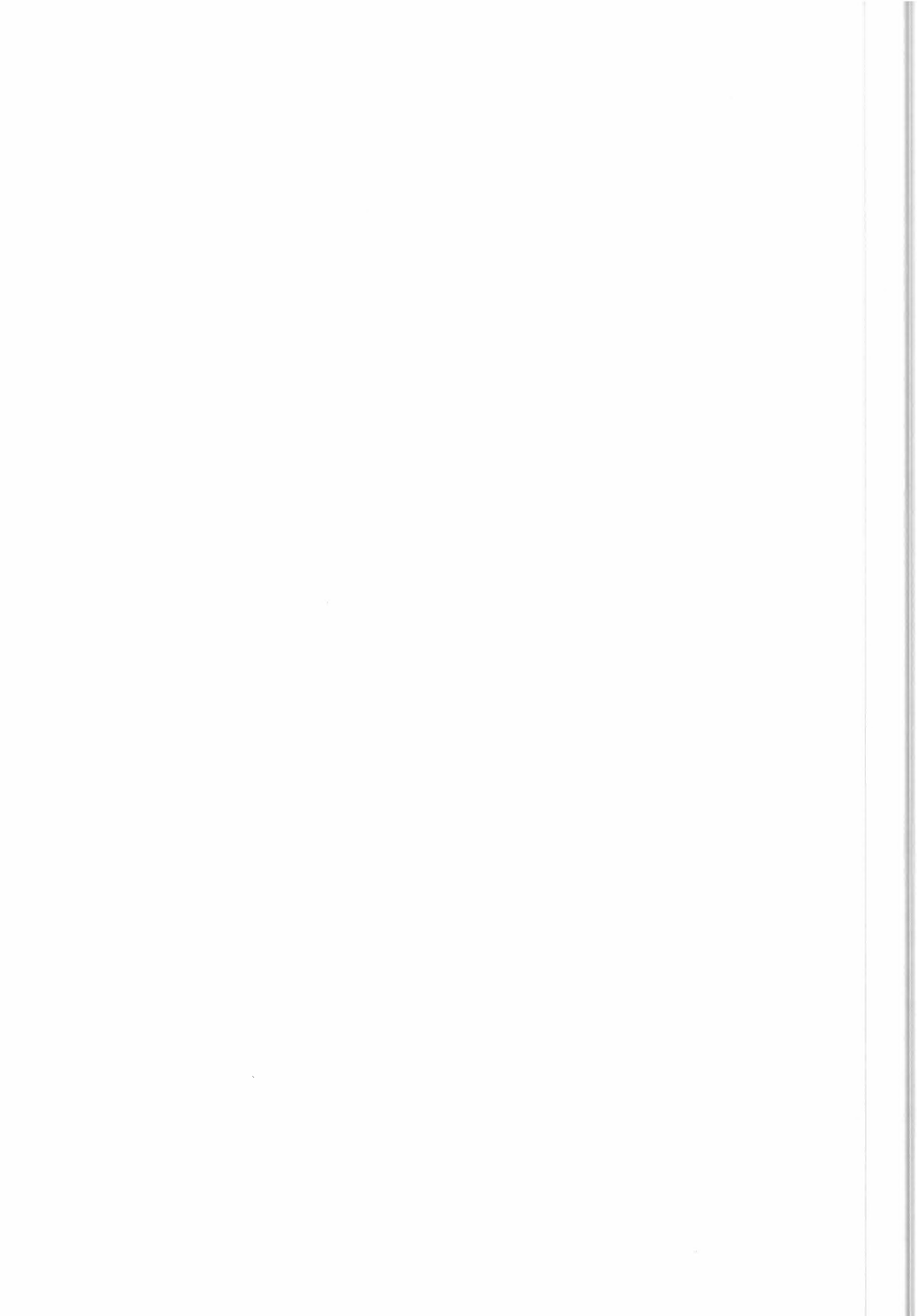
ITAB (2160,144) character * 1

i : latitude index going from 1 to 2160 (180° in latitude)
j : longitude index going from 1 to 144 (120° in longitude)

with the convention : ITAB(I,J) = '1' elementary pixel (5' x 5') is land
ITAB(I,J) = '0' " " " " is sea

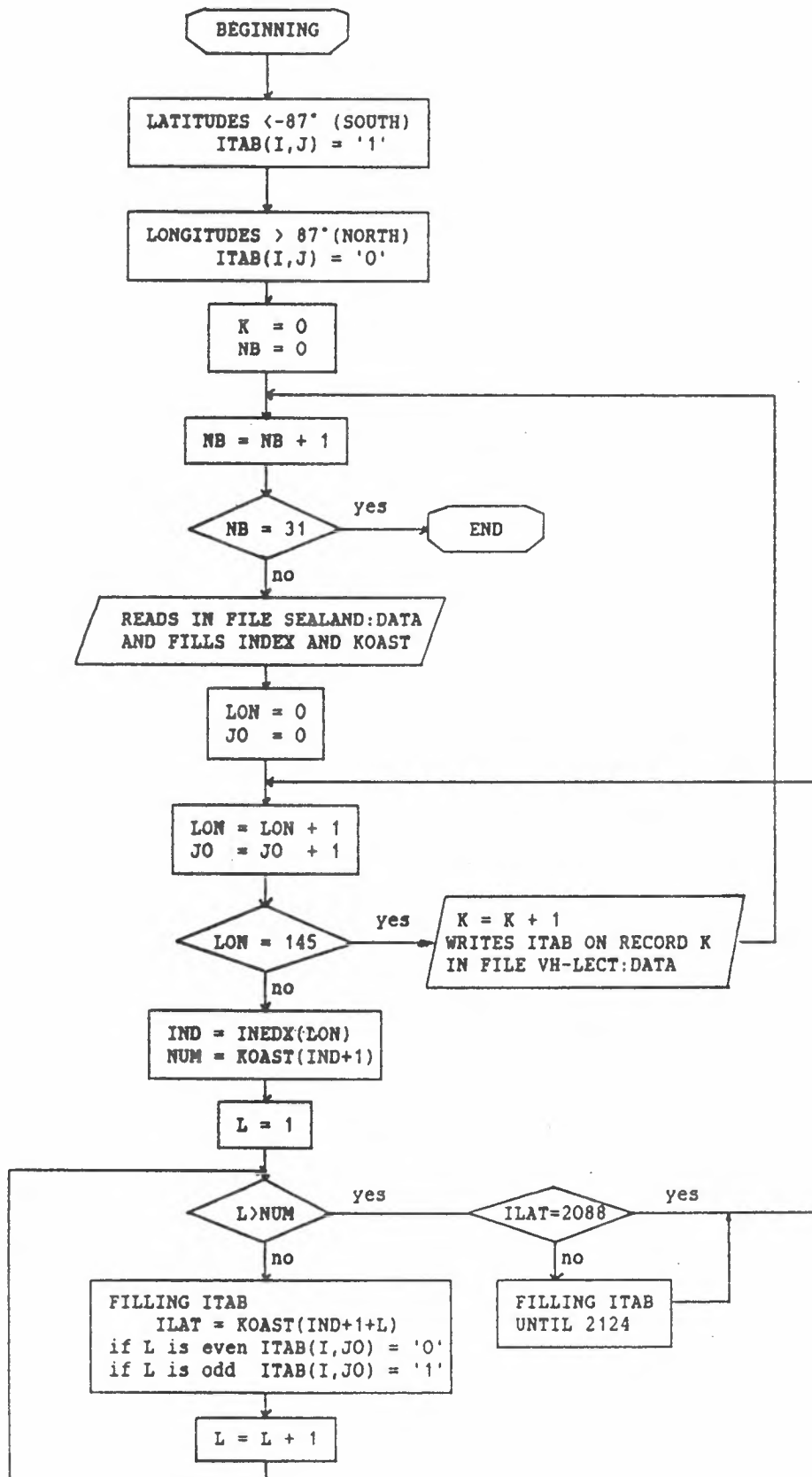
NE : . ILAT is the latitude index for the tables in file SEALAND:DATA and
ILAT = 1 for latitude = -87° (South).

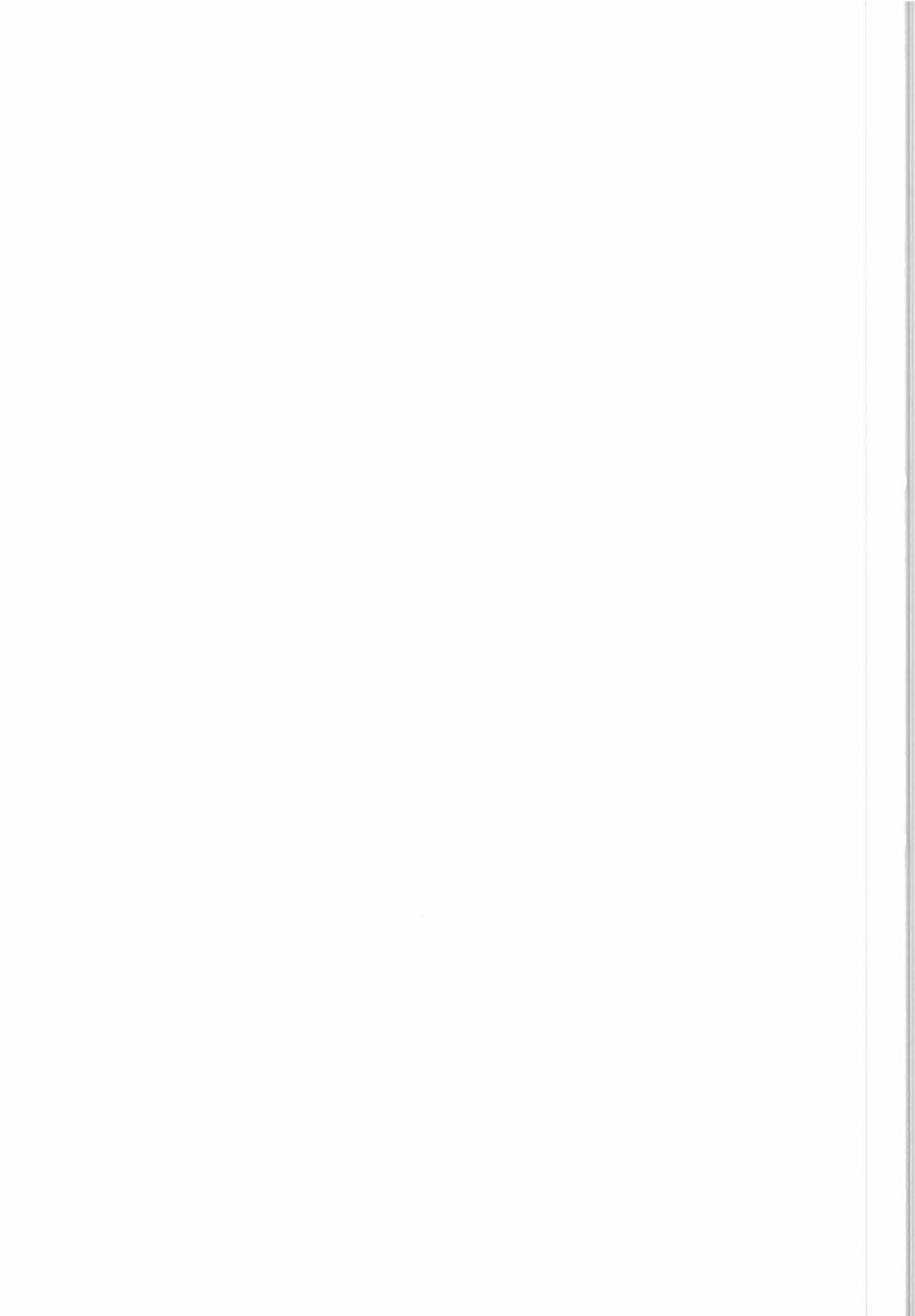
. LAT is the latitude index for the file VH-LECT:DATA and
LAT = 1 for latitude = -90° (South).



If $ILAT = 1$ then $LAT = ILAT + 36$ ($3^\circ \times 12$).

2) Diagram





V - LAND-5:SYMB program description

The second phase is done by program LAND-5:SYMB which reads VH-LECT:DATA to create file TABLES:DATA, containing the two scatterometer-specific land-sea tables. This sequential access file has a length of 138240 bytes, and contains the two tables IND (2160) and XLONG (32400).

IND contains the index value of the first land/sea or sea/land transition in each 5' latitude band. XLONG contains the longitudes of all the transitions (30069) going eastward from the Greenwich meridian over 360° for each latitude band from 90° S to 90° N. An artificial transition 361° is inserted at the end of each latitude band, another at 0° of the following band if there is no real transition between the two elements.

The parameter NMAX (specified by a DATA instruction in the sub-program TABLE5) fixes the maximum number of 5' x 5' elements which may be land in the zone surrounding the element considered. If the number of land elements is greater than NMAX, the central element is declared to be land (that is to say, land contaminated). Presently, in agreement with E.S.A., NMAX has been set to zero.

1) Variables definition

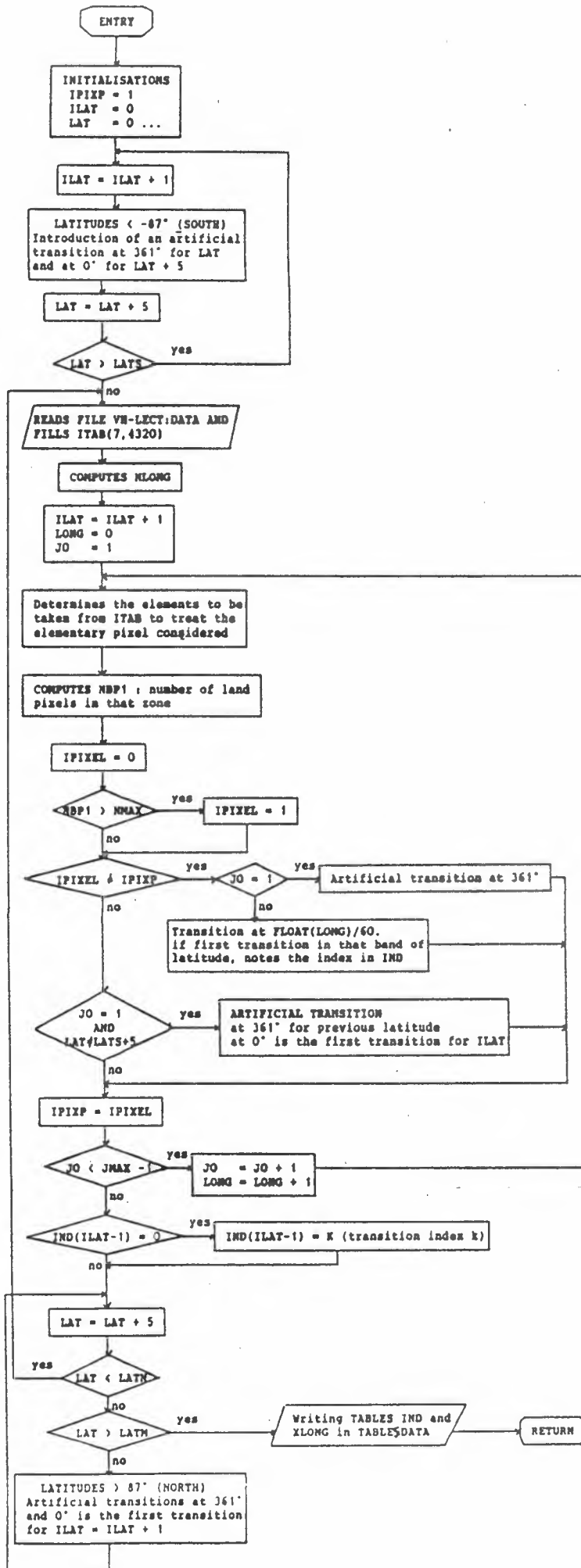
NAME	TYPE	DESCRIPTION
ITAB	Character*1	<p>2 dimensional array ITAB(7,4320) filled by reading the file VH-LECT:DATA.</p> <p>7 is the number of elementary (5' x 5') pixels in latitude</p> <p>4320 = 12 x 360° is the number of elementary pixels in longitude (one 5' latitude band)</p> <p>ITAB(I,J) = '0' for an ocean pixel ITAB(I,J) = '1' of a land pixel</p>
IPERM	Character*1	<p>An array IPERM(6) used in order to reduce the number of readings in the file VH-LECT:DATA</p> <p>In fact :</p> <div style="text-align: center;"> <p style="text-align: center;">J=1 Jmax=4320</p> <p style="text-align: center;">7 6 5 4 3 2 I=1</p> <p style="text-align: right;">band to be treated pixel /pixel</p> </div> <p>For the next band it is only necessary to read a group of 30 records of the input file (one band of 360°).</p>



NAME	TYPE	DESCRIPTION
IND	Integer*4	An array IND(2160) that will contain for each latitude the index corresponding to the first transition land-sea or sea-land found in longitude.
XLONG	Real*4	An array XLONG(32400) that will contain the longitudes of all transitions for each latitude band.
LATM	Integer*4	Maximum latitude in minutes = 10795 (180°)
LATS	"	Southern latitude in minutes = 180 (-87°S between 0° and 180°). Under this latitude all elementary pixels are land.
LATN	"	Nothern latitude in minutes = 10620 (+87°N between 0° and 180°). Above this latitude all elementary pixels are sea.
LAT	Integer*4	Latitude in minutes $LAT = n*5'$
ILAT	Integer*4	Latitude index $ILAT = LAT/5' + 1$
LONG	"	Longitude in minutes $LONG = m*5'$
JO	"	Longitude index varies from 1 to 4320 = JMAX
XLAT	Real*4	Latitude in degrees
XLON	Real*4	Longitude in degrees
NMAX	Integer*4	Maximum number of 5' x 5' pixels declared as land acceptable before setting the flag to land.
NLONG	Integer*4	Number of elementary pixels that covers 25 kms in longitude, varies with the latitude obtained by the formula : $25./(9.26 * \cos(XLAT))$
IPIXEL	Integer*4	IPIXEL = 1 if elementary pixel considered is land IPIXEL = 0 if elementary pixel considered is sea
IPIXP	Integer*4	Initialized to 1 Value of the previous pixel



2) Diagram



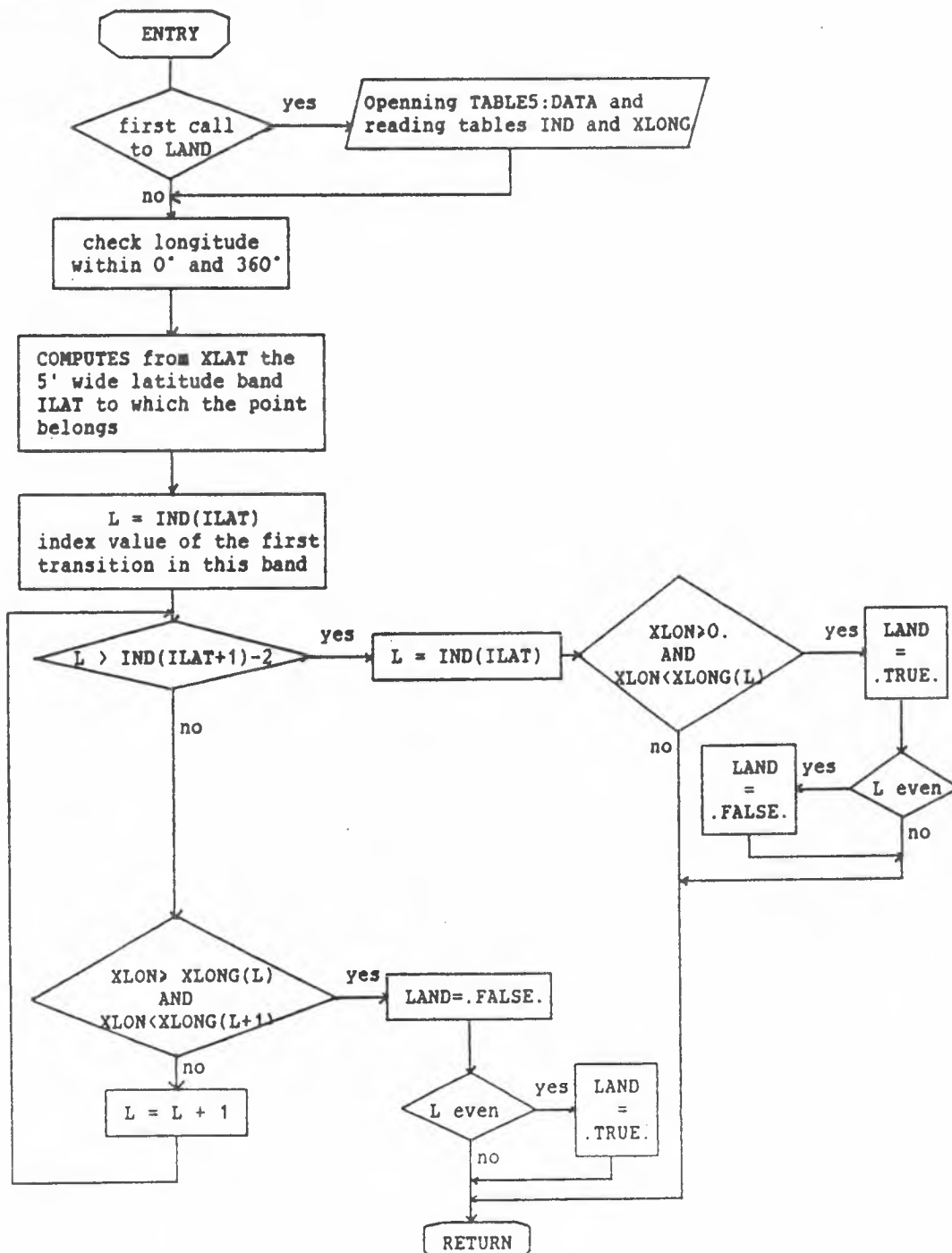
VI - THE LAND (XLAT,XLON) FUNCTION

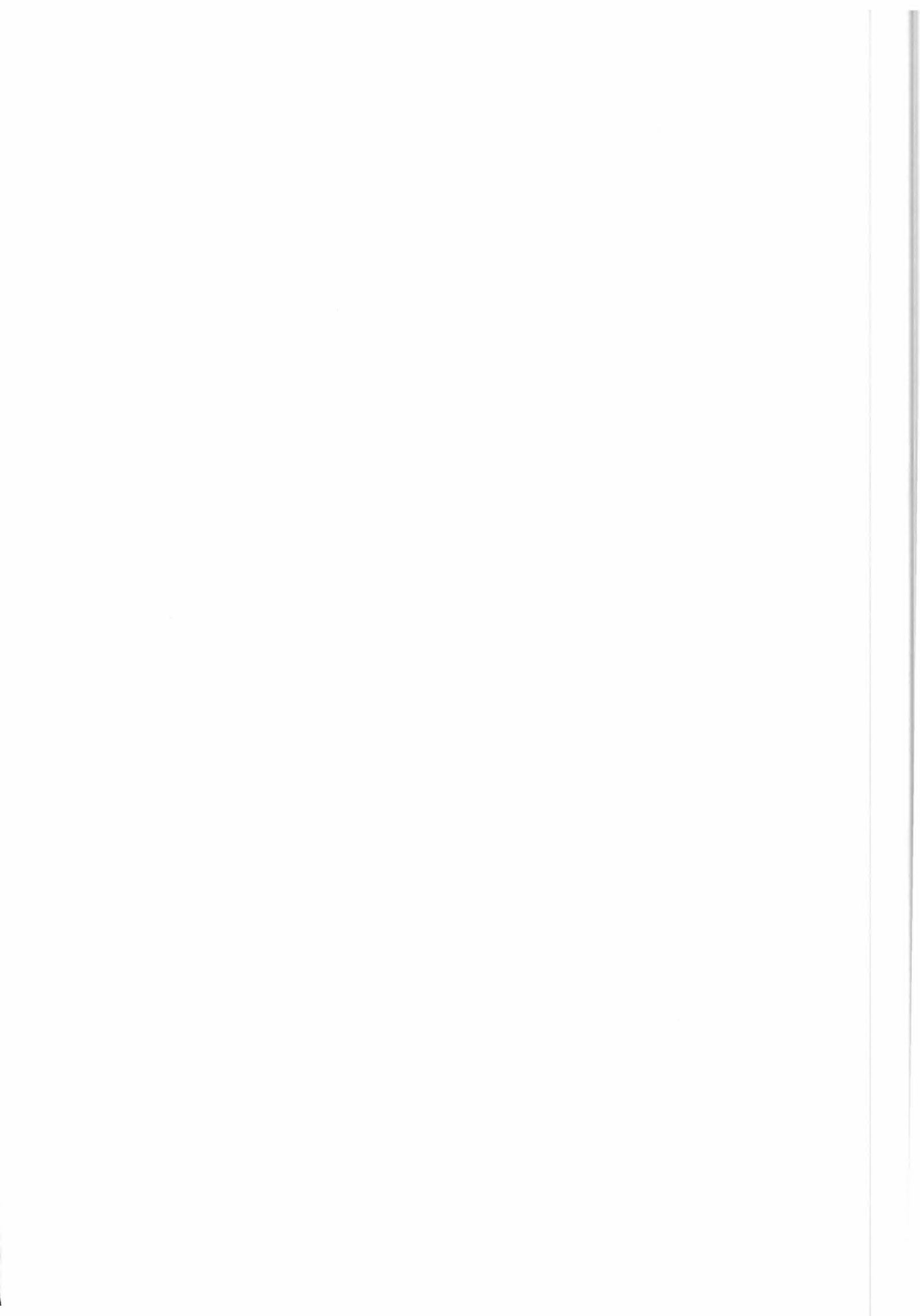
LAND proceeds in the following steps :

- 1) Determine from XLAT the 5' wide latitude band to which the point belongs
- 2) Read from table IND the index value of the first transition (odd if land/sea, even if sea/land) in the latitude band
- 3) Read the longitudes of the transitions successively going eastward. If XLON is less than the longitude of a transition then the point is land or sea if the transition is respectively land/sea or sea/land.

The artificially introduced transitions at 361° and 0° serve to avoid passing from one latitude band to another in the longitude search for transitions.

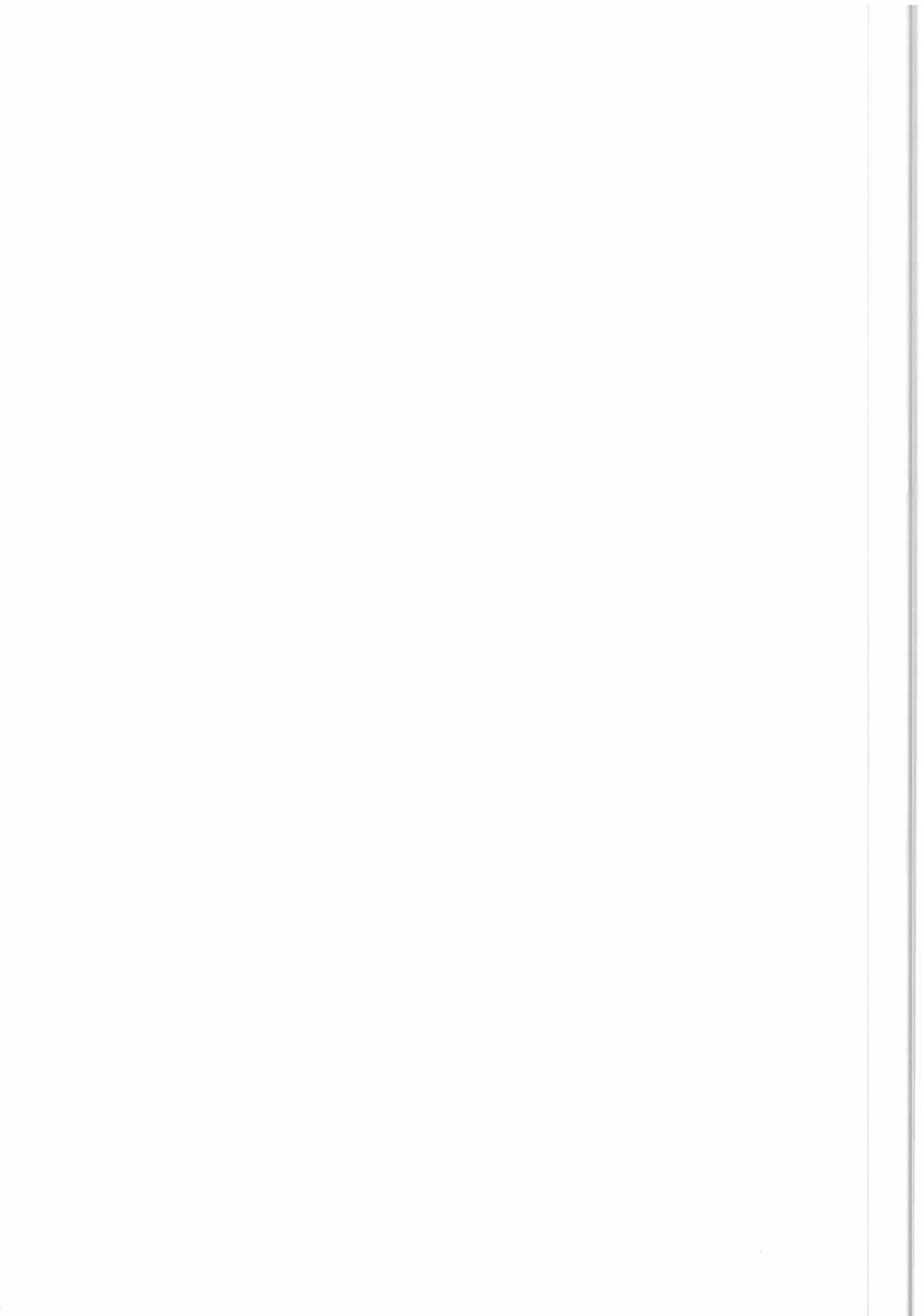
Diagram of this function

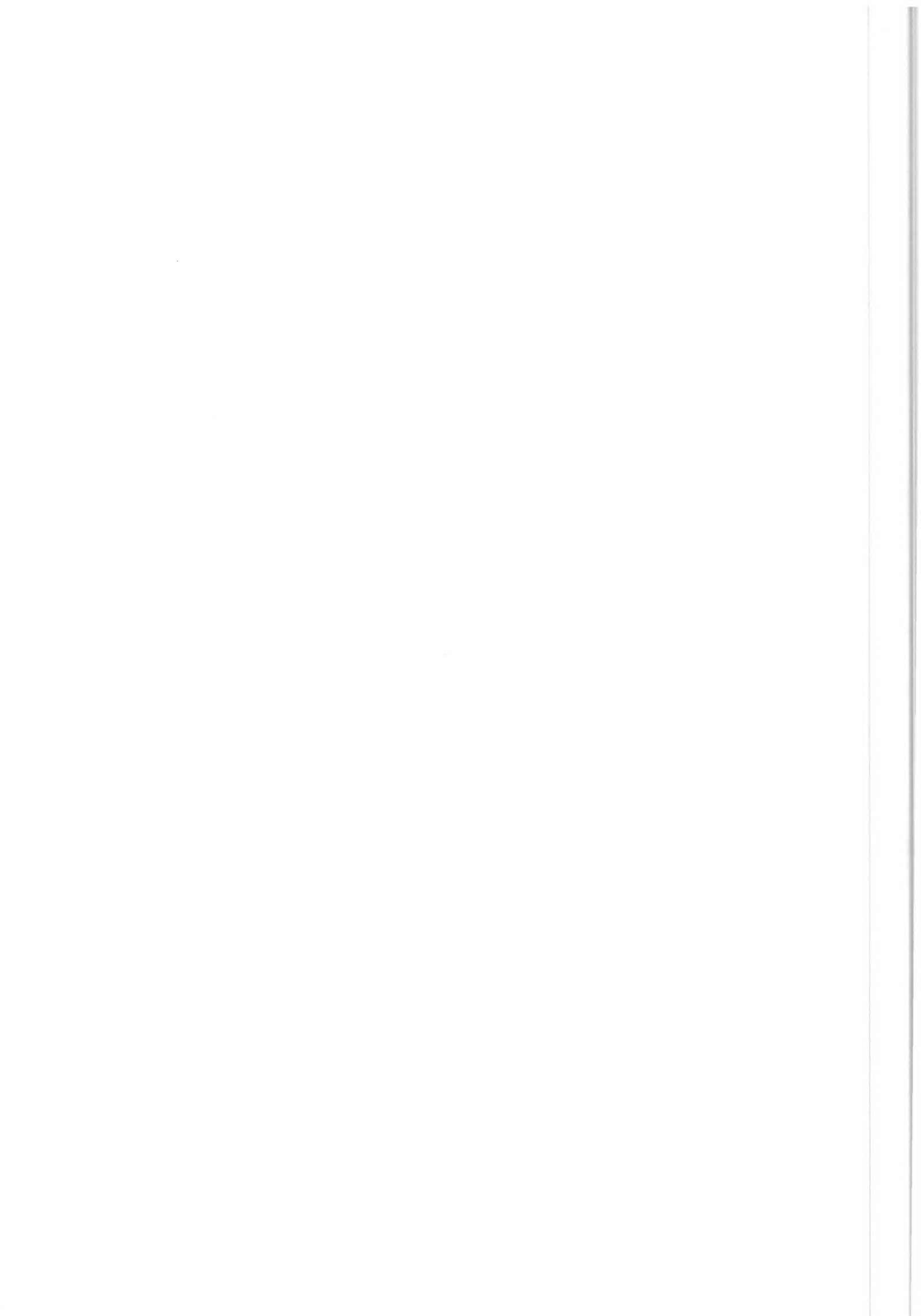


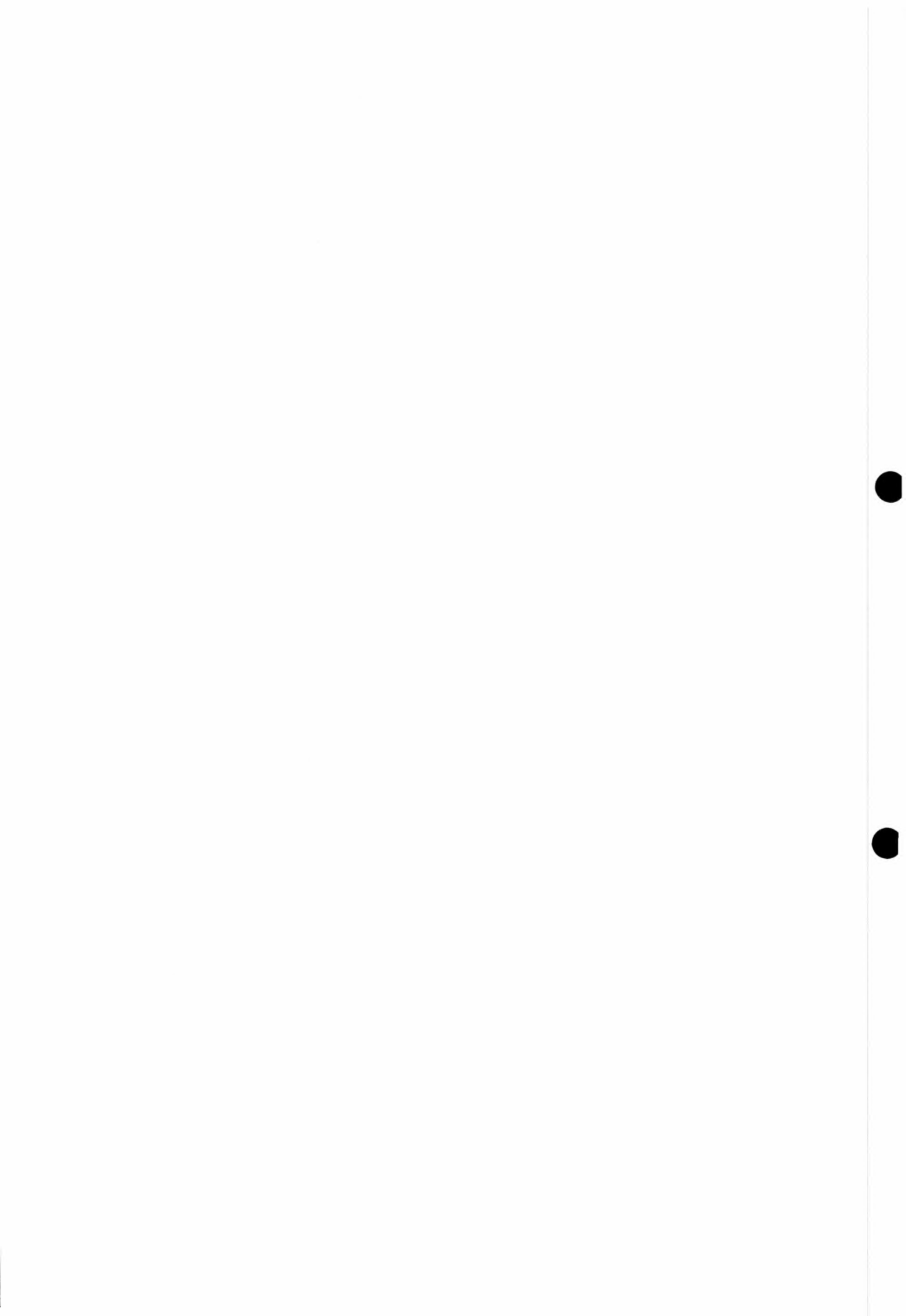


ANNEX 2

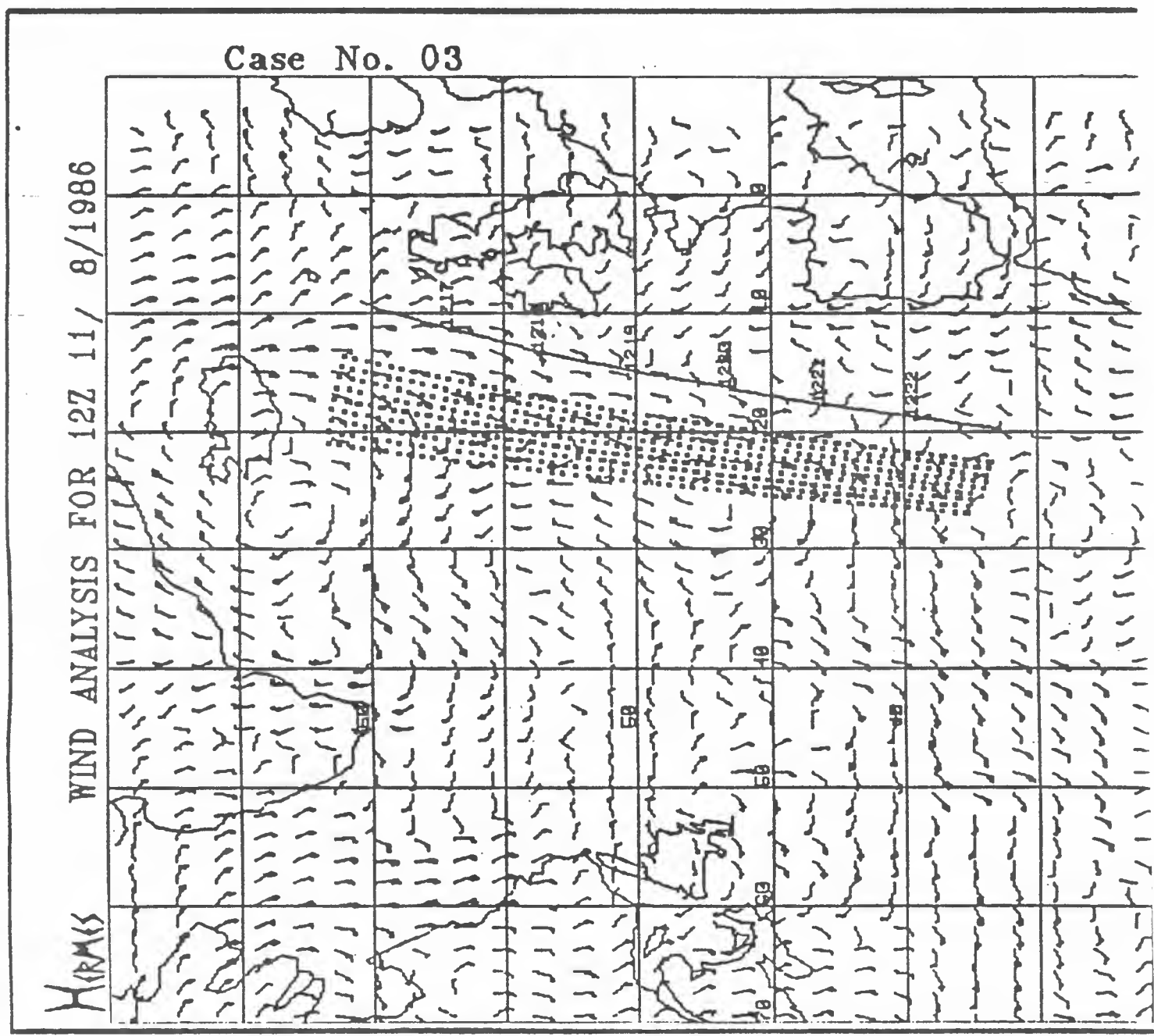
METEOROLOGICAL SITUATIONS OF D. OFFILERS'S TEST FILES

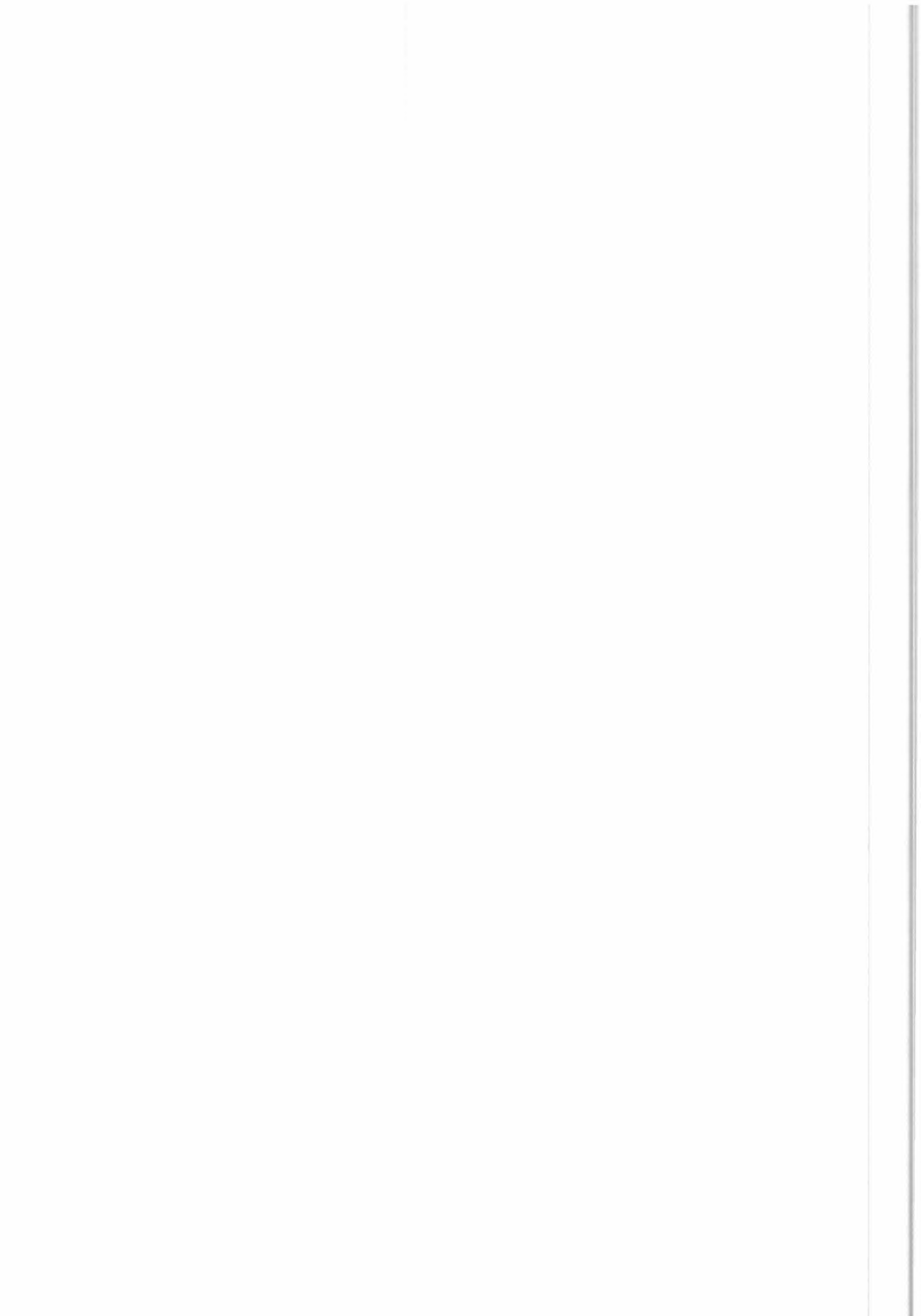






ARGS screen dump taken at 09:16:03 13-AUG-86

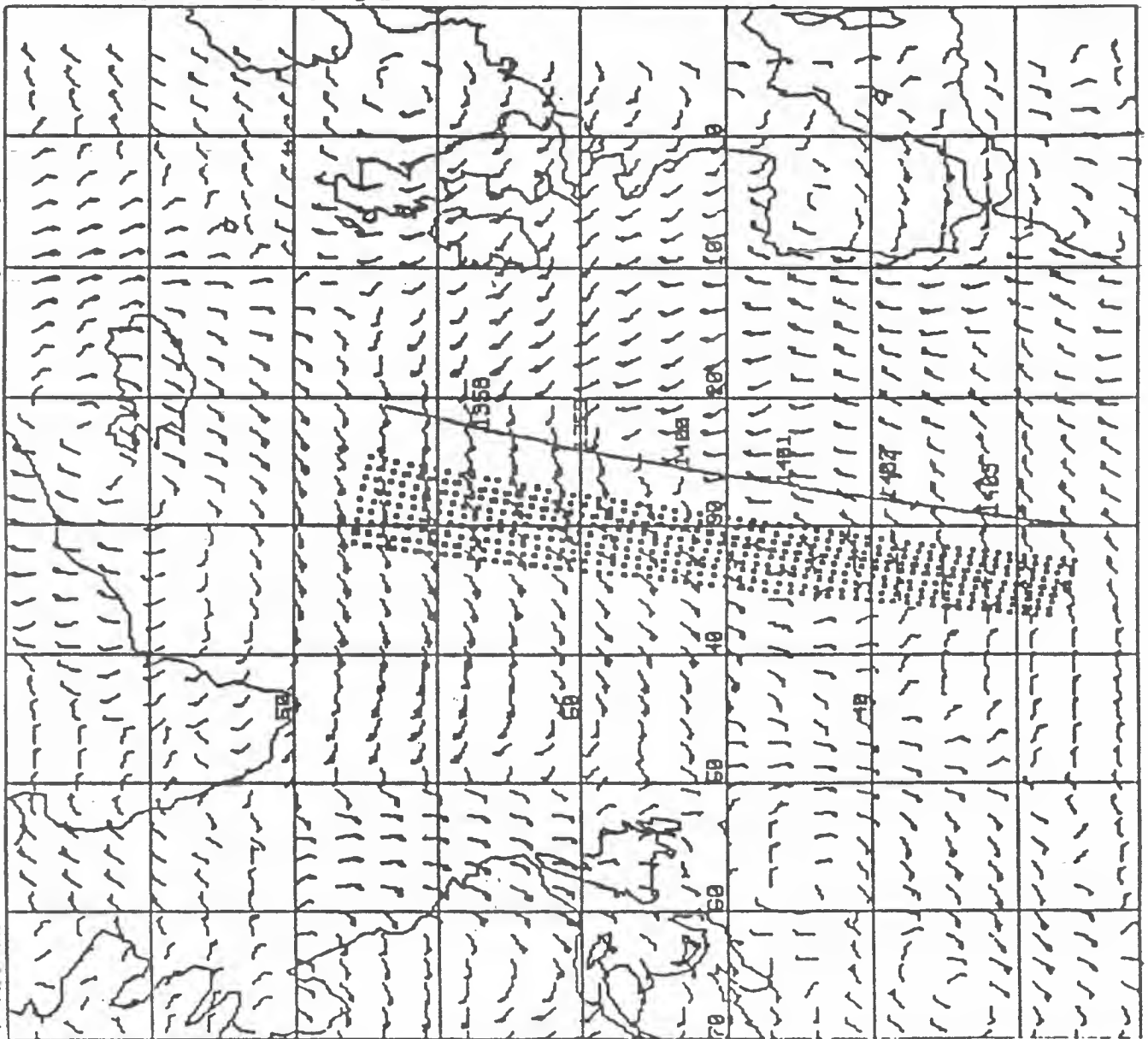


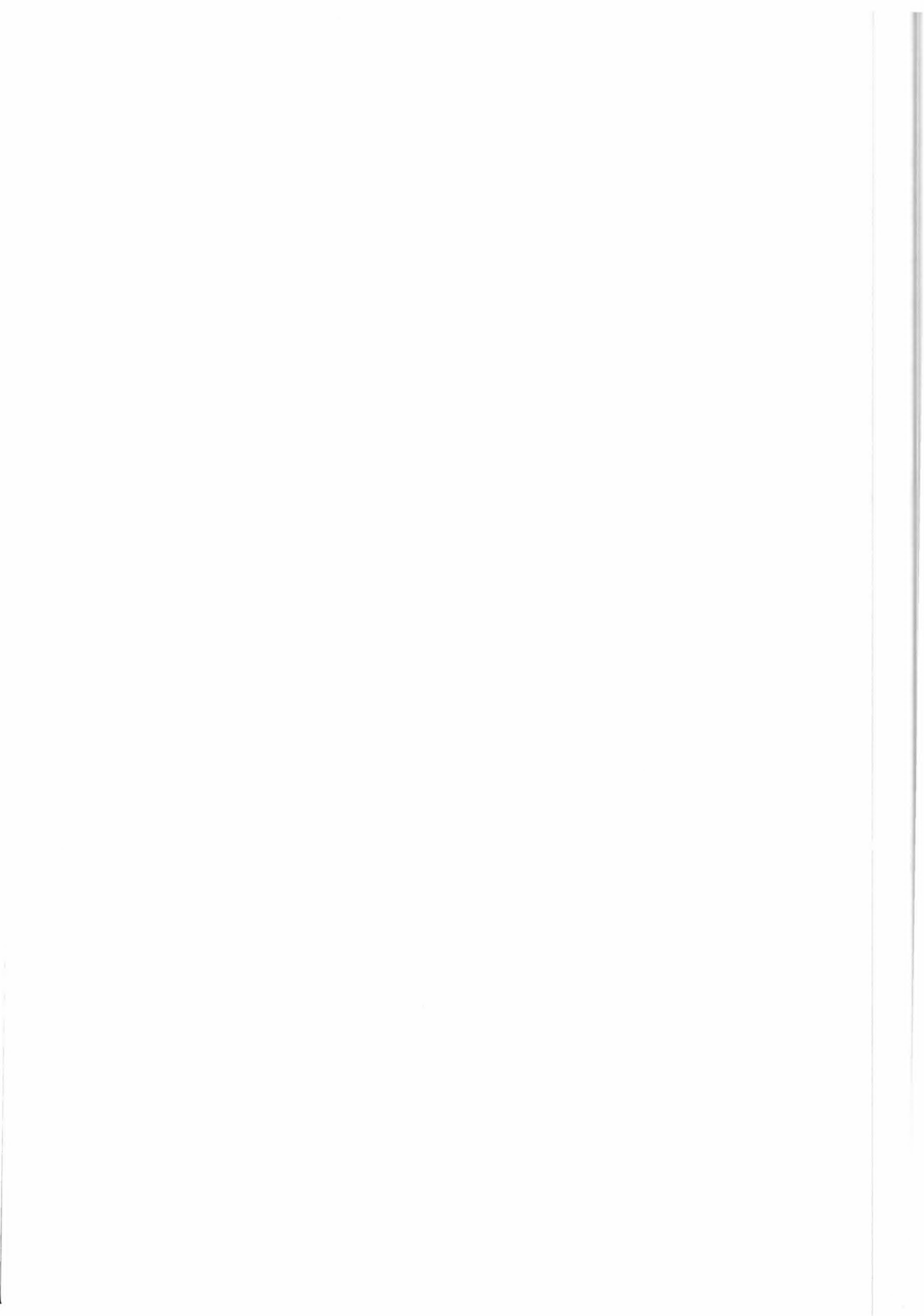


ARGS screen dump taken at 15:39:09 13-AUG-86

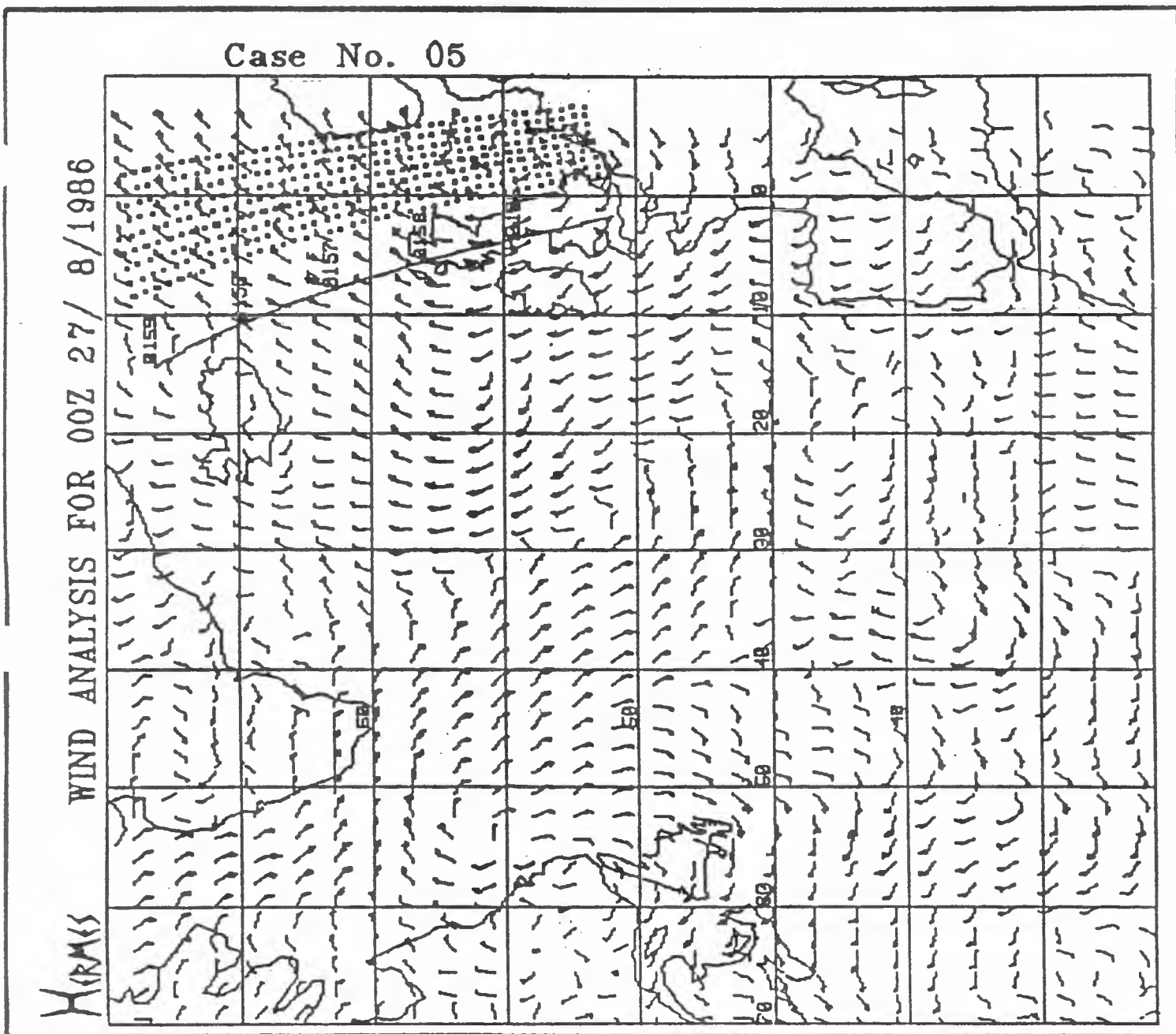
Case No. 04

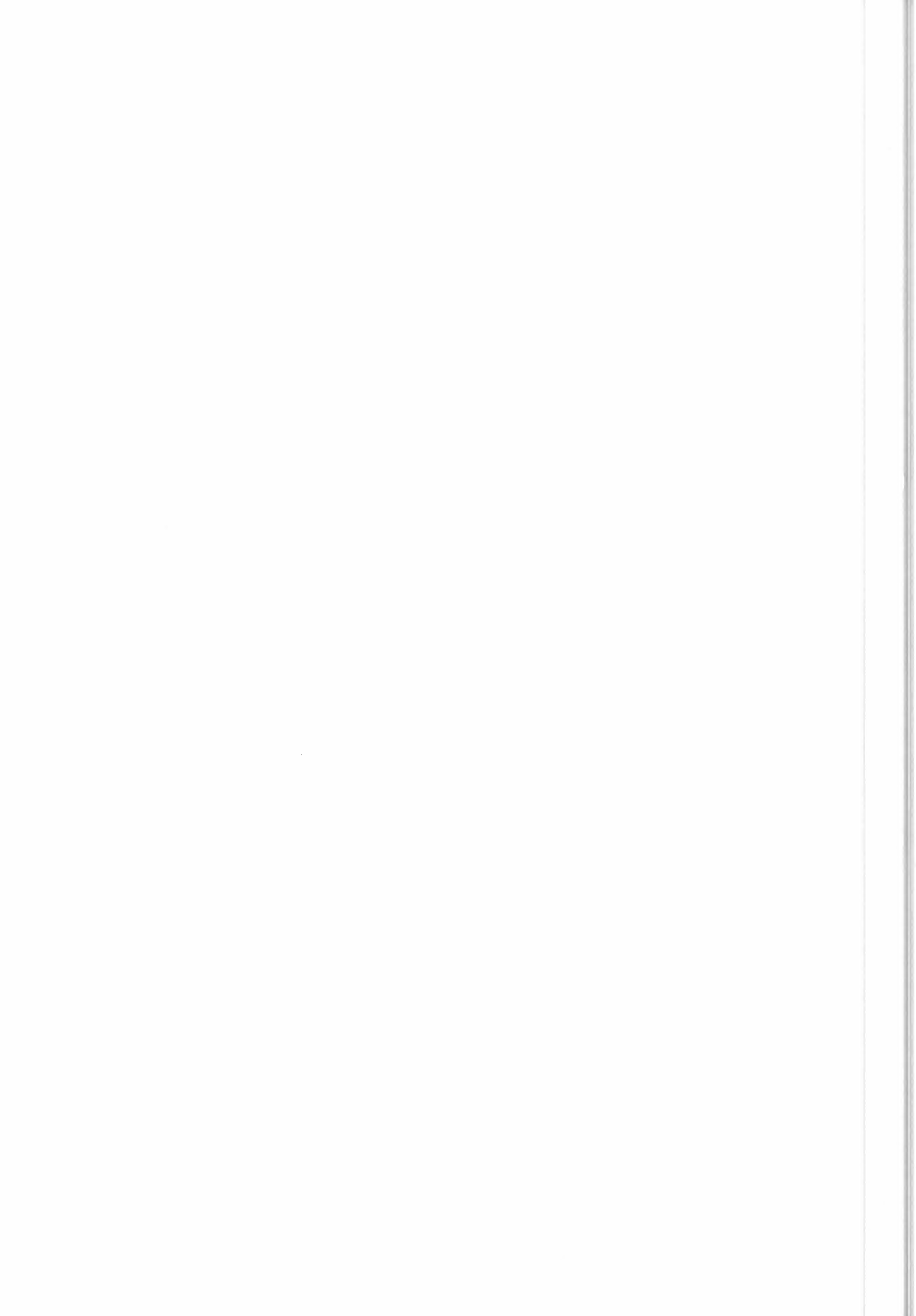
HIRMIS WIND ANALYSIS FOR 12Z 23/ 7/1986





ARGS screen dump taken at 10:24:23 27-AUG-86

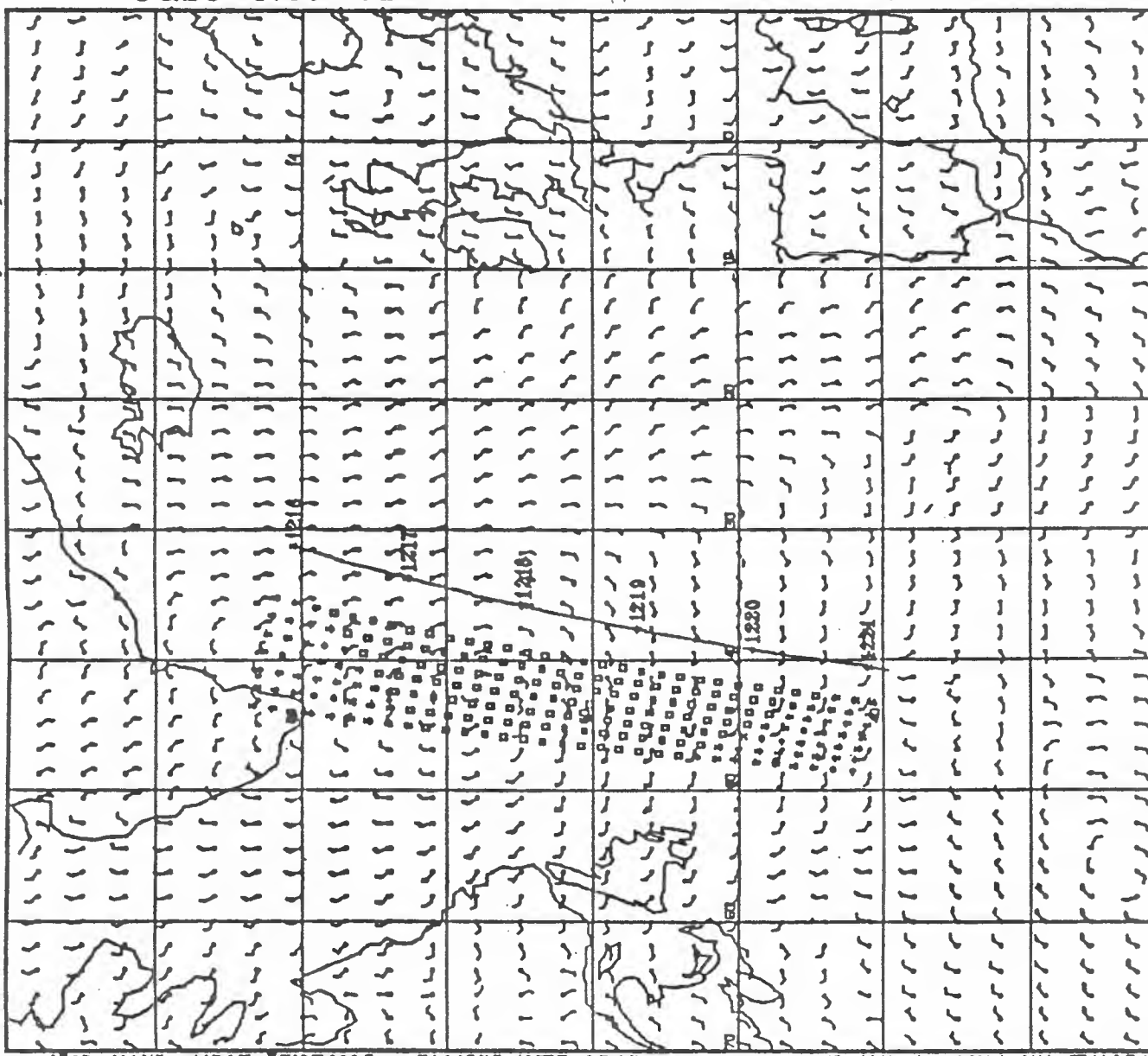




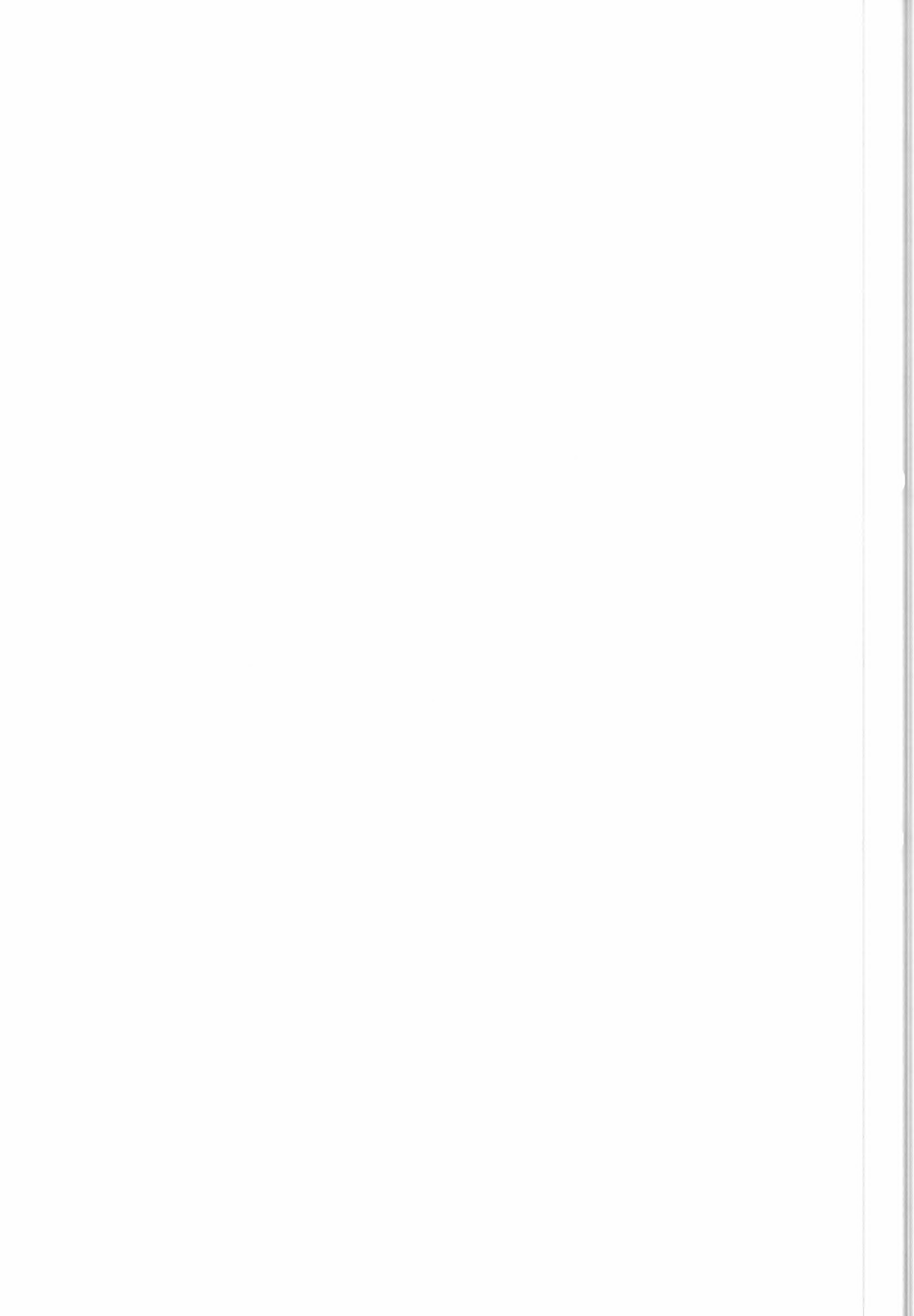
ARGS screen dump taken at 12:05:53 7-JAN-87

Case No. 11

HARMES WIND ANALYSIS FOR 00Z 7/ 1/1987



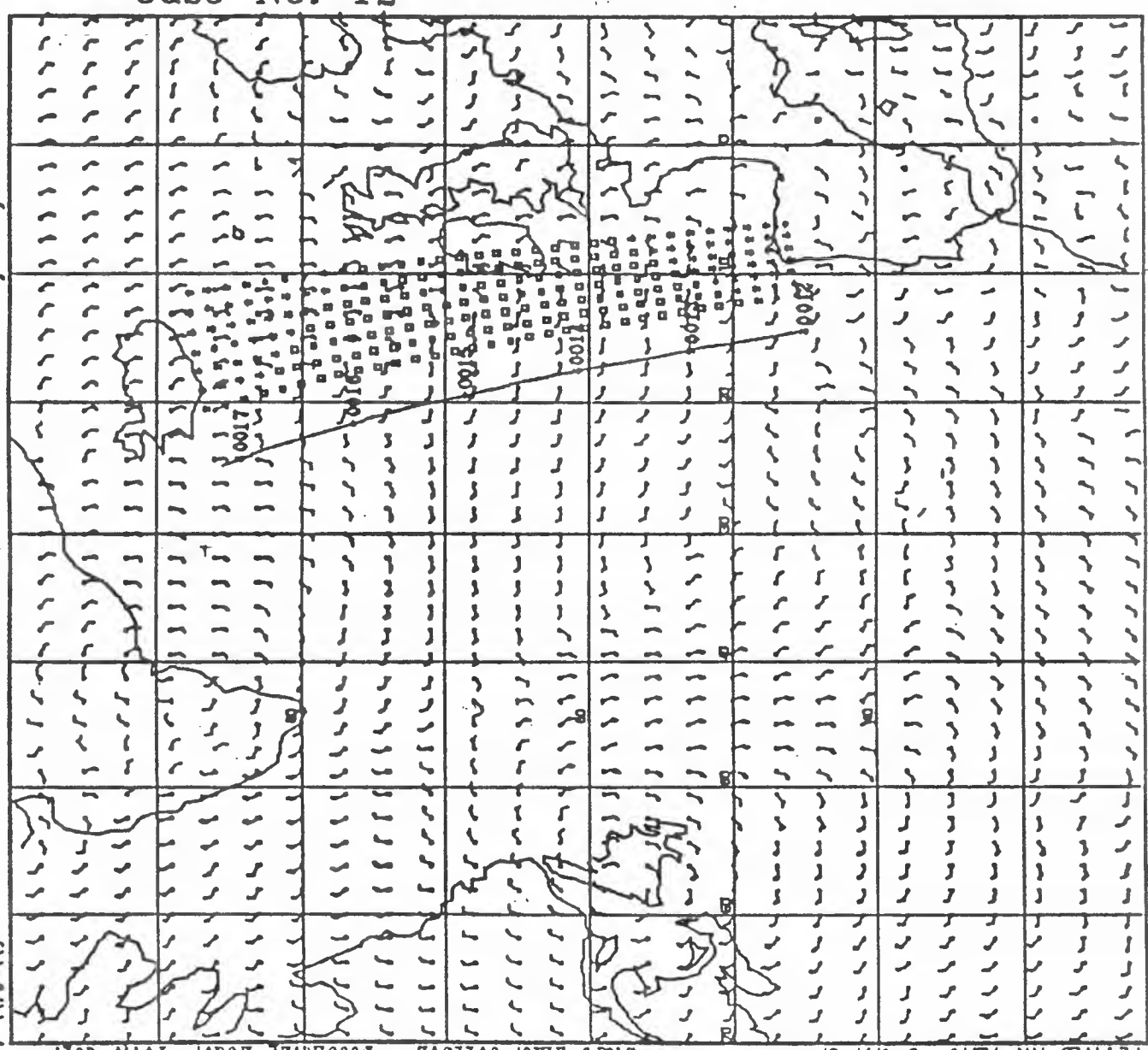
PLOTTED AT: 11:59 7-JAN-87 Start time: 18100Z Receiving node: 126.0 deg.



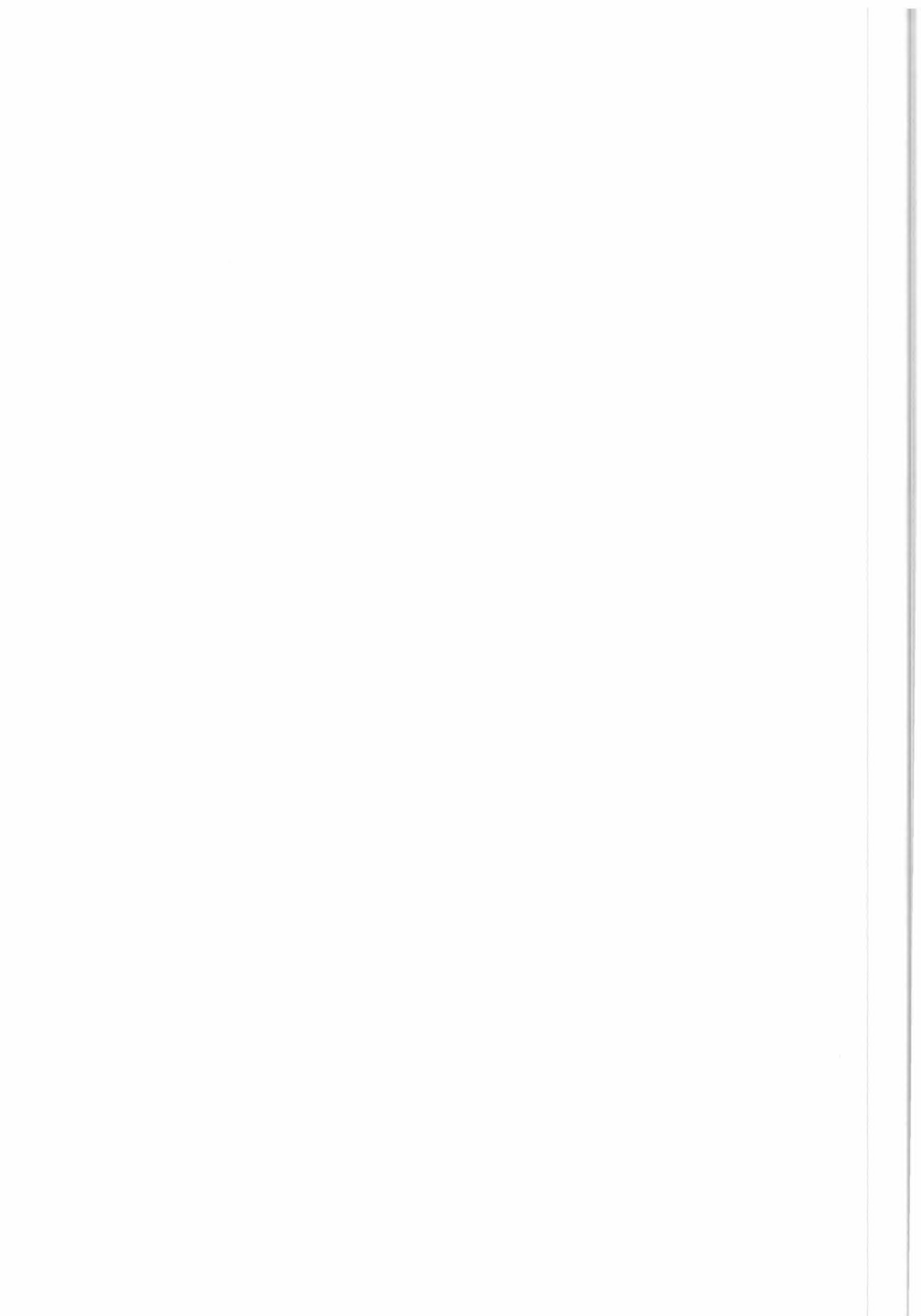
ARGS screen dump taken at 13:01:27 9-JAN-87

Case No. 12

HIRMES WIND ANALYSIS FOR 00Z 9/ 1/1987



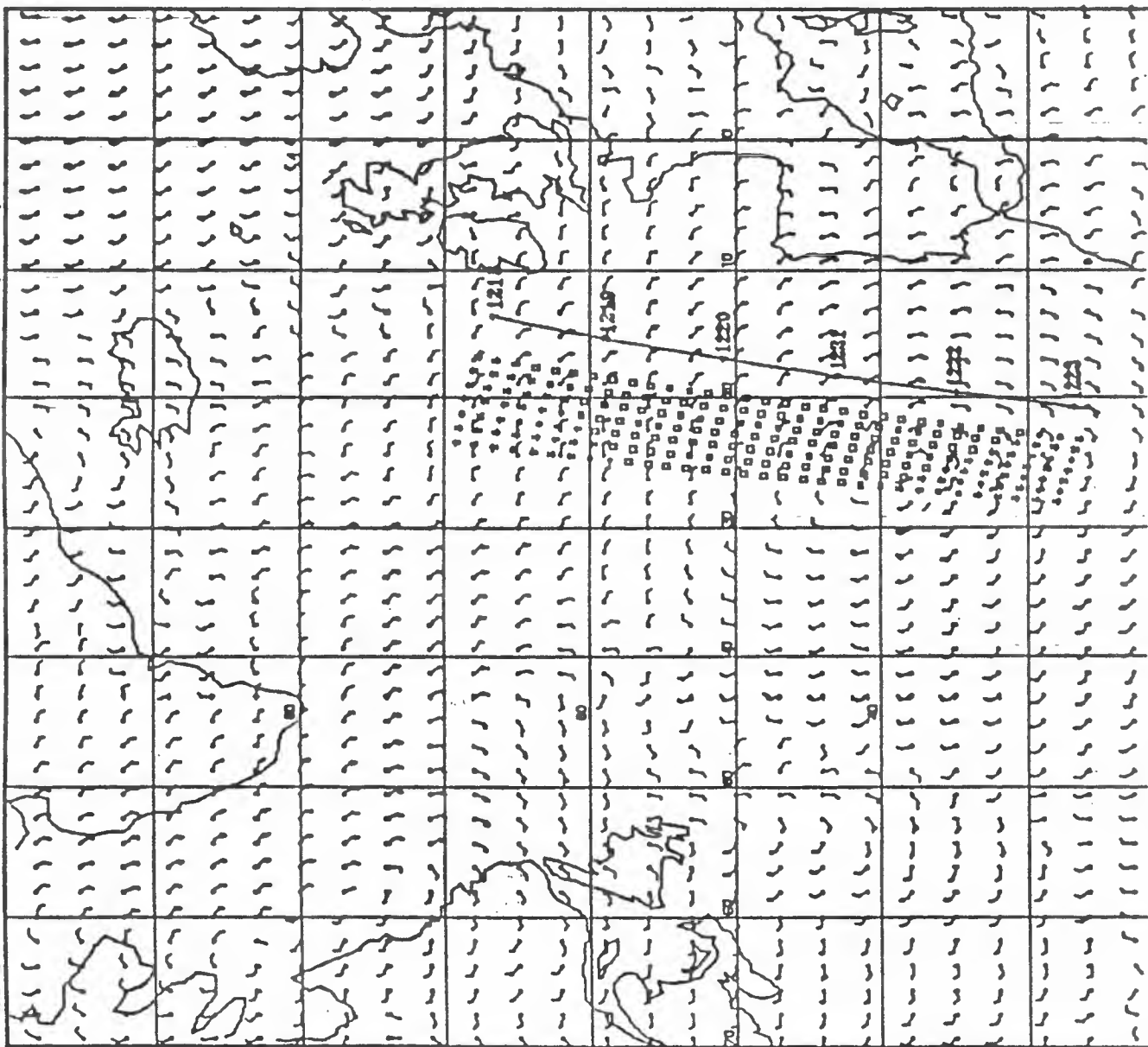
PLOTTD AT: 12:46 8-JAN-87 Start time: 001159Z Recording mode: 164.0 deg.



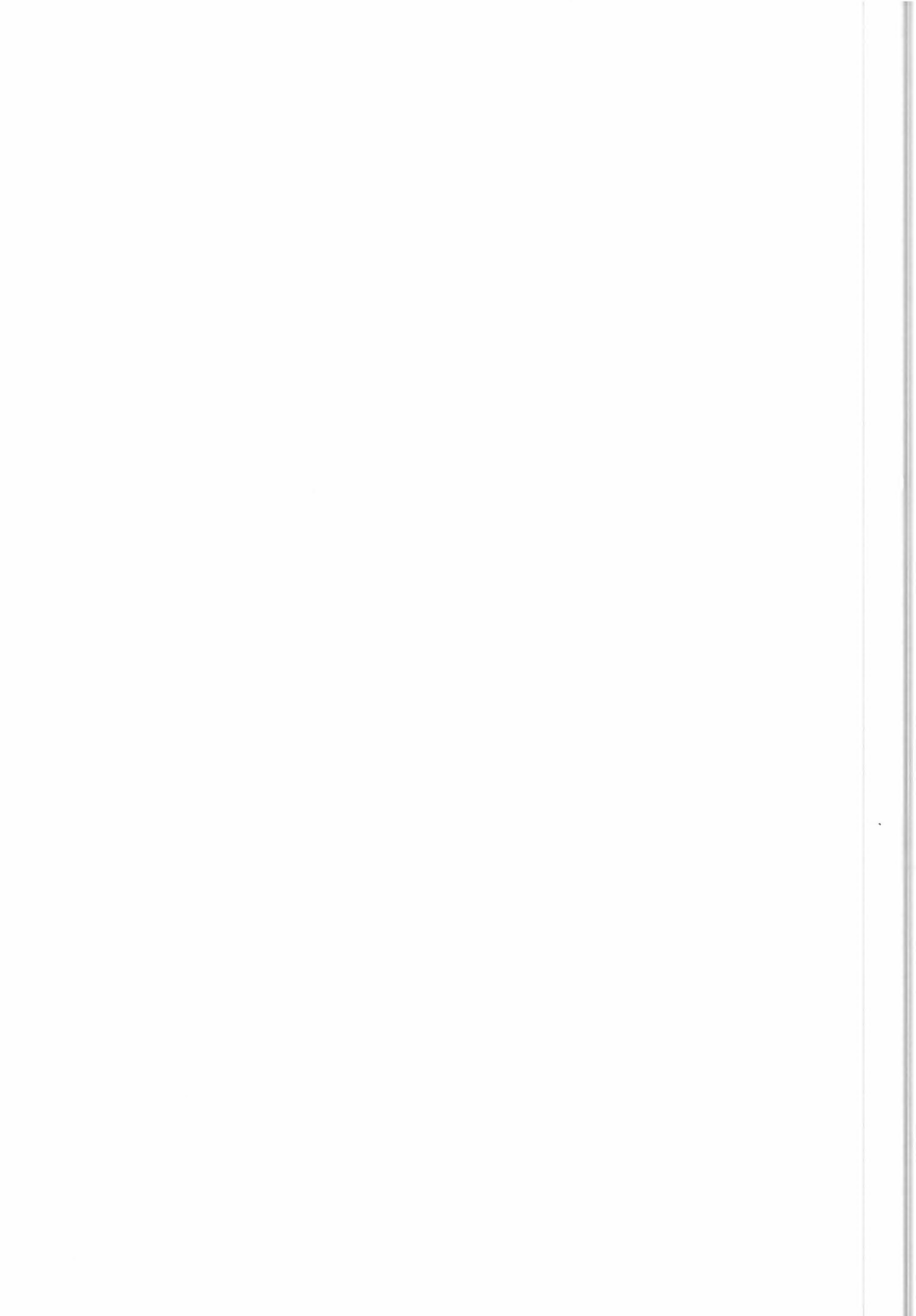
ARGS screen dump taken at 11:27:51 16-FEB-87

Case No. 13

HIRMIS WIND ANALYSIS FOR 12Z 25/ 1/1987



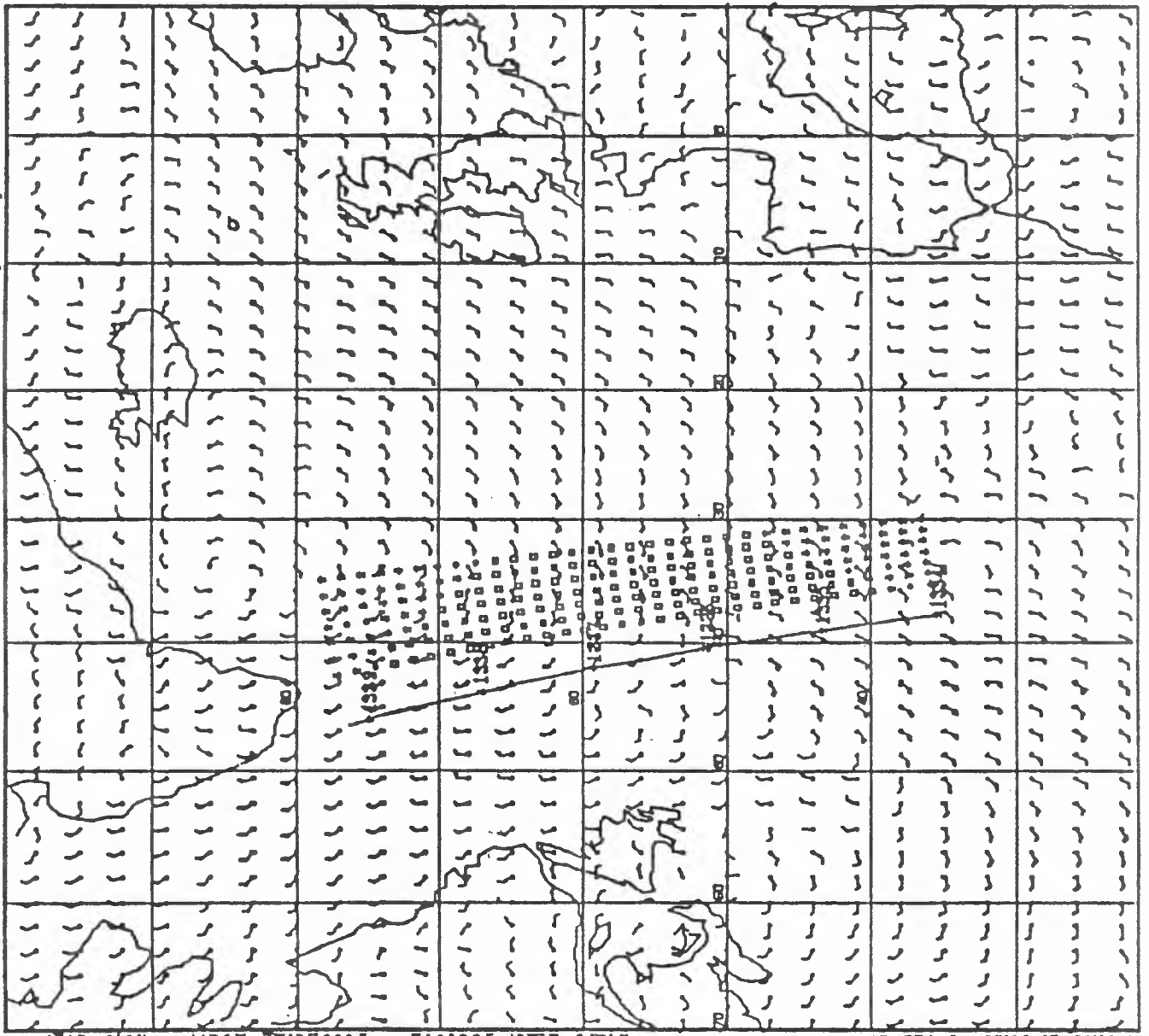
Plotted at 11:24 16-FEB-87 Start time: 181809Z Recording mode: 1479 deg.



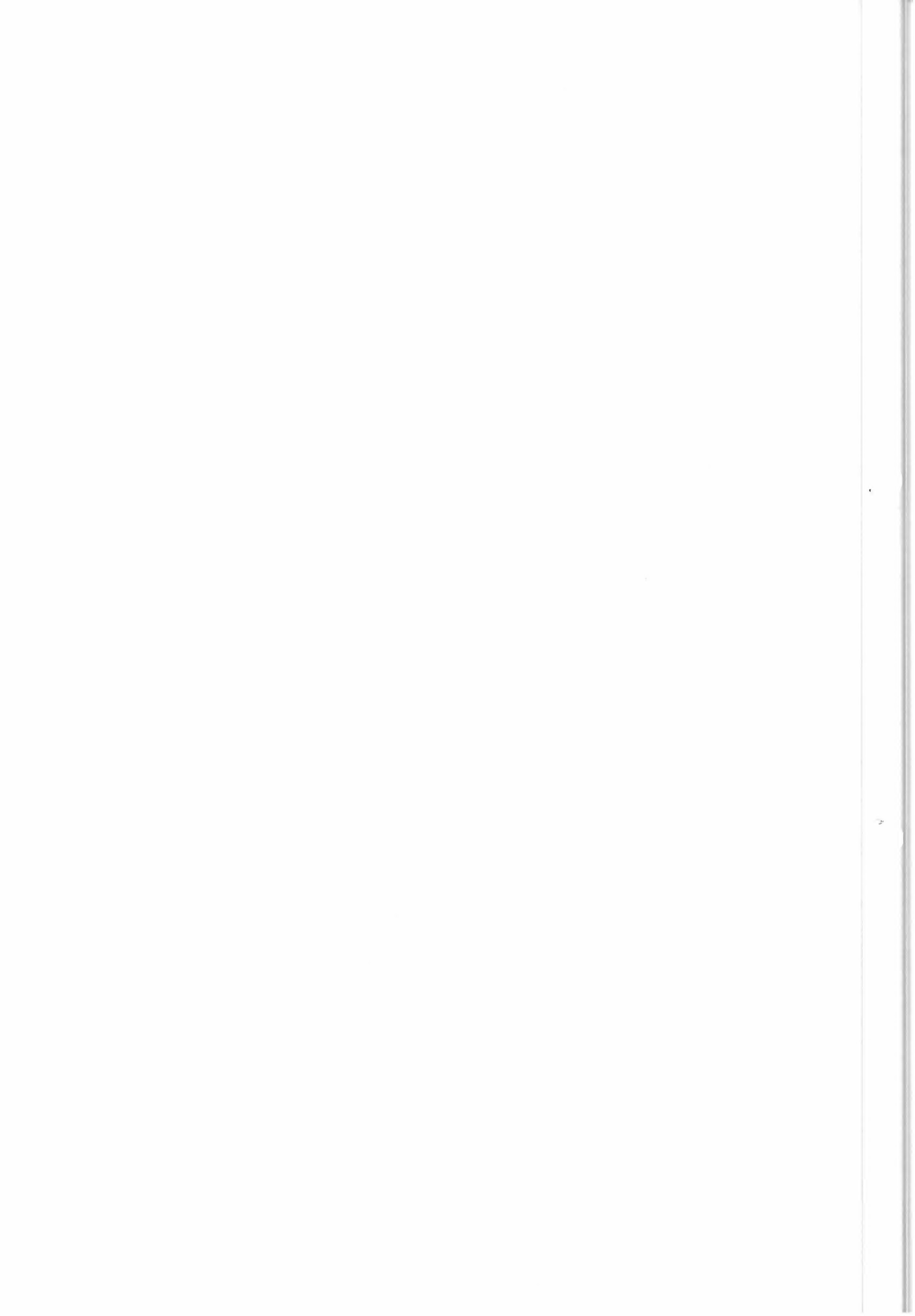
ARGS screen dump taken at 09:38:54 5-FEB-87

HIRMIS WIND ANALYSIS FOR 12Z 4/ 2/1987

Case No. 14



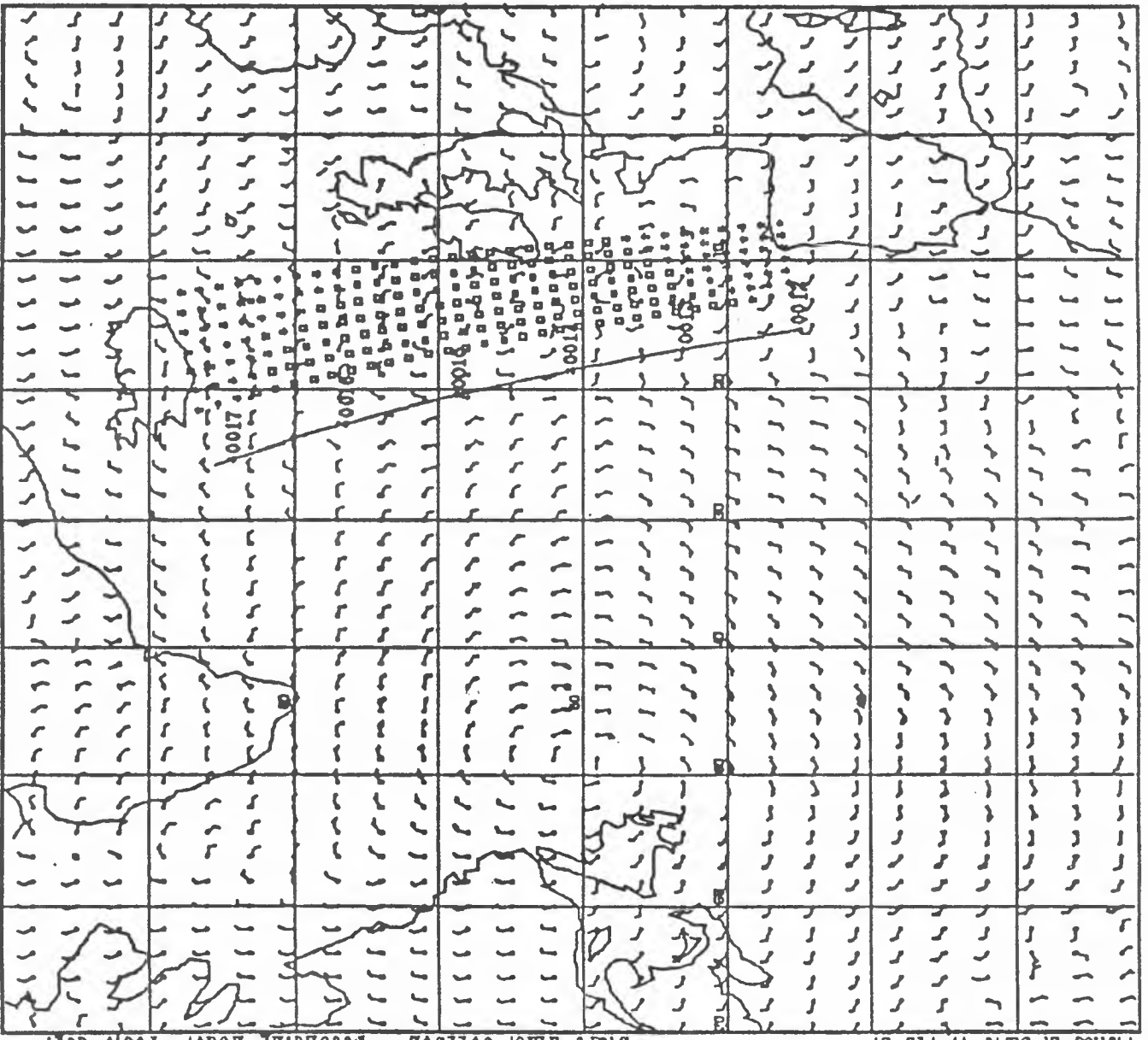
Plotted at 09:28 5-FEB-87 Start time: 183409Z Recording mode: -20.0 deg.



ARGS screen dump taken at 08:54:54 17-FEB-87

Case No. 15

HIRAMS WIND ANALYSIS FOR 00Z 15/ 2/1987



Plotted at 08:48 17-FEB-87 Start time: 001109Z Receiving node: 103.9 deg.

